UNIVERSITY OF Southampton

FACULTY OF MEDICINE

Academic Unit of Human Development and Health

Wnt Protein Delivery to Skeletal Stem Cells for Bone Tissue Regeneration

by

Agnieszka Aleksandra Janeczek

Thesis for the degree of Doctor of Philosophy

September 2015

UNIVERSITY OF SOUTHAMPTON

ABSTRACT

FACULTY OF MEDICINE

Stem Cell Science and Regenerative Medicine

Thesis for the degree of Doctor of Philosophy

WNT PROTEIN DELIVERY TO SKELETAL STEM CELLS FOR BONE TISSUE REGENERATION

Agnieszka Aleksandra Janeczek

There is a pressing need to develop anabolic treatments that enhance bone regeneration. Bone fractures are a major socioeconomic problem, which is likely to increase as our population ages. A promising approach to address this problem may be the delivery of molecules targeted to stem cells responsible for the regeneration of bone. Wnt signalling is involved in regulating skeletal stem cells (SSCs), and is known to be an important regulator of fracture healing. The aim of this study was to test the hypothesis that Wnt protein can augment the osteogenic response of SSCs, and may be delivered in an active form at the fracture site using liposome nanoparticles.

Wnt signalling levels in bone marrow populations rich in SSCs were determined by qPCR. These populations were also transiently exposed to 100 ng/ml of Wnt3A, and their frequency, viability and proliferation were studied by flow cytometry. After 14 days of adherent culture, their colony forming unit fibroblastic and osteoblastic (CFU-F/O) potentials were tested. Osteogenic differentiation was tested in cells exposed to transient and also to sustained Wnt stimulation. Liposomes were then investigated as a means of delivering active Wnt proteins. After optimising their lipid formulation and determining the association of Wnt with the nanoparticles, protein activity, nanoparticle uptake *in vitro* and biodistribution *in vivo* were characterised.

SSC-rich populations had elevated levels of Wnt signalling and were responsive to Wnt stimulation, which, when applied transiently, expanded the subset of osteoprogenitors and increased their osteodifferentiation. However, sustained stimulation inhibited this process. 100 nm liposomes enhanced Wnt activity and were readily taken up by cultured stromal cell populations, as well as by SSC-rich populations within fresh bone marrow isolates. At 24 and 48 hours following systemic injection, liposomes localised at the bone fracture site.

Wnt3A exposure primed SSCs and progenitors within fresh bone marrow isolates to an osteogenic fate, but sustained stimulation dramatically inhibited the osteogenic differentiation. This indicated that the timing of Wnt exposure is crucial, underlining the need for spatiotemporal delivery of this protein. The potential of liposomes to localise at the bone fracture site merits further study into the nanoparticle delivery of Wnt and its effects on bone regeneration.

Contents

List of Tables

List of Figures

Declaration of Authorship

I, Agnieszka Janeczek, declare that this thesis and the work presented in it are my own and have been generated by me as the result of my own original research.

Wnt Protein Delivery to Skeletal Stem Cells for Bone Tissue Regeneration

I confirm that:

This work was done wholly or mainly while in candidature for a research degree at this University;

Where any part of this thesis has previously been submitted for a degree or any other qualification at this University or any other institution, this has been clearly stated;

Where I have consulted the published work of others, this is always clearly attributed;

Where I have quoted from the work of others, the source is always given. With the exception of such quotations, this thesis is entirely my own work;

I have acknowledged all main sources of help;

Where the thesis is based on work done by myself jointly with others, I have made clear exactly what was done by others and what I have contributed myself;

Parts of this work have been published as:

Paper

Janeczek AA, Tare RS, Scarpa E, Moreno I, Rowland C, Jenner D, Newman TA, Oreffo ROC, Evans ND. "Transient canonical Wnt stimulation enriches human bone marrow mononuclear cell isolates for osteoprogenitors". Article first published online: 17 NOV 2015, DOI: 10.1002/stem.2241; Stem Cells.

Book chapter

Janeczek AA, Scarpa E, Newman TA, Oreffo ROC, Tare RS, Evans ND. "Skeletal Stem Cell Niche of the Bone Marrow". Published in: Tissue-Specific Stem Cell Niche. Springer International Publishing 2015. ISBN: 978-3-319-21704-8.

Abstracts

- "Targeting Wnt-loaded nanoparticles to skeletal stem cells for bone regeneration"; Conference of the Tissue and Cell Engineering Society (TCES), Cardiff 2013. TCES abstracts are published in eCells & Materials.
- "Modulating Wnt signalling in skeletal stem cells for bone regeneration"; Conference of the Bone Research Society/British Orthopaedic Research Society (BRS/BORS), Oxford 2013. BRS abstracts are published in: Frontiers in Endocrinology: Bone Research.
- "Influencing the skeletal stem cell niche by targeted liposomal Wnt delivery"; Conference of the TCES, Newcastle 2014. TCES abstracts are published in eCells & Materials.
- "Association of Wnt3A growth factor with PEGylated liposomes for bone tissue regeneration"; Conference of the TCES, Southampton 2015. TCES abstracts are published in eCells & Materials.
- "Wnt-loaded nanoparticles for enhancement of mesenchymal stem cell-mediated bone fracture healing"; Conference of the Tissue Engineering and Regenerative Medicine International Society (TERMIS), Boston 2015. TERMIS abstracts are published in Tissue Engineering Part A.

Signed:

Date:

Contributors

All experiments and data analysis were performed by the author in the Bone and Joint Group laboratory, Academic Unit of Human Development and Health, Faculty of Medicine, Southampton University Hospital, University of Southampton, with the following exceptions:

Section 3.2.2.1

Flow cytometry staining and sampling for blood lineage markers was performed by the author under the supervision of Dr Kam Hussain from the Antibody and Vaccine Group, within the Cancer Sciences Division, Faculty of Medicine, University of Southampton.

Section 5.2.1.1

Particle size measurement by dynamic lights scattering was performed by the author using the equipment at Chemistry Department of University of Southampton, initially under the supervision of Professor George Attard. Nanoparticle tracking analysis and scanning ion occlusion sensing were performed with help of Malvern and Izon Science company representatives, respectively.

Section 5.2.1.2

Preparation of samples for gas chromatography was performed by the author and sample load on the chromatographer and software setup was performed under the supervision of Annette West, Nutrition Group, Human Development and Health, Faculty of Medicine, University of Southampton.

Section 5.2.3.2

Single molecule spectroscopy experiments were performed by the author using the equipment at Chemistry Department of University of Cambridge, under the supervision of Dr Steven Lee and Dr Mathew Horrocks. Data analysis was carried out by Dr Mathew Horrocks.

Section 5.2.4.2

Samples for Image Stream flow cytometry were prepared by the author and the sampling and analysis was performed by Dr Dominic Jenner, Biomedical Sciences Department, DSTL, Porton Down, Salisbury.

Section 5.2.4.2

Confocal imaging was performed under the supervision of Dr David Johnston, in the Biomedical Imaging Unit, University of Southampton.

Section 5.2.4.3

Animal surgeries and liposome injections were performed by Edoardo Scarpa (personal license I1211ECA0), Bone and Joint Research Group, Academic Unit of Human Development and Health, Faculty of Medicine, University of Southampton.

Acknowledgements

Over the course of my PhD studies and the preceding Master of Research, I have been supported by several people, whose help I would like to acknowledge.

First and foremost, I would like to thank my supervisors, Dr Nicholas Evans, Dr Rahul Tare and Professor Richard Oreffo, who were always on hand with comments, advice and guidance. I am very grateful indeed to Dr Nicholas Evans, who always allowed me to express my opinions, and who helped me develop hugely as an independent researcher during the course of my PhD.

I am grateful to all of those within the Bone and Joint Group who have advised me on experimental protocols in the lab, and with whom I shared research ideas, especially to David Gothard, Patrick Stumpf, Edoardo Scarpa and May De Andres Gonzalez.

Most of the laboratory work would not have been possible without the knowledge on bone marrow isolation passed to me by Kate White, for which I am also very grateful.

Many thanks to Nunzia Sposito, Yu Hin Man, David Gibbs, Tsiloon Li, Emma Budd, and Julia Wells for discussions about life, keeping me entertained while working in tissue culture for long hours or when writing up in the office.

Finally, I would like to thank Matthew Loxham, for the enormous support given throughout my PhD, and specifically for the enormous patience during its final stages, and for showing me the light at the end of the tunnel.

Very last of all, I would like to thank my family and especially my sister, for always wholeheartedly supporting me as a scientist, without ever understanding what it is that I am actually working on, to whom I dedicate this thesis.

Abbreviations

3T3	embryonic fibroblast cell line
6C3	phosphorylated cell surface glycoprotein, enzyme with aminopeptidase A activity
AF	Alexa Fluor
ALL	acute lymphoblastic leukaemia
AlphaV	integrin alpha chain V
αMEM	minimum essential medium alpha
ALP	alkaline phosphatase
APC	adenomatous polyposis coli
BGLAP	bone gamma-carboxyglutamic acid-containing protein (gene coding for osteocalcin)
BHT	butyratedhydroxytoluene
BIO	6-bromoindirubin-3'-oxime
BMD	bone mineral density
BMI	body mass index
BMMNCs	bone marrow mononuclear cells
BMPs	bone morphogenetic proteins
BMU	basic multicellular unit
BSA	bovine serum albumin
CAMKII	calmodulin-dependent protein kinase II
CAR cells	CXCL12-abundant reticular cells
CCND1	cyclin D1
CD	cluster of differentiation
cDNA	complementary DNA
C/EBPs	CCAAT-enhancer-binding proteins
CFU-F	colony-forming unit fibroblastic
CFU-O	colony-forming unit osteoblastic
CK1	casein kinase 1
COL1A1	collagen type 1, alpha chain 1
CyTOF	cytometry by time-of-flight
DAPI	4',6-diamidino-2-phenylindole
dH_2O	deionised water

DiI	1,1'-dioctadecyl-3,3,3',3'-tetramethylindocarbocyanine perchlorate
DiO	3,3'-dioctadecyloxacarbocyanine perchlorate
DiR	1,1'-dioctadecyl-3,3,3',3'-tetramethylindotricarbocyanine iodide
Dkk1	dickkopf-related protein 1
DLS	dynamic light scattering
DMEM	Dulbecco's modified Eagle medium
DMPC	1,2-dimyristoyl-sn-glycero-3-phosphocholine
DNA	deoxyribonucleic acid
DOPC	1,2-dioleoyl-sn-glycero-3-phosphocholine
DPPC	1,2-dipalmitoyl-sn-glycero-3-phosphocholine
dsDNA	double stranded DNA
Dsh	dishevelled
DSPC	1,2-distearoyl-sn-glycero-3-phosphocholine
DSPE	1,2-distearoyl-sn-glycero-3-phosphoethanolamine
DTT	dithiothreitol
DXA	dual energy x-ray absorptiometry
ECM	extracellular matrix
EDTA	ethylenediaminetetraacetic acid
EEA1	early endosome antigen 1
EGF	epidermal growth factor
ELISA	enzyme-linked immunosorbent assay
Fab; Fab_2	fragment antigen-binding
FACS	fluorescence-activated cell sorting
FBS	foetal bovine serum
FDA	Food and Drug Administration
FGF	fibroblast growth factor
FRAX	fraction risk assessment tool
FSC	forward scatter
GC	gas chromatography
GD2	disialoganglioside expressed on neuroblastoma and melanoma
GFP	green fluorescent protein
GPA	glycophorin A
GSK3	glycogen synthase kinase 3
HaCaT	human keratinocyte cell line
hADSCs	human adipose-derived stromal cells
HDL	high-density lipoprotein

HER2	human epidermal growth factor receptor 2; ErbB-2
HLA-DR	human leukocyte antigen DR, MHC class II cell surface receptor
HBM	high bone mass
HRP	horseradish peroxidase
HRT	hormone replacement therapy
HSCs	haematopoietic stem cells
HSPGs	heparan sulphate proteoglycans
IGF1	insulin-like growth factor 1
IgG	immunoglobulin G
IgM	immunoglobulin M
IL-6	interleukin 6
iPSCs	induced pluripotent stem cells
ISCT	International Society for Cellular Therapy
IVIS	*in vivo* imaging system
JNK	c-Jun N-terminal kinase
KDR	kinase insert domain receptor, 2 receptor for VEGF
LAMP1	lysosomal-associated membrane protein 1
LDL	low-density lipoprotein
LEF/TCF	lymphoid enhancer-binding factor (LEF)/T-cell factor (TCF) transcription factors
Lepr	leptin receptor
Lrp5/6	low density lipoprotein receptor-related protein 5/6
LUV	large unilamellar vesicle
MACS	magnetic-activated cell sorting
MFI	mean fluorescence intensity
MG63	human osteosarcoma cell line
MLV	multilamellar vesicle
MSCs	mesenchymal stem cells
MVB	multivesicular bodies
NG2	neural/glial antigen 2
NICE	National Institute for Health and Clinical Excellence
NTA	nanoparticle tracking analysis
OCR	osteochondroreticular stem cells
OS	oxidative stress
OSX	osterix
P0	primary passage culture

P1 or P2	passage 1 or 2 culture
PBS	phosphate buffered saline
PDMS	polydimethylsiloxane
PEG	polyethylene glycol
PFA	paraformaldehyde
PKC	protein kinase C
PMN cells	polymorphonuclear cells
PNPP	p-nitrophenyl phosphate
PPARγ	peroxisome proliferator-activated receptor gamma
PSMA	prostate specific membrane antigen
PTH	parathyroid hormone
PVDF	polyvinylidene fluoride
RANK/RANKL	receptor activator of nuclear κB/ligand
RES	reticuloendothelial system
RGD	arginine-glycine-aspartate peptide
RMS	root mean square
RNA	ribonucleic acid
ROS	reactive oxygen species
RT-qPCR	real-time quantitative polymerase chain reaction
RUNX2	runt-related transcription factor 2
SCF	stem cell factor, KIT-ligand
scFv	single-chain variable fragment of antibody
SDS-PAGE	sodium dodecyl sulphate polyacrylamide gel electrophoresis
SIOS	scanning ion occlusion sensing
SOD	superoxide dismutase
SOST	sclerostin
SP7	gene coding for osterix
SPADE	spanning-tree progression analysis of density-normalized events
SPARC	gene coding for osteonectin
SSC	side scatter
SSCs	skeletal stem cells
STRO-1	cell surface trypsin-resistant antigen expressed by CFU-F
SUV	small unilamellar vesicle
TAT	transcriptional activator protein
Tc	transition temperature
TCCD	two-colour coincidence detection

TEM	transmission electron microscopy
TGFβ	transforming growth factor beta
TI	therapeutic index
TIRFM	total internal reflection fluorescence microscopy
upH_2O	ultrapure water
VCAM-1	vascular cell adhesion molecule 1
VEGF	vascular endothelial growth factor
Wnt	Wingless-related integration site

Chapter 1

Introduction

Overview

Our population is aging, increasing the demand for regenerative therapies. In particular osteoporosis, which leads to bone fractures, is a major public health issue affecting the elderly. It is estimated that 1 in 3 women and 1 in 5 men over the age of 50 suffer from osteoporosis, and that fractures to the bone (osteoporotic wrists, vertebrae and hips) cost the European economy €37 billion each year (Holroyd *et al.* 2008, Melton *et al.* 2003). Modern bone regeneration therapies have limitations and long-term effects of current recommended treatments, such as anti-resorptive drugs, are unknown. Therefore the need to develop new anabolic agents is high. These agents could also be used as treatment for non-union fractures. Approximately 1 in 3 people fracture a bone within their lifetime and up to 10 % of those fractures fail to heal properly, resulting in a non-union (Rodriguez-Merchan and Forriol 2004). To address these health problems and improve the quality of life of millions of people, new cutting-edge regenerative medicine approaches towards bone healing/growth are urgently required. This thesis concerns the role of Wnt signalling induction in skeletal stem cell populations of the bone marrow, its potential to expedite bone regeneration, and the development of technology to deliver Wnt protein therapeutically at fracture sites using nanoparticles. A review of biology of bone, fracture healing, Wnt signalling and nanomedicine is therefore appropriate.

1.1 Biological bone environment

1.1.1 Bone structure and composition

Histologically, bone comprises of primary (woven) bone formed early in embryonic skeletal development, which is subsequently replaced with highly structured secondary (lamellar) bone (Clarke 2008).

Woven bone is characterized by a disorganized and irregular pattern of collagen fibrils and mineralization, which makes it flexible but relatively weak. It is present also in early stages of fracture healing, during callus formation.

Lamellar bone is comprised of trabecular bone (also known as cancellous or spongy) and cortical bone (also known as compact). Both have similar biochemical compositions but differ in their physical structure (Buck and Dumanian 2012). Cortical bone surrounds bone marrow cavities and the trabeculae of cancellous bone, and is a major component of the diaphysis of long bones such as the humerus (Figure 1.1A). The basic unit of cortical bone is the osteon, which is composed of successive concentric lamellae. This structure contributes to bone strength by providing bending resistance. Osteocytes, accounting for 90 % of all bone cells, are former osteoblasts embedded in lamellae and forming a complex network within the bone matrix. Osteocytes maintain the viability and structural integrity of bone, mediating calcium homeostasis. At the centre of the osteon, is the Haversian canal, containing blood and lymphatic vessels and nerve fibres (Figure 1.1B).

In contrast to this, trabecular bone is less ordered, with greater surface area. It is the major component of the epiphyses of long bones. Cancellous bone is highly vascularised and contains sinusoids that allow contact between bone structures and marrow. It also has a higher rate of metabolic activity and remodelling than cortical bone, and responds more rapidly to stimuli, because the primary bone cells lie on the surface and are in closer proximity to circulating growth factors and cytokines. The primary function of cancellous bone is allowance of deformation and absorption of loads (Buck and Dumanian 2012).

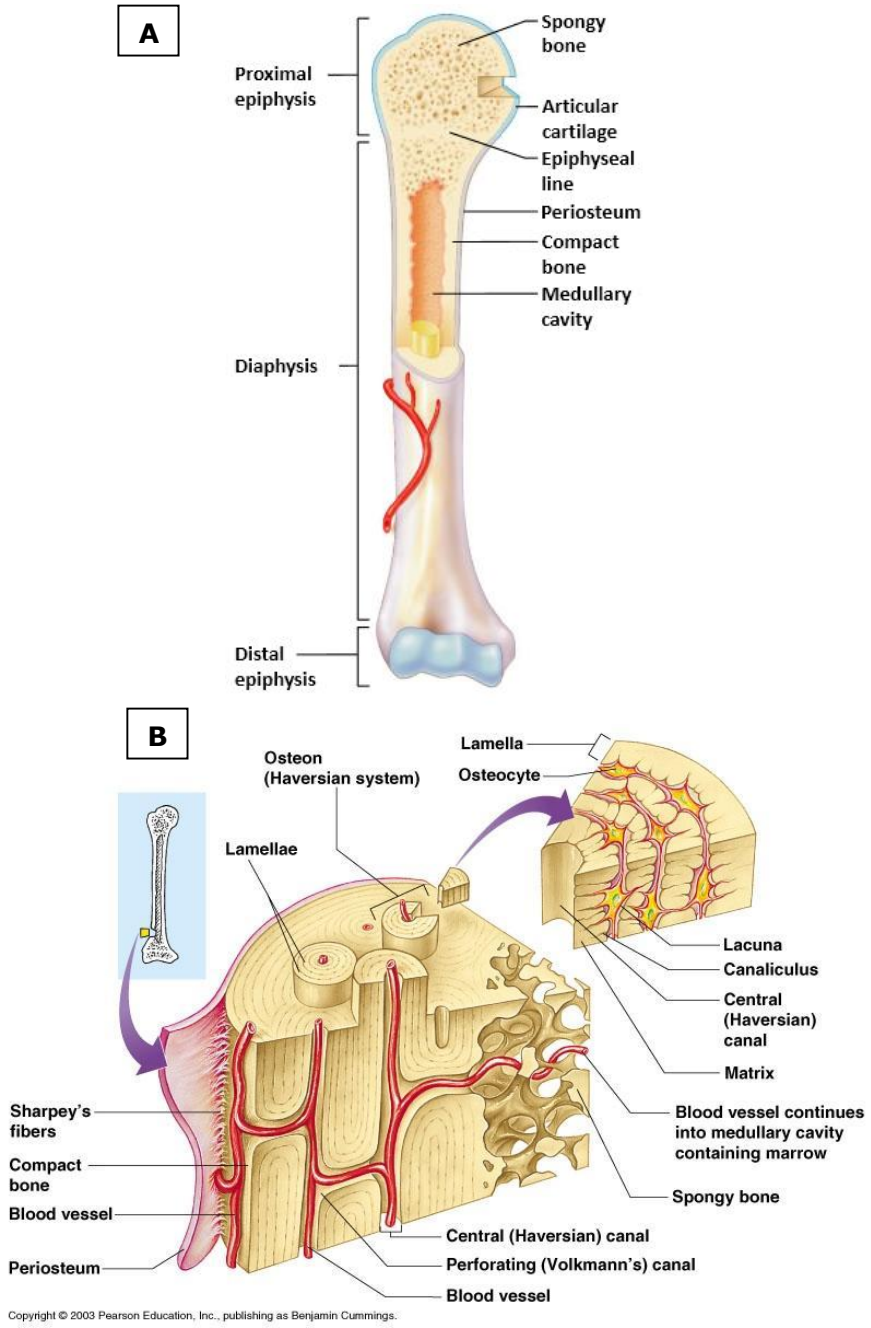

Figure 1.1 Bone structure.

Structure of a long bone (A) and a microscopic structure of cortical bone (B). From: (Marieb 2012). Reprinted by permission of Pearson Education, Inc., New York, New York.

Bone cells make up about 10 % of total bone volume, the rest being bone mineral and organic matrix. Osteoclasts, which are large, multinucleated cells, take part in bone resorption, and are of hematopoietic origin, formed from the precursors of macrophages (Teitelbaum 2000). On the other hand, osteoblasts and osteocytes

(mentioned earlier) are thought to arise from skeletal stem cells (SSCs) (Heino and Hentunen 2008, Palumbo *et al.* 1990). Osteoblasts line the surfaces of bone and are packed tightly against each other. They are considered to be the bone forming cells, as they synthesize and secrete organic bone matrix. Osteoblast activity is marked by alkaline phosphatase (ALP), osteopontin and osteocalcin release, but the most prevalent noncollagenous protein produced is osteonectin (Figure 1.3). These calcium-binding proteins are thought to affect osteoblast maturation and/or proliferation and matrix mineralization. Osteoblasts can either remain quiescent osteoblasts lining the surface of newly formed bone or become "resting" osteocytes, embedded in bone matrix (Clarke 2008).

1.1.2 Bone remodelling

In childhood, bones grow and repair very quickly, but this process slows down as people get older. Bones stop growing in length by the age of 18, but continue to increase in density for about another 10 years. From about the age of 35, gradual loss in bone density is observed (Buck and Dumanian 2012). However, bone remodelling is a process, which occurs continuously throughout life, in order to maintain bone. Remodelling is achieved within discrete areas known as basic multicellular units (BMU). Remodelling allows the substitution of primary bone with secondary bone, achieving greater mechanical competence. It also removes ischaemic or microfractured bone and guarantees a correct calcium homeostasis (Rucci 2008).

Remodelling requires maintenance of a fine balance between tissue resorption by osteoclasts and synthesis by osteoblasts. Briefly, osteocytes sensing a change in mechanical loading or cytokines (i.e. interleukin-6, IL-6) present in the bone microenvironment, trigger an increase of receptor activator of nuclear κB ligand (RANKL) expression on lining cells, which are quiescent osteoblasts. This ligand interacts with receptor activator of nuclear κB (RANK) expressed on pre-osteoclasts and leads to their differentiation toward multinucleated osteoclasts. These osteoclasts adhere to areas of trabecular bone and form pits by secreting hydrogen ions and proteolytic enzymes. This action leads to liberation of factors that are embedded in bone, such as insulin-like growth factor 1 (IGF1), bone morphogenetic proteins (BMPs), transforming growth factor β (TGFβ) and fibroblast growth factors (FGFs).

These in turn recruit and activate osteoblasts, which have been primed to develop from precursor cells by parathyroid hormone (PTH) and 1,25-dihydroxycholecalciferol (calcitriol). Osteoblasts invade the pits and synthetize and secrete osteoid, the organic matrix of the bone. The osteoid is then mineralised and complex calcium phosphate crystals (hydroxyapatites) are deposited. Osteoblasts and their precursors secrete IGF1 (which becomes embedded in osteoid) and other cytokines, such as IL-6, which leads to recruitment and maturation of osteoclasts, a return to the start of the cycle. Bone metabolism and mineralisation therefore involves the action of PTH, the vitamin D family, cytokines and calcitonin (Rucci 2008). The bone remodelling cycle and the site of action of cytokines and also drugs (described in Section 1.2.2) is illustrated in Figure 1.2.

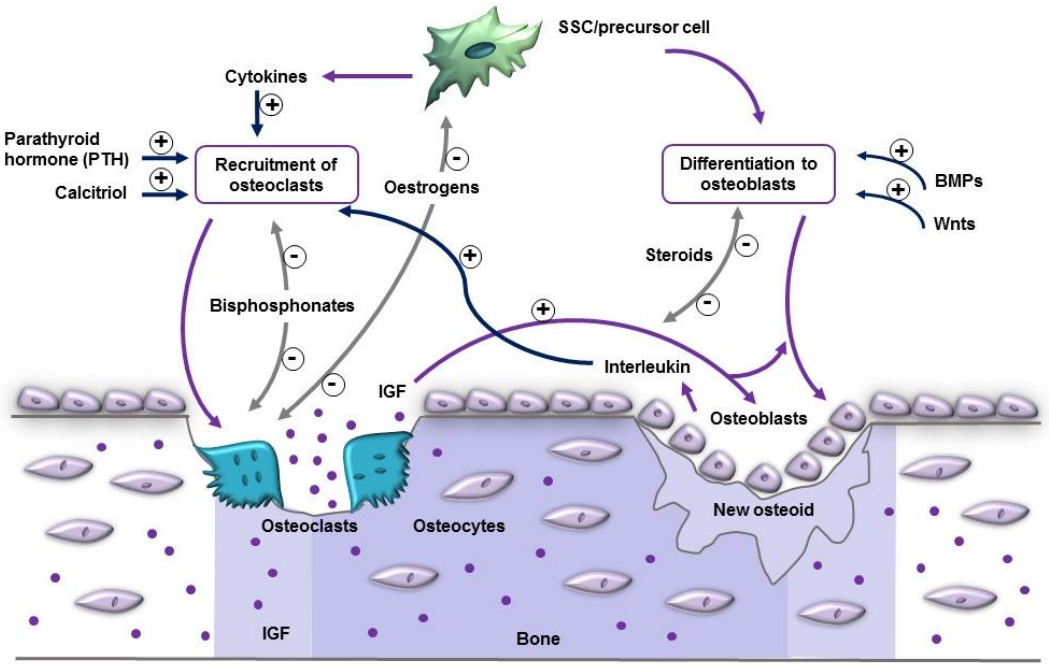

Figure 1.2 The bone remodelling cycle and the site of action of cytokines and drugs.

Bone remodelling cycle, and the action of drugs, as described in Section 1.1.21.2.2. BMPs, bone morphogenetic proteins; IGF, insulin-like growth factor; Wnt, wingless-related integration site. Adapted from: (Ramachandran 2007).

1.1.3 Skeletal stem cells and their niche

Stem cells reside in all adult tissues and are responsible for providing populations of progenitor cells during normal tissue turnover as well as in response to injury (Young and Black 2004). As such, adult stem cells constitute an attractive target for regenerative medicine applications.

Bone marrow stromal cells, firstly described by Friedenstein after their isolation from whole bone marrow aspirates based on differential adhesion properties, contain rare (1 in 10^4 - 10^5) stem cells of the soft fibrous tissue of the marrow stroma (Friedenstein *et al.* 1970, Friedenstein *et al.* 1976). This heterogeneous population serves as a niche for haematopoietic stem cells (HSCs), organises the tissue and contains direct skeletal progenitors (Owen and Friedenstein 1988). These skeletal progenitors are currently referred to as skeletal stem cells (SSCs) or more commonly mesenchymal stem cells (MSCs; as they give rise to cells involved in the process of mesengenesis). In the literature the term "bone marrow stromal cell" is also often used interchangeably, and sometimes inaccurately, to describe SSCs/MSCs. This is because bone marrow stromal cells are an adherent, fibroblast-like, heterogeneous cell population which may contain SSCs/MSCs, and are not stem cells themselves (Beresford 1989, Caplan 1991). Under appropriate *in vitro* culture conditions, SSCs are capable of giving rise to osteoblasts, chondrocytes and adipocytes (Caplan 1991, Prockop 1997). However, the defining feature of SSCs/MSCs is their ability to generate, upon transplantation *in vivo*, heterotopic ossicles. These miniature bone organs, comprised of bone, cartilage and fat, are where the haematopoietic stem/progenitor cells of the recipient animal home into and establish blood production (Bianco *et al.* 2013).

SSCs/MSCs were initially identified by their capacity to form clonogenic cell clusters (colony-forming unit fibroblast, CFU-F) *in vitro*, a common feature among different stem cell populations (Castro-Malaspina et al. 1980, Owen and Friedenstein 1988). The CFU-F assay can also be used as a tool to monitor cell growth (Battula *et al.* 2009). Maturation of SSCs into osteoblasts is pivotal in bone growth, its turnover, fracture healing and the osseointegration of bone implants, and is a process regulated by a number of key factors and signalling pathways, of which Wnt signalling plays a critical role (Hayrapetyan *et al.* 2015). Although the exact stages that a SSC needs to undertake to become an osteoblast are still poorly understood, it has been suggested by several studies, that SSCs express certain non-specific markers during their progression through the differentiation steps towards osteoblasts (Figure 1.3). Osteodifferentiation is initiated by the expression of runt-related transcription factor 2 (RUNX2) (Deng *et al.* 2008, Ducy *et al.* 2000), followed by expression of Osterix (OSX) (Gao *et al.* 2004). Without these transcription factors, bone formation is impaired due to the complete

absence of osteoblasts (Nakashima *et al.* 2002). They activate the transcription of bone-related genes, among which is alkaline phosphatase (*ALP*) and collagen type 1 (*COL1A1*). ALP is important in mineralization of the extracellular matrix (ECM) (Marom *et al.* 2005). Furthermore, the non-collagenous bone ECM proteins, osteonectin, osteopontin and osteocalcin, are commonly used late markers of osteogenic differentiation respectively (Aubin 2001). Therefore, alkaline phosphatase (ALP) staining of colonies or the colony-forming unit osteoblastic test (CFU-O, for cells cultured in osteogenic media) and additional staining for components of cell matrix such as calcium or phosphate deposition can help monitor osteogenic commitment of SSCs, as it marks precursors of functional osteoblasts.

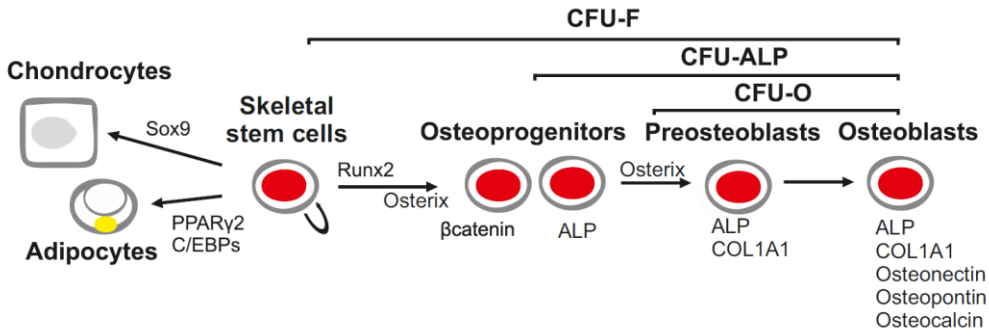

Figure 1.3 Suggested expression of markers of skeletal stem cell commitment.

Schematic illustration of proposed stem cell commitment to various end-stage mesenchymal cell types, focusing on the osteoblast lineage and proposed stage-specific markers. Runx2 is a transcription factor which plays a key role in skeletal development as it is a master gene for osteoblast differentiation, driving the early steps of mesenchymal commitment toward the pre-osteoblast phenotype. Osterix is expressed downstream of Runx2 and, like the latter, is necessary for skeletal formation. Further along the differentiation pathway ALP, COL1A1, osteonectin, osteopontin and osteocalcin are expressed. Based on: (Bilezikian *et al.* 2008) and (Rucci 2008).

Later studies have identified alternative to bone marrow tissue sources of MSCs such as blood, adipose tissue or muscle (Caplan and Bruder 2001) or more recently it has been postulated that all post-natal organs and tissues contain MSCs (da Silva Meirelles *et al.* 2006). It is important to bear in mind that MSCs from different tissue sources vary in their properties (Caplan and Correa 2011). Due to their multipotency and ease of isolation, bone marrow-derived MSCs, herein specifically referred to as SSCs for distinction, are particularly suited for tissue engineering strategies.

Conventional methods for the isolation of SSCs, apart from density-gradient centrifugation (Boyum 1968) also take into account their ability to adhere to tissue culture plastic (Luria *et al.* 1971). However, this not only selects for SSCs but also for reticular cells, macrophages, endothelial cells, resulting in a highly heterogeneous population (Bianco *et al.* 2013, Harichandan and Buhring 2011). It is assessed that by this procedure only approximately 30 % of clonogenic cells are truly multipotent stem cells (Larsen *et al.* 2010).

Alternatively, higher cell purity may be achieved by selection based on surface marker expression. Due to variable results for MSC marker studies, the Mesenchymal and Tissue Stem Cell Committee of the International Society for Cellular Therapy (ISCT) convened in 2006 and published a paper on what they considered a true definition of human MSC. Firstly, they argued MSCs must show plastic adherence under standard culture conditions. Also, they must express CD105 (endoglin), CD73 (membrane-bound ecto-5'-nucleotisidase) and CD90 (Thy-1), and lack the expression of the haematopoietic markers CD45 (tyrosine phosphatase), CD34, CD14 or CD11b (Integrin alpha M, ITGAM), CD79a (immunoglobulin-associated alpha) or CD19 (B-lymphocyte antigen) and HLA-DR (human leukocyte antigen) surface molecules. Finally, it was suggested that MSCs must differentiate into osteoblasts, adipocytes and chondrocytes *in vitro* (Dominici *et al.* 2006). However, critics of these criteria state they do not take into account what truly constitutes a stem cell, namely the ability to self-renew and form multiple lineages from one clone of cells not only *in vitro* but most importantly in *in vivo* transplantation assays (Bianco *et al.* 2013). Therefore, in the literature, there remains no universally accepted definition of this term. In this thesis, the term bone marrow mononuclear cells (BMMNCs) is used to refer to the primary isolates of cells isolated from the bone marrow, and after plating also to stromal cells (those arising from CFU-Fs), STRO-1 enriched BMMNCs for the populations enriched *in vitro* by antibody selection and SSCs for the putative stem cell population referred to by Bianco *et al.* (Bianco *et al.* 2013).

Reliable and sensitive markers for the multipotent fraction referred to by Bianco *et al.* have not yet been identified. The previously mentioned "minimum defining criteria markers" are stably expressed *in vitro* with little variability between donors, however

they might not correlate to the true *"in vivo"* state, and do not allow for purification of clonogenic SSCs to homogeneity. Therefore, other potential markers have also been investigated. The STRO-1 antigen has been shown to be particularly effective in enriching freshly isolated BMMNCs for uncommitted, proliferative, multipotent stromal stem cells (Simmons and Torok-Storb 1991). The STRO-1 antibody was demonstrated to bind approximately 10 % of the BMMNCs isolated from bone marrow aspirates (Tare *et al.* 2008). However, it also selects for glycophorin A^+ (GPA^+) erythroid progenitors and a subset of stromal cells (Simmons and Torok-Storb 1991). Nonetheless, used for over 2 decades, and despite its nonspecificity, it still remains the antibody with the highest affinity and efficiency for isolating clonogenic SSCs as a stand-alone reagent due to the high density of this antigen on the MSC surface (Gronthos *et al.* 2003). CD271 (low affinity nerve growth factor receptor) has been applied to isolate a subset of MSCs from bone marrow and other tissues, however with varying efficacy (Quirici *et al.* 2002, Watson *et al.* 2013). CD106 (vascular cell adhesion molecule 1, VCAM-1) may serve as a marker for the most potent/undifferentiated cell fraction, as sorting for it in combination with STRO-1 has been demonstrated to yield a cell fraction highly enriched for CFU-Fs (Gronthos *et al.* 2003). Expression of both these markers is strongly dependent on the donor, time in cell culture, cell seeding density and many more factors. Furthermore, MSCs share functional properties and gene-expression profile with $CD146^+$ perivascular cells and fibroblasts (Tormin *et al.* 2011) (Covas *et al.* 2008). CD146 (melanoma cell adhesion molecule, MCAM), a pericyte marker, has recently been shown to enrich for MSC populations also in the dentine, but only in combination with STRO-1 (Bakopoulou *et al.* 2013). Attempts to develop novel antibodies for MSC identification, directed to surface markers, were unsuccessful (Andersen *et al.* 2011). Therefore until new markers are identified, STRO-1 serves as a robust candidate for prospective immunoselection.

The lack of an unambiguous *in vivo* MSC marker that identifies this cell population in different tissues highlights the possibility that different cell characteristics may be dictated by the local tissue microenvironment in which they reside (Bianco *et al.* 2008). All stem cell microenvironments, the so-called niches, are implicated in providing relevant cues for stem cells to self-renew and sustain long-term tissue specific regeneration during homeostasis as well as upon injury (Ehninger and Trumpp 2011,

Fuchs and Chen 2013, Kunisaki *et al.* 2013, Li and Clevers 2010). In the bone marrow, SSCs dynamically organise the haematopoietic microenvironment, forming the niche for HSCs and influencing their behaviour towards quiescence or activation. Unfortunately, there are discrepancies with regards to the mechanisms in which SSCs maintain bone homeostasis and their *in vivo* localisation (Bianco *et al.* 2013, Boxall and Jones 2012, Lv *et al.* 2014). As already mentioned, a close link between the microvasculature and tissue progenitors has been demonstrated, proposing SSCs as *in situ* perivascular cells, or cells coinciding with adventitial reticular cells. The majority of data on the interactions and localisation of key bone marrow niche components in sustaining HSCs (Figure 1.4), originated from animal model experiments. Studies which aimed to lineage trace SSCs have used markers expressed under the control of cell type-specific promoters. The most commonly used marker genes for cells with SSC-like properties were Osx, Nestin, neural/glial antigen 2 (NG2) and Leptin receptor (Lepr) (Mendez-Ferrer *et al.* 2015). Various laboratories have shown different, and sometimes confusing outcomes, as to where the skeletal stem cell population might localise. For example, the perivascular Nestin-GFP^{+} population, identified as a SSC-like population (Mendez-Ferrer *et al.* 2010) was shown to be heterogeneous in nature (Kunisaki *et al.* 2013), and depending on perisinusoidal *vs.* arteriolar localisation, the intensity of GFP expression, and co-expression of other markers (Lepr and NG2, respectively) has different functions in sustaining the haematopoietic stem cell population. On the other hand, in the neonatal bone marrow, SSCs appeared to be perisinusoidal Lepr^{+} cells and in adult bone marrow it was the Nestin-GFP^{bright} cells, which were enriched for SSC activity (Mizoguchi *et al.* 2014). Others have provided evidence to suggest that Lepr-cre cells overlap with sinusoidal Nestin-GFP^{+} cells (Ding *et al.* 2012). Also CXCL12-abundant reticular cells (CAR cells) have been postulated as early mesenchymal progenitor cells, supporting HSC maintenance (Greenbaum *et al.* 2013). More recently, other populations have been identified as skeletal stem cell candidates, such as the osteochondroreticular stem cells (OCR), with the use of Gremlin1 promoter (Worthley *et al.* 2015) or cells with the phenotype CD45^{-}Ter119^{-}Tie2^{-}AlphaV^{+}Thy1^{-}6C3^{-}CD105^{-}CD200^{+} (Chan *et al.* 2015). Unsurprisingly, subsets of SSCs identified by expression of genes identified by different conditional reporters seem to differ in their functionality in various studies. This might be a result of an unsatisfactory degree of recombination and off-target

effects of the recombination inducing drug. The commonly used Tamoxifen is known to have anabolic effects on bones or cause apoptosis in certain haematopoietic progenitor subpopulations, thus disrupting homeostasis within the bone marrow niche (Joseph *et al.* 2013, Mendez-Ferrer *et al.* 2015). Therefore, data from the animal models remain complex and sometimes contradictory and, although lineage tracing is an attractive technique with the potential for stem cell identification in mice, it is difficult to transfer this knowledge into the human system due to species differences.

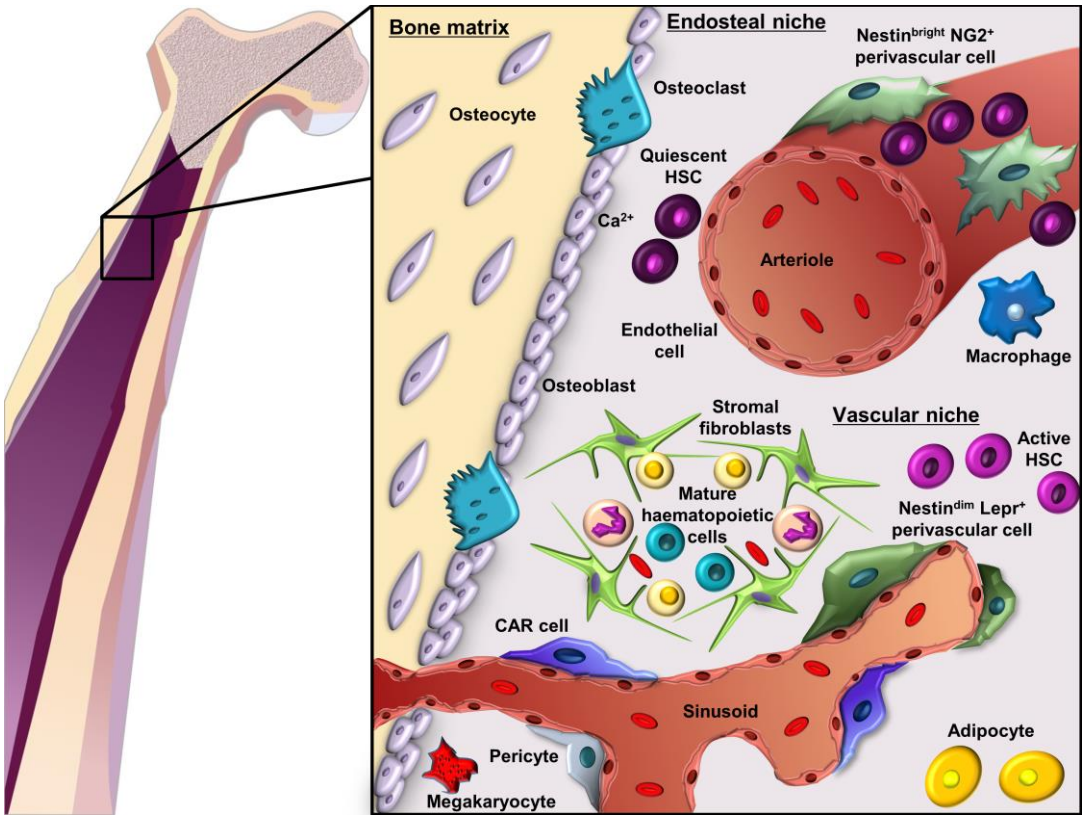

Figure 1.4 Bone marrow stem cell niche and its key components.

In murine models, various cell types have been implicated for their roles in promoting HSC maintenance, including Nestin^{+} perivascular cells, supposedly more differentiated CAR cells (containing adventitial reticular cells and mesenchymal progenitors), endothelial cells and macrophages. Adipocytes, which have been shown to negatively affect HSC maintenance, are increasingly present after chemotherapy or radiation, as well as due to aging. Quiescent HSCs associate with arterioles ensheated with Nestin^{bright} NG2^{+} pericytes (putative SSCs). After activation, HSCs relocate near the Nestin^{dim} Lepr-expressing perisinusoidal area. Osteoblast precursors and CAR cells in the vicinity of the endosteal niche support differentiated phenotypes of HSCs. Identification of these various bone marrow niche components was a major advancement in the field, however, translating these into human physiology, with human-relevant markers and extensive study of overlapping populations may aid resolving other cell populations which might be involved in functioning of the bone marrow niche. CAR cells, CXCL12-abundant reticular cells; HSC, haematopoietic stem cell; SSCs, skeletal stem cells; NG, neural/glial antigen. Figure obtained with kind permission from Springer Science and Business Media, (Janeczek *et al.* 2015).

It is desirable to identify stem cells *in vivo* and understand at a molecular level the regulatory mechanisms underlying the self-renewal and differentiation of skeletal stem cells and their role in normal bone homeostasis, in bone diseases and following injury. Additionally, designing methods for overcoming their replicative senescence (Wagner et al. 2008) and promoting directed differentiation are critical for future regenerative medicine approaches for bone diseases and fracture healing.

1.2 Osteoporosis treatment and bone fracture healing

1.2.1 Pathogenesis of osteoporosis

Osteoporosis is a skeletal disease characterised by low bone mineral density (BMD) and degeneration of the microarchitecture of bone tissue, leading to an increased risk of fractures, most often of the hip, vertebra or wrist (Christodoulou and Cooper 2003). In general, osteoporosis is caused by either failure to achieve an adequate peak bone mass during growth and development or an imbalance in bone remodelling, where bone resorption is higher than bone formation. Therefore the bone becomes more porous and fragile, and hence more prone to fractures (Raisz 2005). Osteoporosis is a major public health concern that affects over 75 million people in the USA, Europe, and Japan, with more than 8.9 million fractures occurring each year as a consequence (Kanis 2007).

The major risk factor for osteoporosis, is called osteopenia, which is characterised by low BMD, and is used to diagnose the disease. Low BMD is defined as a T-score of ≤ 2.5 standard deviations lower than the mean peak bone mass (of sex-matched 30-year olds), measured by dual energy x-ray absorptiometry (DEXA) of the hip and/or spine. Many other factors have been identified in epidemiologic studies, some of which are also used clinically as part of a questionnaire-based assessment called FRAX (Fracture Risk Assessment Tool). FRAX is commonly used to diagnose the risk of osteoporotic fracture, and considers risk factors such as: advanced age, female sex, family history of osteoporotic fracture, physical inactivity, medication with corticosteroids or anticoagulants, smoking, excess alcohol consumption, low body mass index (BMI) and malnutrition (calcium, vitamin D). Another key predictor of an increased risk of bone loss and fragility fractures is the rate of bone remodelling,

measured by the level of collagen breakdown products (for assessing bone resorption), or bone specific alkaline phosphatase, osteocalcin and procollagen peptide levels (for assessing bone formation). To further improve diagnosis, techniques that can safely analyse the microarchitecture of the bone are being developed (Raisz 2005).

The modern view on the pathogenesis of osteoporosis shifts from the oestrogen-deficiency paradigm towards the effects of aging and age-related oxidative stress (OS) complemented with the effects of oestrogen (Manolagas 2010). Loss of bone tissue is correlated partly with age-related changes in other organs and tissues, such as the ovary (oestrogen deficiency), the adrenal gland (glucocorticoid excess or hyperresponsiveness), the kidney (loss of nephrons, reduced calcitriol synthesis, calcium malabsorption and secondary hyperparathyroidism) and muscle (sarcopenia, inactivity, reduced mechanical loading). However, excessive accumulation of reactive oxygen species (ROS) contributes to age-related changes in many tissues and in bone it also contributes to age-related bone loss and strength. There are multiple defence mechanisms against oxidative stress, including enzyme-mediated or FoxO transcription factors, which up-regulate free radical scavenging and DNA-repair enzymes. The latter is linked to Wnt signalling *via* β-catenin, as β-catenin is an essential co-activator of FoxO. There are implications for FoxO being involved in controlling the generation of new osteoblasts from their mesenchymal stem cell progenitors and modulating their proliferation and differentiation. In general, with increasing age and higher ROS generation, β-catenin is diverted from TCF- to FoxO-mediated transcription, meaning that Wnt signalling is being attenuated, leading to decreased osteoblastogenesis (see Section 1.3.2). It is therefore noteworthy that the anti-osteoporotic effect of oestrogens is not only due to their activity in slowing the rate of bone turnover, but also due to their ability to protect against oxidative stress thus complementing the OS theory. Loss of oestrogens and androgens has been shown to accelerate the effects of aging on bone by decreasing defence against OS (Manolagas 2010).

1.2.2 Treatment for osteoporosis

Prevention and treatment of osteoporosis, which aim to avoid the occurrence of future fractures, involve lifestyle changes regarding diet (calcium and vitamin D

supplementation), physical activity and minimising the risk of falling for elderly people. According to 2008 National Institute for Health and Clinical Excellence (NICE) guidance, pharmacological treatment for primary and secondary prevention of osteoporotic fragility fractures, is comprised of anti-resorptive and anabolic drugs. The site of action of cytokines and drugs during the bone remodelling cycle is depicted in Figure 1.2 in Section 1.1.2.

Anti-resorptive drugs, which include oestrogen, selective oestrogen receptor modulators (raloxifene), and bisphosphonates (alendronate, risedronate, etidronate), act by reducing bone resorption (and subsequently bone formation), preserving BMD. Unlike oestrogen, raloxifene, which is a non-steroidal benzothiphene prescribed for secondary prevention of osteoporotic fragility fractures, does not stimulate endometrial hyperplasia or increase the risk of breast cancer. However, the risk of blood clots, heart disease and strokes still remains (Ettinger *et al.* 1999, Miller *et al.* 2002, Rossouw *et al.* 2002), and although raloxifene increases BMD, it does not reduce the fracture risk, which is why hormone replacement therapy (HRT) is not generally used as a treatment for osteoporosis. Bisphosphonates (alendronate, risendronate, ibandronate, zoledronic acid) have many side-effects, including intolerance defined as persistent upper gastrointestinal disturbance, and can lead to osteonecrosis of the jaw and subtrochanteric fractures (McGreevy and Williams 2011), but they still remain the drugs of choice due to their potency and ease of frequency of administration.

The only currently available anabolic drugs, such as full-length parathyroid hormone (PTH1-84) and teriparatide (PTH1-34), are prescribed as injections for secondary prevention only in high risk patients for up to 2 years (Hodsman *et al.* 2005). They stimulate bone formation (but also subsequently bone resorption) and improve bone micro-architecture, thereby increasing BMD. Common side effects include hypertension, hypercalciuria, hypercalcemia and nausea, and treatment is limited to 2 years, after which time it becomes ineffective. Moreover, there are suggestions of increased risk of developing osteosarcomas after PTH treatment, although this has only been observed in some strains of rats (McGreevy and Williams 2011). The main disadvantages of this treatment are problems with patient compliance and high costs.

Strontium ranelate is another agent which reduces fracture risk. It possesses both anabolic and anti-catabolic effects. It exerts effects on bone remodelling, most likely by potentiating osteoblast proliferation and differentiation in parallel with inhibition of osteoclast activity at resorption sites, but its exact mechanism of action is still unclear. However, this drug may cause persistent nausea or diarrhoea and lead to memory loss or hypersensitivity reactions with systemic symptoms including hepatitis and nephritis (Pernicova *et al.* 2008).

Denosumab, approved by Food and Drug Administration (FDA) in 2010, is a fully human monoclonal antibody designed to inhibit RANKL, and therefore block maturation of pre-osteoclasts to osteoclasts. Denosumab, which is an anti-resorptive and anabolic agent, showed greater efficacy in reduction of osteoporotic fractures in comparison to bisphosphonates, restoring cortical bone density (Cummings *et al.* 2009, Seeman *et al.* 2010). However, because RANKL is also expressed by B cells and T cells in the immune system, the adverse effects after treatment with this antibody include infections of the urinary and respiratory tracts, the ear and skin as well as increased risk of malignancies (McGreevy and Williams 2011).

There are other treatments generally only prescribed when others are not appropriate, such as calcium or cholecalciferol/calcitriol (the hormonally active form of vitamin D). Calcium supplements have been shown to increase BMD but have limited effect on fracture reduction. Vitamin D increases the level of calcium in the blood by increasing the uptake of calcium from the gut, and possibly increasing the release of calcium into the blood from bone. However, calcium supplements should not be prescribed alone, as they have been associated with a possible increase in cardiovascular events (Bolland *et al.* 2010), and beneficial effects of vitamin D are strongly correlated with appropriate dosing (Brincat *et al.* 2015, Ross 2011).

Due to significant mortality and morbidity associated with osteoporotic fractures as well as high annual costs, estimated at €37 billion in the EU and $19 billion in the US, osteoporosis is a major socioeconomic burden to countries with aging populations (Burge *et al.* 2001, Burge *et al.* 2007). Taking into consideration the poor efficacy of treatments primarily designed to reduce fracture risks by preventing bone loss, rather than elevating bone mass and increasing bone regeneration after a fracture has

occurred, there is a great need to develop new, more easily administered anabolic agents for therapeutic intervention in the treatment of osteoporosis and bone fractures it may lead to (Salari Sharif *et al.* 2011).

1.2.3 Bone fracture healing and non-unions

In vertebrates, bone fracture healing is a remarkable process as in contrast to other tissues, bone can regenerate without forming a fibrous scar (McKibbin 1978). Skeletal fractures may occur as a consequence of bone fragility as well as trauma, and are a significant public health problem. Following the initial trauma, bone heals by either direct intramembraneous healing, or indirect fracture healing, which consists of both intramembraneous healing and endochondral bone formation. Fracture healing comprises several phases of regeneration involving different types of bone cells and the interactions between them, growth factors, and extracellular matrix (Marsell and Einhorn 2011). It involves an acute inflammatory response (following haematoma formation), and recruitment of mesenchymal stem cells in order to generate a primary soft cartilaginous callus, which undergoes revascularisation and calcification, ultimately being remodelled to restore a normal bone structure (Figure 1.5).

It has recently been discovered that, in young animals, a stage of natural reduction occurs between the stages of soft and hard callus formation, driven by a bidirectional growth plate at the fracture site induced by muscle contraction, exerting growth in both directions and therefore a force straightening the fragments (Rot *et al.* 2014). SSCs can also directly trigger an intramembranous ossification response that generates a hard callus, without the involvement of a cartilage template (Karsenty 2003). Bone healing then occurs by direct remodelling of lamellar bone (Marsell and Einhorn 2011). It is generally accepted that during fracture healing, instability and motion at the site of the fraction lead to the formation of cartilaginous callus, whereas rigid stabilisation leads to reduced cartilage formation and direct repair by intramembranous ossification (Thompson *et al.* 2002). This direct process occurs with surgical procedures after reduction of fracture ends and immobilisation or a stable surgical fixation.

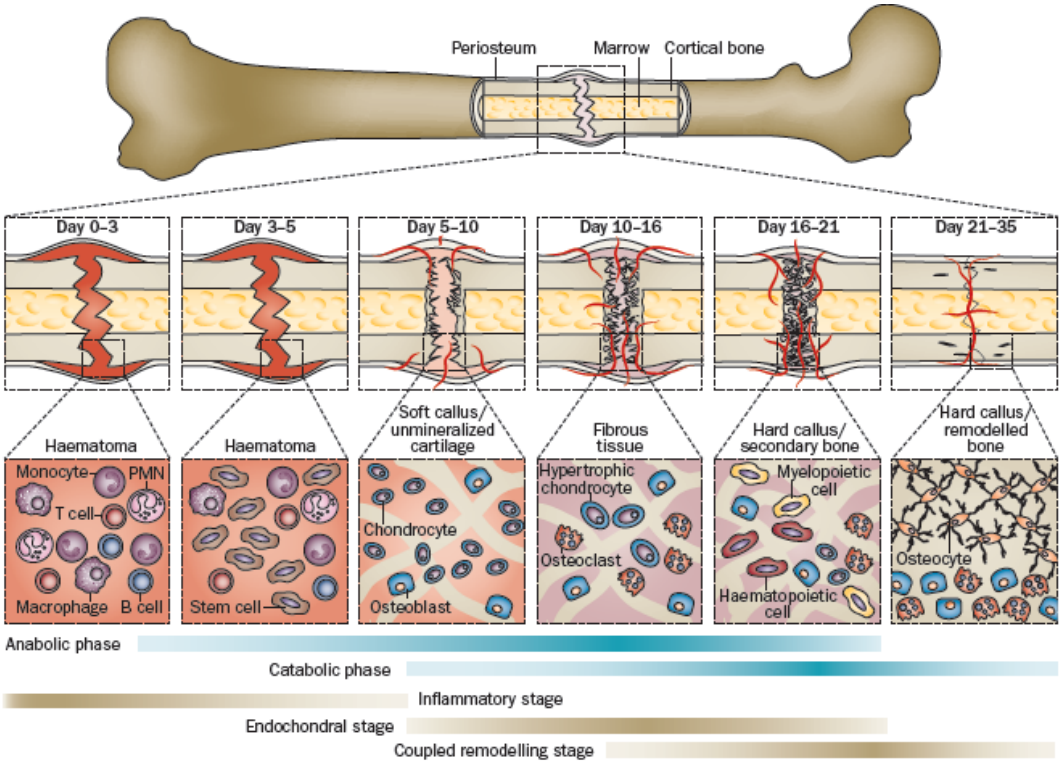

Figure 1.5 Phases of bone fracture healing.

The major metabolic phases (blue bars) of fracture healing overlap with biological stages (brown bars). The primary metabolic phases (anabolic and catabolic) of fracture healing are presented in the context of three major biological stages (inflammatory, endochondral bone formation and remodelling) that encompass these phases. The primary cell types found at each stage, and the time span of their prevalence in each stage, are denoted. The time scale of healing is equivalent to a mouse closed femur fracture fixed with an intramedullary rod. PMN, polymorphonuclear cells. Reprinted by permission from Macmillan Publishers Ltd: Nature Reviews Rheumatology (Einhorn and Gerstenfeld 2015), copyright (2015).

However, the healing process sometimes fails, leading to non-unions, especially in tibial fractures. There is no universally agreed definition of non-union of a fracture, but it is widely accepted that if a fracture does not heal within the time usually required (up to 6 - 8 months), it is designated as a non-union. 10 % of all bone fractures fail to heal properly, resulting in non-unions (Rodriguez-Merchan and Forriol 2004, Tzioupis and Giannoudis 2007). Non-unions are generally classified into three types according to defined radiological and histological criteria (Megas 2005). Hypertrophic non-unions are often linked with insufficient fracture stability and appear to have an adequate blood, oxygen, and nutrient supply. Therefore, they exhibit a better healing response than atrophic non-unions, which are generally poorly vascularized. In defect

non-unions, fracture healing is affected by a lack of contact among fracture fragments (Megas 2005). Studies conducted on the bone marrow in non-union cases showed that problems with bone consolidation may be caused by a reduction in bone-producing stem cells as well as their differentiation potential in the fracture haematoma (Hofmann *et al.* 2008).

Several strategies may be used to promote fracture healing in the event of delayed union. For example, commonly used is surgical treatment, which includes removal of the scar tissue, formed between the fracture fragments, and subsequent immobilisation of the fracture (Hak 2011). This can be achieved with the use of metal plates, rods, pins, bone grafts or biomaterials. Bone autografts are a gold standard in treatment augmenting bone healing, providing a source of bone progenitors, osteoinductive proteins and an osteoconductive framework for bone growth. However, due to underlying illnesses, tissue source is not always available or not of expected quality, and harvesting the bone graft may lead to donor site morbidity (Goulet *et al.* 1997).

To address this issue, various osteoconductive or osteinductive biocompatible materials are being developed (Laurencin *et al.* 2006). Synthetic materials include bioceramics or hydrogels, which can be loaded with growth factors (Dawson and Oreffo 2013, Wang *et al.* 2014), as well as SSCs and osteoprogenitors (Gomez-Barrena *et al.* 2015). The efficacy of cell therapy solutions, however, needs further study, as the clinical data regarding the advantages offered by delivery of stromal cell/stem cell populations are inconclusive (Gomez-Barrena *et al.* 2015).

The only drugs approved by the FDA and European Medicines Agency for fracture repair are osteoinductive BMPs in bone graft material or as an alternative to autografts. However, these drugs are not approved for systemic delivery. Two members of the BMP family, BMP7 and BMP2, have been approved for long-bone fracture non-unions and lumbar spinal fusion, respectively. Despite this, they are still used very infrequently due to side effects, which include ectopic bone formation, osteolysis or soft tissue swelling, and also due to the high cost of the therapy ($6000 - $10000) (Lissenberg-Thunnissen *et al.* 2011). Moreover, since FDA approval of BMP2 therapy, several trials re-examining the efficacy of this protein in the treatment of tibial fractures have failed to show advantages over current standards of care (Aro *et al.*

2011, Lyon *et al.* 2013). BMP signalling is inevitably linked to the Wnt signalling pathway, as both cooperatively regulate bone formation presumably *via* osteoblast differentiation (Mbalaviele *et al.* 2005). BMPs and Wnts each regulate each other's gene expression; in fact the Wnt/β-catenin signalling pathway has been shown to be an upstream activator of BMP2 expression in osteoblasts (Zhang *et al.* 2013).

It has also been indicated that anabolic PTH, which has already been approved by the FDA for osteoporotic fracture prophylaxis, might be effective in fracture healing (Aspenberg 2013). Multiple studies suggest that the molecular mechanism of its action in induction of bone formation may be *via* inhibition of Sclerostin (*Sost)* and Dickkopf-related protein 1 (*Dkk1)*, in osteocytes and osteoblasts, both of which are inhibitors of the Wnt signalling pathway (Guo *et al.* 2010, Leupin *et al.* 2007).

Due to the lack of efficacious drugs, either systemically or locally applied, that are currently available, there is an urgent need to develop new therapeutics. One potential target for such therapeutics is the Wnt signalling pathway.

1.3 The Wnt signalling pathway

1.3.1 The Wnt signalling pathway as a regulator of stem cells

The Wnt (Wingless-related integration site) gene name originates from the segment polarity gene name Wingless (*Wg*) in Drosophila (Baker 1987) and the proto-oncogene *Int1* in mouse (Nusse and Varmus 1982), which have been found to belong to an evolutionarily conserved family of extracellular signalling molecules. The 19 human *WNT* genes, also subjected to alternative splicing, code for a family of secreted glycoproteins, characterised by several conserved cysteine residues (Miller 2002). The Wnt proteins initiate signalling by binding to their membrane receptor complex, which consists of a serpentine receptor of the Frizzled family and Lrp5/6, a member of low-density lipoprotein (LDL) receptor family.

The main part of the Wnt signalling pathway, referred to as the canonical Wnt cascade (Reya and Clevers 2005), involves β-catenin (a cytoplasmic protein) stabilisation and translocation into the nucleus. Figure 1.6 shows a schematic illustration of this process. After binding of the Wnt receptor, Dishevelled (Dsh), an Axin binding protein,

inhibits the formation of the "destruction complex" and the pool of stabilised cytoplasmic β-catenin localises to the nucleus and interacts with transcription factors and co-activators, promoting Wnt target gene expression (many of which are genes responsible for pluripotency or differentiation of stem cells). β-catenin binds to the lymphoid enhancer-binding factor (Lef)/T-cell factor (Tcf) family of repressor proteins and transiently converts them into transcriptional activators. The "destruction complex" present when the receptor is unbound by Wnt normally consists of the tumour suppressors adenomatous polyposis coli (APC), Axin, and two kinases: casein kinase 1 (CK1) and glycogen synthase kinase 3 (GSK3). By phosphorylating β-catenin, the destruction complex guides it to ubiquitin-mediated proteasomal degradation.

Non-canonical Wnt signalling involves all Wnt-activated cell signalling pathways that do not specifically promote β-catenin stabilization, for example a pathway guiding cell movements during gastrulation (Veeman *et al.* 2003). In addition, a Wnt/Ca^{2+}-dependent pathway has been identified, in which Wnts stimulate intracellular calcium release and activate calmodulin-dependent protein kinase II (CAMKII) and protein kinase C (PKC), supposedly in a G-protein-dependent manner (Kuhl *et al.* 2000). Others involve c-Jun N-terminal kinase (JNK) or Rho signalling (Ling *et al.* 2009). The classification of signalling into canonical or non-canonical Wnt signalling is determined primarily by the Wnt receptors of a particular cell, as several Wnt proteins can act through both pathways, augmenting the effect of signalling or even antagonising one another (Ishitani *et al.* 2003). However, according to published classification, Wnt1, 2, 3 and 3a, 8, 8b and 10b are regarded as the canonical Wnts, and Wnt4, 5a, 5b, 6, 7a and 11 as the non-canonical (Ling *et al.* 2009, Miller 2002).

Wnt proteins regulate development, cell polarity, proliferation, motility and cell fate determination (Ling *et al.* 2009). The Wnt signalling pathway, more precisely the canonical Wnt cascade, depicted in Figure 1.6, is one of the most important in the self-renewal of stem and progenitor cells. Indeed, dysregulation of Wnt signalling has been linked to tumorigenesis in different tissues (Reya and Clevers 2005). Furthermore, Wnt signalling not only plays an essential role in embryonic cell maintenance or iPS cell reprogramming (Ding *et al.* 2010, Marson *et al.* 2008, Miki *et al.* 2011, Wray and Hartmann 2012), but also in adult stem cell biology (Reya and Clevers 2005). For

example, the Wnt signalling pathway is considered to be a major regulator of HSC self-renewal, as shown in lethally irradiated mice, where Wnt has been seen to directly promote the reconstitution of the haematopoietic system (Willert *et al.* 2003). However, while several reports suggest that Wnt signalling directly sustains the haematopoietic stem cell and progenitor pool (Reya *et al.* 2003), there have been various conflicting findings on the influence of Wnt signalling on the stromal microenvironment, which forms the haematopoietic stem cell niche. For many years now, Wnt signalling has been known to be particularly important in bone homeostasis, and again, this may have a great deal to do with the importance of this pathway in the control of bone stem cells.

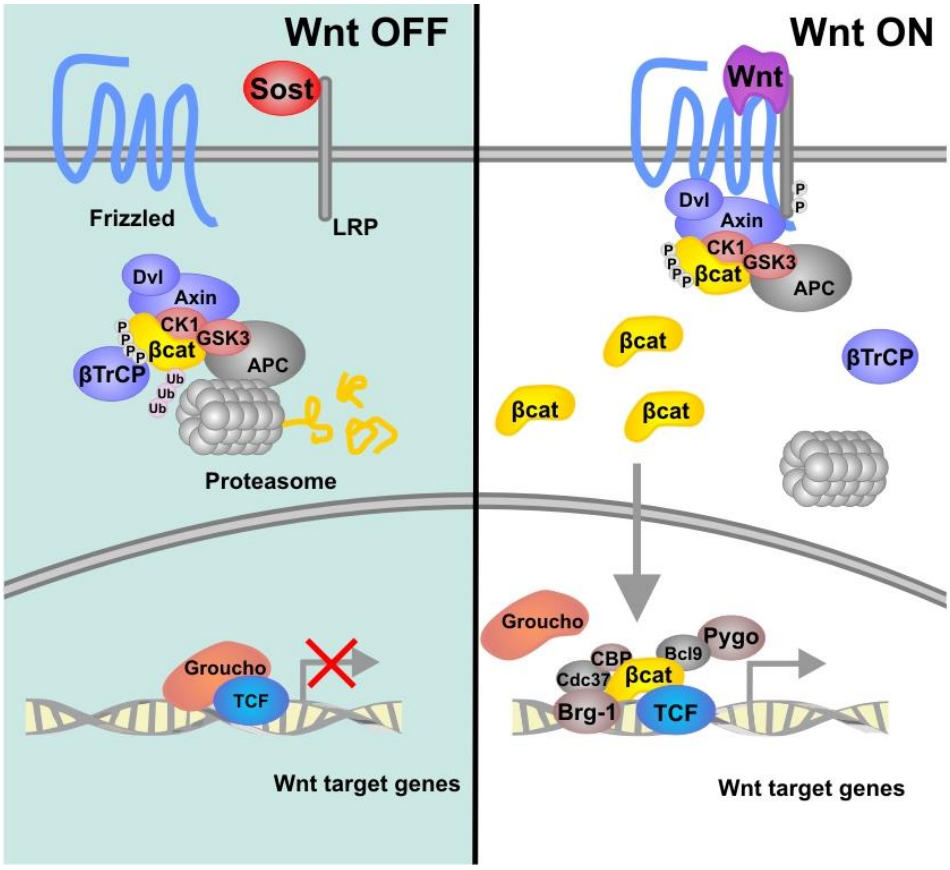

Figure 1.6 The canonical Wnt signalling pathway.

In the absence of Wnt signalling, which can be caused by inhibitors, such as Sost (left panel), β-catenin resides in a destruction complex in the cytoplasm with Axin, APC and GSK3, and becomes phosphorylated and targeted for degradation by β-TrCP. The proteasome recycles the complex by degrading β-catenin. In the presence of Wnt signalling (right panel), the intact complex associates with phosphorylated LRP. After binding to LRP, the destruction complex still captures and phosphorylates β-catenin, but ubiquitination by β-TrCP is blocked. Newly synthesized β-catenin accumulates and translocates to the nucleus, where it binds Lef/Tcf transcription factors, thus activating target genes. Based on: (Clevers and Nusse 2012).

1.3.2 The Wnt signalling pathway in bone physiology and skeletal stem cell biology

The role of Wnt signalling in bone anabolism has been the subject of numerous studies for more than a decade. Rare human mutations causing alterations in bone density have been identified in the components of the Wnt signalling pathway. These mutations lead to diseases such as High Bone Mass (HBM) disease, sclerosteosis, or Van Buchem disease, demonstrated by either *LRP5* gain-of-function mutations or *SOST* loss-of-function mutations (Balemans *et al.* 2001, Boyden *et al.* 2002, Gong *et al.* 2001), or osteoporosis-pseudoglioma syndrome (Gong *et al.* 2001), demonstrated by lack of *LRP5* or loss-of-function mutations thereof.

A plethora of animal studies have confirmed the importance of Wnt signalling in bone homeostasis, where activation of the Wnt/β-catenin pathway has been shown to be crucial in bone formation, whereas suppression of this pathway or loss-of-function *LRP5* mutations lead to bone-related pathologies (Babij *et al.* 2003, Day *et al.* 2005, Gong *et al.* 2001, Kato *et al.* 2002, Pinzone *et al.* 2009). The absence of Wnt10b, normally expressed in the developing bone, has been shown to lead to loss in trabecular bone (Bennett *et al.* 2005, Stevens *et al.* 2010), and confirmed that this molecule is an endogenous regulator of bone formation acting on mesenchymal precursors (Cawthorn *et al.* 2012). As described previously, in addition to bone homeostasis, Wnt signalling is also crucial in bone fracture healing, and many Wnts have been shown to be expressed/upregulated at the bone fracture site (Hadjiargyrou *et al.* 2002). Furthermore, several elements of the Wnt signalling pathway have been identified as being expressed in the bone marrow niche by putative SSCs themselves - Wnt ligands such as: Wnt2, Wnt4, Wnt5a, Wnt11, Wnt16 and various Wnt receptors, co-receptors and inhibitors (Etheridge *et al.* 2004). Whereas activation of Wnt/β-catenin signalling has been shown to suppress adipogenesis through inhibition of C/EBPα- and PPARγ-expression (Christodoulides *et al.* 2009, Kang *et al.* 2007), and the majority of studies report inhibition of chondrogenesis as well (Chun *et al.* 2008), there are substantial discrepancies in findings regarding the effects of Wnts in osteoblastogenesis.

For example, LRP5 overexpression, which elevates Wnt signalling, has been reported to increase the proliferation of SSCs (Baksh *et al.* 2007). Several studies have shown that Wnt3A-induced activation of Wnt signalling preserves SSC proliferation capacity in addition to suppressing their differentiation or apoptosis (Baksh and Tuan 2007, Boland *et al.* 2004, Cho *et al.* 2006, de Boer *et al.* 2004, Liu *et al.* 2009, Quarto *et al.* 2010).

In direct contrast to this, other studies have shown that Wnt signalling inhibits proliferation and promotes SSC differentiation (Babij *et al.* 2003, Bennett *et al.* 2005, Gregory *et al.* 2005, Qiu *et al.* 2007). Constitutive activation of Wnt signalling by retroviral transfection showed that high levels of Wnt signalling can stimulate osteoblast differentiation (Bain *et al.* 2003). It has also been observed that the activation of Wnt signalling mediated through the inhibition of the kinase GSK3, preventing β-catenin degradation, resulted in increased bone mass *in vivo* due to an increase in the osteogenic potential of SSCs at the expense of adipogenesis (Gambardella *et al.* 2011). Interestingly, links between Wnt, the BMP signalling pathway and Runx2 have been identified; Wnt signalling increases Runx2, osteoblast maturation and *via* stimulation of BMP9 or BMP2, increases alkaline phosphatase expression (Kang *et al.* 2007, McCarthy and Centrella 2010, Rawadi *et al.* 2003).

The discrepancies between these studies may be a result of difference in study design, such as different Wnt exposure times, concentrations, and involvement of direct or indirect Wnt pathway inducers/inhibitors. Also, the use of different cell sources/types prevents direct comparison between studies of the mechanism of Wnt involvement in stromal cell proliferation/differentiation. Furthermore, different Wnt proteins (canonical Wnt3A *vs.* non-canonical Wnt5A) have been shown to have different effects on SSCs (Baksh and Tuan 2007). As described previously, mixed population of stromal cells were analysed, consisting supposedly of stem cells and precursors at different stages of osteogenic commitment. Thus, the reported pleiotropic effects of Wnt might be due to varying responses of different cells within this population (Liu *et al.* 2009, Quarto *et al.* 2010). However, it is worth noting that the Wnt3A protein has been indicated as a clinically viable compound by exerting a rapid (in 2 days) and efficient effect in recruitment of CFU-Fs from bone marrow (Baksh and Tuan 2007).

Although most studies on Wnt signalling in bone biology focus on β-catenin dependent Wnt signalling, a potential role of non-canonical Wnt signalling in bone homeostasis is becoming increasingly acknowledged (Baron and Kneissel 2013). Furthermore, alternative from β-catenin routes for Lrp5-mediated signalling are emerging, as it has also been postulated to play a role in the control of bone formation *via* inhibition of serotonin synthesis in the duodenum, and not through the Wnt pathway (Ducy and Karsenty 2010, Yadav *et al.* 2008, Yadav *et al.* 2010). These studies underline the need for a systemic approach when analysing the *in vivo* effects of Wnts. Elucidating how the Wnt signalling pathway influences the recruitment, maintenance and maturation of bone marrow-derived SSCs might be of great interest due to their potential use in regenerative medicine. However, studies which aim to address this issue are hindered due to the complexity of this signalling pathway and the lack of specific markers for the SSCs. Once a solution is found, and a consensus reached, targeted and timed delivery of Wnt proteins or their agonists to stem cell populations at the site of injury might be able to enhance bone healing and promote tissue regeneration.

1.3.3 Potential of Wnts in therapy

Down-regulation of factors involved in the Wnt signalling pathway has been identified in cases of non-union. Several groups have shown that damage to the skeleton upregulates Wnt signalling at the site of injury during fracture healing and that Wnt signalling also accelerates fracture repair (Chen *et al.* 2007, Hadjiargyrou *et al.* 2002, Kim *et al.* 2007, Secreto *et al.* 2009). A summary of *in vivo* studies of the role of Wnt signalling in fracture healing has been published, and lists multiple approaches of pathway induction or targeting its inhibitors (Xu *et al.* 2014). These *in vivo* studies of the role of Wnt signalling in fracture healing have led to various investigations of Wnts as therapeutics for systemic delivery to accelerate fracture healing and reduce fracture-associated complications. A variety of Wnt modulators is already in preclinical or clinical trials mainly for the treatment of cancer, but also for osteoporosis, osteolytic disease, and bone fracture healing (Rey and Ellies 2010). Table 1.1 lists the proteins, antibodies and small molecules tested in the studies. One of those most advanced in preclinical development is an anti-sclerostin humanised antibody developed by Amgen (Romosozumab). Sclerostin binds to LRP5/6 co-receptor and antagonises canonical

Wnt signalling (Li *et al.* 2005). Studies into sclerostin-related genetic disorders in humans showed both increased bone formation and reduced bone resorption, suggesting agents that supress sclerostin might have both anabolic and anti-catabolic properties (see 1.3.2; (Balemans *et al.* 2001)). In Phase I clinical trials, a single-dose of Romosozumab antibody caused an increase in bone density in the hip and spine in healthy men and postmenopausal women (Padhi *et al.* 2011). In a Phase II trial, one year of the antibody treatment in osteoporotic women increased bone density more than bisphosphonate and teriparatide treatment (McClung *et al.* 2014). It demonstrated short-term anabolic responses in excess of those seen with teriparatide, the only currently available anabolic skeletal agent, and it produced only mild side-effects. However, Amgen is no longer pursuing its trials into Romosozumab as a drug for fracture healing (ClinicalTrials.gov identifier: NCT01081678), although planning for Phase III clinical trials for the treatment of osteoporosis was continued. At the time of writing, these trials are underway (ClinicalTrials.gov identifier: NCT01575834).

Other sclerostin antibodies, designed for the treatment of osteoporosis, namely Blosozumab, developed by Eli Lilly, and BSP804, by Novartis, have completed Phase II trials, and have shown increased bone mineral density in the lumbar spine of post-menopausal women with low BMD (ClinicalTrials.gov identifier: NCT01144377; ClinicalTrials. gov identifier: NCT01406548, respectively).
In addition, OsteoGeneX is developing small molecule inhibitors of sclerostin (Rey and Ellies 2010).

Another potential target is the Wnt inhibitor Dkk1. Dkk1 forms a complex with Lrp5/6 and disrupts the Wnt signalling pathway (Glinka *et al.* 1998). Inhibition of Dkk1 enhanced the healing process, resulting in mechanically stronger bone at the fracture site in a rodent model (Li *et al.* 2011). Indeed, antibodies against Dkk1 are undergoing clinical trials (Pfizer, Nuvelo), also in multiple myeloma patients for treatment of bone metastases (Iyer *et al.* 2014) (Novartis).

R-spondins positively regulate canonical Wnt signalling by reducing Wnt receptor turnover, thereby increasing β-catenin stabilization. R-spondins are prominently expressed in the developing skeleton and contribute to limb formation, particularly the distal digit. Additionally, results suggest that R-spondins may contribute to the

maintenance of adult bone mass by regulating osteoblastogenesis and bone formation (Knight and Hankenson 2014). However, the development of recombinant R-spondin proteins as a therapeutic for bone diseases was discontinued by Nuvelo after Phase I trials.

Table 1.1 Wnt modulators of bone biology in the biotech pipeline.

Adapted from: (Rey and Ellies 2010).

	Company	Therapeutic	Target	Technology	Development
Extracellular Modulators					
Bone	Nuvelo	R-Spondin NU206	LRP6	Biologic	Phase I (discontinued)
Bone	Nuvelo	LRP5 Mab	LRP5	Biologic	Discovery
Bone	Nuvelo	Dkk1 Mab	Dkk1	Biologic	Discovery
Bone	Amgen	Dkk1 Mab	Dkk1	Biologic	Preclinical
Bone	Pfizer	Dkk1 Mab PF-04840082	Dkk1	Biologic	Phase I
Bone in multiple myeloma	Novartis	Dkk1 Mab BHQ880	Dkk1	Biologic	Phase I
Bone	Amgen/UCB	AMG785 Sclerostin Mab (romosozumab)	SOST	Biologic	Phase III
Bone	Novartis	BPS804 Sclerostin Mab	SOST	Biologic	Phase II
Bone	Eli Lilly	Sclerostin Mab (blosozumab)	SOST	Biologic	Phase I
Bone	Wyeth	WAY-316606	SFRP	Small Molecule	Preclinical
Bone	Enzo Biochem	IIIC3a	Dkk1	Small molecule	Preclinical
Bone	OsteoGeneX	Anti-Sclerostin	SOST/LRP	Small molecule	Preclinical
Bone	Galapagos	?	LRP5	Small molecule	Discovery
Intracellular Modulators					
Stem cell renewal	Asahi Kasei Corporation	IQ1	PP2A	Small molecule	Discovery
Stem cell renewal	Rockefeller	BIO	GSK3	Small molecule	Discovery
Cancer, **Bone**, Obesity	OsteoGeneX	?	Various Wnt pathway	Small molecule	Lead optimisation, preclinical
Bone, Diabetes	Eli Lilly	603281-31-8	GSK3 inhibitor	Small molecule	Preclinical
Bone	Roche	?	GSK3 inhibitor	Small molecule	Preclinical

Although increased Wnt signalling has the potential to strengthen bones, it may also cause adverse side-effects in other tissues, such as articular cartilage, causing its degradation (Enochson *et al.* 2014, Lodewyckx and Lories 2009).

For bone fracture healing purposes, it is essential that the treatment activating the Wnt signalling pathway starts as soon as possible after the fracture occurs, as it has also been suggested that β-catenin signalling plays varying roles in different phases of fracture repair (Chen *et al.* 2007, Minear *et al.* 2010). The effects of Wnt on

angiogenesis also need to be tightly controlled, as it has been postulated that both inducers and inhibitors of Wnt can promote new blood vessel formation, depending on the timing of action (Min *et al.* 2011).

Therefore, Wnt modulators should ideally be delivered in a time-controlled manner, enhancing retention at the bone fracture site, but the delivery should also be targeted to the desired cell populations, in order to minimise the detrimental side-effects. One possible approach to achieve these aims may be the encapsulation of Wnt in delivery vesicles such as liposomes.

1.3.4 Wnt protein structure and biology

Although Wnts are predicted to be hydrophilic proteins based on their protein sequence, they are in fact highly hydrophobic. Previous findings showed that Wnts are hydrophobic owing to the posttranslational addition of palmitate and/or palmitoleic acid to one or two amino acid residues by a protein called Porcupine (Gao and Hannoush 2014, Hofmann 2000, Willert *et al.* 2003). The structure of any Wnt protein remained unknown until 2012, when the crystal structure of Xenopus Wnt8 was published, albeit in complex with its receptor (Figure 1.7 (Janda *et al.* 2012)). This highly unusual two-domain structure forms a protein fold, called a "thumb and index finger" structure, which has not previously been identified in any other protein. It is now clear that the fatty acid molecules interact with the Frizzled receptor. It is possible, though unproven, that these moieties are also involved in docking Wnt to the liposomal membranes (Lorenowicz and Korswagen 2009).

The hydrophobic nature of Wnts argues against the simple model of passive diffusion in the extracellular milieu. Because of this, various studies have investigated mechanisms by which Wnts are transported in the extracellular space. Some studies have shown that they associate with different vesicles during transport, such as multivesicular bodies (MVB), argosomes (exogeneously derived lipoproteins) and LDL/HDL (Greco *et al.* 2001, Korkut *et al.* 2009, Neumann *et al.* 2009, Panakova *et al.* 2005). Wnts are also thought to be able to associate with the lipid bilayer of the liposomes (Dhamdhere *et al.* 2014, Morrell *et al.* 2008), as suggested by researchers investigating their use as a therapeutic. A large body of evidence also suggests that

components of the extracellular space, such as glypicans (Capurro *et al.* 2005), biglycans (Berendsen *et al.* 2011) and heparan sulphate proteoglycans (HSPGs) modulate Wnt-receptor interactions, as well as maintain activity and solubility of Wnt proteins by preventing their aggregation in low serum conditions (Fuerer *et al.* 2010). Wnts form morphogen gradients and HSPGs concentrate Wnt molecules at the cell surface. What is more, mutations of enzymes that synthesise these ECM components phenocopy Wnt mutations (Hacker *et al.* 1997), suggesting that these proteins are involved in Wnt transport. As previously noted, Wnts are chaperoned during their transport and interestingly lipoprotein particles, which have also been indicated to play a role in the transport of Wnts, have themselves been shown to interact with HSPGs (Eugster *et al.* 2007).

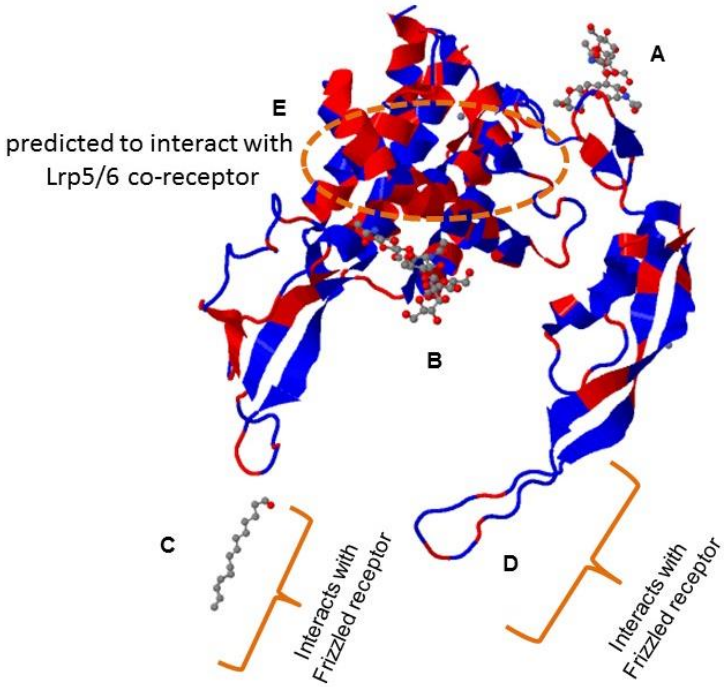

Figure 1.7 Xenopus Wnt8 structure.

The crystal structure of first of the Wnt, Xenopus Wnt8 (352 amino acid residues; ~40kDa), in the formation adopted when in complex with its Frizzled receptor. Wnt8 has 2 glycosylation sites (A and B) which surround the domain which is predicted to interact with Wnt co-receptors, and one palmitoleic acid residue (C). The previously unseen protein folding structure is called a "hand" with a "thumb" (C) and "index finger" (D) structure, where both the thumb and the index finger interact with the Frizzled receptor. Hydrophobic amino acid residues are shown in red, whereas hydrophilic residues are shown in blue. Adapted from Protein Data Base submission by Janda *et al.* Science 2012.

1.4 Liposomes as therapeutic delivery nanoparticles

1.4.1 Nanoparticles as drug delivery vehicles

Nanoparticles are particles in the 10^{-9} - 10^{-7} m size range, used in medicine for the diagnosis, prevention, detection and treatment of disease. In particular, nanotechnology has been used to design and develop targeted drug delivery systems which could safely deliver therapeutics to injury sites or specific cells (Mills and Needham 1999). Potential benefits of nanoparticles include improved solubility of the clinical formulation of the drug, protection of the entrapped therapeutic drug from degradation, modification of the pharmacokinetic and tissue distribution profile of the drug to avoid side effects and reduce toxicity, and increased cellular uptake/internalization. Nanocarriers can be divided into organic, inorganic and organic/inorganic hybrid nanoparticles, and include dendrimers, liposomes, solid lipid nanoparticles, polymersomes, polymer-drug conjugates, polymeric nanoparticles, peptide nanoparticles, micelles, nanoemulsions, nanospheres, nanoshells, carbon nanotubes, and iron, gold or silica nanoparticles. In all of these types of nanoparticles, drugs can be entrapped inside the particle, dissolved in the matrix, covalently linked to the backbone, or adsorbed on the surface (Gao *et al.* 2014). Due to their biological properties, lipid-based preparations have attracted great attention as drug delivery systems and among these, liposomes are the most widely used and studied examples. The beneficial properties of liposomes include good biocompatibility, biodegradability, low immunogenicity, and the ability to deliver both hydrophilic and hydrophobic drugs.

1.4.2 Physicochemical properties of liposomes

Liposomes were first described in the 1960s by the British scientist Alec Bangham, who observed them by looking under an electron microscope after negatively staining dry phospholipids, the liposomes being formed spontaneously when certain lipids are diffused in aqueous solutions (Bangham and Horne 1964). The pictures served as the first evidence that the cell membranes consist of a lipid bilayer.

The name "liposome" originated from Greek, "lipo" meaning "fat" and "soma" meaning "body", as the liposomes mainly consist of phospholipids. Liposomes are spherical, self-closed structures formed by one or more concentric lipid bilayers with

an aqueous phase inside and between the lipid bilayers. Depending on the size and the number of lamellae (single or multiple bilayer membranes), liposomes can be divided into three groups:

- MLVs – multilamellar vesicles, >0.1 μm in size
- LUVs – large unilamellar vesicles, >0.1 μm in size
- SUVs – small unilamellar vesicles, ≤ 0.1 μm in size.

Generally, liposome size may vary from very small (0.025 μm) to large vesicles (2.5 μm). Liposomes can be composed of natural and/or synthetic phopsho- and sphingolipids. They can also contain other bilayer constituents, such as cholesterol or hydrophilic polymer (polyethylene glycol, PEG)-conjugated lipids (Lasic 1993).

The physicochemical properties of the lipids which comprise liposomes, such as size, membrane fluidity, surface charge density and steric hindrance, determine the liposomes' interactions with blood components and other tissues after systemic administration. As liposomes have the ability to encapsulate hydrophilic agents in their core, while hydrophobic agents remain entrapped within the lipid bilayer, the nature and extent of liposome-cell interaction determines the mode of intracellular delivery of the carried cargo (Gregoriadis 1976). Liposome formulations can be optimised in terms of the above mentioned properties.

The main problem with systemic administration of liposomes is their opsonisation and therefore rapid clearance by the reticuloendothelial system (RES). SUVs are opsonised less rapidly and less extensively than LUVs, therefore leading to slower uptake by the RES. Also, a reduction in liposome size has been correlated with increased accumulation in tumour tissue or areas of inflammation, due to prolonged circulation half-life and increased permeability of blood vessels (Yuan *et al.* 1994).

In terms of bilayer fluidity, lipids composing the liposomes have a characteristic phase transition temperature (Tc). Below Tc, they exist in a rigid, well-ordered arrangement, called the solid "gel-like" phase, while above Tc in a liquid crystalline "fluid-like" phase (Figure 1.8). The fluidity of the bilayer, and therefore its leakage, can be altered by using phospholipids with different Tc values, which vary between -20°C to 90°C depending on the length and saturation of the fatty acid chains of the lipid. The presence of high Tc lipids (>37°C) makes the liposome bilayer less fluid, and hence

less leaky at physiological temperatures, as well as lowering their uptake by the RES. Incorporation of cholesterol into the lipid bilayer can also alter the fluidity of the membrane. At high concentrations (>30 molar %), cholesterol eliminates the phase transition and decreases the membrane fluidity, which stabilises the liposomes and reduces leakage (Cullis 1976).

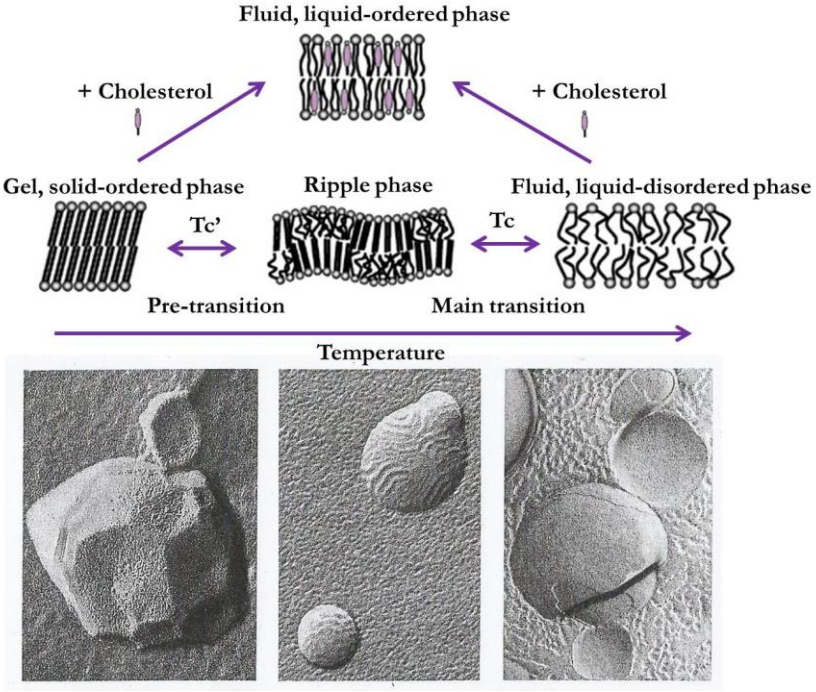

Figure 1.8 A schematic presentation of membrane phase transitions.

At Tc', tilted subgel transforms into gel (the so-called pretransition) and at Tc frozen hydrocarbon chains melt and a liquid crystalline phase is formed (main transition). These phases can also be seen in freeze fracture EM micrographs. In the liquid crystalline phase, the surface is mostly smooth, where in the gel phase the surface often shows characteristic ripples, and at T<Tc', liposomes are often faceted polyhedra because tilted bilayers cannot be packed into a closed sphere (from right to left). From: (Lasic 1993).

The surface charge of the liposome, which is dependent on the lipid composition, can affect how the liposomes interact not only with the desired cell target but also with the RES. Lack of surface charge can lead to liposome aggregation, whereas anionic liposomes are more easily taken up by cells by endocytosis, and unfortunately also by the RES, leading to rapid plasma clearance. Cationic liposomes, on the other hand, have been proposed to deliver their contents by fusion with cell membranes.

Addition of small fractions (5 - 10 molar %) of compounds bearing hydrophilic groups, such as PEG, reduces the interaction of liposomes with cells and blood

components, sterically stabilising them. Hydrophilic surface coating offers steric hindrance to opsonin adsorption, which reduces the rate of uptake by the RES and prolongs the circulation half-life by up to 10-fold (Klibanov *et al.* 1990). However, higher concentrations of PEG can lower drug encapsulation efficiency, and also lead to macromolecular syndrome of the liver, instead of being normally excreted in urine or faeces (Veronese and Pasut 2005). PEGylated liposomes are often called "stealth" liposomes or long-circulating liposomes.

Another advance in liposome technology, proposed in the 1990s, has been the addition of targeting moieties to the liposome surface. This technology enables active targeting of the liposome-encapsulated drugs to the desired cell populations.

Figure 1.9 shows an overview of the last 40 years in liposome technology. Over two decades ago, triggered-release liposomes were introduced. These liposomes can release their cargo when activated by remote triggers such as heat, ultrasound, and light, and local triggers intrinsic to the disease site or cellular organelles, such as enzymes and pH changes. A thorough review of triggered-release liposomes has recently been published (Bibi *et al.* 2012). The new millennium has seen the development of lipoplexes, the most recent generation of liposomes comprised of cationic lipids, containing siRNA, oligopeptides, DNA or plasmids.

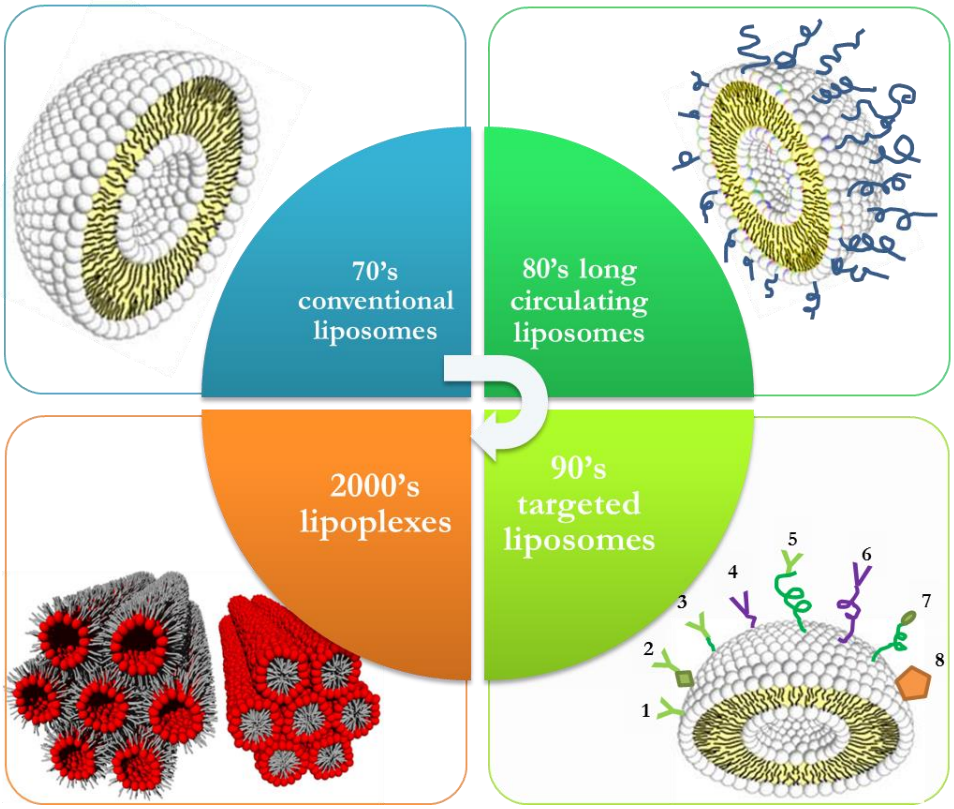

Figure 1.9 Overview of the last 40 years in liposome technology.

During the 1970s a simple lipid shell containing an active molecule was used. In the 1980s, liposome pharmacokinetics have been improved thanks to hydrophilic polymers grafted onto the surface of liposomes. With this improvement, they began to be called long-circulating or sterically stabilized "stealth" liposomes. In the 1990s active targeted liposomes as well as immunoliposomes were developed for a wide range of cancer applications. 1. represents whole antibody simply adsorbed on liposome surface; 2. represents the whole antibody-hapten binding technique; 3. represents covalent binding between whole antibody and liposome surface; 4. represents Fab' or Fab2 antibody fragment covalently attached on the surface of liposome; 5. represents covalent binding of whole antibody on the extremity of PEG chains; 6. represents a covalent binding of Fab' or Fab2 antibody fragment on the extremity of PEG chains; 7. represents the most recent generation of immunoliposomes containing a scFv fragment covalently linked to liposomes PEG chains; 8. represents targeting peptides. The new millennium has seen the birth of the most recent generation of liposomes containing siRNA, oligopeptides, DNA or plasmids, called lipoplexes. Adapted from: (Tresset 2009), (Urbinati *et al.* 2012).

1.4.3 Liposomes as delivery vesicles

Liposomes are widely used in the pharmaceutical industry as delivery vesicles for multiple drugs, such as antibiotics, vaccines, or anti-cancer drugs (Table 1.2). Applications of liposomes in drug delivery are developed when they can offer superior therapeutic efficacy and safety over existing formulations (Juliano and Stamp 1978). Hydrophobic drugs, such as cyclosporine or paclitaxel, when formulated in surfactants or organic co-solvents, caused toxicity at the doses needed to deliver the appropriate amount of drug. In contrast, liposomes, which are made of lipids, are relatively

biocompatible and biodegradable, non-toxic and non-immunogenic molecules. They can encapsulate a wide range of water-insoluble drugs and increase their therapeutic index (TI), because they can contain greater concentrations of the drug compared to the extracellular fluid. The toxicity of drugs with a narrow TI can be minimized by reducing their biodistribution after encapsulating them in liposomes, thus decreasing their delivery to critical organs. Liposomes have been shown to be taken up poorly by tissues such as heart, kidney or gastrointestinal tract, which are major sites for toxicity (Szoka 1990). Among the examples of the superiority of liposomal delivery, is Amphotericin B or doxorubicin, which produced severe dose-limiting nephrotoxicity and cardiac toxicity, respectively, before their reformulation into liposomes (Sharma and Sharma 1997).

Table 1.2 Current list of clinically approved liposomal drugs.
Based on: (Allen and Cullis 2013).

Name	Trade name	Company	Indication
Amphotericin B	Abelcet	Enzon	Fungal infections
Amphotericin B	Ambisome	Gilead Sciences	Fungal and protozoal infections
Cytarabine	Depocyt	Pacira (formerly SkyePharma)	Neoplastic meningitis
Daunorubicin	DaunoXome	Gilead Sciences	HIV-related Kaposi's sarcoma
Doxorubicin	Doxil	Janssen-Cilag	HIV-related Kaposi's sarcoma, metastatic breast cancer, metastatic ovarian cancer
	Caelyx	Janssen-Cilag	
	Lipo-dox	Sun Pharma Global	
	Myocet	Zeneus	
IRIV vaccine	Epaxal	Crucell	Hepatitis A
IRIV vaccine	Inflexal V	Berna Biotech	Influenza
Morphine	DepoDur	SkyePharma, Endo	Postsurgical analgesia
Verteporfin	Visudyne	QLT, Novartis	Age-related macular degeneration, pathologic myopia, ocular histoplasmosis
Proteins SP-B and SP-C	Curosurf	Chiesi Farmaceutici, S.p.A.	pulmonary surfactant for Respiratory Distress Syndrome
Vincristine	Marquibo	Spectrum Pharmaceuticals	Acute Lymphoblastic Leukemia (ALL) and Melanoma

There are different ways in which liposomes can release their cargo to cells (Canton and Battaglia 2012, Petros and DeSimone 2010, Torchilin 2005). Figure 1.10 shows potential mechanisms of cellular uptake of nanoparticles and nanoparticle-cell interactions. However, the preference for a specific mechanism is also dependent on the nanoparticle formulation, therefore each composition requires testing.

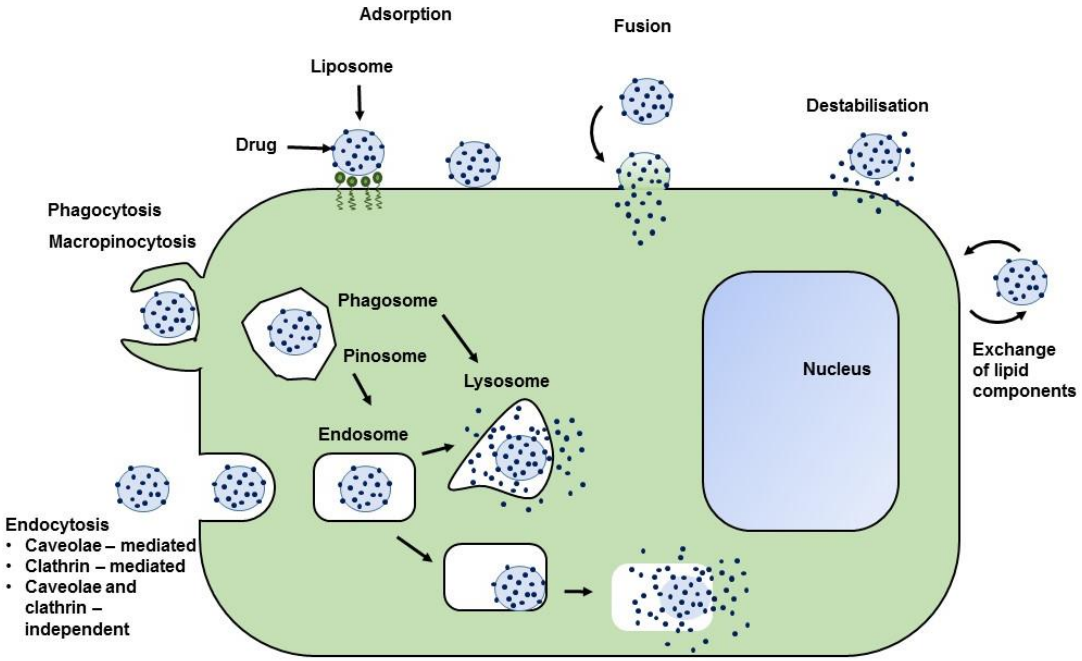

Figure 1.10 Mechanisms of cellular uptake of liposomes and liposome-cell interactions.

Drug-loaded liposomes can specifically or non-specifically adsorb onto the cell surface. Liposomes can also fuse with the cell membrane with subsequent release of their contents into the cell cytoplasm, or can be destabilised by certain cell membrane components when adsorbed on the surface, so that the released drug can enter the cell. Furthermore, liposomes can undergo direct or transfer protein-mediated exchange of lipid components with the cell membrane, or be subjected to specific or nonspecific endocytosis. In the case of endocytosis, a liposome can be delivered by the endosome into the lysosome or, while being transported to the lysosome, the liposome can provoke endosome destabilization, which results in drug liberation into the cell cytoplasm. Liposomes modified with specific viral peptides and loaded with a drug can specifically interact with cells, provoke endocytosis, and, *via* the interaction of viral components with the inner membrane of the endosome, permit drug efflux into the cell cytoplasm. Liposomes can also enter cells through phagocytosis or macropinocytosis. Mechanisms of cellular uptake are dependent on the nanoparticle formulation and size. Based on: (Canton and Battaglia 2012, Petros and DeSimone 2010, Torchilin 2005).

1.4.4 Liposomes as protein delivery vesicles

Proteins, including enzymes, peptide hormones, and cytokines have become drugs of choice for the treatment of various diseases during the past three decades. Encapsulation of these molecules into liposomes has been a subject of many different studies, which showed their superior therapeutic efficacy in comparison to free proteins or peptides (Torchilin 2005). Liposome-encapsulated asparaginase improved the survival of animals with asparagine-dependent tumours, superoxide dismutase reduced ischaemia-reperfusion oxidative stress, and tissue plasminogen activator used for thrombolytic therapy allowed minimization of the dose. Liposomes were also

tested for interleukin-2, with increased blood circulation time of the drug, and both oral and parenteral delivery of insulin (Torchilin 2005).

1.4.5 Liposomes as Wnt protein delivery vesicles

Wnt protein incorporated into the liposome structure has been shown to be biologically active and potent throughout a longer period of time, in comparison to the purified protein. This shows the advantage of association with lipid membranes and has been proposed to better resemble the natural secretion of Wnt (Lum and Clevers 2012, Morrell *et al.* 2008, Zhai *et al.* 2004). Recently, an encouraging study on Wnt3A protein packaged in liposomal vesicles and delivered into skeletal defects in mice has been shown to result in faster bone regeneration through stimulation of proliferation of skeletal progenitors and acceleration of their differentiation into osteoblasts (Minear *et al.* 2010). Liposomal Wnt3A delivery resulted also in enhancement of implant osseointegration in murine bone defects (Popelut *et al.* 2010). This encapsulation technology has also been shown to be advantageous for the protein itself, prolonging and extending its activity (Dhamdhere *et al.* 2014).

The major issue while considering Wnt signalling modulation by Wnt proteins in order to promote bone anabolism and healing is to provide specific delivery of this potent factor at the injury site, preferably also to a specific stem cell population. This targeted delivery is necessary to avoid potentially harmful non-specific effects of Wnt signalling elevation as well as to ensure a sufficient concentration of the Wnt protein (Tsaousi *et al.* 2011).

1.4.6 Liposomes in targeted delivery

Site-specific delivery, a concept first proposed by Paul Ehrlich in 1906, involves the delivery of a drug to the target site and a reduction in exposure of healthy tissues (Strebhardt and Ullrich 2008). It increases liposomal drug accumulation in the desired tissue, producing more efficacious and selective therapeutic activity. Liposomes have been exploited for both passive and active targeting of drugs. Passive targeting is used, where due to the size or properties of the liposomal formulation alone, the liposomes accumulate in certain tissues. In active targeting, liposomes can be directed specifically

to the desired cell population by attachment to their surface of targeting components, such as peptides or antibody fragments.

Passive targeting of drugs involves the natural tendency of certain cell types, such as circulating macrophages or Kupffer cells in the liver, to phagocytose foreign particles, such as liposomes (Kelly *et al.* 2011). Immunostimulators or immunosuppressive drugs have been successfully delivered in liposomal formulations to lymphatic tissues, such as the spleen. Passive targeting is a common approach used in the delivery of vaccines. Recently, accumulation of liposomes in bone marrow has also been suggested, as bone marrow macrophages seemingly have a role in the delivery of lipids to the bone marrow, where they are used as a source of energy, for membrane biosynthesis or in the delivery of fat-soluble vitamins for haematopoiesis (Sou *et al.* 2011). As previously discussed, passive targeting also occurs when SUVs accumulate in solid tumour tissue undergoing angiogenesis, due to leaky vasculature and a lymphatic system which is not fully functional.

Active targeting of liposome encapsulated drugs may be accomplished by coupling specific antibodies or peptides to the vesicles. These immunoliposomes have several advantages over antibody-drug conjugates, as they can carry significantly larger amount of drug (Gregoriadis 1995). The drugs can also reach their intracellular targets by diffusion, after release from immunoliposomes associated with the target tissue. Therefore, unlike antibody-drug conjugates, they may not have to undergo receptor-mediated endocytosis, in order to deliver their contents intracellularly.

Some of the tested immunoliposome formulations with peptides contain folate or hyaluronic-modifications, transferrin or transferrin receptor antibodies (as these receptors are over expressed in many cancers), arginine-glycine-aspartate peptides (RGD) to target integrins present in the tumour vasculature, or transcriptional activator protein to enhance liposome internalisation (Hatakeyama *et al.* 2004, Platt and Szoka 2008, Tseng *et al.* 2002, Zhang *et al.* 2010). A transferrin-targeted liposomal oxaliplatin formulation has completed Phase II clinical trials and a transferrin-targeted lipid-based nanocomplex containing the p53 gene has completed a phase I trial (Suzuki *et al.* 2008, Xu *et al.* 2001). Liposomes with a $(AspSerSer)_6$-surface moiety (for

interaction with calcium-rich bone surfaces) have been used for *in vivo* evaluation of osteogenic siRNA delivery for a potential bone anabolic therapy (Zhang *et al.* 2012).

Among antibodies used for active targeting of liposomes, anti-HER2 (for breast cancer) and anti-CD19 (for leukaemia and lymphoma) are the most regularly exploited in preclinical studies (Cheng and Allen 2008, Goren *et al.* 1996, Park *et al.* 2002). A liposomal doxorubicin formulation targeted *via* anti-HER2-scFv formulation has progressed to Phase I clinical trials (Nellis *et al.* 2005). Other antibody-conjugated liposomes, such as anti-GD2 (for neuroblastoma), the anti-KDR domain of VEGF (anti-angiogenic treatment), anti-CD22 (for B-cell lymphoma), anti-EGF and anti-VCAM-1 (overexpressed in many tumours) are also being investigated (Benzinger *et al.* 2000, Gosk *et al.* 2005, Loomis *et al.* 2010, Mamot *et al.* 2005, Raffaghello *et al.* 2003). For the diagnosis and treatment of osteoarthritis, immunoliposomes conjugated with a type II collagen antibody are being tested in animal models (Cho *et al.* 2013). Aptamers are also often investigated *in vitro* and *in vivo* as targeting moieties on the liposome surface, and these include preparations targeting CD44 and prostate specific membrane antigen (PSMA) (Alshaer *et al.* 2015, Baek *et al.* 2014).

Given the evidence suggesting that spatiotemporal modulation of the Wnt signalling pathway might be an attractive target for bone anabolic therapies, design of novel therapeutics that offer the possibility to regulate this pathway at the fracture site is greatly desired. However, the effects of Wnt signalling induction specifically on stem cell populations and osteoprogenitors within the bone marrow niche are not well known and need further investigation. Translation of this knowledge into a bone fracture scenario would help produce effective particles regulating the Wnt signalling pathway, tailored for bone regeneration purposes. In order for these Wnt therapeutics to be beneficial, they would have to be delivered in a targeted and timed fashion to bone stem cells of the bone marrow niche at specific phases of bone fracture healing. This way, liposomal therapy could offer an efficacious but also a safe approach for delivering Wnt anabolic agents.

Hypothesis and aims

The aim of this thesis was to determine the effect of Wnt stimulation on the osteogenic response of populations of cells in human bone marrow, to establish a method of incorporating Wnt proteins in nanoparticle carriers, to prove the protein/liposome association, and to develop a technology for spatiotemporal delivery in fracture healing. These aims were devised to test the hypotheses that temporal control of Wnt stimulation promotes osteogenesis in human SSCs, that Wnt proteins associate with liposomes and retain their activity, and finally that this technology could be used for spatiotemporal delivery of Wnts in fracture healing.

The specific aims were as follows:

- To measure the frequency of skeletal stem cells in fresh bone marrow isolates;
- To determine intrinsic levels of Wnt signalling in fresh bone marrow isolates between populations of cells with various levels of skeletal stem cell marker expression;
- To assess the frequency of skeletal stem cell-rich populations and haematopoietic populations within fresh bone marrow isolates after transient Wnt stimulation;
- To measure CFU potential of bone marrow isolates after transient Wnt stimulation;
- To assess the osteogenic differentiation of bone marrow isolates after a transient and ongoing Wnt stimulation;
- To characterise and optimise the formulation of liposomes;
- To determine suitability of liposomes as delivery vesicles for Wnt3A protein;
- To measure the uptake of liposomes *in vitro* and distribution *in vivo*.

Chapter 2

Methodology

2.1 Materials

2.1.1 Cells

Bone marrow mononuclear cells (BMMNCs) were isolated from femoral samples obtained from haematologically normal individuals undergoing hip replacement surgery, due to osteoporosis or osteoarthritis, at Southampton General Hospital or Spire Hospital Southampton, with the approval of the appropriate Local Research Ethics Committee (LREC 194/99/1). A list of isolates can be found in the Appendix, Table A.7.

MG63 human osteosarcoma cell line, used as a positive control for STRO-1 antibody, was purchased from Sigma (St. Louis, USA). The human keratinocyte cell line HaCaT, used as a negative control for the STRO-1 antibody, was a gift from Professor Eugene Healy (Faculty of Medicine, University of Southampton). The 3T3 murine fibroblast Wnt reporter cell line was purchased from Enzo Life Sciences (Farmingdale, USA).

2.1.2 Cell Culture Medium, Buffers, Reagents

Chemicals and reagents used in the experiments are listed in the Appendix, Table A.1 - Table A.5. FBS was batch tested in the Bone and Joint Research Group.

2.1.3 Equipment

Equipment used in experiments is listed in the Appendix, Table A.6.

2.2 Methods

2.2.1 BMMNC isolation

BMMNCs were isolated from bone marrow samples aspirated from patients' femurs, often containing small pieces of trabecular bone and traces of fat. The donated tissue usually comprised of ~1 - 2 ml of bone marrow aspirate and varying volumes of trabecular bone. When the trabecular bone volume was low in the donated sample, additional trabecular bone fragments were extracted from the neck of the femoral head as trabecular bone samples have been shown to contain similar numbers of nucleated cells as bone marrow (Sakaguchi *et al.* 2004). This standardised the amount of tissue

from which cells could be subsequently extracted, and increased cell yield. Samples were washed thoroughly with medium A (Minimum Essential Medium alpha, αMEM, containing 100 U/ml penicillin and 100 µg/ml streptomycin; see Appendix Table A.1 for detailed media contents), through repeated vigorous shaking with ~10 ml of medium, and transferral of each 10 ml portion to a 50 ml Falcon tube, until the bone appeared to be white (cell-deprived). This mechanical process assisted in the release of cells from the marrow. The remains of the sample were discarded into Virkon (DuPont, Wilmington, USA). The cell suspension was then supplemented with medium A up to 50 ml and centrifuged for 5 minutes at 18°C, 240x *g*. After decanting fat and most of the medium into Virkon, 10 ml of fresh medium A was used to resuspend the cell pellet thoroughly before straining through a 40 µm filter into a new 50 ml Falcon tube to remove residual bone chips and other unwanted tissue. The filtered cell suspension was then diluted in total of 50 ml medium A. The sample was divided into two 25 ml samples, each of which was transferred delicately with a Pasteur pipette onto 25 ml of density gradient medium, Lymphoprep™ (Axis-Shield, Dundee, UK), in a 50:50 ratio and centrifuged for 40 minutes at 18°C, 800x *g*. This density gradient separation enables the isolation of BMMNCs and the removal of the majority of red blood cells from the sample, although blood clots sometimes remain in the interphase (Boyum 1968). Figure 2.1 shows the phase separation of cells after centrifugation.

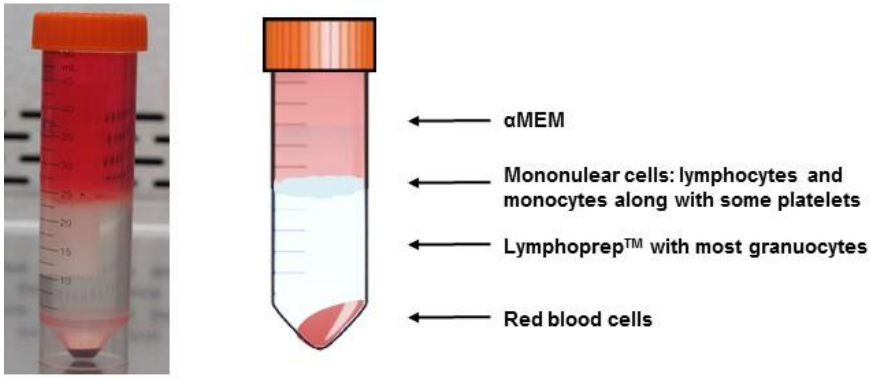

Figure 2.1 Lymphoprep separation of bone marrow samples.

After transferring the interphase between αMEM and Lymphoprep™, containing BMMNCs, into a new 50 ml Falcon tube, cells were washed twice in 20 ml of medium

A, by centrifuging at 240x *g*, for 5 minutes at 18°C. Finally, cells were resuspended in medium B (αMEM containing 5 % FBS and 100 U/ml penicillin and 100 μg/ml streptomycin) and counted. The total number of viable cells was counted using the trypan blue dye exclusion assay (Sigma). To exclude remaining red blood cells from the count, Easy Lyse Erythrocyte Lysing Reagent (Dako, Glostrup, Denmark) was used, according to the manufacturer's protocol. Briefly, cells were incubated in 20x diluted lysing reagent, for 5 minutes at room temperature.

2.2.2 STRO-1-enrichment of BMMNCs - MACS isolation

STRO-1 MACS isolation was carried out on a subset of BMMNCs isolated previously by Lymphoprep™ or, in the case of assessment of intrinsic Wnt signalling level, on BMMNCs which were in culture and provided sufficient cell number. These previously cultured cells were digested with collagenase and trypsin (see Section 2.2.4), MACS-selected, and their RNA was subsequently extracted. Generally, for STRO-1-enrichment, the cell pellet was first deprived of erythrocytes with Easy Lyse Erythrocyte Lysing Reagent (see above) in the case of fresh BMMNCs, or directly resuspended in 2 ml of blocking buffer (see Appendix for ingredients of all buffers, Table A.2) and incubated for 30 minutes at 4°C, with agitation every 10 minutes. The suspension was then centrifuged at 240x *g* for 5 minutes at 4°C and washed with 10 ml of chilled MACS buffer. 1 ml of STRO-1 primary antibody in the form of unpurified hybridoma supernatant (see Appendix for antibody details, Table A.5) was then added for 30 minutes and incubated at 4°C, with agitation every 10 minutes. Next, cells were washed three times with 20 ml of MACS buffer and finally resuspended in 800 μl of this buffer. After the addition of 200 μl of MACS rat anti-mouse IgM microbeads and 30 minute incubation at 4°C, with agitation every 10 minutes, cells were again washed three times with 20 ml of MACS buffer and resuspended in 2 ml MACS buffer. Magnetic separation of the sample was performed using the LS separation column and QuadroMACS magnetic field (Miltynei Biotec, Bergisch Gladbach, Germany). The column was equilibrated by a 3 ml wash with MACS buffer. 2 ml of the immunolabelled cell suspension was then separated on the column, the negative (unlabelled) fraction passing through to a collection tube and the STRO-1$^+$ fraction remaining magnetically bound. After three 3 ml washes with MACS buffer to ensure removal of the unbound cells, the positive fraction was eluted. By removing the

column from the magnetic stand, adding 5 ml of MACS buffer, and pressing a plunger through the column, STRO-1^+ cells were flushed out of the column and collected in a separate collection tube. After washing twice in PBS, the cell pellet was suspended in cell lysis buffer and further processed for RNA extraction or, if the cells were to be cultured, the washes were performed in medium A before final resuspension at the required seeding density and media for each experiment.

2.2.3 Wnt3A protein treatment

For each short-term Wnt exposure experiment, different numbers of BMMNCs were incubated for 24 hours with Wnt3A protein (R&D Systems, or solvent only as control) in suspension on a MACSmix™ tube rotator (Miltenyi Biotec), rotating at 8 rpm to avoid aggregation of cells at the bottom of the tubes (Figure 2.2). For every 10^6 cells, 2 ml of medium B was used. The concentration of Wnt3A protein was 100 ng/ml. Following treatment, cells were either assayed immediately or plated on tissue culture plastic in basal culture medium or osteogenic medium. 5 days post isolation, adherent cells (BMMNCs or STRO-1-enriched BMMNCs), both containing skeletal stem cells (SSCs), attached to the tissue culture dish, and the remaining non-adherent cells (most haematopoietic cells) were disposed of by washing twice with PBS before media change.

Figure 2.2 Wnt induction during rotation culture.

BMMNCs incubated for 24 hours in suspension on a MACSmix™ tube rotator to avoid cell aggregation at the bottom of the tubes.

For long-term Wnt exposure experiments, cells were seeded onto tissue culture plastic immediately after isolation, and Wnt3A protein at 100 ng/ml (unless stated otherwise)

was added after 5 days (from the initial adherence to tissue culture plastic), as part of the first media change.

In short- and long-term Wnt exposure experiments, BMMNCs and STRO-1-enriched BMMNCs were cultured for a total of 14 days in basal or osteogenic media after tissue culture plastic adherence. Both basal and osteogenic media, with or without Wnt, were changed three times a week. The time-frames for short- and long-term exposure to Wnt3A are shown in Figure 2.3.

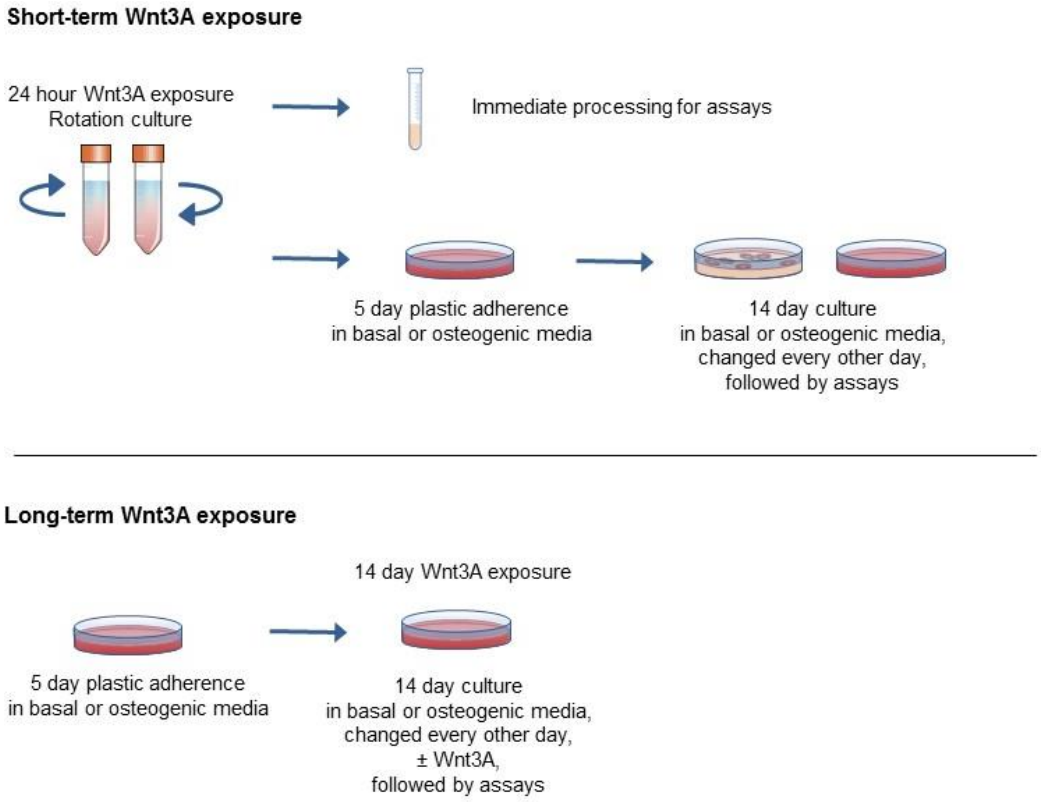

Figure 2.3 Experimental protocol for short- and long-term exposure of cells to Wnt3A.

2.2.4 Cell culture

The majority of research presented in this thesis was conducted using BMMNCs or STRO-1-enriched BMMNCs from primary (P0) passage culture. However, a subset of nanoparticle uptake assays was carried out using BMMNCs at P1, including flow cytometry and confocal imaging, to examine a population with a greater degree of homogeneity. For subculture, cells at 80 % confluence were detached with the use of 1 mg/ml collagenase IV (Sigma) for 45 minutes at 37°C and then trypsinised (Lonza, Basel, Switzerland) with 0.5 mg/ml trypsin. The ratio for passaging was 1:3 – 1:6.

HaCaT and MG63 cells used as a negative and positive control, respectively, for the STRO-1 antibody, were cultured in Dulbecco's Modified Eagle Medium (DMEM) supplemented with 10 % FBS and 100 U/ml penicillin and 100 µg/ml streptomycin. Passaging was carried out at a 1:3 – 1:8 ratio when the cells reached 60 % confluence. Cells were centrifuged at 300x *g* for 5 minutes.
The 3T3 murine fibroblast Wnt reporter cell line was cultured in DMEM supplemented with 10 % FBS and 100 µg/ml penicillin/streptomycin and maintained at 10 – 60 % confluence. Passaging was carried out at a 1:8 ratio every 3 days. The seeding density was 3.5 x 10^3 - 1.5 x 10^4 cells/cm^2 and cells were centrifuged at 800x *g* for 5 minutes.
All cells were maintained at 37°C in a humidified 5% CO_2 atmosphere.

2.2.5 Experimental analyses

Pictorial summaries of the experimental methods used are shown in the introduction to each results chapter. Detailed below are the procedures for assays carried out throughout this thesis.

2.2.5.1 Immunostaining of cells in suspension for flow cytometry, Image Stream cytometry and FACS

Prior to staining, BMMNCs were treated with Easy Lyse Erythrocyte Lysing Reagent (DAKO). For flow cytometry analysis, 10^6 - 10^7 cells were stained, each sample having an isotype-matched control. All cells gated as positive showed a fluorescence intensity greater than that detected on 99 % of the cells labelled with the isotype-matched control. Non-specific antibody binding was reduced by a 30 minute incubation at room temperature with flow cytometry blocking buffer (see Appendix, Table A.2). Staining was performed with the relevant antibodies (listed in the Appendix, Table A.5) in 100 µl of flow cytometry buffer at 4°C for 30 minutes, followed by two washes with flow cytometry buffer. When required, a secondary antibody staining was conducted in 100 µl of flow cytometry buffer at 4°C for 30 minutes, followed by two washes with the buffer and subsequent analysis on a flow cytometer (sometimes with a prior 20 minute fixation of the samples in 2 % PFA in flow cytometry buffer). The same staining procedure was applied to HaCaT cells used as a negative control for the STRO-1 antibody, and MG63 cells used as a positive control.

For phenotyping, the Human Mesenchymal Stem Cell Multi-Color Flow Kit (R&D Systems, Minneapolis, USA) and the Human Haematopoietic Stem Cell Flow Kit (R&D Systems) were used, following the same staining procedure. For analysis of proliferation, a Click-iT® EdU Alexa Fluor® 488 Flow Cytometry Assay was used (Life Technologies, Carlsbad, USA). The test was conducted according to the manufacturer's protocol, with 6 hours of incubation with EdU. For apoptosis/necrosis detection, Annexin V Apoptosis Detection Kit eFluor® 450 (eBioscience, San Diego, USA) was used. Single-stained positive controls for apoptosis and necrosis were acquired by incubating cells for 15 minutes at 70°C. Where possible, compensation controls for the fluorophores were prepared with OneComp eBeads (eBioscience) according to the manufacturer's protocol. Briefly, 5 µl of antibody was added to a drop of beads, vortexed, and incubated for 30 minutes in the dark at 4°C. Following this, the beads were washed with flow cytometry buffer, with centrifugation at 400x *g* for 5 minutes. Samples were assayed on a FACS Calibur/Canto II cytometer (BD Biosciences, San Jose, USA) or Guava (Merck Millipore, Billerica, USA) and analysed using FlowJo v10 software (Ashland, USA).

Image Stream cytometry was used for analysis of the morphology and frequency of $CD45^-/GPA^-/STRO\text{-}1^+$ cells, as well as for analysis of STRO-1 expression after Wnt stimulation, as a confirmation of conventional flow cytometry observations. Samples were stained according to the procedures described previously. Data was acquired using a dual camera ImageStream X MkII (Merck Millipore). Data was collected using a 60x objective lens with a numerical aperture of 0.9 and image resolution of ~0.33 µm/pixel. Data capture was performed with INSPIRE® software v.2 (Merck Millipore), with a minimum of 1.2×10^5 and maximum of 6×10^5 in-focus and nucleated cells captured for each sample, leading to a minimum of 500 cells possessing the phenotypes of interest. Single stained controls were run for each fluorophore used, and a compensation matrix was created to calculate spectral overlap. All image display properties were adjusted linearly on representative cell population images for each channel based on the pixel range of the signal, and then applied to the entire data file. The gating and analysis strategy, where relevant, is shown in the respective Figures. The Aspect Ratio Intensity for STRO-1 assesses the distribution of the staining on cells and weights it accordingly. Therefore, cells with an even distribution will have a

value approaching 1, whereas those without an even distribution have a value nearer 0. A data analysis template was generated from the established settings and selected gates, and used for all subsequent analyses.

For fluorescent sorting of different cell populations based on the level of expression of the STRO-1 antigen, MACS STRO-1 isolation was performed using the protocol described in Section 2.2.2, with two additional steps incorporated after the incubation with rat anti-mouse IgM Microbeads. Briefly, cells were incubated with an AF488-conjugated secondary antibody for 20 minutes at 4°C. After two subsequent washes with MACS buffer, samples were separated on magnetic columns.
Sorting based on STRO-1 expression resulted in three different cell populations: STRO-1^{bright}, STRO-1^{+} and STRO-1^{-} fractions as well as the control BMMNC fraction. Granulocytes were gated out of all of these populations. Samples were then used directly for RNA extraction and measurement of Wnt target gene expression.

2.2.5.2 Immunostaining of adherent cells for fluorescence microscopy

Adherent cells were stained for the STRO-1 antigen to assess expression of this marker in BMMNCs straight after adhering in 24-well plates, as well as in positive and negative control cells (MG63 and HaCaT, respectively). Osteopontin staining was conducted on cells subjected to short- and long-term Wnt exposure and cultured in 24-well plates for 14 days. Briefly, prior to staining, the cells were washed twice with PBS and fixed in 4 % PFA for 20 minutes at room temperature, followed by 2 washes in PBS. Non-specific antibody binding was blocked by incubation with 300 µl of blocking buffer for 30 minutes at 4°C. Wells were then incubated with 300 µl of primary antibody: neat STRO-1 hybridoma supernatant per well, containing the anti-STRO-1 antibody, or the Osteopontin antibody at a 1/50 dilution in 1 % BSA in PBS, or 1 % BSA in PBS alone (negative, secondary antibody only control), overnight at 4°C on the rocker. The next day, after 3 washes with 0.5 % Tween/PBS, 300 µl of relevant secondary antibody was added per well (1/100 dilution in 1 % BSA in PBS). Plates were incubated on the rocker in the dark, for 1 hour at room temperature. After washing again twice with 0.5 % Tween/PBS, the nuclei of cells were stained with 4',6-diamidino-2-phenylindole (DAPI, Life Technologies) at 50 µg/ml for 5 minutes. Cells

were kept under PBS and images were taken on a Zeiss Axiovert microscope using AxioVision imaging software (Zeiss, Jena, Germany).

2.2.5.3 CFU-F/CFU-O assays and alkaline phosphatase (ALP) staining

The CFU-F and CFU-O (cultured in basal and osteogenic media, respectively, see Appendix for media composition, Table A.1) potential of SSCs from transiently stimulated BMMNCs was determined by plating cells in different densities in T75 culture flasks or 6-well tissue culture plates. Three different cell seeding densities for each donor were used, due to high inter-donor variability in colony forming potential (5×10^4 cells/cm^2, 1×10^4 cells/cm^2, 5×10^3 cells/cm^2). After 7 days of culture, cells were washed twice with PBS and media were changed. Following another 7 days of culture, cells were washed with PBS and fixed with 95 % ethanol for 10 minutes. Subsequently, after washing fixed cells with dH_2O, cells were stained for alkaline phosphatase (ALP). All reagents were supplied by Sigma. 600 μl of ALP staining solution (400 μl of Napthol AS-MX Phosphate Alkaline Solution and 2.4 mg of Fast Violet B Salts in 9.6 ml of dH_2O) was added to each well. Plates were then incubated for 45 minutes at 37°C. The reaction was stopped by rinsing wells with dH_2O. Colonies which comprised of more than 50 cells with more than 50 % of their area histologically stained (bright purple) were counted as positive. Next, counterstaining was performed, by addition of 600 μl of Gill no.3 hematoxylin for 10 minutes at room temperature, which stains nuclei blue. After rinsing the wells with dH_2O, negative colonies were counted. CFU results are presented as the number of colonies per 10^4 seeded cells, and their ALP expression is shown as proportion of positive colonies of the total number of colonies. Images were taken both before and after counterstaining on a Zeiss Axiovert microscope with the use of AxioVision imaging software (Zeiss) or Zeiss Stemi 2000 microscope with Canon Power Shot G10 digital camera.

2.2.5.4 Alkaline phosphatase (ALP) activity measurement

Measurement of alkaline phosphatase activity was carried out on BMMNCs and STRO-1 selected cells, either after transient exposure to 100 ng/ml Wnt3A (short-term) or continuously subjected to 100 ng/ml Wnt3A for a period of 14 days (long-term) in both basal and osteogenic media. Cells were seeded in 24-well plates, at 2×10^5 cells/cm^2 for BMMNCs and 8×10^4 cells/cm^2 for STRO-1-enriched cells. Briefly,

after the exposure period, cells were digested with collagenase and trypsin, and the pellets resuspended in 600 µl of 0.05 % of Triton-X to lyse cells. After a series of 3 freeze-thaw cycles, lysates were pressed through a syringe with a 0.5 mm needle in order to attain homogeneity of the samples. The colorimetric assay was performed using 10 µl of each sample and 90 µl of substrate solution (0.04g phosphatase substrate (p-nitrophenyl phosphate, PNPP), 10ml 1.5M alkaline buffer solution and 20 ml distilled water). Standards (100 µl/well) were prepared from known p-nitrophenol (end product of ALP enzymatic reaction) concentrations. All reagents were purchased from Sigma. Plates were placed in an incubator at 37°C and protected from light. The incubation time for samples from different patients ranged between 15 - 60 minutes, and was stopped by the addition of 1M NaOH (100 µl/well) before any sample reached a greater intensity of yellow than the highest standard. The colour intensity was measured using an ELx800 microplate reader (Biotek, Winooski, USA) with the absorbance wavelength set to 415nm. Absorbance values were converted into concentrations using the calibration curve from the standards. Results were adjusted for DNA content measured by the PicoGreen assay.

2.2.5.5 dsDNA quantification assay – PicoGreen assay

A dsDNA quantification assay was performed on cell lysates from the above ALP activity assay to control for cell number. The concentration of dsDNA was quantified with the use of Quant-iT™ PicoGreen® dsDNA Reagent (Thermo Fisher, Waltham, USA) according to manufacturer's protocol. Briefly, 10 µl of lysate per well was pipetted into a black 96-well plate, and diluted with 90 µl of TE buffer (Tris/EDTA). A standard curve of known DNA concentration (0, 50, 100, 250, 500, 750 and 1000 ng/ml; 100 µl per well) was prepared from 2 µg/ml stock solution of Lambda DNA standard (Thermo Fisher). Next, 100 µl of 0.5 % PicoGreen in TE buffer was added to all wells, and the plates were incubated in the dark for 5 minutes at room temperature. Fluorescence was measured on an FLx800 fluorescence microplate reader (Biotek) with the excitation/emission wavelength set to 480/520nm, respectively. Results were converted into DNA concentrations using the standard curve.

2.2.5.6 Calcium deposition quantification - Alizarin red S staining

Alizarin red S is a dye which binds selectively to calcium salts and is widely used for calcium histochemistry. It binds ~2 mol of Ca^{2+} per mol of dye in solution (Puchtler *et al.* 1969). Cells cultured in 24-well plates and fixed with 95 % ethanol were stained with a 40 mM (2 %) solution of Alizarin red S at pH = 4.2, for 20 minutes on a rocker. When calcium deposits appeared orange-red, plates were rinsed delicately but thoroughly with dH_2O, and imaged. Next, Alizarin Red was extracted by dissolving in 300 µl of 10 % cetypyridinium chloride solution (in 10mM sodium phosphate Na_2HPO_4, pH = 7.0) per well, with incubation at 37°C for 2 hours to solubilise the stain (Stanford *et al.* 1995). 100 µl of the product was transferred into a clear 96-well plate in duplicates and sample absorbance was measured on a Varioscan Flash microplate reader (Thermo Scientific) at 540nm alongside a standard curve (2 mM, 1 mM, 0.5 mM, 0.25 mM, 0.125 mM, 0.0625 mM, 0.0313 mM, 0 mM, all in 10 % cetylpyridinium chloride solution). The absorbance values were converted into concentrations using the calibration curve from the standards. The values from each condition were normalised to the corresponding cellular DNA concentration, and the data were presented as µM Alizarin Red S/µg DNA.

2.2.5.7 RT-qPCR

RNA extraction

For the short-term and long-term Wnt exposure experiments followed by qPCR for osteogenic gene expression, BMMNCs were seeded in both basal and osteogenic media onto tissue culture plastic at 10^5 cells/cm^2. Subsequent media changes (with or without Wnt) were carried out three times a week after initial tissue culture plastic adherence of the cells, for up to 14 days. Total RNA was extracted using an RNeasy Mini Kit (Qiagen, Venlo, Netherlands). Briefly, cell samples were lysed in 350 µl of buffer RLT. 350 µl of 70 % ethanol was added, and mixed lysates were transferred onto spin columns and centrifuged at 8000x *g* for 15 seconds. Flow-through was discarded, and the columns were washed with 700 µl of buffer RW1 and centrifuged at 8000x *g* for 15 seconds. After discarding the flow-through, the columns were washed twice in 500 µl of RPE, with the final wash centrifuged for 2 minutes at 8000x *g*. The columns were then placed into fresh collection tubes and RNA was released by

addition of 30 µl of RNAse-free water followed by centrifugation at 8000x *g* for 1 minute.

For measurement of Wnt target gene expression in cultured samples, total RNA was extracted using the same procedure, from the same donor BMMNCs, and donor-matched MACS STRO-1-enriched cells (after ~2 weeks of culture).

For measuring the Wnt target gene expression in fresh samples, the PicoPure RNA Isolation Kit (Thermo Fisher) was used, suitable for small cell samples. RNA was extracted from cells after sorting by FACS into STRO-1^{bright}, STRO-1^{+}, STRO-1^{-} and BMMNC populations, not containing granulocytes. Briefly, cell pellets were incubated with 100 µl of Extraction Buffer for 30 minutes at 42°C. After centrifugation for 2 minutes at 3000x *g*, the supernatant was transferred to an equal volume of 70 % ethanol and subsequently onto a pre-conditioned purification column. The samples were centrifuged for 2 minutes at 100x *g* to bind the RNA, immediately followed by centrifugation at 16000x *g* for 30 seconds. The columns were then washed with 100 µl of Wash Buffer 1 and Wash Buffer 2, respectively, with 1 minute centrifugations at 8000x *g*. Another wash with 100 µl of Wash Buffer 2 was followed by a 4 minute centrifugation at 16000x *g*. The columns were then placed into fresh collection tubes and RNA was released by the addition of 11 µl of RNAse-free water and centrifuging at 1000x *g* for 1 minute, followed by 16000x *g* for 1 minute.

RNA concentrations and quality were determined using a NanoDrop ND-1000 spectrophotometer (Thermo Fisher). Samples with a 260nm/280nm absorbance ratio of ~2.0 were considered to be pure RNA.

Reverse transcription

500 ng of RNA from cultured cells was reverse transcribed using the SuperScript® VILO™ cDNA Synthesis Kit, according to the manufacturer's instructions, with the reaction conditions listed in the Appendix, Table A.9. For fresh uncultured cells, 300 ng of RNA was used for reverse transcription. After reverse transcription, each sample was diluted 5x in upH_2O.

Primer design and validation

All Wnt target gene primers were designed to amplify specifically the gene of interest, verified by the BLAST database (http://blast.ncbi.nlm.nih.gov), and checked for

possible secondary structure formation, such as hairpins or primer-dimers, by Primer Analyzer and NetPrimer tools (premierbiosoft.com/netprimer, primerdigital.com/tools/PrimerAnalyser). Primers were designed to span an exon-exon junction and amplify fragments of 65-130 bp. A detailed list of primers (synthesised by Sigma) can be found in the Appendix, Table A.10.
Before RT-qPCR experiments, primers were validated for use in the ΔΔCt method of data interpretation. RT-qPCR was run on a series of dilutions of a cDNA sample from STRO-1^+ cells, and the efficiency of the new primers was assessed and compared with the efficiency of *ACTB* primers. The Ct values for each dilution were used to produce a linear graph, from which the slope of standard curve value (of the linear equation) was used to calculate the efficiency of the primer pair:

$$\text{efficiency } [\%] = (10^{1/\text{slope}} - 1) * 100\ \%$$

The recommended efficiency for RT-qPCR primers is 80 % - 120 %. Primer efficiencies were then compared to the efficiency of *ACTB* primers on another graph, with a slope value below 0.1 (<10 %) indicating that the ΔΔCt method could be used for data interpretation (see Appendix, Figure A.6 - Figure A.12).
Osteogenic marker primers had been designed previously in-house, at the Bone and Joint Research group (listed in the Appendix, Table A.10).

RT-qPCR

The ΔΔCt method of relative quantification of real-time qPCR was performed using Applied Biosystems reagents and the 7500 Real Time PCR detecting system (Applied Biosystems, Foster City, USA). Each 25 μl sample contained 1 μl of cDNA from the reverse transcription reaction mixture, 5 μM of each primer, and 50 % (vol:vol) of SYBRGreen Master Mix. The cycling conditions used were: 50°C for 2 minutes, 95°C for 10 minutes, 40 cycles at 95°C for 15 seconds and 60°C for 1 minute. All reactions were performed in duplicate and the specificity of products was evaluated with the use of melting curves. Amplification products with Ct values >35 were considered artefactual, and the transcript absent. Expression of two housekeeping genes was tested (*ACTB* and *GAPDH)*, and finally relative gene expression levels were normalized using *ACTB* as a reference gene.

Agarose gel electrophoresis

Primer amplification products were visualised by running standard agarose (Sigma) gel electrophoresis (4 % agarose gel in 1X TAE buffer) with 7 µl (per 100 ml of gel) of Gel Red Nucleic Acid Stain (Biotium, Hayward, USA), at 80V for 3 hours, and imaged on an InGenius transilluminator (Syngene, Cambridge, UK). The size of the amplicons was verified as compared to the 50 bp GeneRuler DNA ladder (ThermoFisher; see Appendix, Figure A.7 and Figure A.13).

2.2.5.8 ELISA

ELISA assay (Figure 2.4) was performed in order to quantify the STRO-1 IgM antibody produced in the hybridoma supernatant.

Briefly, 96-well Nunc Maxisorp plates were coated overnight at 4°C with 100 µl of goat anti-mouse IgM antibody in PBS as a capture antibody (see Appendix, Table A.5, for list of antibodies and dilutions used). After three subsequent washes with washing buffer (0.05 % Tween in PBS), the plates were incubated with 300 µl of blocking solution (1 % BSA in PBS) on a rocker for 1 hour at room temperature. After removal of the blocking solution and three further washes in washing buffer, 50 µl of appropriate controls, standards and samples were added. The control was hybridoma culture media at a dilution parallel to sample and PBS. The standards used for the dilution curve comprised of an isotype control antibody to mouse IgM from murine myeloma and commercially available purified STRO-1 antibody. For the standard curves, 5x dilutions starting at 10 ng/ml were used. The hybridoma supernatant was added at 2x dilutions starting from 1 in 20 000. All dilutions were made in 1 % BSA in PBS. Plates were incubated for 2 hours at room temperature on a rocker. After three washes with washing buffer, 50 µl of anti-mouse IgM peroxidase-conjugated antibody was added and incubated for 2 hours at room temperature on a rocker. After another three washes, 50 µl 3,3' tetramethylbenzidine (TMB) ELISA Substrate Solution (eBioscience) was added and incubated for 20 minutes in the dark. The reaction was stopped by the addition of 25 µl of 2M HCl. Colour intensity was measured using an ELx800 microplate reader (Biotek) with the absorbance parameters set to 450nm with 540nm plate correction. The absorbance values were converted into concentrations using the calibration curves.

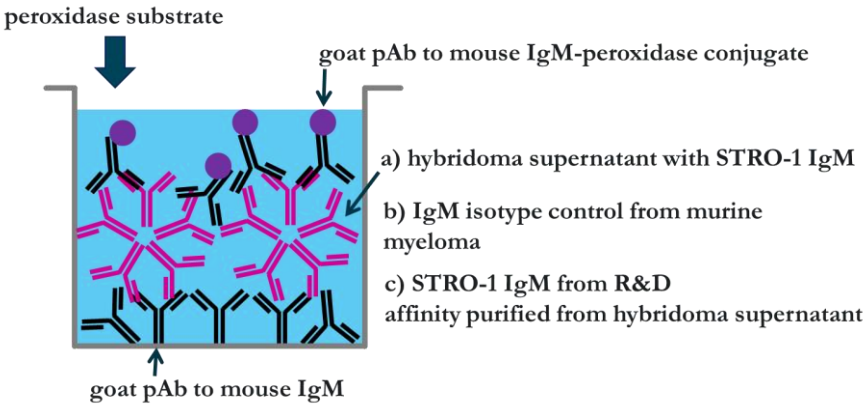

Figure 2.4 STRO-1 antibody ELISA.

One well representation of antibody reactions. a) or b) or c) represent different tested options – either the IgM content of the hybridoma supernatant (a) or isotype (b) or purified (c) controls for acquiring standard curves. pAb, polyclonal antibody.

2.2.5.9 Liposome preparation

Liposomes were prepared using the extrusion method (see Figure 2.5). Briefly, depending on the composition of liposomes, a combined total of 14 μM of different lipids were dissolved in 1 ml chloroform:methanol (3:1) in a 10 ml round-bottomed flask, and dried to a thin film under a nitrogen gas stream for 5 minutes, with further evaporation overnight at room temperature in a vacuum cabinet. Several different lipid compositions were attempted and a detailed list of molar ratios can be found in the Appendix, Table A.12 and Table A.13. Lipids with different carbon chain lengths and saturation were tested. PEGylation was achieved by adding 5 molar % DSPE/PEG lipid. For lipid composition optimisation experiments, the thin lipid layer was hydrated the next day with 1 ml PBS, placed in a water bath for 1 hour at 37°C (or 56°C for DSPC lipid), ensuring it was above the gel to liquid phase transition temperature (Tc) of the main lipid in the composition. The lipid solutions were vortexed every 10 minutes. Extrusion was carried out on a heating block (Avanti Polar Lipids, Alabaster, USA) at 37°C (or 56°C for DSPC lipid), 41 times through a 100 nm membrane (GE Healthcare/Whatman, Little Chalfont, UK). In order to minimise the contamination of the liposome samples with free lipids, the solutions were ultracentrifuged at 100 000x *g* for 60 minutes at 4°C. The liposome pellet was then resuspended in 1 ml PBS and liposomes were subsequently stored at 4°C until used, for up to three weeks.

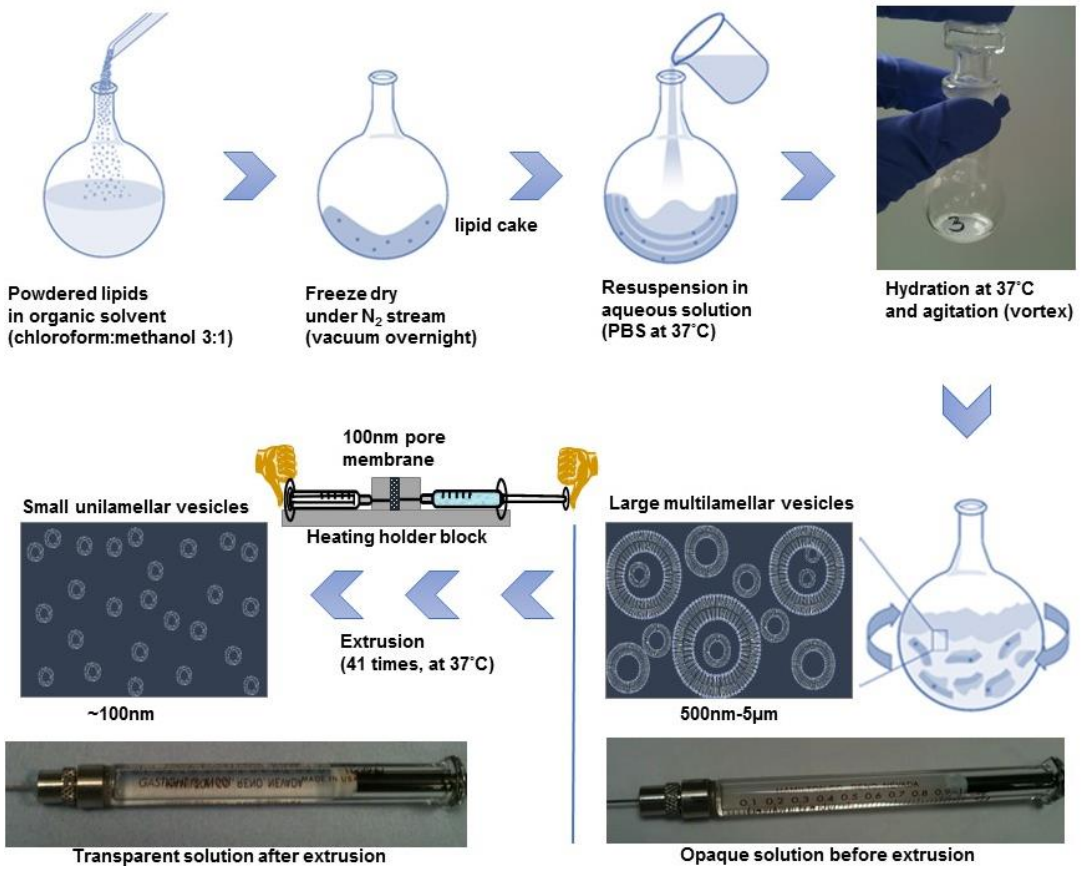

Figure 2.5 Liposome preparation.

When Wnt3A protein was to be incorporated into the liposome preparations, two approaches were adopted. Firstly, loading was carried out during the lipid cake resuspension step, with 2 µg/ml of Wnt3A (50 nM total) being dissolved in PBS at 37°C used for hydration. Therefore, Wnt3A protein was encapsulated/incorporated within the liposomes while they were forming. Another approach involved incubating the already-formed liposomes with 2 µg/ml Wnt3A protein at room temperature. The highest possible liposome concentration was used for Wnt3A incorporation (~10^{14} particles/ml), to allow for the maximum possible loading efficiency of the protein. Assuming the protein associated with the membrane, due to its hydrophobicity, 10^{14} liposome particles, each with surface area ~30 000 nm^2, were sufficient to accommodate 3 x 10^{16} Wnt3A protein molecules of approximate diameter of 3 nm; approximated for ~40kDA proteins (Erickson 2009). After Wnt incorporation, the liposomes were ultracentrifuged at 100 000x *g* for 60 minutes at 4°C to get rid of the unbound protein, and resuspended in PBS at the initial volume.

For visualisation of liposomes for uptake studies, the particles were stained with lipophilic dyes (3,3'-dioctadecyloxacarbocyanine perchlorate, DiO or 1,1'-dioctadecyl-3,3,3',3'-tetramethylindocarbocyanine perchlorate, DiI, Life Technologies) after preparation, by incubation with 3 µl of 1 mM dye solution per 1 ml of liposomes. Subsequently, to get rid of unbound dye, particles were ultracentrifuged at 100 000x *g* for 60 minutes at 4°C, and liposomes were resuspended at the initial volume with PBS. To monitor the uptake of liposomes in fresh bone marrow isolates or their distribution *in vivo*, lipophilic dyes (100 µM DiO or 1,1'-dioctadecyl-3,3,3',3'-tetramethylindotricarbocyanine iodide, DiR) were incorporated into the liposomes during their preparation, where they were mixed with lipids before the freeze-drying step. Visualisation of liposomes was also possible when a biotinylated lipid (DSPE-PEG Biotin, 2 molar %) was incorporated into the preparation, and after formation, the liposomes were incubated with 30 µl of 0.5 mg/ml streptavidin-AF647 conjugate per 1 ml of liposomes (~1:1 biotin to streptavidin ratio) for 20 minutes at room temperature. Next, liposomes were ultracentrifuged at 100 000x *g* for 60 minutes at 4° to get rid of the unbound protein, and resuspended to their initial volume with PBS. Liposomes were also stained by incorporating 100 mM sodium fluorescein, during the lipid cake resuspension step, where this dye was dissolved in PBS used for hydration. This hydrophilic dye self-quenches at high concentrations when encapsulated in the core of nanoparticles, but upon uptake of nanoparticles by cells, the dye is released into the cytoplasm, resulting in fluorescence (Weinstein *et al.* 1977).

2.2.5.10 Liposome characterisation

Transmission electron microscopy (TEM)

Liposomes were examined for unilamellarity and an approximation of size under TEM. An aliquot of the sample was diluted 1000x in PBS and fixed for 5 minutes. 2.5 % glutaraldehyde was chosen as a fixative, as it reacts with phospholipids containing free amino groups (i.e. phosphatidylserine or phosphatidylethanolamine), and such lipids were used for the liposome preparations. 5 µl of fixed liposome sample was applied to carbon-coated electron microscope grids coated with formvar. Grids were immediately negatively stained with 1 % ammonium molybdate solution (with 1 % ammonium acetate and 1 % of sucrose) for 10 seconds. The grids were examined

using a H7000 Transmission Electron Microscope (Hitachi, Tokyo, Japan) at an accelerating voltage of 75kV at 20 000-100 000x magnification.

Dynamic light scattering (DLS) analysis

Size distribution of all liposome preparations was examined by dynamic light scattering (DLS, also called photon correlation spectroscopy) on a Beckman Coulter N4 PLUS Particle Size Analyzer (Beckman Coulter, Brea, USA). This technique is based on the fact that differentially sized particles scatter light and undergo Brownian motion in a different manner (principle in Figure 2.6; further description in Section 5.1). Each sample was placed in a cuvette at a concentration giving between 5 x 10^4 – 1 x 10^6 counts/s (standard cuvette: 1ml of upH_2O + 50 µl of sample; narrow cuvette: 300 µl of upH_2O + 15 µl of sample). The samples were subjected to laser light at 90° and 23° angles twice for 300 seconds. Data analysis resulted in a mean size distribution for particles in each sample tested.

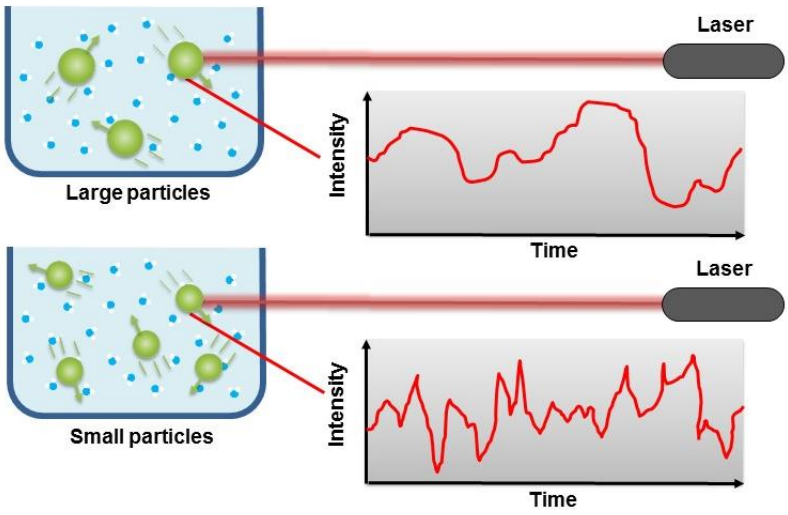

Figure 2.6 Dynamic light scattering.

Hypothetical DLS of large and small particles, and fluctuations of scattering over time due to the fact that molecules in solution are undergoing Brownian motion.

Nanoparticle tracking analysis (NTA)

The size distribution and concentration of a subset of liposome preparations was analysed by nanoparticle tracking analysis (NTA) on a NanoSight LM10 (Malvern Instruments, Malvern, UK) using NTA3.0 software. This technique is similar to DLS, but because the particle paths are recorded under a microscope, it allows analysis of

particles on individual basis, as well as the analysis of particle concentration when a microfluidics setup is used (Figure 2.7; see Section 5.1 for further description). Before analysis, samples were diluted 250 000x in PBS and videos were recorded at 25 frames/second, with 1500 frames analysed.

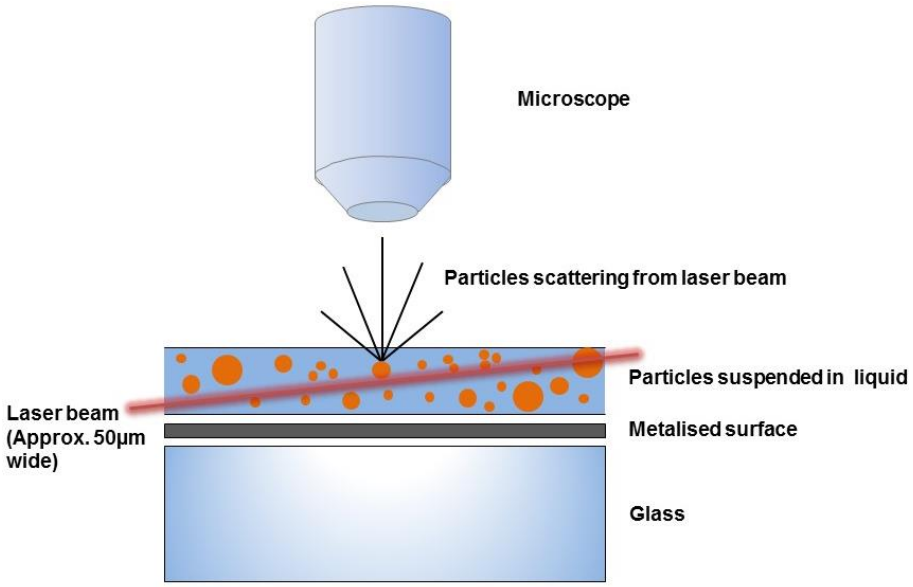

Figure 2.7 Nanoparticle tracking analysis.

Due to the presence of a CCD camera and a microfluidic system, nanoparticle size is assessed on a particle by particle basis and concentration of the particles can be determined.

Scanning ion occlusion sensing (SIOS)

The size distribution and concentration of liposomes upon prolonged storage (>1.5 months at 4°C) was assessed by scanning ion occlusion sensing (SIOS) on a qNano benchtop device (further description in Section 5.1), as it offers higher resolution than the DLS and NTA techniques. Before analysis, samples were diluted 100x in PBS. An NP100 pore size was used for analysis.

Gas chromatography (GC)

Liposome formation efficiency and the degree of PEGylation of liposome preparations were assessed by GC. Separation of fatty acids by GC is based on the difference in temperatures at which they become volatile, which in turn is dependent upon carbon chain length and number and position of double bonds. Separation also depends on the interaction between fatty acids and the lining of the GC column. The

method used for processing the samples for GC involved the addition of a methyl group to the carboxylic end of the fatty acid to form a fatty acid methyl ester (FAME) by reaction with a methyl donor in the presence of the catalyst. This allowed for separation at moderate temperatures and released the fatty acids from phospholipids. A lipid with known concentration, different from the lipids used in the liposomes (15:0), was added to each sample and used as a standard for subsequent lipid concentration calculations. A 150 µl aliquot of each sample in a glass tube was diluted up to 1 ml and 50 µl of 2 mg/ml standard was added to each sample, followed by the addition of 5 ml of chloroform:methanol (2:1), containing 50 µg/ml butyratedhydroxytoluene (BHT) antioxidant. Next, 1 ml of 1M NaCl was added, followed by vortexing and centrifugation at 680x *g* for 10 minutes at room temperature, with low brakes. The lower phase was subsequently collected with a glass Pasteur pipette, transferred to a fresh glass tube, and dried under a nitrogen gas stream at 40°C for 20 minutes. Next, 0.5 ml of dried toluene was added and vortexed, before addition of 1 ml of methylation reagent (methanol containing 2 % (v/v) H_2SO_4), and gentle mixing by inversion. The capped tubes were heated for 2 hours at 50°C, after which they were allowed to cool. Next, 1 ml of neutralising solution (0.25M $KHCO_3$, 0.5M K_2CO_3) and 1 ml of dry hexane was added and the solution was vortexed, and centrifuged at 200x *g*, for 2 minutes at room temperature, with low brakes. Subsequently, the upper phase was collected into a new glass vial, and dried under nitrogen gas stream at 40°C, and dissolved in 75 µl of hexane. The sample was then transferred into a GC autosampler vial, and any remaining lipid in the previous vial was again extracted with 75 µl of hexane, added to the GC vial. Samples were stored in -20°C before being analysed on the Agilent G1530A 6890 series chromatograph. Peaks on the chromatogram were identified automatically using ChemStation software (Agilent Technologies, Santa Clara, USA), based on their retention times, set manually by running defined standards beforehand, and the area of the peaks was used for concentration calculations, based on the following equation:

$$Fatty\ acid\ concentration\ (\mu g/ml) = \left(\frac{Ap}{Ai}\right) \times\ mi\ \times\ V$$

where:

Ap – area of peak of interest,
Ai – area of peak of internal standard,
mi – mass of internal standard added,
V – volume of sample extracted.

2.2.5.11 Luciferase assay – liposomal and neat Wnt3A activity

The luciferase assay was performed on a 3T3 mouse embryonic fibroblast cell line (Enzo Life Sciences), which was modified to expresses the firefly luciferase reporter gene under the control of Wnt-responsive promoters (TCF/LEF). The change in chemiluminescence measured after the addition of luciferase substrate acts as an indicator of active Wnt signalling. Cells were used for the assay between passages 2-5 after defrosting, and no later than passage 11 overall, as the responsiveness of the cell line diminishes at higher passages. Briefly, cells were seeded onto white, clear-bottomed, 96-well plates, at 1.5 x 10^4 cells/well in 50 µl assay medium (Enzo Life Sciences or made in house, see Appendix, Table A.1) and incubated overnight at 37°C. Next, agonists (BIO, LiCl or Wnt3A protein) or liposomal Wnt3A preparations were added at a total volume of 50 µl/well in DMEM, in duplicate. In the case of tested liposomes, the volume added was 5, 10 or 15 µl/well. Plates were again incubated overnight at 37°C for ~18 hours, unless stated otherwise, before addition of 100 µl/well of luciferase substrate diluted in luciferase buffer (Steady-Glo, Promega, Madison, USA). After 10 minutes of reaction and cell lysis, the chemiluminescence signal was read (0.1 second/well) on a Varioscan Flash microplate reader (Thermo Scientific). To control for cell count, cell lysates were analysed for dsDNA content, as described previously (Section 2.2.5.5).

2.2.5.12 Protein quantification within lipids – liposomal Wnt3A incorporation

Quantification of Wnt3A protein in liposomal preparations was carried out using a fluorescent CBQCA Protein Quantitation Kit (Molecular Probes, Eugene, USA), according to the manufacturer's protocol. Briefly, Wnt3A protein standards (10, 20, 50, 100, 200 ng) and liposomal Wnt3A (150 µl) were dissolved in 0.1 M sodium borate at pH = 9.3, to achieve a final volume of 270 µl. Next, 10 µl of 20 mM of KCN was added to each sample and vortexed. Following this, 20 µl of 5 mM ATTO-TAG CBQCA solution was added, and samples were incubated protected from light for 3

hours at room temperature. After the incubation period, each sample had fluorescence read in duplicate in a black 96-well plate, with excitation wavelength of 465 nm and an emission wavelength of 550 nm, using a Varioscan Flash microplate reader (Thermo Scientific). The values were converted into concentrations using the calibration curve from the neat Wnt3A protein.

2.2.5.13 Western blotting – liposomal Wnt3A release

Gel electrophoresis for Western blotting was performed using Bio-Rad equipment. 10 % resolving gels were made (all recipes in Appendix, Table A.3) with 10 wells in a stacking gel (ProtoGel, National Diagnostics, Atlanta, USA). 10 µl of molecular weight marker (Precision Plus Protein All Blue Standards, Bio-Rad, Hercules, USA) was used to allow visualisation of movement of the proteins down the gel during electrophoresis and as an evaluation of Western blot transfer efficiency. Liposome and protein samples were prepared at a 1:1 ratio with SDS Blue Loading Buffer (New England BioLabs, Ipswich, USA) with 10 % dithiothreitol (DTT, BioLabs) and were heated at 95°C for 5 minutes. In total 50 µl of liposome samples and 20 µl of Wnt3A protein as standards (5, 10, 50 ng) were pipetted into wells and 10 µl of loading buffer was pipetted into empty wells. Electrophoresis was performed at 150V for ~80 minutes. Next, methanol-activated polyvinylidene fluoride (PVDF) membranes (Immobilon-P, Merck Millipore) were used for protein transfer, which was run at 100V for 60 minutes at 4°C. Membranes were then incubated with the primary anti-Wnt3A antibody, diluted at 1/10000 in 10 ml 5 % milk for 2 hours at room temperature on a shaker. Next, membranes were washed three times for 5 minutes each in washing buffer (0.05 % Tween in PBS), before being incubated with the secondary antibody conjugated with horseradish peroxidase (HRP), diluted at 1/3000 in 5 % milk for 1 hour at room temperature. Membranes were then washed again with washing buffer before treatment with Immobilon™ Western Chemiluminescent HRP Substrate (Merck Millipore). Membranes were imaged within 5 minutes using Versadoc (Bio-Rad) and quantified using Quantity One Software Version 4.6.8 (Bio-Rad).

2.2.5.14 Association of Wnt3A with liposomes – single molecule spectroscopy

Protein tagging for single molecule spectroscopy

To assess whether Wnt3A protein was associating with the liposomes, single-molecule spectroscopy experiments were carried out. However, to enable visualisation, both liposomes and Wnt3A protein required a fluorescent label. Liposomes were stained by incubation with DiO (see 2.2.5.9), but a "carrier-free" version of the Wnt3A protein (R&D Systems) was conjugated with a fluorescent tag. This process required a high degree of optimisation, and initially 3 different dyes were tested: Atto680-maleimide (Sigma), AF647-maleimide (Molecular Probes) and Atto680-NHS (Sigma) at 3:1 or 10:1 dye:protein ratios, in PBS, or $NaHCO_3$ buffers with pH = 8.3 or 9. This was initially performed on BSA protein and subsequently on Wnt3A. Finally, a protocol was created where 75 µl (4 µg/1 µM) of Wnt3A protein was tagged or 75 µl (6.5 µg, 1 µM) BSA as control with 10 µM dye, for 2 hours at room temperature with gentle agitation (50 rpm). Following this, the protein was purified from the unbound dye on Micro Bio-Spin Chromatography Columns (BioRad). The buffer in the columns was exchanged with 0.5 % CHAPS, 0.1 mM EDTA, to match the Wnt3A solvent used by the supplier prior to protein lyophilisation. Briefly, 500 µl aliquots were applied to the columns and centrifuged for 1 minute at 1000x *g*, and this process was repeated 4 times. Next, 75 µl of samples was applied directly to the centre of the columns, and centrifuged for 4 minutes at 1000x *g*. Purified, tagged protein was stored at 4°C for up to 1 month.

The fluorescent tag was visualised using sodium dodecyl sulfate polyacrylamide gel electrophoresis (SDS-PAGE) and a far red fluorescent scanner (described below) and the activity of the tagged protein was tested on the luciferase reporter cell line (see 2.2.5.11).

SDS-PAGE

Gel electrophoresis and sample preparation was carried out as described in Section 2.2.5.13, but ~30 µl of tagged-protein sample (50-500 ng protein) was pipetted into wells. The fluorescent tag on the protein within the gel was imaged on the LI-COR Odyssey system (LI-COR, Lincoln, USA), using the 700nm channel. The quantity of loaded protein was assessed by subsequent staining of the gel with a Proteo Silver

Stain Kit (Sigma). All procedures were carried out at room temperature with gentle agitation. Briefly, the gel was fixed in 50 ml of fixing solution (50 % ethanol, 10 % acetic acid) for 1 hour, followed by a 10 minute wash in 50 ml of 30 % ethanol and a 10 minute wash in 100 ml of upH_2O. Next, the gel was incubated with 20 ml of the sensitizer solution (1 % ProteoSilver Sensitizer) for 10 minutes, washed twice with 100 ml of upH_2O, and incubated with 20 ml of silver solution (1 % ProteoSilver Solution) for 10 minutes. The gel was then washed with 100 ml of upH_2O for 1 minute and the developer solution (5 % ProteoSilver Developer 1, 0.1 % ProteoSilver Developer 2) was added for 4 - 12 minutes until bands were clearly visible, at which point the reaction was stopped by adding 1 ml of the ProteoSilver Stop Solution for 5 minutes. Finally, the gel was washed with 100 ml of upH_2O and imaged on an HP G4010 Scanjet Photo Scanner.

Single molecule spectroscopy - Total internal reflection fluorescence microscopy (TIRFM) measurements

Firstly, glass slides for single molecule analysis by TIRFM were prepared. Borosilicate glass coverslips (VWR, Radnor, USA) were cleaned using an argon plasma cleaner (PDC-002, Harrick Plasma) for 1 hour to remove any fluorescent residues. 9 x 9 mm Frame-Seal Incubation Chambers (Bio-Rad) were affixed to the glass coverslips, and 75 µl of 0.01 % poly-L-lysine solution (Sigma) was added on the inside of the chamber and incubated for at least 30 minutes, before being washed twice with filtered PBS. Next, 100 µl of 100x diluted liposome sample was placed on each slide immediately prior to imaging, and 1 µl of 4000x diluted protein was added to the slide and mixed by pipetting. As a negative control, 0.1 % of Triton-X in PBS was added to destroy the liposomes. Imaging was performed using a total internal reflection fluorescence microscope constructed "in house" (Figure 2.8). This imaging technique restricts the detectable fluorescence signal to within 200 nm from the sample slide. For each dataset, 3 x 3 image grids were measured in three different regions of the cover slide. The distance between the 9 images measured in each grid was set to 100 µm, and was automated to prevent user bias. Images were recorded at 33 frames per second for 100 frames, firstly from the red channel (AF647 emission) with 641 nm illumination, followed by 100 frames in the green channel (DiO emission) with 488 nm illumination.

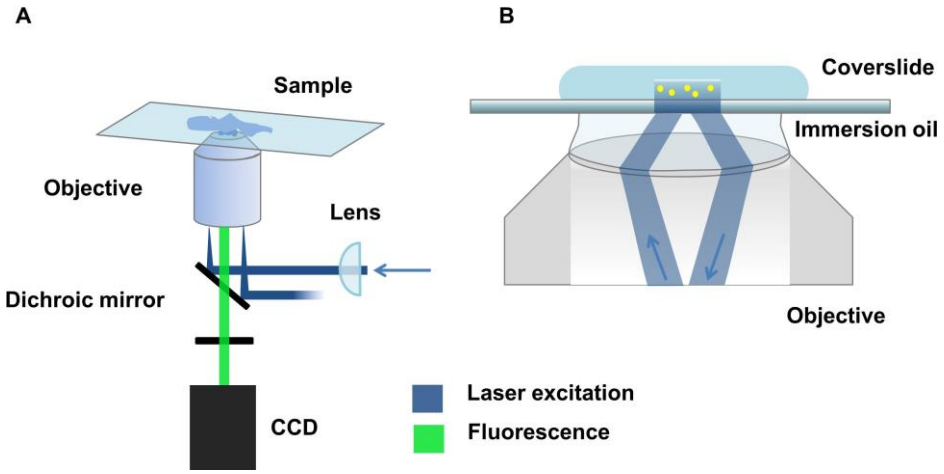

Figure 2.8 Total internal reflection fluorescence microscopy.

A schematic of TIRF microscope setup (A) and a side-view of the excitation volume (B), showing that the illumination is limited to a region close to the coverslip surface.

Single molecule spectroscopy - Two-colour coincidence detection (TCCD) measurements

Samples were diluted to concentrations of approximately 100 pM, before being immediately added to a gel-loading tip attached to the inlet of a simple one-channel polydimethylsiloxane (PDMS) microfluidic device measuring 25 μm high and 100 μm wide, mounted onto the single-molecule confocal microscope (Figure 2.9). The confocal volume was focused into the centre of the channel, and the sample was passed through the channel by withdrawing it from the device at the outlet channel at a flow rate of 100 μL/hour, achieved by attaching the outlet to a syringe pump (Harvard Apparatus, Holliston, USA). Laser wavelengths were 488 nm and 633 nm, and their intensities at the back-port of the instrument were 2 mW. Data were collected for 400 seconds (photons counted in time-bins of 50 μs). As a negative control, 0.025 % solution of CHAPS was added to destroy the liposomes.

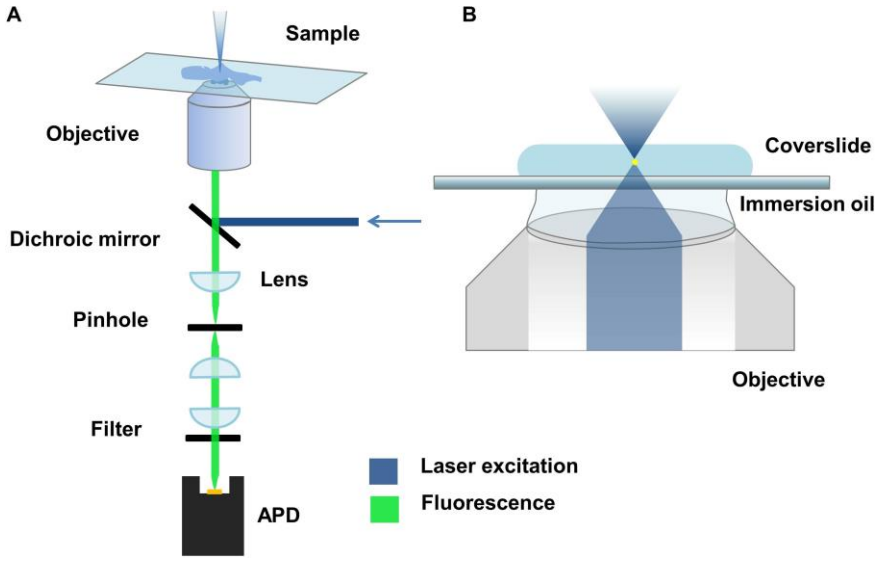

Figure 2.9 Two-colour coincidence detection.

A schematic of the confocal microscope setup (A) and side-view of the confocal volume (B), showing that the excitation is restricted to a small volume (~1 um diameter, ~0.5 fL); by working at subnanomolar concentrations, less than one fluorophore on average will be excited at any given time.

Data from TIRFM and TCCD was analysed using custom-written procedures in Igor Pro (Wavemetrics, Portland, USA). The coincidence (Q) for both methods was calculated according to the following equation:

$$Q = \frac{C - E}{A - E}$$

Where :

Q – association quotient,
C – number of coincident events in both red and green channels,
E – estimated rate at which coincident events occur by chance,
A – events rate in the green channel.

2.2.5.15 Liposome cytotoxicity - cell viability assay

To test for potential cytotoxicity of the liposomes on adherent BMMNCs, a RealTime-Glo™ MT Cell Viability Assay (Promega) was performed, according to the manufacturer's protocol. This method allows for real-time determination of cell viability, by measuring their reducing potential and therefore their metabolism. Viable cells reduce the cell-permeant pro-NanoLuc® substrate, and generate a substrate for NanoLuc® luciferase, both of which are added to culture. The bioluminescent signal correlates with the number of viable cells. Briefly, BMMNCs at P1 were seeded onto

white, clear-bottomed, 96-well plates, at 1.5 x 10^3 cells/well in 50 µl of αMEM supplemented with 5 % FBS and antibiotics (100 U/ml penicillin and 100 µg/ml streptomycin) and maintained at 37°C. After 1 hour, 50 µl of 2x concentrated reaction compound (substrate and enzyme) was added to each well, followed by luminescence signal readout (0.1 second/well) on a Varioscan Flash microplate reader (Thermo Scientific). Next, 5 µl of liposomes (~10^7 particles/cell; or PBS as a control) and 5 µl of 2x concentrated reaction compound were added in triplicate wells, followed by luminescence signal readout at 1, 3, 6, 18, 24 and 48 hours of culture at 37°C.

2.2.5.16 *In vitro* liposome uptake – cytometry and confocal microscopy

Flow cytometry

Uptake of liposomes, double-labelled with sodium fluorescein and DiI, by adherent BMMNCs at P1 was studied by flow cytometry. Cells were seeded into 6-well plates at 4 x 10^4 cells/well, allowed to adhere overnight, and serum starved (2 ml αMEM supplemented with 0.5 % FBS and 100 U/ml penicillin and 100 µg/ml streptomycin per well) for 24 hours. Next, 10 µl of liposomes were added per well (~10^7 particles/cell). After 1, 3, 6, and 24 hours cells were trypsinised and assayed by flow cytometry on a Guava Easycyte Mini Flow Cytometer (Merck Millipore).
Next, uptake of DiO-labelled or AF647-labelled liposomes was studied by flow cytometry on both adherent BMMNCs at P1 and fresh bone marrow isolates after 3 hours of incubation with ~10^6 liposomes/cell. For the cultured cells, the setup was as above, but with 10x lower seeding density. For fresh bone marrow isolates, 100 µl liposomes were added to 10^7 cells in suspension rotation culture. Following the 3 hour incubation at 37°C, cells were assayed by flow cytometry on a FACS Canto II cytometer (BD Biosciences, San Jose, USA). All flow cytometry experiments were analysed using FlowJo v10 software (Ashland, USA).

Image Stream cytometry

Uptake of DiO-labelled or AF647-labelled liposomes was studied by Image Stream cytometry. Fresh bone marrow isolates (10^7 cells) were incubated for 3 hours with 100 µl liposomes (~10^6 liposomes/cell) in suspension rotation culture. Following this, immunostaining for CD14, STRO-1 and GPA was carried out as described previously (Section 2.2.5.1). Depending on whether the cells were incubated with DiO-labelled or

AF647-labelled liposomes, a secondary antibody against STRO-1 was used conjugated with AF647 or AF488, respectively. Data were acquired and analysed as described previously (Section 2.2.5.1).

Confocal microscopy

Uptake of liposomes by cells, and colocalisation of liposomes with endosomes or lysosomes, were studied by confocal microscopy. BMMNCs at P1 were seeded onto glass coverslips (10^5 per coverslip) in a 6-well plate, and allowed to adhere for 6 hours in culture medium (1.5 ml of αMEM supplemented with 10 % FBS and 100 U/ml penicillin and 100 µg/ml streptomycin per well), followed by overnight culture in starving medium (1.5 ml αMEM supplemented with 0.5 % FBS and 100 U/ml penicillin and 100 µg/ml streptomycin per well). Next, 50 µl of DiO-labelled liposomes (~10^7 particles/cell) were added to each well in fresh medium (1.5 ml αMEM supplemented with 5 % FBS and 100 U/ml penicillin and 100 µg/ml streptomycin per well), and cultured for 1, 3 or 24 hours. Subsequently, the cells were washed twice with PBS and fixed in 4 % PFA for 20 minutes at room temperature, followed by two washes in PBS. Staining was then carried out at room temperature. Briefly, cells were incubated for 1 hour in blocking and permeabilisation buffer (see Appendix, Table A.2), followed by 3 hours of incubation with anti-LAMP1 or anti-EEA1 antibodies (Appendix, Table A.5). After washing twice with 0.5 % Tween/PBS, appropriate secondary antibodies, conjugated with AF594, were added. After washing again twice with 0.5 % Tween/PBS, nuclei of cells were stained with DAPI at 2 µg/ml for 20 minutes. Next, cells were washed twice with PBS and coverslips were mounted with Fluoromount™ Aqueous Mounting Medium on a glass slide. Images were taken at 63x magnification on a Leica DMi8 confocal microscope.

2.2.5.17 *In vivo* liposome distribution

Animal work was carried out under the project license 30/2880, with personal licence number of the operator I1211ECA0, on 7.5 week old MF1 male mice (n = 3). Mice were anaesthetised by intraperitoneal injection of 250 µl of 1:1 Hypnorm/Hypnovel, and a 5 mm incision was made and the left femur surface was exposed while carefully preserving the periosteum. Next, a 1mm drill bone defect was created in the femur of the animals (Figure 2.10). Within 1 hour of the procedure, 200 µl of liposomes in PBS

were injected systemically *via* the tail vein, and the animals were imaged on IVIS Lumnia series III, with the Living Image Software 4.3.1 (PerkinElmer, Waltham, USA), using a 0.5 second exposure, directly after the injection (0 hours), and 24 and 48 hours after the injection. After 48 hours, the animals were euthanised and their organs (liver, spleen, lung, kidney, femurs) were imaged, before preservation in 4 % PFA fixative. Two mice received an injection of DiR-labelled liposomes, and one was treated as a control, with injection of non-labelled liposomes.

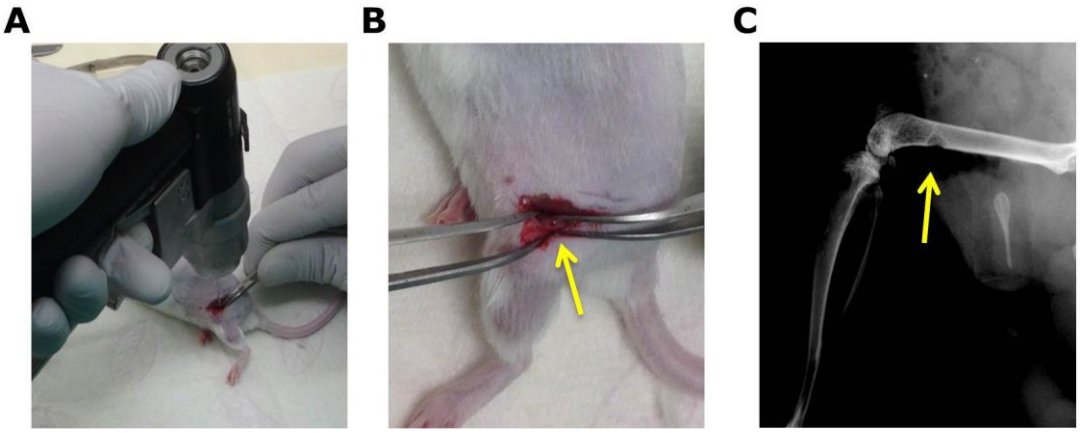

Figure 2.10 Drill bone defect in murine femur.

The defect was created by drilling a whole in the murine left femur (A) and is clearly visible (B). X-ray picture (C) of the drill defect courtesy of Dr Janos Kanczler, Bone and Joint Research Group, University of Southampton.

2.2.6 Statistical analysis

Statistical analysis was performed using GraphPad Prism 6 software (GraphPad, La Jolla, USA) and Sigmaplot 13 software (Systat Software, San Jose, USA). Differences in all the assays were analysed first by testing for the normality of data distribution with Shapiro-Wilk's test. For data not normally distributed, nonparametric tests were used. For the same donor samples exposed to Wnt protein or to control, paired analysis was conducted. The significance threshold was set at $p < 0.05$. Details about data presentation (mean *vs.* median) and statistical tests used can be found in figure legends.

Chapter 3

Identification and analysis of putative skeletal stem cell populations in human bone marrow

3.1 Introduction

The aim of this chapter was to develop flow cytometric techniques for the study of freshly isolated human bone marrow, to determine the cellular composition of human bone marrow related to age or sex, to identify putative stem cells based on previous published surface marker characteristics, and to measure intrinsic levels of Wnt signalling in these populations, for future studies to address how therapeutic interventions may influence the behaviour of human skeletal stem cells.

Bone marrow is soft tissue residing in the cavities of bones, and contains blood cell lineage and stromal components, which provide the niche for haematopoietic and skeletal stem cells (SSCs; see Section 1.1.3 for details on the bone marrow niche). The bone marrow is known to contribute substantially to the tissue that forms after fracture, probably because it is rich in the stem cell/progenitor cell populations. It is therefore a very suitable model tissue for studying how therapeutic molecules may affect these stem cell populations and how they may be developed to enhance fracture healing clinically. Human bone marrow is often surplus material after hip replacement surgery and so is a particularly convenient cell source for the studies described in this thesis. However, before this can be done, it is necessary to have a fast and convenient technique for studying the phenotypic and functional characteristics of these cells. Several methodologies fit for this purpose have been developed to date, the most prominent of which is flow cytometry.

Flow cytometry is a technique developed by Wallace Coulter in the 1950s, when he designed the "Coulter counter" to count red blood cells in suspension (Coulter 1956). The device allowed cell sizing to take place based on a detectable change in the electrical characteristics of the path whenever a cell passed through it, and the technology was called the "Coulter principle". The first fluorescence-based flow cytometry was developed by Wolfgang Göhde from University of Münster in 1968, to measure cellular DNA content stained with fluorescent dyes (Dittrich and Gohde 1969). The first fluorescence-activated cell sorting (FACS) machine, designed by Len Herzenberg at Stanford University (Herzenberg *et al.* 1976), which combined fluorescent flow cytometry and subsequent cell sorting, was commercialised by Beckton Dickinson in 1974. Since then, with the discovery of new fluorescent dyes

and the development of monoclonal antibodies in 1975 by Georges Köhler and César Milstein (Kohler and Milstein 1975), the field has evolved very rapidly to become one of the main analytical methods in cell biology.

In flow cytometry, cells labelled with fluorescent dyes or dye-conjugated antibodies flow in a single file stream past a series of lasers, causing the dyes to be excited and detected specifically according to their individual excitation and emission wavelengths. Therefore, it is possible to measure the intensity for each fluorescent parameter and extrapolate it to the expression level of the antibody-targeted antigen of interest, for every cell. Flow cytometry also measures the light scattering properties of cells. The forward scatter (FSC) enables assessment of the relative size of the cell, as large cells refract more light than smaller ones leading to high forward scatter signals (and *vice versa*). Conversely, the side scatter (SSC) provides information about the granularity of a cell or the smoothness of a cell's membrane. It can be inferred that a rough apoptotic cell or an eosinophil with many granules would have high side scatter signals. A correlated measurement of FSC *vs.* SSC can allow for cell type differentiation within heterogeneous populations, such as in the case of blood analysis, where lymphocytes, monocytes and granulocytes can be easily distinguished without the need for fluorescent labels. For sorting, a charge is placed on each droplet containing a cell, after its fluorescence or light scatter intensity measurement, and the droplets are diverted into containers based on their charge (Figure 3.1). Nowadays, a state-of-the art flow cytometer supports up to 10 lasers and theoretical detection of up to 24 parameters although, due to limitations such as spectral overlap of fluorescent dyes, the maximum number of detectable parameters is 18.

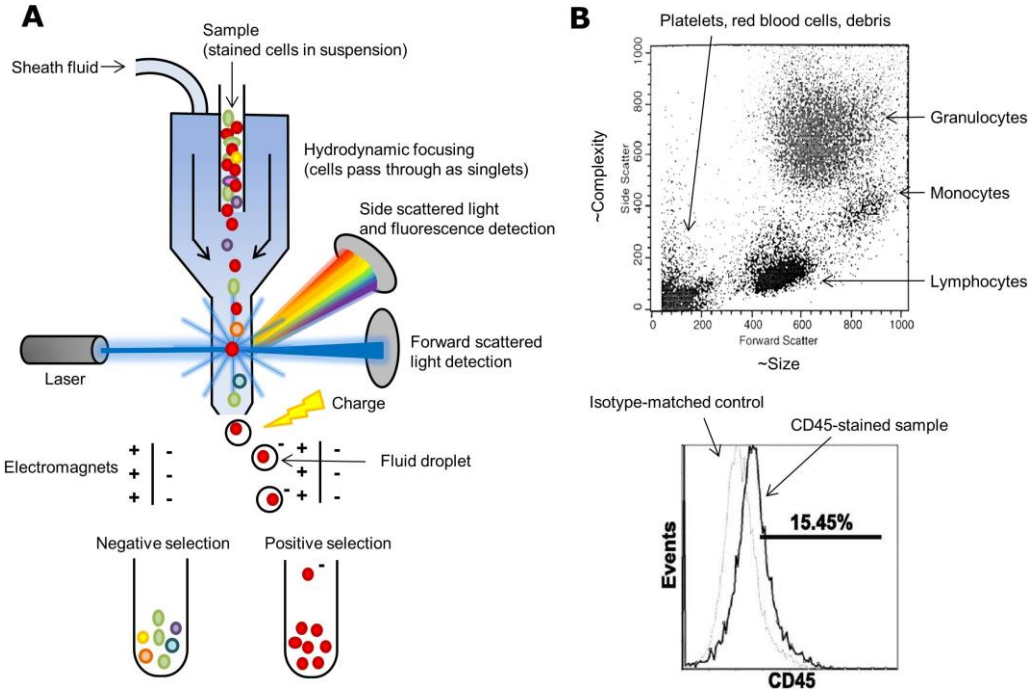

Figure 3.1 Flow cytometry and FACS schematic.

A: When particles pass in the fluid stream through the laser intercept, they scatter laser light. Any fluorescent molecules present on the particle fluoresce. The scattered and fluorescent light is then focused by appropriately positioned lenses. A combination of beam splitters and filters steers the scattered and fluorescent light to the appropriate detectors. The detectors produce electronic signals proportional to the optical signals striking them. FACS provides a method for sorting a heterogeneous mixture of biological cells, one cell at a time, based upon the specific light scattering and fluorescent characteristics of each cell. A charge is placed on the liquid droplets containing the cells, and the electrostatic deflection system directs the droplet accordingly into two or more containers.
B: Data can be displayed as a single parameter on the histogram, where the horizontal axis represents the parameter's signal value in channel numbers and the vertical axis represents the number of events per channel number. Alternatively, two parameters can be displayed simultaneously on a plot, with one parameter on the x-axis and another on y-axis. FSC *vs.* SSC dot plot presents lysed whole blood and its distinguishable populations of granulocytes, monocytes and lymphocytes, as indicated, and the histogram shows low CD45 blood antigen expression (black line) in freshly adherent murine bone marrow isolates, as calculated with regards to the matched-isotype control (grey line). Graphs reproduced by permission from Jon Wiley and Sons: Cytometry Part A (Bossuyt *et al.* 1997), copyright (1998) and The American Physiological Society (Wong *et al.* 2007), copyright (2007).

Since its introduction in 1989 (Bertoncello *et al.* 1989), the magnetic-activated cell sorting (MACS) technology has also been used extensively for cell separation in immunology and stem cell research, most often in clinical applications for quick enrichment of haematopoietic stem and progenitor cells for transplantations (Gaipa *et al.* 2003). It uses non-toxic, biodegradable, 50 nm superparamagnetic particles that are

conjugated to highly specific antibodies against a particular antigen on the cell surface, and a magnet stand to enable positive or negative selection of cells.

Another technology, the Image Stream (George *et al.* 2004), overcomes the limitation posed by flow cytometry, in that flow cytometry only provides information on a whole cell basis. Instead of measuring the light/fluorescence intensity from the entire cell, Image Stream enables visualisation of the fluorescently tagged molecule within or on the cell surface, by combining flow cytometry and microscopy. By producing multiple high-resolution images of every cell directly in flow, including brightfield and darkfield (SSC), it also enables visualisation of cellular morphology. Currently, Image Stream can be equipped with up to 5 lasers and up to 12 channels of detection.

As discussed in Section 1.1.3, skeletal stem cells are cells found in BMMNCs that are capable of multilineage differentiation into osteoblasts, adipocytes and chondrocytes, and thus apart from providing the niche for haematopoietic stem cells, they have the potential to regenerate bone tissue. Therefore, they are a very useful source of cells for tissue engineering applications and so over several decades researchers have sought to find ways of purifying them. Research published so far has focused on prospective selection of putative SSCs with a set of non-specific markers, which especially when used in combination, enrich the BMMNCs for colony forming unit-fibroblastic cells (CFU-Fs). Markers used for selection of SSCs include STRO-1 (Simmons and Torok-Storb 1991), CD106 (Gronthos *et al.* 2003), CD146 (Tormin *et al.* 2011) and CD271 (Quirici *et al.* 2002). STRO-1 is a particularly attractive marker, as it is known to enrich BMMNCs for CFU-Fs, and it selects approximately 10 % of BMMNCs, but these include glycophorin A^+ (GPA^+) erythroid progenitors and a subset of stromal cells. For this reason, a negative selection with an antibody to GPA has been investigated and it was found that >95 % of STRO-1^+ cells are nucleated erythroid cells (Simmons and Torok-Storb 1991). Sorting the STRO-1^+ fraction for a subpopulation with the highest expression of this antigen, the so called STRO-1^{bright}, resulted in substantial CFU-F enrichment (Gronthos *et al.* 2003), in the same manner as a combination of STRO-1^{bright} with GPA (Zannettino *et al.* 2007). Panels of antibodies used for characterisation of putative skeletal stem cells isolated with all these different markers often comprise CD90 (also expressed in most fibroblasts and myofibroblasts), CD105

(also a marker for endothelial and smooth muscle cells), and CD146 (also a marker for cells that are components of the blood vessel wall, including vascular endothelial cells, smooth muscle cells and pericytes).

Although the aforementioned selection markers were used for prospective isolation or immunophenotyping of cells which have already been cultured, to date there is no evidence in the literature of flow cytometry being used for assessing the skeletal stem cell population within fresh bone marrow isolates after response to treatment or other stimuli. This kind of research could be a useful tool for investigating the influence of potential drugs on the heterogeneous population of BMMNCs and the stem cells within it. MACS and flow cytometry/FACS, as well as Image Stream, were used in this chapter to characterise the fresh bone marrow isolates and the SSC population within, focusing mostly on analysis within cell suspensions, as opposed to cells cultured on plastic. These data were generated to assess the possibility of studying these stem cells by flow cytometry, and to apply appropriate gating strategies, within the populations they are normally surrounded by in the bone marrow niche. Additionally, the MACS technology in this chapter was used to enrich heterogeneous bone marrow isolates for putative skeletal stem cells, to enable the assessment of this population and its purity for further studies described in the next chapter, where it was used to delineate the directness of the Wnt effects after exposure.

Furthermore, given the evidence that several elements of the Wnt signalling pathway have been identified as being expressed by SSCs, such as Wnt ligands, various Wnt receptors, co-receptors and inhibitors (Etheridge *et al.* 2004), this chapter aimed to assess intrinsic Wnt signalling levels in STRO-1$^+$, believed to be the putative stem cells, *vs.* unsorted BMMNCs. Therefore, qPCR analysis of Wnt target genes, such as *CMYC* (Hiyama *et al.* 2011), *CCND1* (Shtutman *et al.* 1999), *AXIN2* (Jho *et al.* 2002), and *LEF* and *TCF4* (Hovanes *et al.* 2001) were conducted to compare their expression levels in tissue culture plastic adherent cells (cultured for ~2 weeks) as well as in freshly isolated cells, between populations containing various levels of the STRO-1 marker. Additionally, as Osterix-expressing cells (Osx$^+$) within the murine bone marrow have recently been identified as a population both producing Wnts and responsive to Wnt signals (Tan *et al.* 2014), expression of this gene in the STRO-1$^+$ cells was tested.

The assessment of intrinsic Wnt signalling levels laid ground for the following chapter where external Wnt cues and their effects were studied.

In summary, the aim of the work in this chapter was to:

- isolate human bone marrow mononuclear cells and identify the putative skeletal stem cell population in fresh non-cultured samples;
- enrich for this population and characterise the purity of this enrichment;
- measure intrinsic Wnt signalling levels in skeletal stem cells.

These studies were performed to test the hypothesis that skeletal stem cells can be studied in fresh bone marrow isolates after application of appropriate gating strategies, and these stem cells can be characterised by elevated levels of Wnt signalling.
A pictorial summary of the experimental protocols is shown in Figure 3.2.

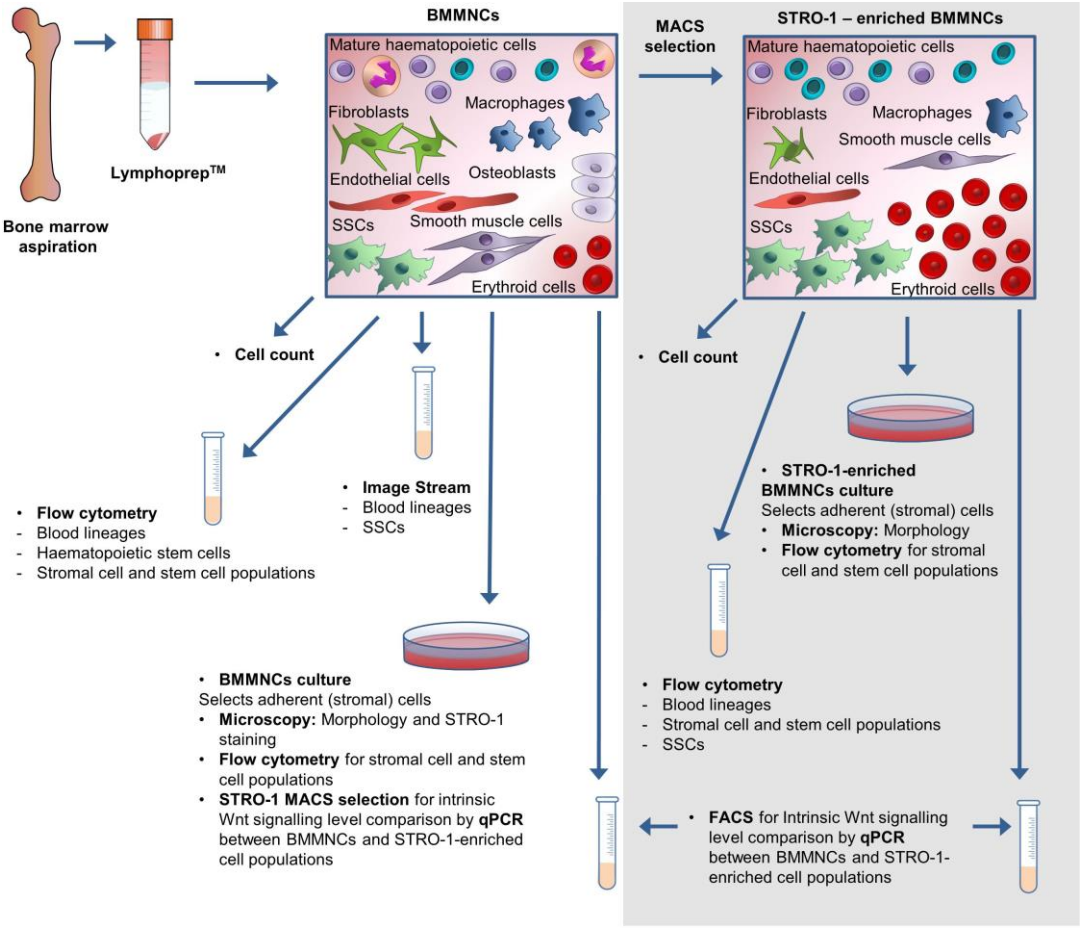

Figure 3.2 Overview of methodologies used and described in this chapter for characterisation of bone marrow isolates.

BMMNCs were isolated from bone marrow aspirates by Lymphoprep™, and a subset of samples was further enriched by MACS selection for the STRO-1 antigen. Flow cytometry was the main method used in this chapter, which enabled comparison between BMMNCs and STRO-1-enriched samples, with regards to their composition, as well as allowing for sorting of populations assayed for intrinsic Wnt signalling levels. BMMNCs, bone marrow mononuclear cells; MACS, magnetic activated cell sorting; FACS, fluorescence-activated cell sorting; SSCs, skeletal stem cells.

3.2 Results

3.2.1 Cell isolation

Bone marrow mononuclear cells (BMMNCs) were isolated from bone marrow samples donated by patients undergoing hip replacement surgery at local hospitals (see Methods Section 2.2.1, and Appendix for a detailed list, Table A.7). BMMNCs used in the experiments throughout this thesis came from a total of 74 donors (mean age 73 ± 11, range 53 - 97), of which 43 were females (mean age 75 ± 12, range 54 – 97) and 31 males (mean age 70 ± 10, range 53 – 91), as depicted in Figure 3.3A. The age distribution between female and male donors was not statistically different, nor was the number of cells extracted from female and male donors (mean 145 ± 151 x 10^6 *vs.* 142 ± 158 x 10^6 cells, respectively; Figure 3.3B). However, a negative correlation between females' age and the number of cells isolated from bone marrow samples from female donors was observed, whereas for male donors only a trend was noticeable (Figure 3.3C).

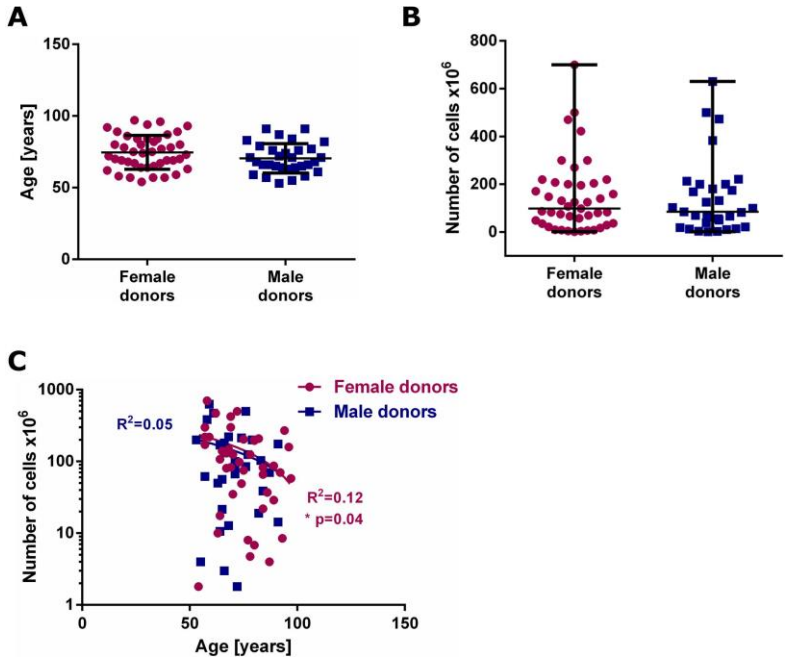

Figure 3.3 Comparison between donor age and sex and the number of isolated BMMNCs.

After isolation of BMMNCs, cell numbers from samples from female and male donors were counted to assess the variation. A: Female and male donor age distributions for the acquired samples were not significantly different. Data analysed by t-test, presented as mean ± SD. B: Number of cells isolated from female and male donor samples were not significantly different. Data analysed by Mann-Whitney test, presented as median ± range. C: A negative correlation was observed between female donor age and cell numbers isolated from their bone marrow (n = 43, $p<0.05$), whereas for male donors only a trend was observed (n = 31, ns). Data analysed by Spearman's rank correlation.

3.2.2 Characterisation of bone marrow isolates by flow cytometry

To characterise the composition of the bone marrow isolates, flow cytometry was used. This allowed for a closer analysis of the extracted tissue, based on blood lineage marker expression, haematopoietic cell marker expression and expression of markers of stromal/mesenchymal cell types, described in the following paragraphs.

3.2.2.1 Blood lineage markers

The bone marrow is the haematopoietic microenvironment, and thus blood cell rich; hence blood cell population distribution was examined first. Figure 3.4A depicts a typical flow cytometry FSC *vs.* SSC dot plot of bone marrow cell populations in the tissue isolates. In order to gate out the platelets, any remaining red blood cells and most of all dead cells and cell debris, propidium iodide (PI) staining was conducted (Figure 3.4B and C). The overlay in C shows the contaminating cells on the left side of the FSC *vs.* SSC dot plot gated out from any subsequent flow cytometry analyses.

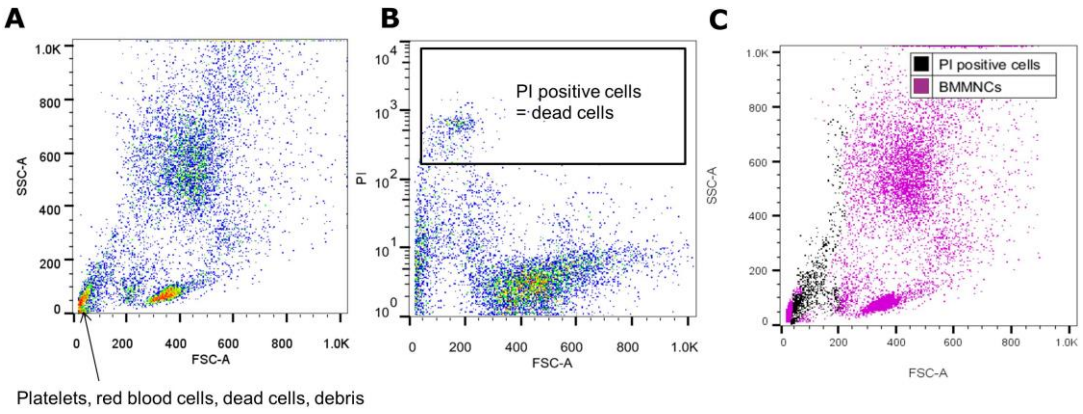

Figure 3.4 Localisation of dead cells within BMMNC isolates.

A: A representative flow cytometry dot plot depicting bone marrow cell populations based on their FSC *vs.* SSC properties, showing possible platelet, red blood cell, dead cell and cell debris contamination, as pointed out. B and C: PI staining for dead cell exclusion from analyses, with the PI^+ population overlaid on FSC *vs.* SSC, and localising, as expected, in the low FSC region. FSC, forward side scatter; PI, propidium iodide; SSC, side scatter.

As expected, different populations (granulocytes, monocytes and lymphocytes) are distinguishable based solely on their scatter properties. To confirm this distribution, a general panel of antibodies against common markers of granulocytes (CD66b), monocytes (CD14) and lymphocytes (CD56 for NK cells, CD3 for T cells, CD19 for B cells) was used, and the populations were subsequently overlaid on the FSC *vs.* SSC

dot plot (Figure 3.5A and B). The staining colocalised with the expected light scatter properties of each of these fractions, therefore the gating strategy for further experiments in which blood lineage markers were not used (depicted in Figure 3.5C) refers to the granulocytic, monocytic and lymphocytic light scatter parameters of these populations. Figure 3.5D shows quantification of granulocyte, monocyte and lymphocyte marker expression in the bone marrow isolates. Although bone marrow was layered onto Lymphoprep™ media for mononuclear cell separation, there was still a high percentage of granulocytes (65 ± 6.5 %) contaminating all preparations. However, for the purpose of consistency and simplicity in this thesis, these isolates will retain the designation of BMMNCs. Blood cell lineages comprised 85 ± 3.2 % of BMMNC isolates (detected with the aforementioned set of markers) in total, with coverage >90 % when analysing only the granulocyte and lymphocyte gate, but >70 % for the monocyte gate. This indicated a greater presence of unlabelled cells within the monocyte gate compared to the granulocyte and lymphocyte gates.

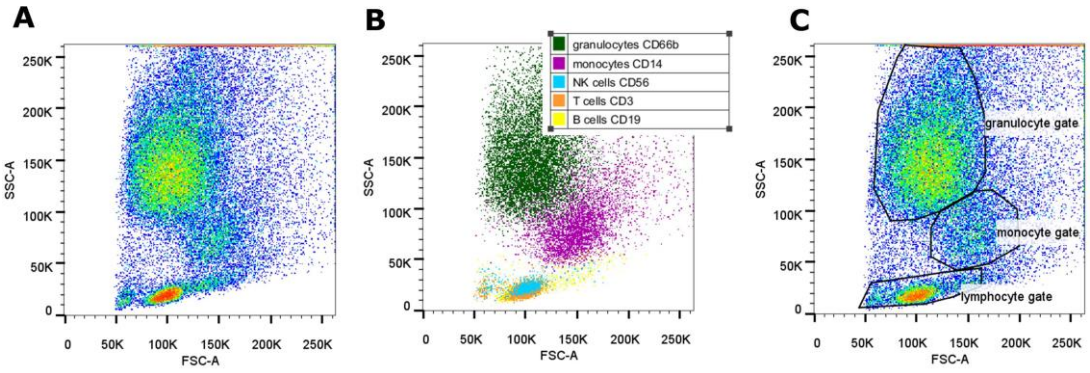

D

Cell type		Percentage stained out of all BMMNCs		Percentage stained within the set gate
Granulocytes		65 ± 6.5 %		93.4 ± 2.5 %
Monocytes		6.6 ± 1.3 %		73.4 ± 3.4%
Lymphocytes	NK cells	13.2 ± 0.9%	2.9 ± 0.7%	91 ± 6.3 %
	T cells		6.4 ± 0.6 %	
	B cells		3.9 ± 0.9 %	
	Total	85 ± 3.2 %		

Figure 3.5 Blood cell lineages in the BMMNC isolates.

A: A representative flow cytometry dot plot depicting bone marrow cell populations based on their FSC *vs.* SSC properties, with cell debris gated out. B: Overlay of positively stained bone marrow cell populations on the FSC *vs.* SSC dot plot. Antibodies against markers of granulocytes (CD66b), monocytes (CD14) and lymphocytes (CD56 for NK cells, CD3 for T cells and CD19 for B cells) were used. Gating strategy is detailed in the Appendix, Figure A.1. C: A representative dot plot depicting gating strategy based on FSC *vs.* SSC with polygon gates set for granulocytic, monocytic and lymphocytic cells, used in further experiments where staining for specific bone marrow cell populations was not applied, but the populations were sufficiently distinguishable to allow gates to be set manually. D: Percentages of granulocytes, monocytes and lymphocytes within the bone marrow, based on staining with specific antibodies, expressed as a proportion of all BMMNCs, or of events within specific granulocyte/monocyte/lymphocyte gates; n = 3 donors.

3.2.2.2 Haematopoietic stem cells

A commercial marker panel (see Methods, 2.2.5.1) was employed to detect haematopoietic stem cells in the bone marrow isolates. Quantification of populations of cells with the proposed haematopoietic phenotypes of $CD11b^-/CD38^-/CD34^+/SCF^+$ and $CD11b^-/CD38^-/CD34^+/CD90^-$ was carried out (Figure 3.6). Due to insufficient numbers of the populations of interest in the analysed isolates, data is represented by quadrant density plots to aid interpretation. On average, 0.7 ± 0.31 $CD11b^-/CD38^-/CD34^+/SCF^+$ cells out of 10 000 BMMNCs (n = 3) were haematopoietic stem cells, as defined by the markers used in the staining panel. However, it is worth noting that the inter-donor variability was high with regards to putative HSC numbers, and the staining pattern for CD34 varied between samples as well, with donor 2 and 3 representing a $CD34^{dim}$ population in comparison to donor 1.

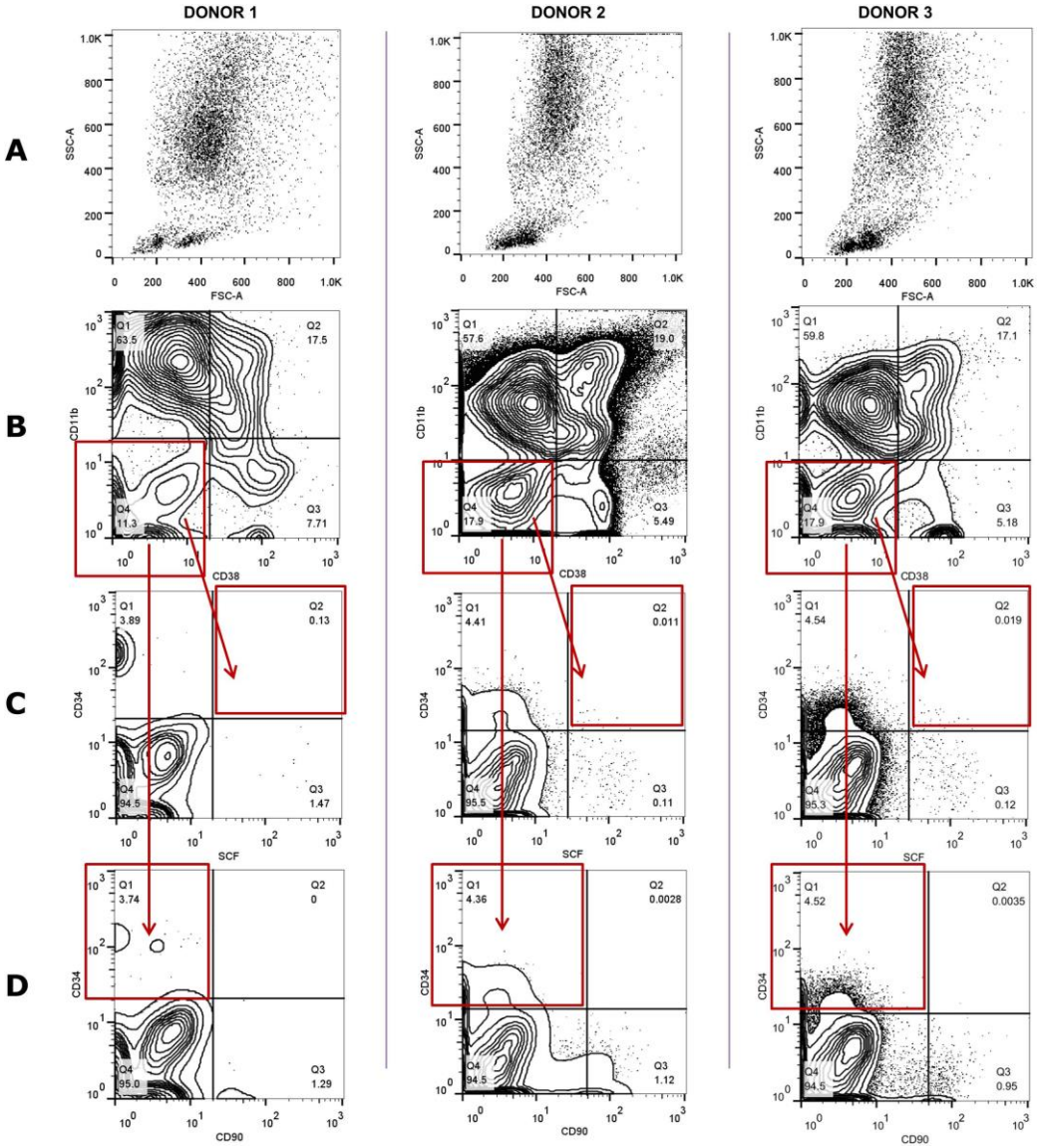

Figure 3.6 Analysis of haematopoietic stem cell numbers present in bone marrow isolates.

Samples from 3 donors were analysed with the haematopoietic stem cell marker panel. A: Flow cytometry FSC *vs.* SSC dot plots of BMMNCs. B: Gating on the $CD11b^-/CD38^-$ fraction of the BMMNCs in a quadrant density plot. C: Quantification of the $CD34^+/SCF^+$ events in the gated $CD11b^-/CD38^-$ fraction. For each donor the number of $CD11b^-/CD38^-/CD34^+/SCF^+$ cells was 12 in ~10^5, 40 in ~2 x 10^6 and 51 in ~1.5 x 10^6 analysed cells, respectively. D: Quantification of the $CD34^+/CD90^-$ events from the gated $CD11b^-/CD38^-$ fraction. The vertical and horizontal lines in the quadrant graphs were set to the reactivity levels obtained with the isotype-matched control antibodies, and all cells gated as positive showed a fluorescence intensity greater than that detected on 99 % of the cells labelled with the isotype-matched control. See Appendix Figure A.2 for isotype controls.

3.2.2.3 Stromal cell and stem cell populations

To identify skeletal stem cells in BMMNCs, the CD45 marker was used to distinguish between blood cells and other cell types, as the stromal/skeletal cells lack the

expression of this marker. On average, 7.8 ± 1.7 % of the analysed BMMNCs (n = 3) were CD45$^-$. Next, in this fraction, the expression of CD90, CD105 and CD146 was examined. A combination of these markers is proposed to distinguish mesenchymal/skeletal stem cell populations, and the antibodies were included in a commercial marker panel (see Methods, 2.2.5.1). The CD45$^-$ fraction colocalised with the lymphocytic and monocytic cells on a flow cytometry FSC *vs.* SSC plot (Figure 3.7A), whereas the stromal/skeletal cell populations in the CD45$^-$ fraction localised mostly where the monocytic cells would be, based on their light scattering properties only (Figure 3.7B).

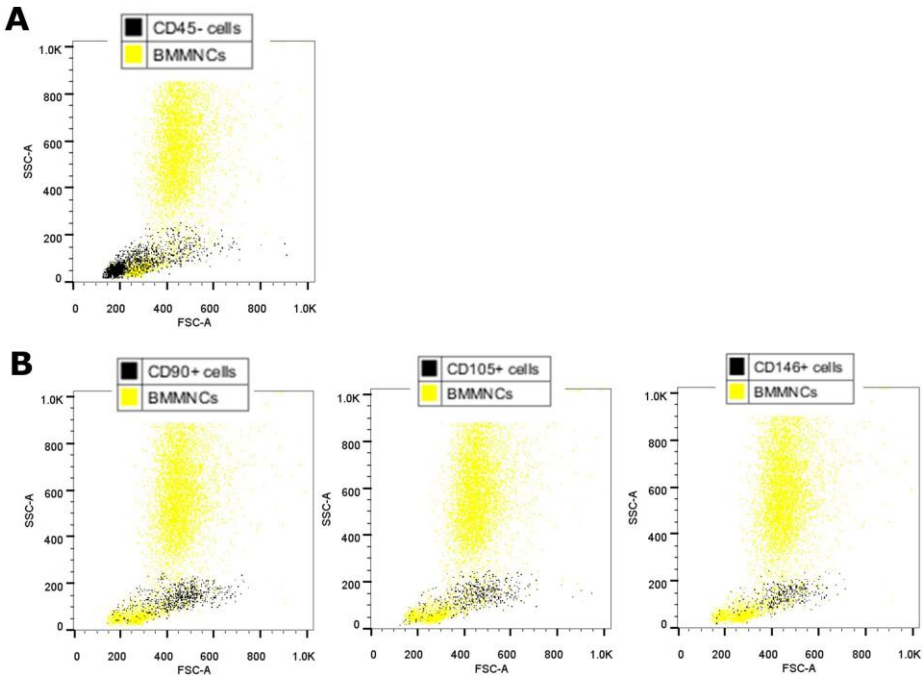

Figure 3.7 Stromal cell populations in the BMMNC isolates.

BMMNCs were stained with CD45 and markers of stromal populations: CD90, CD105 and CD146. A: A flow cytometry FSC *vs.* SSC dot plot depicting cell populations negative for the blood cell marker CD45 (black) overlaid on all BMMNCs (yellow). B: Expression of markers of stromal cells/skeletal stem cells within the CD45 negative fraction: CD90 for fibroblasts and myofibroblasts, CD105 for endothelial and smooth muscle cells, and CD146 for cells that are components of the blood vessel wall, including vascular endothelial cells, smooth muscle cells and pericytes. Populations positive for these markers are overlaid in bulk in black (due to overall low expression in fresh marrows, <1 %) on all BMMNCs (yellow), for ease of visualising their localisation within the "monocytic/stromal" region based on light scattering on the FSC *vs.* SSC dot plots.

Next, staining for the more broadly expressed STRO-1 marker, known to enrich BMMNCs for putative skeletal stem cells, was conducted. This marker is thought to be expressed by stem cells, but may also be present on other cells. STRO-1 expression in

the BMMNCs was 8.85 ± 4.66 % (n = 7; representative histogram of the antibody staining depicted in Figure 3.8A). Negative and positive controls for the antibody can be found in the Appendix, Figure A.4. Although positively stained cells were found throughout the entire marrow, they colocalised predominantly within the monocyte gate based on their light scattering properties. However, the STRO-1$^+$ population was distinct from the monocyte population identifiable by CD14 expression, as the colocalisation of both markers was <1 % (Figure 3.8A, Q2). Furthermore, STRO-1 expression on other blood cell lineages was also negligible (Figure 3.8B, Q2).

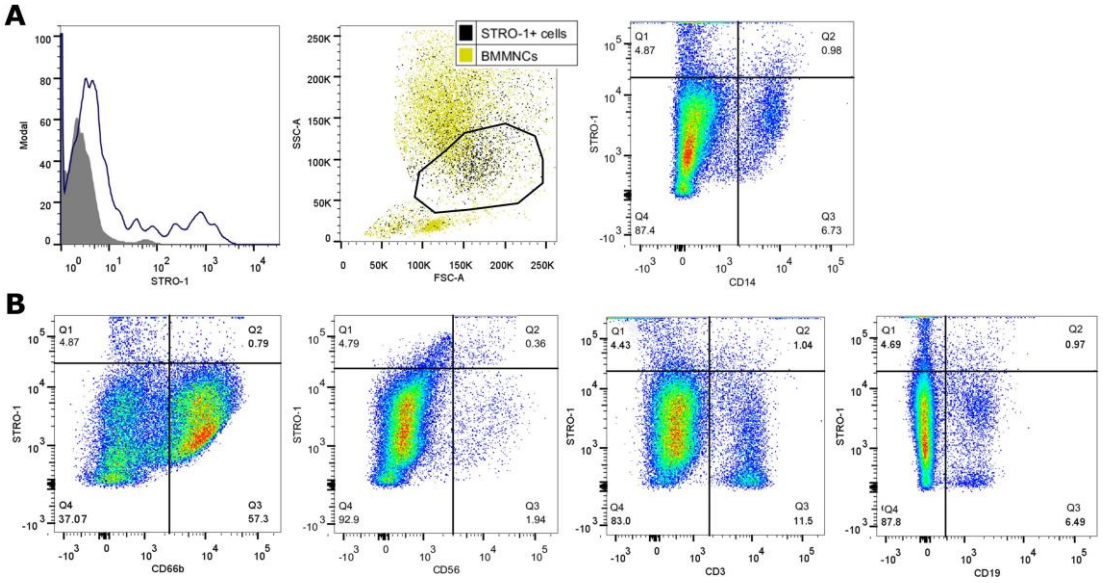

Figure 3.8 Staining for the STRO-1 marker within the BMMNCs.

Staining for the STRO-1 marker was conducted on BMMNCs in conjunction with haematopoietic cell lineage markers. A: Histogram showing STRO-1 expression within the BMMNCs (blue line) *vs.* isotype control (filled grey), and overlay of these STRO-1$^+$ cells (black) within all BMMNCs (yellow) on the following flow cytometry FSC *vs.* SSC dot plot. Polygonal gate shows "monocytic" localisation of the majority of STRO-1$^+$ events, however only a small subset of cells (0.98 %, Quadrant 2, following dot plot) is positive for both STRO-1 and the CD14 monocyte marker. B: Quadrant dot plots depicting negligible colocalisation (Q2) of STRO-1 with CD66b, CD56, CD3 and CD19 markers. The vertical and horizontal lines in the quadrant graphs were set to the reactivity levels obtained with the isotype-matched control antibodies (see Appendix Figure A.3), and all cells gated as positive showed a fluorescence intensity greater than that detected on 99 % of the cells labelled with the isotype-matched control.

3.2.3 STRO-1-enriched cell isolation

The MACS technique was used to enrich the BMMNC samples, from a subset of the aforementioned donors, for cells expressing the STRO-1 marker (see Methods, Section 2.2.2). The reason for this was to study a population with higher content of the

putative skeletal stem cells and less blood lineage cells. These STRO-1-enriched BMMNC samples used in the experiments came from a total of 39 donors (mean age 73 ± 11, range 53 – 97), of which 23 were females (mean age 75 ± 13, range 57 – 97) and 16 males (mean age 71 ± 9, range 53 – 84), as depicted in Figure 3.9A. The age distribution between female and male donors was not significantly different, neither was the number of cells extracted from female and male donors (means 6.2 ± 4.8 x 10^6 *vs.* 7.3 ± 5.8 x 10^6; Figure 3.9B). No correlation was observed between the age of female and male donors and the number of cells isolated from bone marrow samples, or percentages of STRO-1-enriched cells out of all BMMNCs (Figure 3.9C and D).

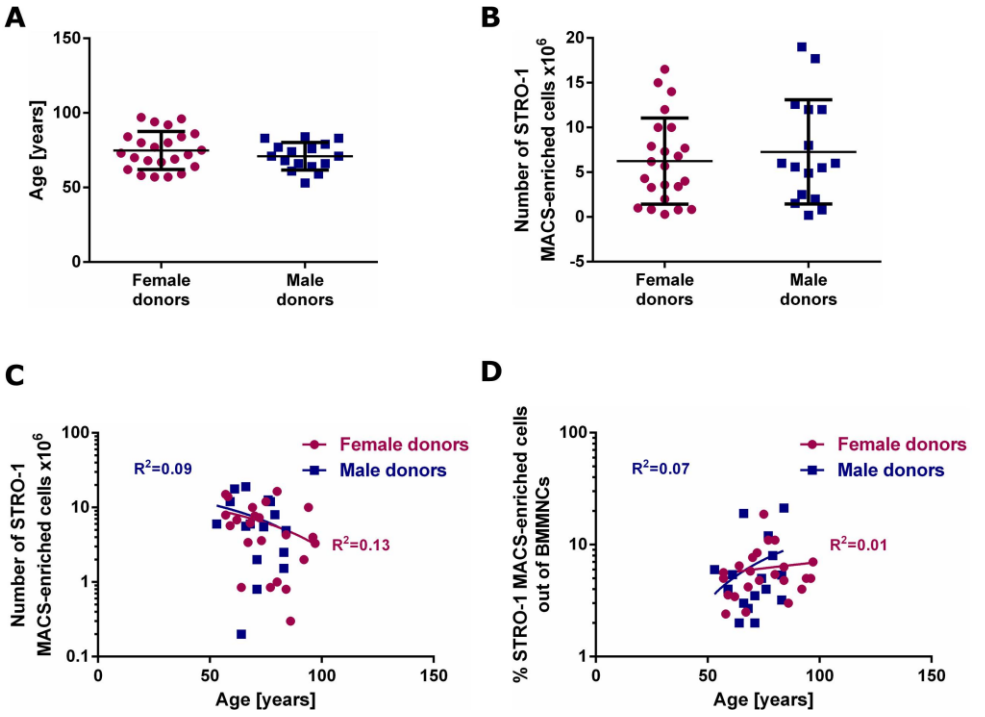

Figure 3.9 Comparison between donor age and sex and the number of isolated STRO-1-enriched BMMNCs.

After MACS isolation, cell numbers from samples from female and male donors were counted to assess the variation. A: Female and male donor age distribution was not statistically different. Data analysed by t-test, presented as mean ± SD. B: Number of cells isolated from female and male donor samples was not statistically different. Data analysed by t-test, presented as mean ± SD. C: No correlation was observed between female and male donor age and STRO-1$^+$ cell numbers isolated from bone marrow. Data analysed by Pearson's correlation. D: No correlation was observed between female and male donor age and percentage of STRO-1$^+$ cell numbers out of all BMMNC numbers. Data analysed by Spearman's rank correlation.

STRO-1-enriched cells comprised 6.35 ± 4.58 % of the general BMMNC isolates, which was not statistically different from the measured expression of the STRO-1 marker in BMMNCs described in Section 3.2.2.3. However, it was observed that the

range of stained STRO-1^+ cells was between 2.93 - 14.90 %, whereas the MACS selection for STRO-1 resulted in enrichment with a range of 2.00 - 21.28 %. The maximum value seen with the MACS selection might suggest that the hybridoma antibody used for MACS selection may be less specific than the commercially available antibody used for staining. Therefore, a characterisation similar to that conducted on BMMNC isolates was carried out on the STRO-1-enriched fraction.

3.2.4 Characterisation of STRO-1-enriched bone marrow isolates by flow cytometry

In order to determine what cell populations might be present in the STRO-1-enriched fraction of the BMMNCs, and to assess the purity of the fraction obtained using this selection method, blood cell lineage staining and staining for the stromal cells and stem cell markers was conducted.

3.2.4.1 Blood lineage markers

Figure 3.10A depicts typical flow cytometry FSC *vs.* SSC dot plots of bone marrow cell populations in the BMMNCs and STRO-1-enriched isolates, visualising an equivalent number of cells. Different populations (granulocytes, monocytes and lymphocytes) are distinguishable based solely on their scatter properties, but a decrease in the granulocytic fraction and enrichment of the monocytic and lymphocytic fractions is visible in the STRO-1-enriched sample *vs.* BMMNCs. To confirm this distribution, a general panel of antibodies against common markers of granulocytes (CD66b), monocytes (CD14) and lymphocytes (CD56 for NK cells, CD3 for T cells, CD19 for B cells) was used as previously, and the populations were subsequently overlaid on the flow cytometry FSC *vs.* SSC dot plot (Figure 3.10B, C). The staining colocalised with the expected light scatter properties of each of these fractions, therefore the gating strategy for further experiments in which blood lineage markers were not used (depicted in Figure 3.10D) refers to the granulocytic, monocytic and lymphocytic light scatter parameters of these populations. Figure 3.10E shows granulocyte, monocyte and lymphocyte markers expression in bone marrow isolates.

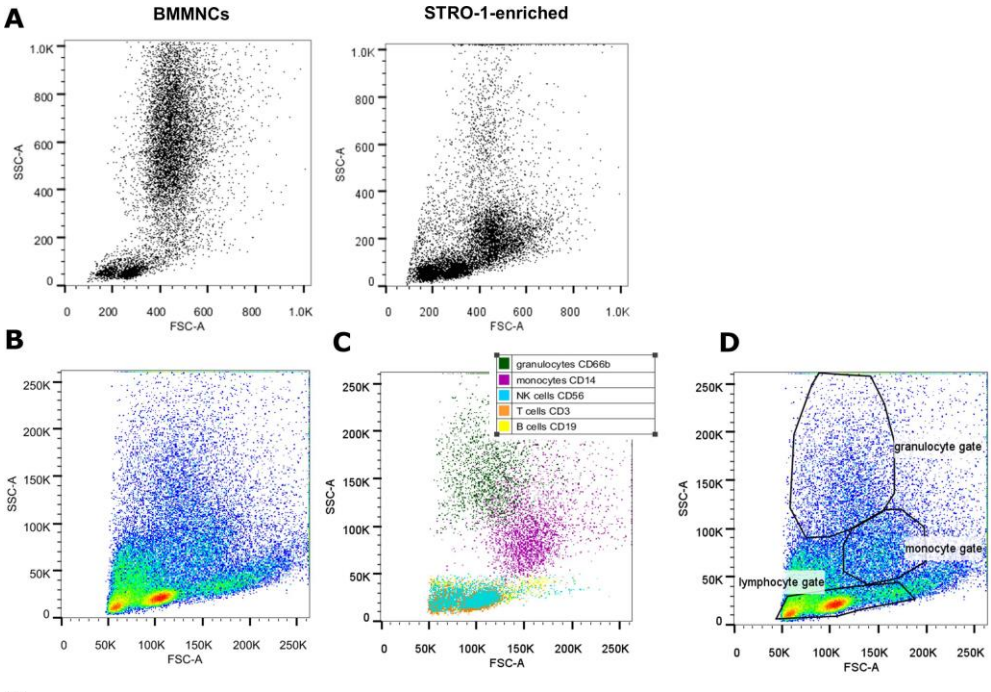

E

Cell type		Percentage within the MACS STRO-1-enriched cells		Percentage stained within the set gate
Granulocytes		5.6 ± 0.2 %		82.6 ± 1.3 %
Monocytes		6.6 ± 0.3 %		36.4 ± 2.7 %
Lymphocytes	NK cells	44.5 ± 3.2 %	13.9 ± 0.9 %	78.3 ± 6.3 %
	T cells		26.0 ± 1.95 %	
	B cells		4.6 ± 0.5 %	
	Total	57 ± 3.2 %		

Figure 3.10 Blood cell lineages in the MACS STRO-1 enriched cell isolates.

A: Flow cytometry dot plots depicting the same overall cell number of BMMNCs and STRO-1-enriched cells. A decrease in the granulocytic fraction and enrichment of the monocytic and lymphocytic fractions is visible. B: A representative dot plot depicting cell populations within the STRO-1-enriched fraction of the bone marrow based on their FSC *vs.* SSC properties. C: Overlay of positively stained bone marrow cell populations on the FSC *vs.* SSC dot plot. Antibodies against markers of granulocytes (CD66b), monocytes (CD14) and lymphocytes (CD56 for NK cells, CD3 for T cells and CD19 for B cells) were used. These cell types were all still present after the STRO-1-enrichment. Gating strategy can be found in the Appendix, Figure A.1. D: A representative flow cytometry dot plot depicting gating strategy based on FSC *vs.* SSC with polygon gates set for granulocytic, monocytic and lymphocytic cells based on settings for unenriched BMMNCs, used in further experiments where staining for specific bone marrow cell populations was not performed. E: Percentages of granulocytes, monocytes and lymphocytes within the MACS STRO-1-enriched fraction of the bone marrow, based on staining with specific antibodies, expressed as a proportion of all STRO-1-enriched events, or of events within specific granulocyte/monocyte/lymphocyte gates; n = 1, mean ± SD of 3 technical replicates.

57 ± 3.2 % of STRO-1-enriched bone marrow isolates were accounted for by blood cell lineages detected with the aforementioned set of markers, indicating that MACS selection method and the use of the hybridoma-produced unpurified antibody allowed for the extraction of blood cells, mostly from the lymphocytic lineage, although the

colocalisation of STRO-1 marker expression on blood cells was negligible based on staining conducted with the commercially-sourced STRO-1 antibody (Figure 3.8). The blood lineage marker coverage reached >78 % for the granulocyte and lymphocyte gate, and >36 % for the monocyte gate, indicating presence of other non-blood cell populations mostly within the monocyte gate.

3.2.4.2 Stromal cell and stem cell populations

The blood lineage marker panel stained 57 ± 3.8 % of STRO-1-selected BMMNCs. Therefore staining with markers for stromal cells and putative skeletal stem cells was conducted. The CD45 marker was selected again to distinguish between blood cells and other cell types, as stromal/skeletal cells lack the expression of this marker. On average, 41.5 ± 3.9 % of the analysed STRO-1 enriched samples (n = 3) were $CD45^-$, indicating an increase as compared to non-selected BMMNCs, where 7.8 % was seen (Figure 3.11A and B). In this $CD45^-$ fraction, the expression of CD90, CD105 and CD146 was examined as with BMMNCs before. The $CD45^-$ fraction colocalised with the lymphocytic and monocytic cells as judged by scattering properties (Figure 3.11A), whereas the stromal/skeletal cell populations in the $CD45^-$ fraction localised with the monocytic cells (Figure 3.11C). Figure 3.11D depicts histograms comparing the expression of all these markers in BMMNCs *vs.* STRO-1-enriched isolates, showing that there were no differences in their expression of CD90, CD105 and CD146 between the two populations.

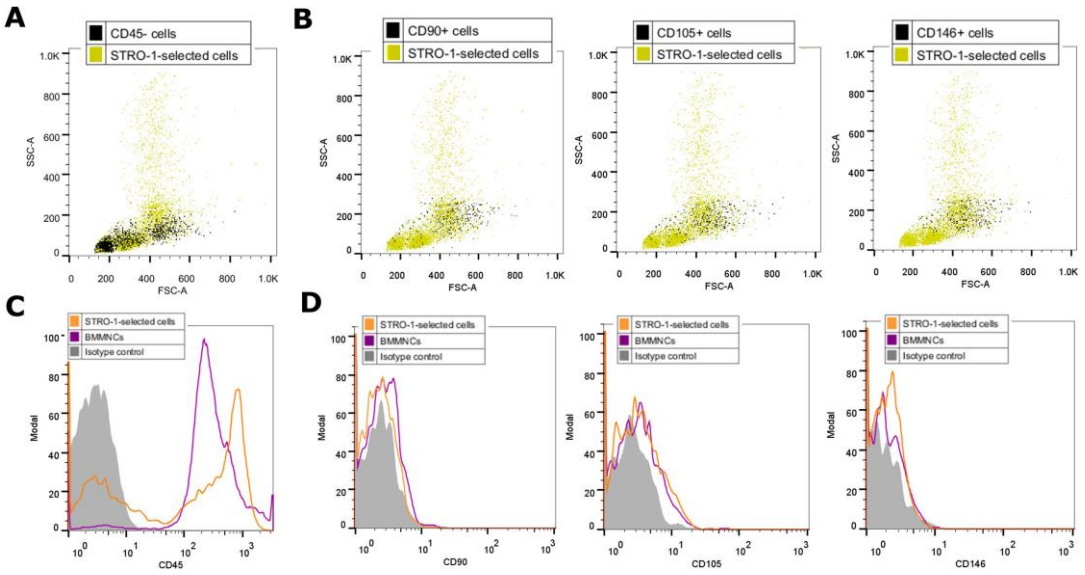

Figure 3.11 Stromal cell populations in the STRO-1-enriched bone marrow isolates.

STRO-1 MACS-enriched cells were stained with CD45 and markers of stromal populations: CD90, CD105 and CD146. A: A flow cytometry dot plot depicting cells populations negative for the blood cell marker CD45 (black) overlaid on all STRO-1-enriched bone marrow cells (yellow). B: Expression of markers of stromal cells / mesenchymal stem cells within the CD45 negative fraction: CD90 for fibroblasts and myofibroblasts, CD105 for endothelial and smooth muscle cells, and CD146 for cells that are components of the blood vessel wall, including vascular endothelial cells, smooth muscle cells and pericytes. Populations positive for these markers are overlaid in bulk in black (due to overall low expression in fresh marrows, <1 %) on all STRO-1-enriched bone marrow cells (yellow), for ease of visualising their localisation within the "monocytic" region of light scattering on the FSC *vs.* SSC dot plots. C: A histogram comparing CD45 expression in BMMNCs (purple line; MFI: 111) and in STRO-1-enriched bone marrow isolates (orange line; MFI: 46.6). Grey filled histogram represents staining with matched isotype control (MFI: 1.47). STRO-1 selection clearly enriched the $CD45^-$ population. D: Histogram comparing CD90, CD105 and CD146 expression in BMMNCs (purple line) and in STRO-1-enriched bone marrow isolates (orange line). Grey filled histograms represent staining with matched isotype controls. Expression of all these markers is low and no different in BMMNCs *vs.* STRO-1-enriched isolates. MFI, mean fluorescence intensity.

As previously noted, STRO-1 staining with the antibody produced by the hybridoma and the MACS selection process might result in a lower purity of population for subsequent analysis in comparison to staining with the commercially available STRO-1 antibody. By staining with a fluorescently-labelled secondary antibody in conjunction with a magnetic bead-labelled antibody during the MACS protocol, subsequent flow cytometry analysis allowed the determination of the impurity introduced by the magnetic separation process itself.

Figure 3.12A shows overlaid STRO-1^+ cells stained with the fluorescent secondary antibody (black), out of all STRO-1-enriched cells after the MACS protocol (yellow).

Unfortunately, due to economic reasons (antibody volume and cost), the MACS selection and STRO-1 staining on these isolates could only be conducted with the hybridoma antibody. Therefore, direct comparison of the STRO-1 stain pattern between the hybridoma and commercially available antibody is not possible. However, the acquired data suggest that the hybridoma antibody might be marking some populations non-specifically (Figure 3.12A *vs.* Figure 3.8A; see Appendix for hybridoma antibody concentration assessment by ELISA, Figure A.5 and Table A.8), indicating that the MACS selection is less stringent for STRO-1 selection than flow cytometry, with only 62.53 ± 9.06 % (n = 3) in MACS samples staining positively for STRO-1 by flow cytometry.

The GPA marker has previously been used with success for negative selection of the STRO-1-expressing erythroid precursors in the STRO-1 MACS-selected samples, and accompanied sorting of cells which are brightest for STRO-1 (see Section 3.1). Therefore, STRO-1 staining for the MACS-enriched samples was conducted in conjugation with GPA staining, to purify the skeletal stem cell population further. As a result, the majority of the STRO-1^+ population were GPA^+ (89.33 ± 4.39 %; Figure 3.12B, Q2 and E). Gating on the GPA^-/STRO-1^+ subset (Figure 3.12B, Q3) and its subsequent overlay (Figure 3.12C), as well as gating on the GPA^-/STRO-1^{bright} subset (Figure 3.12B, R1) and its subsequent overlay (Figure 3.12D) resulted in gradual purification of the stromal cells, as evidenced by the enrichment in the region where stromal cell populations were previously shown to localise (marked by polygonal gates). Quantification of this staining within specific gates conducted on 3 donor samples is depicted in Figure 3.12E.

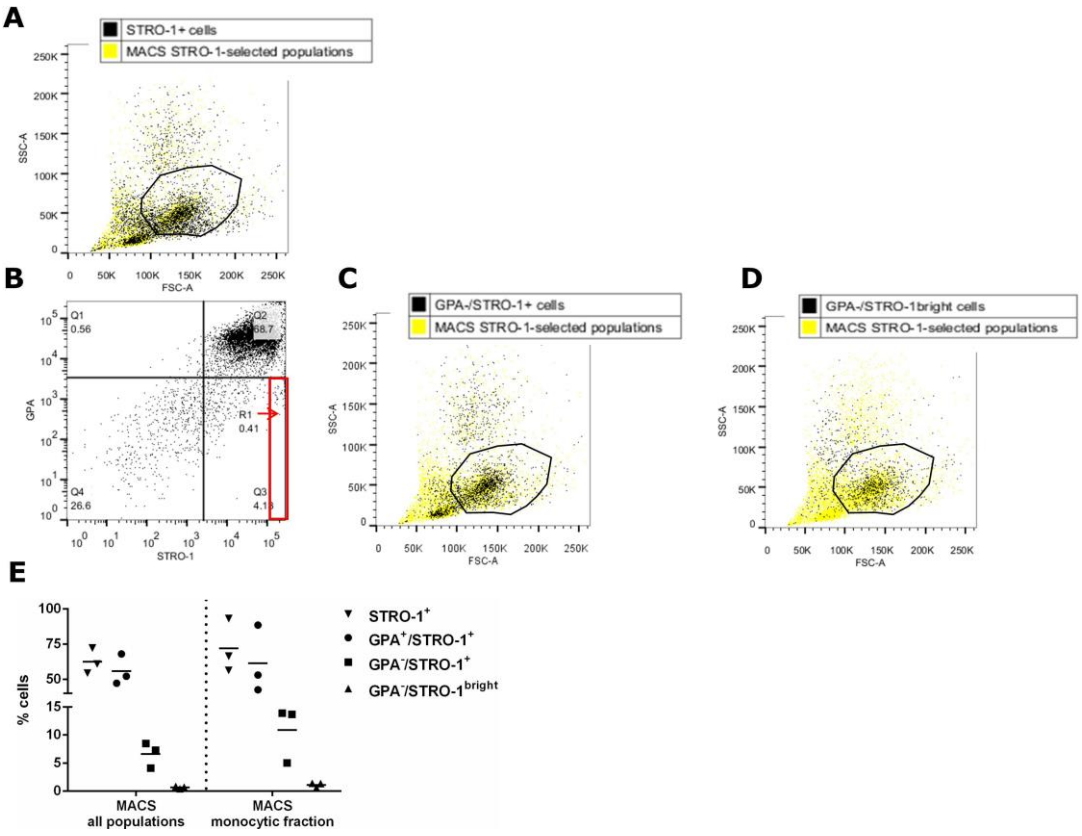

Figure 3.12 STRO-1-enrichment efficiency and further skeletal stem cell characterisation.

STRO-1 and GPA staining was conducted on STRO-1 MACS-enriched populations. A: A flow cytometry FSC *vs.* SSC dot plot depicting stained STRO-1$^+$ cells (black), out of all STRO-1-enriched cells after the MACS protocol (yellow). B: Colocalisation of STRO-1 and GPA marker, showing that the majority of the STRO-1$^+$ fraction is also GPA$^+$ (Q2). Q3 is the GPA$^-$/STRO-1$^+$ gate and R1 (marked in red) is the top 10 % of cells within that gate used for further overlays in C and D. E: Quantification of the STRO-1 staining, also in conjunction with GPA, in the entire MACS-selected sample and within specific "monocytic/stromal" gate set based on light scattering properties; n = 3 donor samples. GPA, glycophorin A.

3.2.5 Characterisation of bone marrow isolates by Image Stream

Because the different light scattering properties of GPA$^-$/STRO-1$^+$ skeletal stem/progenitor cells and GPA$^+$/STRO-1$^+$ erythroid precursors would indicate the presence of morphological differences within the STRO-1$^+$ cell populations, a general analysis of morphology and phenotype of bone marrow cells was conducted using Image Stream. This involved distinguishing blood cell populations and cells expressing the STRO-1 marker. The protocol can be found in Methods, Section 2.2.5.1.

Firstly, as cells for Image Stream need to be acquired from highly concentrated solutions, a gating strategy was applied to distinguish between single cells and possible clumps/doublets formed due to this high concentration (Figure 3.13). Only single cells in focus were analysed.

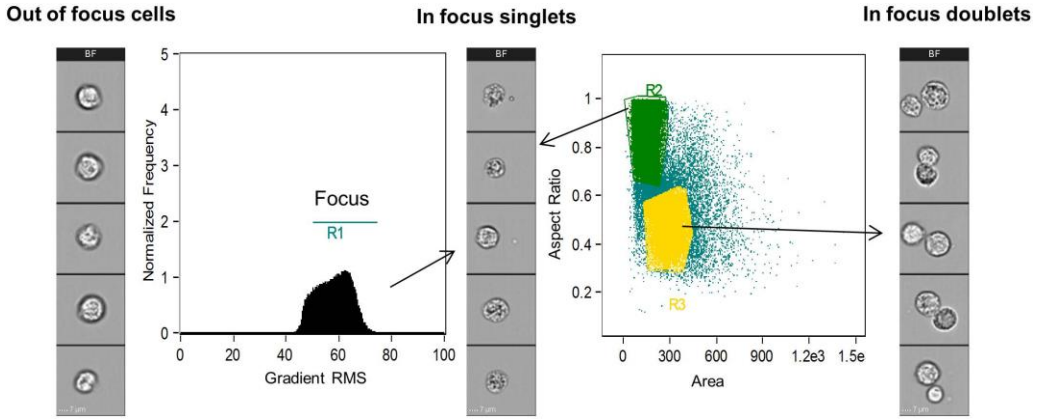

Figure 3.13 Focusing and gating procedure on Image Stream.

The Image Stream technology requires highly concentrated samples during sample acquirement, therefore settings were adjusted so only the "in focus" events would be analysed, based on Gradient RMS gating. Gradient RMS is the root mean square of the rate of change of the image intensity profile. Of these in focus events, only single cells would be analysed, as gated based on the Aspect Ratio *vs.* Cell Area dot plot. RMS, root mean square.

The bone marrow sample was stained with the CD45 marker to characterise the blood cell lineages. The intensity of the SSC and CD45 dot plot shows a clear distinction between the $CD45^-$ population and the three blood cell lineage populations (granulocytes, monocytes and lymphocytes), based on their SSC properties (Figure 3.14A). In this sample, other markers were also used in conjunction with CD45: either CD14 and STRO-1, or GPA and STRO-1, to better distinguish the monocytes and skeletal stem cells. The blood cell lineages were negative for both GPA and STRO-1 and the images for the $CD45^+$ populations are shown in Figure 3.14B and C.

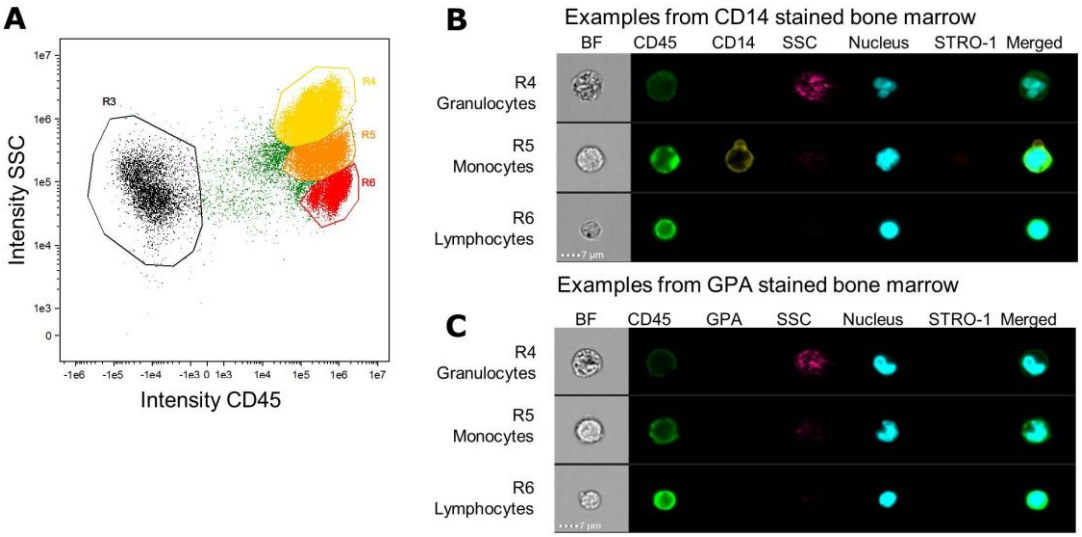

Figure 3.14 Blood cell lineage morphology pictured by Image Stream.

BMMNCs were stained with CD45, STRO-1 and either CD14 or GPA markers, to distinguish between the various blood cell populations. A: Dot plot of Intensity SSC *vs.* CD45, dividing the bone marrow into distinctive blood cell lineages (R4 – granulocytes, R5 – monocytes, R6 – lymphocytes) and a $CD45^-$ subset. B: Representative images of granulocytes, monocytes and lymphocytes in the subset of bone marrow co-stained with CD14. C: Representative images of granulocytes, monocytes and lymphocytes in the subset of bone marrow co-stained with GPA. GPA is not expressed on blood cell lineages. BF, brightfield; GPA, glycophorin A; SSC, side scatter.

The $CD45^-$ population was then examined for subpopulations expressing STRO-1 and GPA (Figure 3.15A). The dot plot of STRO-1 intensity *vs.* GPA intensity shows the gating strategy applied for distinguishing between erythroid precursors and putative skeletal stem cells, representative images of which are shown in Figure 3.15B.

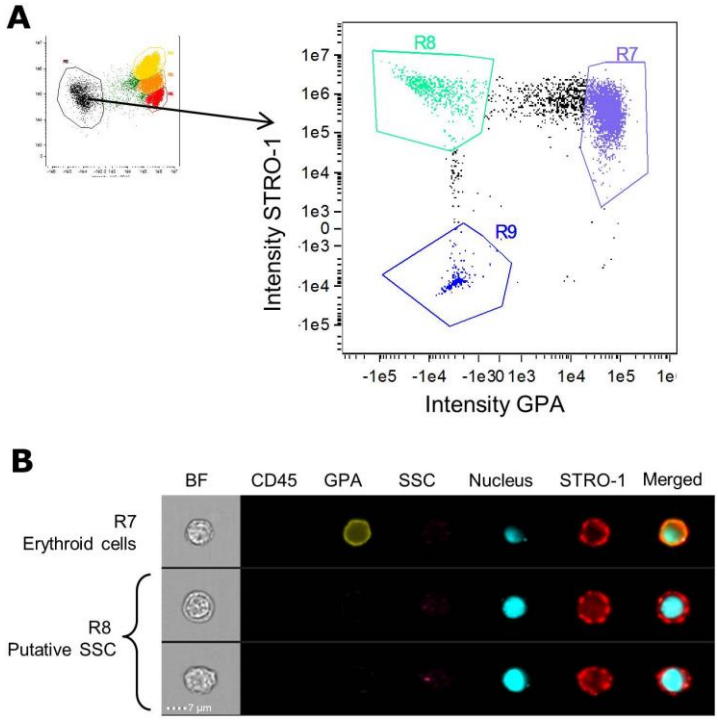

Figure 3.15 Skeletal stem cell *vs.* erythroid cell phenotype on Image Stream.

A: Analysis of the CD45$^-$ subset of the bone marrow for populations expressing STRO-1 and GPA. R7 – GPA$^+$/STRO-1$^+$ erythroid cells; R8 – GPA$^-$/STRO-1$^+$ putative skeletal stem cells; R9 – GPA$^-$/STRO-1$^-$ cells. B: Representative images of erythroid cells and putative skeletal stem cells, included in the R7 and R8 gate, respectively. BF, brightfield; GPA, glycophorin A; SSC, side scatter (top) or skeletal stem cell (left).

Previous flow cytometry data indicated that skeletal stem cell populations were localised within the "monocytic/stromal" region based on the FSC *vs.* SSC, as opposed to erythroid precursors, which had lower FSC properties. A similar comparison was performed on Image Stream, where the intensity of SSC *vs.* area of these cells was plotted (Figure 3.16A). Further analysis of these subsets confirmed that the CD45$^-$/GPA$^-$/STRO-1$^+$ skeletal stem cells were bigger (median area: 124.67 *vs.* 82.78 μm^2) and less round (median aspect ratio: 0.55 *vs.* 0.88) than erythroid cells (Figure 3.16B). The R9 gate, of cells double-negative for GPA and STRO-1, which may comprise of other stromal subsets, spans across both R7 and R8 characteristics.

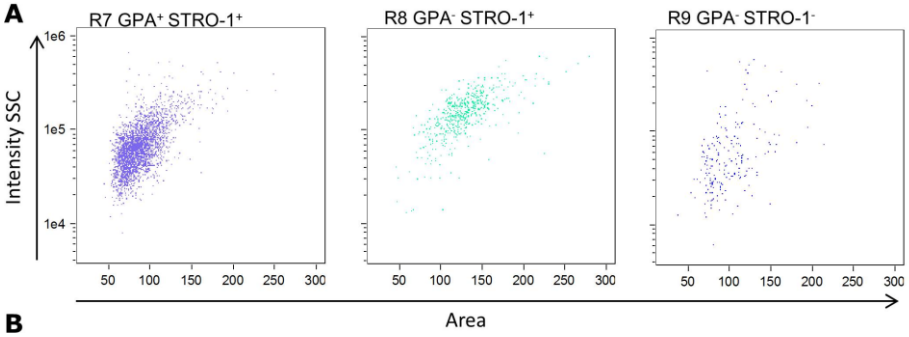

B

	Phenotype	Mean Area µm²	Median Area µm²	Mean ASR	Median ASR
R7	GPA⁺STRO-1⁺	86.31	82.78	0.859	0.876
R8	GPA⁻STRO-1⁺	127.9	124.67	0.841	0.547
R9	GPA⁻STRO-1⁻	101	94.11	0.816	0.839

Figure 3.16 Skeletal stem cell *vs.* erythroid cell morphology on Image Stream.

A comparison between the Intensity SSC vs. Area of cells stained with GPA and STRO-1 within the CD45⁻ fraction, revealing the morphological differences between skeletal stem cells and erythroid cells. A: Intensity SSC *vs.* Area dot plots of cells within the three CD45⁻ populations. Clear differences between GPA⁺/STRO-1⁺ erythroid cells and GPA⁻/STRO-1⁺ putative skeletal stem cells are noticeable, whereas the double-negative cells for GPA and STRO-1 within the R9 gate encompass both R7 and R8 populations. B: Mean and median cell areas and aspect ratios for the three populations. A minimum of 500 cells of the listed phenotype was analysed. ASR, aspect ratio.

The Image Stream technology therefore allowed for similar analysis to flow cytometry with regards to distinguishing between the population containing skeletal stem cells and erythroid cells based on marker expression, but also in addition it provided data on the morphological differences between the cell types of interest and possibility to distinguish between them without the requirement of staining.

3.2.6 Intrinsic Wnt signalling in skeletal stem cells

Since STRO-1⁺ cells contain a multipotent population of stem cells, and data suggests that Wnt signalling controls the self-renewal of stem cells, RT-qPCR analysis for Wnt target genes was conducted to test whether the intrinsic Wnt signalling level differed between unsorted BMMNCs and STRO-1-expressing populations.

3.2.6.1 Wnt signalling in cultured cells

Firstly, adherent BMMNC cultures with subsequent MACS selection were assessed. Cells from different donors differed in their proliferation capacities and it was difficult to culture them for ~14 days to obtain adequate amounts of cells for magnetic separation, while maintaining them at a low confluence (max. 60 %) in order to ensure they will still be expressing a sufficient level of STRO-1 antigen, and at the lowest

possible passage. A flow cytometry staining test was conducted on cells at passage 2, cultured for 14 days at 60 % confluency, in order to measure their STRO-1 expression levels. Approximately 15 % of cells were positive after staining (Figure 3.17). RNA was extracted from five suitable samples, which were first divided into 2 groups: yielding a small subset of BMMNCs and 6 x mores cells subsequently processed for selection based on the expression of STRO-1 antigen (Table 3.1). RNA samples were free from DNA contamination as assessed using NanoDrop spectrophotometer (260nm/280nm absorbance ratio >2.0), and the concentrations were sufficient to conduct reverse transcription of 500 ng of RNA. All cDNA samples were assessed together by qPCR for the expression of Wnt target genes.

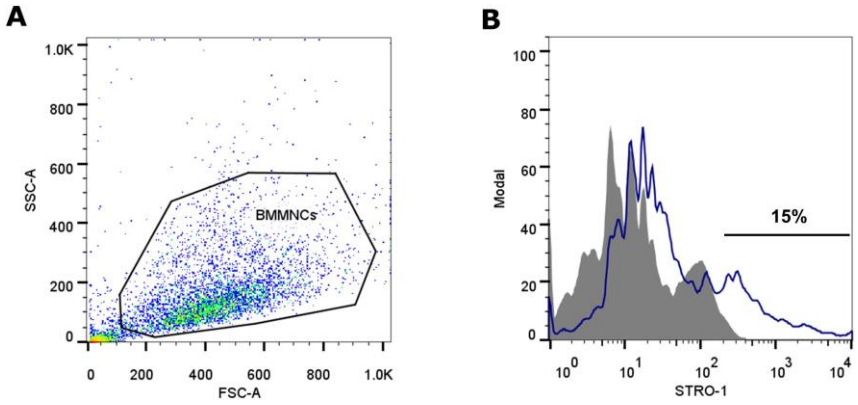

Figure 3.17 STRO-1 expression in cultured BMMNCs.

Example of STRO-1 expression, passage 2 cells, 14 days in culture after isolation. A: Flow cytometry FSC *vs.* SSC dot plot showing the BMMNC population after adherent culture; B: A histogram showing the level of STRO-1 expression (blue line), overlaid on the matched isotype control (grey filled).

Table 3.1 Percentages of STRO-1$^+$ cells after MACS selection of cultured cells.

Differences in the percentages of STRO-1$^+$ cells between different cultured samples and variability of the number of cells for RNA extraction.

Donor number	Sample	Passage	Cell count	% STRO-1+ cells after MACS selection	Days in culture
1	1 BMMNCs	P1	1 300 000		15
1	2 STRO-1$^+$	P1	450 000	5.6	15
2	3 BMMNCs	P2	785 000		15
2	4 STRO-1$^+$	P2	925 000	16.8	15
3	5 BMMNCs	P2	636 000		16
3	6 STRO-1$^+$	P2	250 000	5.5	16
4	7 BMMNCs	P1	1 680 000		13
4	8 STRO-1$^+$	P1	1 770 000	15.0	13
5	9 BMMNCs	P1	1 200 000		16
5	10 STRO-1$^+$	P1	150 000	2.1	16

Relative gene expression levels of *CMYC, CCND1, AXIN2, LEF1* and *TCF4* in cDNA samples from matching BMMNCs and STRO-1$^+$ cell samples, calculated by the ΔΔCt method, after normalisation to *ACTB* housekeeping gene and then to normalised expression in BMMNCs, are shown in Figure 3.18. The efficiencies for these newly designed primers are detailed in the Appendix, Figure A.8 - Figure A.12. There were no statistically significant differences in gene expression levels between unsorted BMMNCs and matching STRO-1-enriched cells. Considering previous results engaging the STRO-1 hybridoma antibody for MACS selection, and also the fact that these cells have been in culture, an alternative method of assessing the intrinsic Wnt signalling was sought.

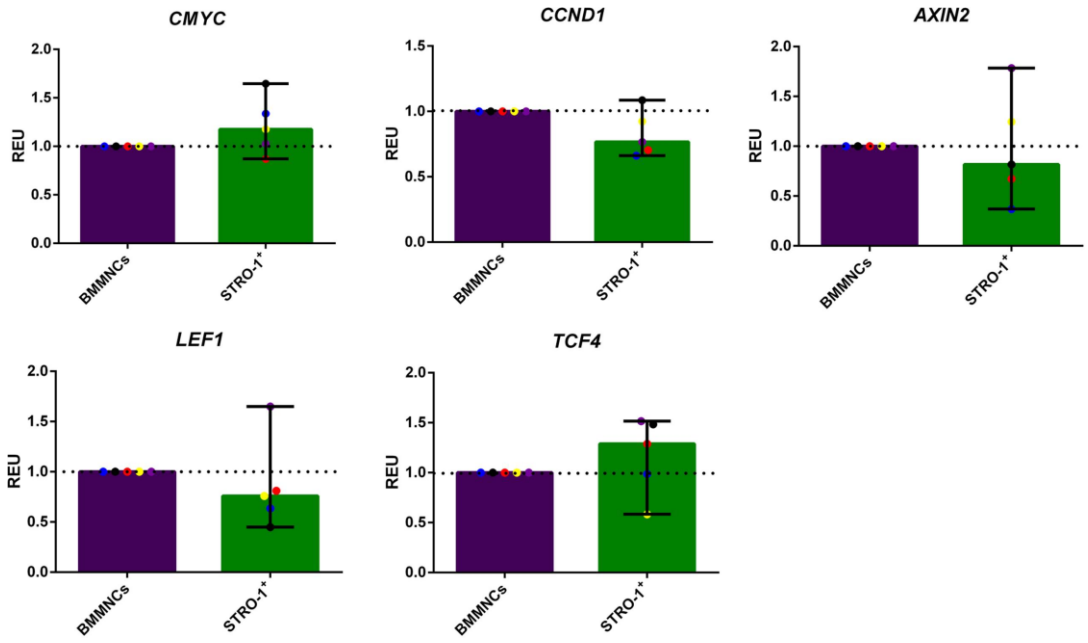

Figure 3.18 Wnt target gene expression in cultured BMMNC *vs.* STRO-1$^+$ cells.

BMMNCs were in culture for ~14 days and subsequently divided into BMMNCs and a subset processed for MACS STRO-1-enrichment, followed by RNA extraction. mRNA expression of *CMYC*, *CCND1*, *AXIN2, LEF1* and *TCF4* in STRO-1$^+$ cells as relative to BMMNCs is shown. Gene expression was normalised to *ACTB* and then to normalised expression in BMMNCs in the same donor sample; n = 5, same colour data points represent same donor sample, data presented as median ± range. No statistical significance between groups has been observed, as assesed by Kruskal-Wallis test wth Dunn's correction. REU, relative expression units.

3.2.6.2 Wnt signalling in freshly isolated cells

Because there were no differences in Wnt target gene expression in cultured cells between unselected and STRO-1-enriched populations, FACS was employed on fresh samples to more accurately sort between populations with different levels of STRO-1

expression. This was made possible by the acquisition of an RNA extraction kit which allows isolation from small numbers of cells.

RNA was extracted from STRO-1^{bright}, STRO-1^{+} (without the STRO-1^{bright}), STRO-1^{-} and BMMNCs populations, with the large contaminating granulocyte population gated out. The cells came from four different donor bone marrow samples (Table 3.2). The STRO-1^{bright} fraction constituted the top 10 % of the STRO-1^{+} population, after magnetic sorting and confirmation by fluorescent sorting. Figure 3.19A illustrates the procedure of sorting cells into the aforementioned populations based on the intensity of STRO-1 expression. RNA samples were free from DNA contamination as assessed *via* NanoDrop (260nm/280nm absorbance ratio >2.0), and the concentrations were sufficient to conduct reverse transcription of 300 ng of RNA. All cDNA samples were assessed together by qPCR for the expression of Wnt target genes.

Table 3.2 Cell numbers after FACS sorting for populations with different expression of STRO-1.

Numbers of BMMNCs and various populations divided according to STRO-1 expression levels after MACS selection and FACS of freshly isolated cells for subsequent RNA extraction. The STRO-1+ population does not contain the STRO-1^{bright} fraction.

Donor number	Sample	Cell count	% STRO-1+ cells after MACS selection	Estimated cell count after FACS
1	1 BMMNCs	86 000 000		
1	2 STRO-1^{-}			
1	3 STRO-1^{+}	4 500 000	5.3	1 500 000
1	4 STRO-1^{bright}			170 000
2	5 BMMNCs	70 000 000		
2	6 STRO-1^{-}			
2	7 STRO-1^{+}	3 000 000	4.2	1 370 000
2	8 STRO-1^{bright}			115 000
3	9 BMMNCs	125 000 000		
3	10 STRO-1^{-}			
3	11 STRO-1^{+}	7 700 000	5.6	1 800 000
3	12 STRO-1^{bright}			250 000
4	13 BMMNCs	100 000 000		
4	14 STRO-1^{-}			
4	15 STRO-1^{+}	2 600 000	2.6	830 000
4	16 STRO-1^{bright}			55 000

Relative gene expression levels of *CMYC, CCND1, AXIN2, LEF1* and *TCF4* in cDNA samples from matching BMMNCs, STRO-1$^-$ and STRO-1$^+$ cell populations, calculated by the ΔΔCt method, after normalisation to *ACTB* housekeeping gene and to 1 for cDNA from BMMNCs, are shown in Figure 3.19B and C. Statistically significant differences were observed in *CMYC* transcription between the STRO-1 expressing cells and non-selected BMMNC populations and in *CCND1* between the STRO-1^{bright} cells specifically and STRO-1$^-$ and non-selected BMMNC populations. For *AXIN2,* a non-significant trend was observed.

As it has recently been shown that Osterix/SP7-expressing cells can produce Wnts and respond to Wnt signalling to control bone homeostasis, the expression of SP7 was tested in the STRO-1-expressing cells as well. The results showed that STRO-1^{bright} cells expressed higher levels of SP7 than unsorted BMMNCs (Figure 3.19D).

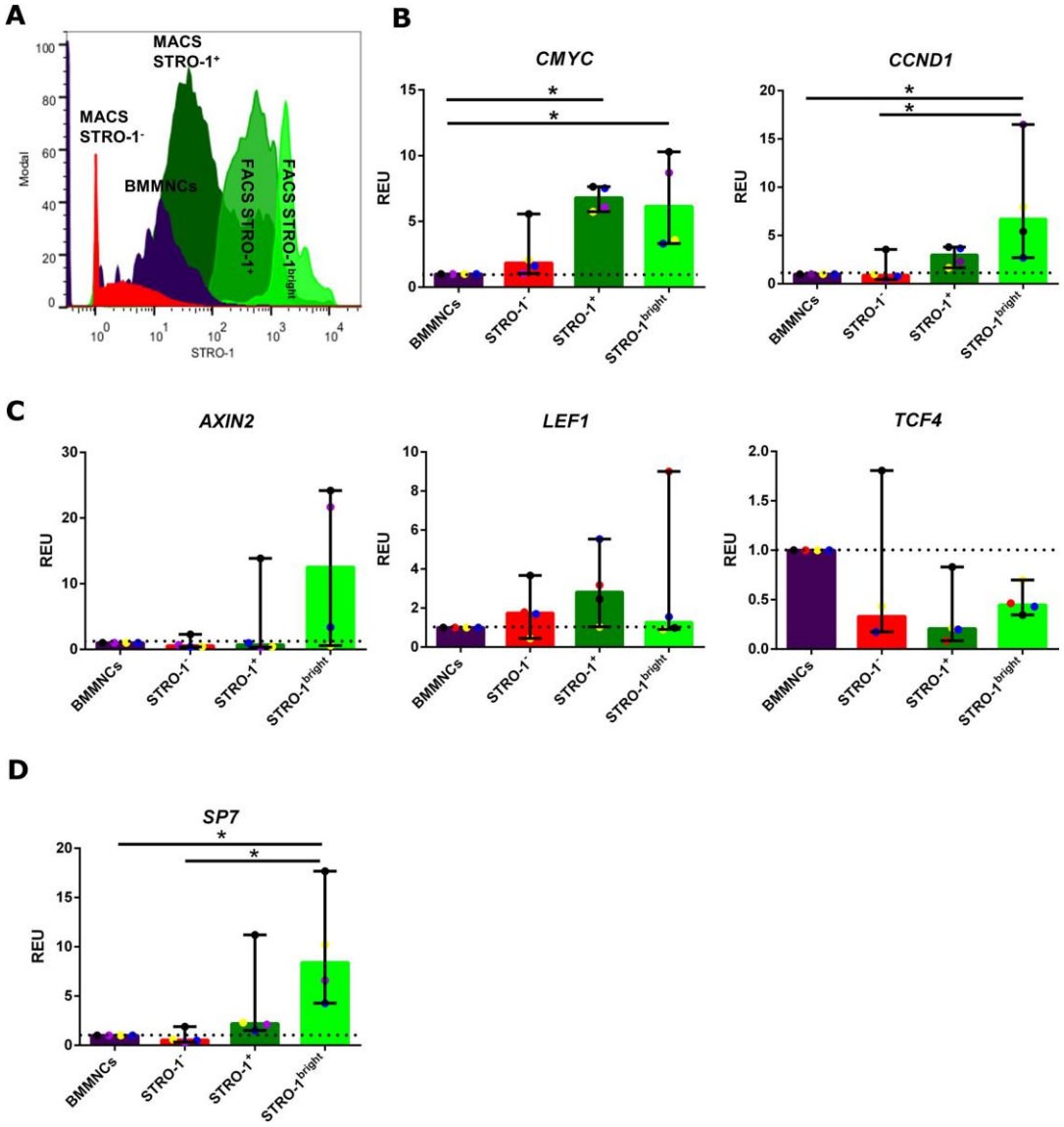

Figure 3.19 Wnt target gene expression in freshly isolated BMMNCs *vs.* cells with different degrees of STRO-1 antigen expression.

MACS and FACS were conducted in order to obtain various enrichments of fresh BMMNCs for STRO-1$^+$ subsets. A: Overlay of flow cytometry histograms showing various fractions of the bone marrow with regards to their STRO-1 expression and the procedure of sorting into STRO-1$^+$ and STRO-1^{bright} populations based on FACS. The STRO-1^{bright} fraction constituted the top 10 % of the STRO-1$^+$ population according to FACS. The STRO-1 MACS-selected fraction had a high degree of STRO-1$^-$ cells and hence was not analysed, but used solely for enrichment before FACS staining to provide sufficient numbers of STRO-1$^+$ cells for subsequent RNA extraction. B: mRNA expression of *CMYC* and *CCND1* in STRO-1$^-$, STRO-1$^+$ and STRO-1^{bright} cells as relative to BMMNCs. C: mRNA expression of *AXIN2, LEF1* and *TCF4* in STRO-1$^-$, STRO-1$^+$ and STRO-1^{bright} cells as relative to BMMNCs. D: mRNA expression of *SP7* in STRO-1$^-$, STRO-1$^+$ and STRO-1^{bright} cells as relative to BMMNCs. Gene expression was normalised to *ACTB* and then to normalised expression in BMMNCs in the same donor sample. n = 4, same colour data points represent same donor sample, data presented as median ± range. Statistical significance assessed by Kruskal-Wallis test with Dunn's correction, *p<0.05.

3.2.7 Comparison between cultured BMMNCs and STRO-1-enriched bone marrow isolates

When the BMMNC isolates and the STRO-1-enriched isolates were seeded onto tissue culture plastic, their morphology was mostly fibroblast-like, typical for stromal cell / skeletal stem cell populations (Figure 3.20). There were no apparent differences in adherent cell types between the two BMMNC and STRO-1-enriched isolates, as contaminating macrophage-like cells (round, fried egg-like) were apparent in both cultures. For the purpose of this thesis, the nomenclature "BMMNCs" and "STRO-1-enriched/selected cells" will be used to differentiate between the two isolates, even after seeding onto tissue culture plastic, in order to maintain consistency.

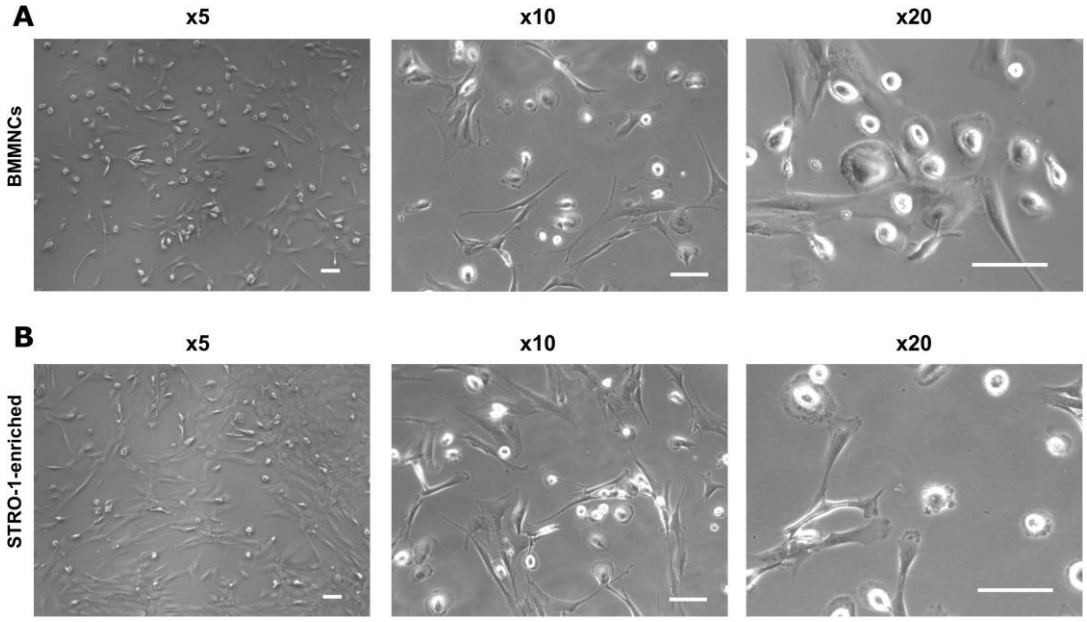

Figure 3.20 Morphology of adherent cultures of BMMNCs and STRO-1-enriched cell isolates at passage 0.

After isolation, both BMMNCs and STRO-1-enriched cells were seeded onto tissue culture plastic. Images were taken 7 days of adherent culture after the initial attachment and media change (total 12 days in culture). A: BMMNCs at increasing magnifications; B: STRO-1-enriched cells at increasing magnifications. Scale bars = 100 μm.

After passaging, all cultures contained only the stromal cell lineages. When plated at low density, clonal growth of the fibroblastic cells could be observed (Figure 3.21).

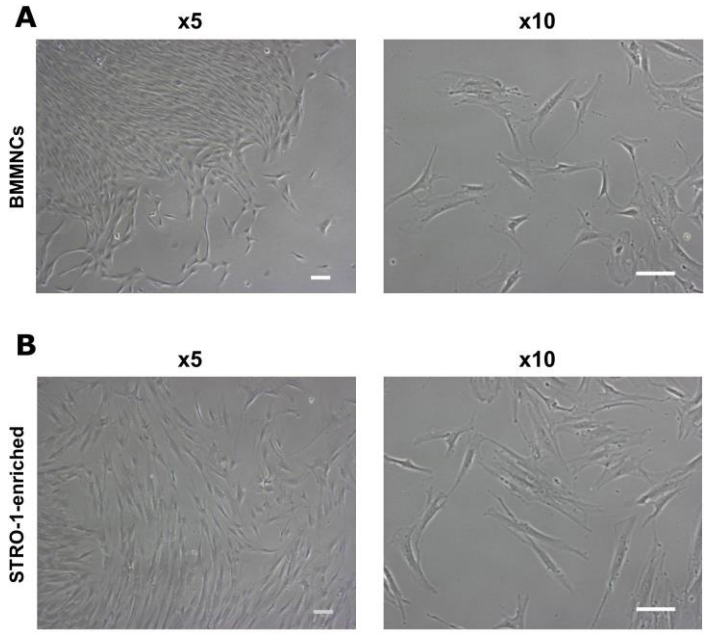

Figure 3.21 Morphology of adherent cultures of BMMNCs and STRO-1-enriched cell isolates after passaging.

A: BMMNC colony edge and cells at the edge at a higher magnification; B: STRO-1-enriched cell colony edge and cells at the edge at a higher magnification. Scale bars = 100 μm.

Because no apparent differences in the morphology of the BMMNCs *vs.* STRO-1-enriched BMMNCs were found, STRO-1 staining using a hybridoma antibody (used for MACS STRO-1-enrichment) was conducted following plastic adherence of isolated non-selected BMMNCs (5 days of culture, Figure 3.22). All cells that adhered to plastic were STRO-1^+, as marked by the hybridoma antibody staining.

Therefore the STRO-1 hybridoma antibody selected for all stromal lineages capable of plastic adherence even without the MACS enrichment step. To assess whether there were differences in the numbers of different stromal cell types between BMMNCs and the STRO-1-enriched fraction of BMMNCs, quantification of CD90, CD105 and CD146 markers expression was conducted by flow cytometry on cells cultured until 60 % confluent after adherence. Figure 3.23 shows that there were no apparent differences in expression of the stromal markers between these two fractions, apart from a slight difference in expression of the CD146 marker, which was higher in the STRO-1-enriched fraction. When stained with the commercially available STRO-1 antibody, STRO-1-enriched cells had a higher expression of STRO-1 than BMMNCs (Figure 3.23D).

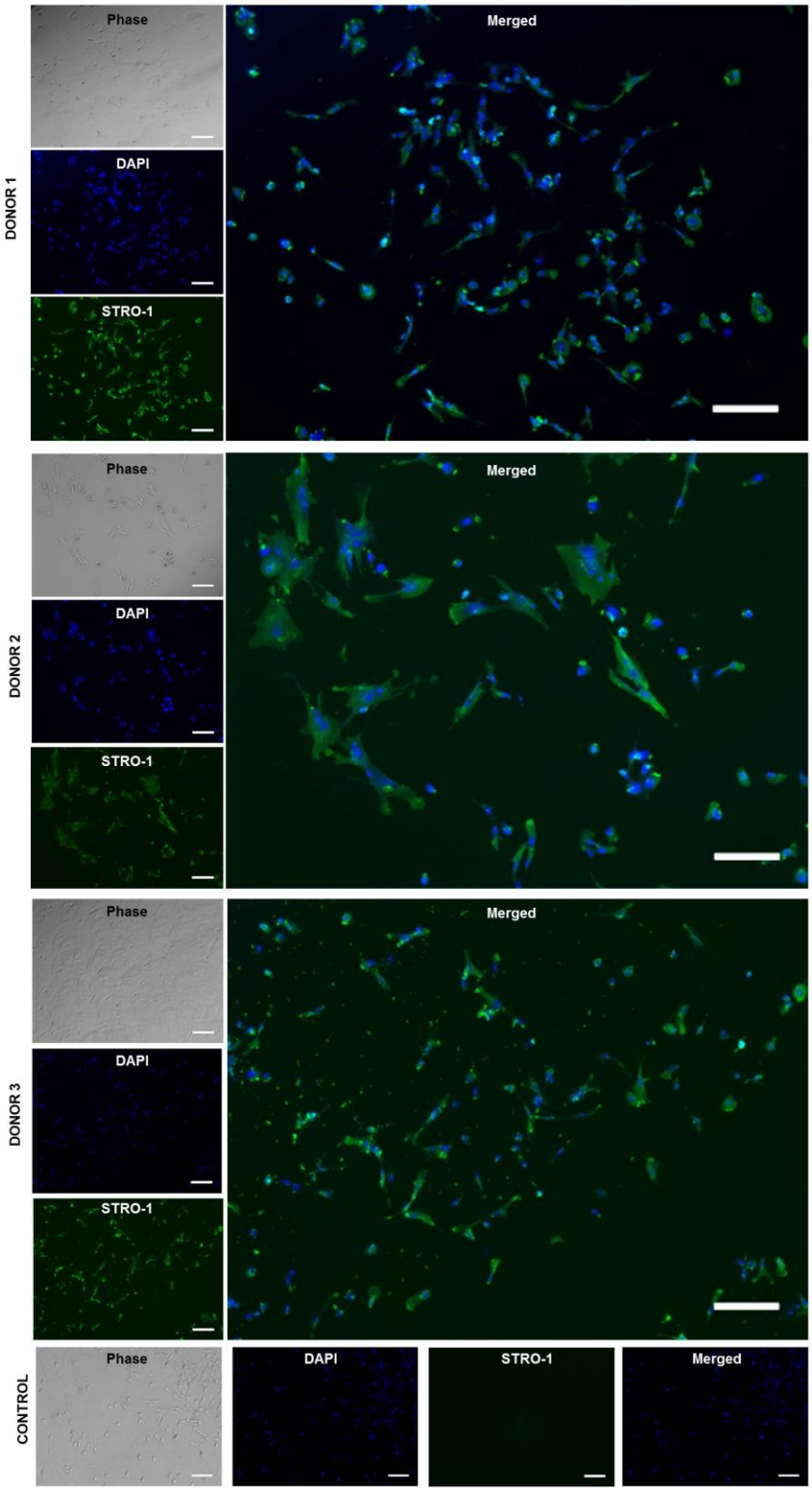

Figure 3.22 STRO-1 staining on BMMNCs 5 days after seeding.

BMMNC samples from 3 donors were stained with DAPI (nucleus) and the STRO-1 hybridoma antibody immediately after adhering to plastic (day 5). After this staining, all adherent cells were found to be positive for the STRO-1 antigen (merged). Isotype-matched antibody was used as a negative control. Scale bars = 100 μm.

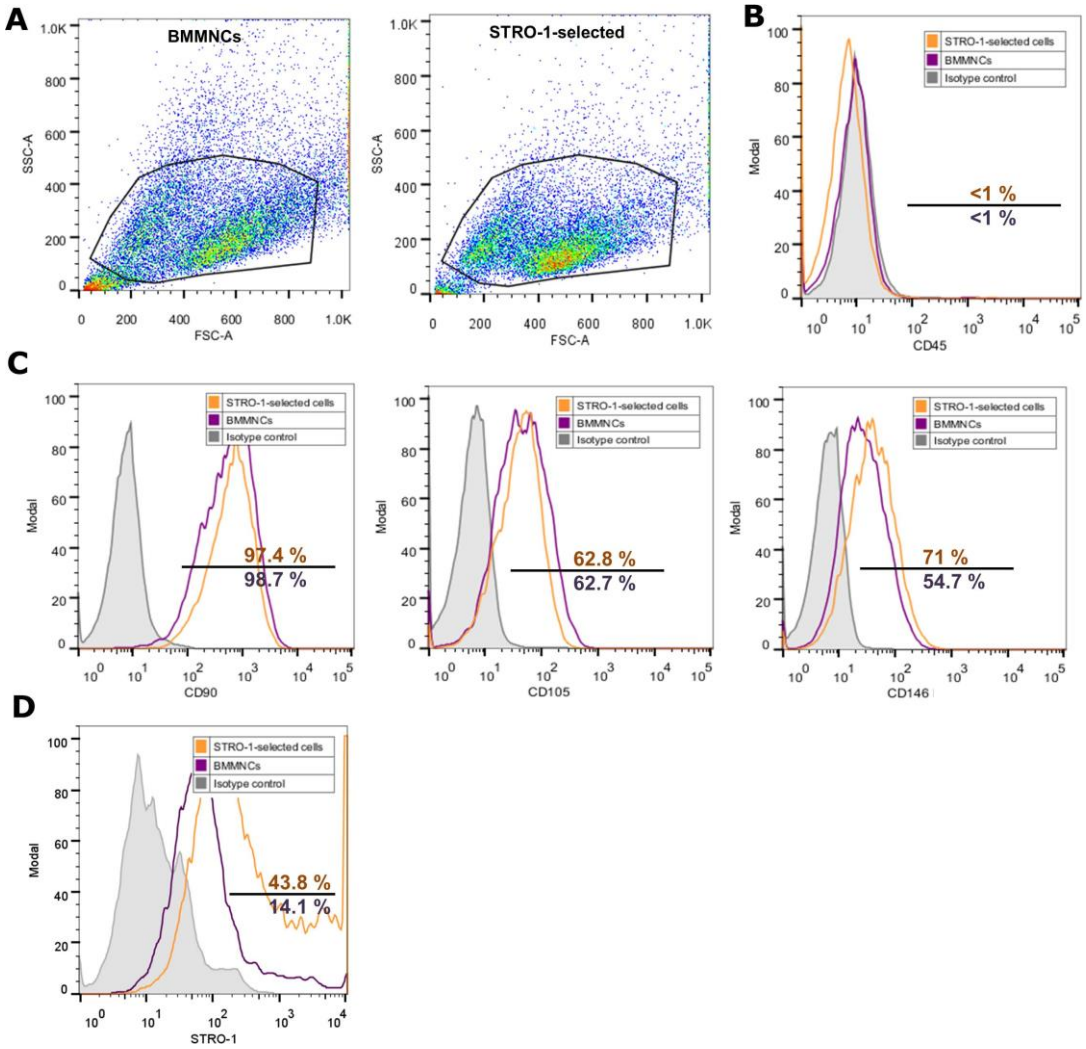

Figure 3.23 Stromal cell populations in BMMNCs *vs.* STRO-1-enriched BMMNCs after adherent culture on plastic.

A: Flow cytometry FSC *vs.* SSC dot plots of BMMNCs and STRO-1-enriched BMMNCs. B: All adherent cells were negative for CD45. C: There were no apparent differences in the expression of CD90 or CD105 between BMMNCs (purple line) and STRO-1-enriched BMMNCs (orange line). All cells gated as positive showed a fluorescence intensity greater than that detected on 99 % of the cells labelled with the isotype-matched control, presented as grey-filled histograms. According to these gates, for CD90 they were 97.4 % and 98.7 % cell positive, and for CD105 62.7 % and 62.8 %, respectively in the two populations compared. CD146 was expressed on 54.7 % of BMMNCs and 71 % of STRO-1-enriched fraction. D: STRO-1 expression was notably higher in the STRO-1-enriched cells *vs.* BMMNCs when stained with the commercially available antibody (43.8 % *vs.* 14.1 %, respectively, when gated as described). n = 1.

3.3 Discussion

All bone marrow samples used in this thesis came from osteoporotic or osteoarthritic patients undergoing hip replacement surgery, which was either scheduled or took place following a traumatic bone injury. During hip arthroplasty, the femoral head and neck is excised and the bone marrow is often aspirated to fit the prosthetic implant, therefore generating surplus biological material which would normally be discarded if not used for research. As the purpose of this thesis was to investigate a potential therapeutic treatment for bone fractures and its effects on skeletal stem cells, using samples from donors which could be the main targets of the potential therapy was considered advantageous.

After attempts to normalise the tissue volume from which cells were extracted, the mean BMMNC yield from bone marrow samples was ~140 x 10^6 cells. For female donors this number decreased with age, whereas for male donors the decline was not significant. Notably, samples used in this thesis came from donors suffering from osteoporosis or osteoarthritis, and osteoporotic patients have higher contents of fat in their marrow (Yeung *et al.* 2005). Nevertheless, there was no gender difference in the distribution of both types of diseases in the donors selected for studies. There is a possibility that the situation is similar in diseased donors as in healthy individuals, in which case the difference between the sexes might be due to the fact that in older females (>60 years old), the bone marrow fat content has been reported to be 10 % higher than in males (Griffith *et al.* 2012). This might have led to the decreased numbers of BMMNCs from older female donors.

As the STRO-1 antigen is known to enrich BMMNCs for putative stem cells, both MACS-selection for this marker and flow cytometry staining were used to assess the fraction of the bone marrow represented by STRO-1-expressing cells. The usual STRO-1-enriched BMMNC cell yield was ~6.66 x 10^6 cells, which constituted on average ~6.35 % of BMMNCs. This value was comparable to that reported in literature, with ~6.5 % incidence of STRO-1^+ cells in the BMMNC samples from MACS selection (Gronthos *et al.* 2003). There was no significant correlation between donors' sex and age, as seen for the BMMNCs. This might be due to the fact that

fewer samples were used for STRO-1-enrichment, and therefore the weak negative correlation was not reached.

Both flow cytometry and Image Stream analysis revealed a high percentage of blood lineage cells in the bone marrow preparations, which was substantially lower in the STRO-1-enriched fraction of the BMMNCs compared to non-selected BMMNCs (~57 % *vs.* ~85 %). During staining, the STRO-1 antibody was previously demonstrated to bind to approximately 10 % of the BMMNCs from bone marrows of healthy donors (Simmons and Torok-Storb 1991), and this number was close to the STRO-1 expression in the BMMNCs from donors used in this thesis, assayed by flow cytometry (~8.85 %). It is worth noting that STRO-1^+ cells colocalised with monocytes on the FSC *vs.* SSC, but constituted a distinct population (as they were negative for CD14), with only coincidental similarities to monocytes in their light scatter properties. Moreover, immunoselection by MACS yielded a population with ~62.5 % STRO-1^+ cells, which was similar to the figure of ~75.3 % previously reported for healthy donors (Gronthos *et al.* 2003). However, as expected, the majority of STRO-1^+ cells (>95 %) were GPA^+ erythroid cells (Simmons and Torok-Storb 1991). To exclude erythroid cells, STRO-1 staining was conducted in combination with GPA staining. Moreover, because of the highly heterogeneous STRO-1 staining pattern due to the use of hybridoma antibody, in addition a subpopulation characterised by very high levels of STRO-1 staining (STRO-1^{bright}, ~10 % of the STRO-1^+) was assessed. These selection criteria have previously been reported to offer substantial enrichment for CFU-Fs (0.04 – 9 % of plated enriched cells), during prospective selection of BMMNCs by MACS and FACS (Gronthos *et al.* 2003, Zannettino *et al.* 2007). After selection and staining with the hybridoma antibody in combination with negative selection with GPA and selection of only the highest 10 % of cells expressing STRO-1, the staining pattern more closely resembled that of whole BMMNC staining with the commercially available STRO-1 antibody. The hybridoma antibody used at high concentrations and the MACS technique itself could have resulted to some degree in non-specific selection. The antibody produced by the hybridoma was used unpurified from the bioreactor media, and being an IgM antibody, no effective and cost efficient protocol could be applied for the in-house purification. Although attempts were made to use it for staining at the same

concentration as the commercially available purified STRO-1 IgM, for MACS the hybridoma antibody had to be used at high concentrations. Even 24 hours after MACS, the antibody was present on the cell surface, as perhaps the magnetic bead conjugated to the secondary antibody prevented it from internalising. For future research with the antibody produced by the hybridoma, it would be preferable to investigate the option of switching the class of the antibody from IgM to IgG and thus start incorporating a simpler purification process at the end of production. This could be done by selection of naturally occurring class switch variants or genetic engineering of desired variable region genes into specially designed vectors containing constant region genes (Morrison *et al.* 1984, Spira *et al.* 1984). However, due to the pentameric structure of the IgM antibody and hence its high avidity for the antigen, a monomeric IgM antibody should be tested first to assess whether the affinity of the individual antibody molecule is high enough, before switching to the monomeric IgG.

Staining for other stromal/skeletal stem cell markers in fresh bone marrow samples, as well as STRO-1-enriched samples, resulted in the localisation of these cells similar to the monocytes based only on light scattering properties on FSC *vs.* SSC. Image Stream analysis of the $CD45^-/GPA^-/STRO\text{-}1^+$ fraction confirmed these results as well, as the putative stem cells had the highest SSC and cell area out of $CD45^-$ populations. Therefore for analysing the skeletal stem cell population, gating on the "monocytic/stromal" fraction based on FSC *vs.* SSC was used in addition to antibody markers, in order to narrow down the analysis to putative stem cells.

Although the $STRO\text{-}1^+$ population is highly heterogeneous and the marker is expressed mostly on erythroid progenitor cells in the bone marrow, it offers some advantages while being used as a sole marker for analysis/selection. For example, as opposed to CD105 marker, which is also expressed on monocytes/macrophages (Pierelli *et al.* 2001), and hence should be used in conjunction with negative CD45 selection, STRO-1 marker is generally not expressed by blood cell lineages. Also its expression on erythroid progenitor cells is not an issue when it comes to adherent cell culture, which efficiently negatively selects for suspension cells or when "monocytic/stromal" gating is applied for analysis of fresh isolates. For several years, investigations of human putative skeletal stem cells have mainly focused on sorting for

cells expressing different sets of suspected markers and assaying their CFU-F and differentiation capability *in vitro* and more rarely *in vivo*. In this chapter, the purpose of staining bone marrow populations with various markers was to localise the skeletal stem cell fraction within the fresh non-adherent bone marrow isolates for future studies. STRO-1 staining with the commercially available antibody in conjunction with appropriate "stromal" gating for the BMMNCs, as well as STRO-1 hybridoma staining in conjunction with GPA and "stromal" gating for MACS-enriched samples, was chosen as the methodology for future assessment of skeletal stem cells in fresh bone marrow isolates and in their stem cell enriched fractions, respectively.

When cultured, the BMMNCs and STRO-1-enriched samples had a similar morphology and expressed CD90 and CD105 markers to the same extent. However, STRO-1 and CD146 expression were higher in the STRO-1-enriched subsets. CD146 is an interesting marker, as its expression on MSCs has been linked to their pericyte topography and function, although it was also postulated that its expression on skeletal stem cell subsets is dependent on their *in situ* localisation (Crisan *et al.* 2008, Tormin *et al.* 2011). As STRO-1-selection enriched the bone marrow isolates for the CD146 marker, and the use of this marker has been shown to enrich for MSC populations in the dentine, but only in combination with STRO-1 (Bakopoulou *et al.* 2013), a combination of these two markers might possibly be used for prospective isolation of highly purified putative skeletal stem cells. Selection for another marker, CD106, has been used previously for sorting in combination with STRO-1, yielding a cell fraction highly enriched for CFU-Fs (Gronthos et al. 2003). However, to study the putative skeletal stem cells in fresh bone marrow isolates, these markers would ideally have to be used in conjunction with negative selection markers, such as GPA or CD45.

In order to see whether STRO-1$^+$-enriched cells, comprising the putative stem cells, differ from unsorted BMMNCs in their intrinsic Wnt signalling levels, as one would expect from a true stem cell population, qPCR experiments for Wnt target genes, such as *CMYC* (Hiyama *et al.* 2011), *CCND1* (Shtutman *et al.* 1999), *AXIN2* (Jho *et al.* 2002), *LEF* and *TCF4* (Hovanes *et al.* 2001) were conducted. Their expression levels between populations containing STRO-1$^+$ cells of varying purity were compared.

The results from cultured cells did not show any significant differences in the expression of tested genes between non-selected (BMMNCs) and STRO-1$^+$ populations. This may be due to the fact that STRO-1 isolation was conducted on cells cultured for ~2 weeks, to ensure testing a more homogenous population with the ability to adhere to tissue culture plastic. The STRO-1$^+$ cells were further down their developmental pathway and hence similar to unsorted populations. To clarify this, further studies are recommended to compare Wnt target gene expression in cells after plastic selection at P0, P1 and P2. It is well known that STRO-1 marker expression declines with prolonged culture (Simmons and Torok-Storb 1991). Also, it has been indicated previously that Wnt signalling is lower in fresh *vs.* cultured MSCs, because in tissue homeostasis low levels are sufficient and because *in vitro* expansion activates the pathway (Churchman *et al.* 2012, Qian *et al.* 2012). This could be another factor contributing to the fact that no difference between STRO-1$^+$ cells and BMMNCs was seen. Therefore, further experiments focused on determination of intrinsic Wnt activity in freshly isolated and FACS-sorted cells.

The significantly elevated levels of *CMYC* and *CCND1* genes, cell cycle markers, and the similar but non-significant trend for *AXIN2*, targets of the Wnt signalling pathway, in cells brightly staining for STRO-1, suggests that this population has higher intrinsic Wnt signalling, and hence a higher stem cell content. Interestingly, *TCF4* followed a reverse trend, with lower TCF expression in STRO-1^{bright} fraction *vs.* BMMNCs approaching significance ($p = 0.053$). It has been proposed that the expression of this transcription factor can be supressed in MSCs with high expression of β-catenin, and hence increased Wnt signalling (Kim *et al.* 2015). However, the experiments comparing the transcriptional profiles of low *vs.* high β-catenin-expressing MSCs were conducted on retrovirally transduced cells; hence the results may not be comparable to the naturally occurring Wnt signalling levels.
As the STRO-1^{bright} fraction has been shown to contain the majority (74 %) of CFU-Fs within the BMMNCs and offers a 950 fold enrichment over BMMNCs (Gronthos *et al.* 2003), a higher Wnt target gene expression in this stem cell-rich fraction *vs.* STRO-1$^+$ population (not containing the STRO-1^{bright} fraction) was expected. However, possibly due to the purity of sorting (85 - 95 %) or due to high inter-donor variability, the differences between the expression of Wnt target genes in STRO-1^{bright} *vs.* STRO-

1^+ populations were insignificant. As mentioned before, the STRO-1 staining histograms vary between the donors, and the "bright" cells are a small and incompletely resolved subpopulation. Therefore for the purpose of consistency, in this thesis it has been set on cells with the upper 10 % of fluorescence. It is possible that this somewhat arbitrary STRO-1^{bright} gate is not strict enough to differentiate between the stem cell-rich fraction and the remaining fraction. Moreover, it is important to remember that the STRO-1 marker is expressed mostly on erythroid cells (Simmons and Torok-Storb 1991), hence all STRO-1^+ fractions comprise of these cells as well, providing high background noise in the qPCR experiments. However, it would be futile to incorporate an additional negative selection marker for erythroid cells (for example GPA) in the current experimental setup, as RNA extraction from such small cell subsets would be inefficient. Even with prior enrichment of the fraction of interest, the cell numbers acquired are a limitation in this protocol, which also negatively affects the sample sorting time. To circumvent these issues, in the future, single cell qPCR could potentially be used for determining the genetic profile of GPA$^-$/STRO-1^{bright} cells after FACS selection (Sanchez-Freire *et al.* 2012).

It has recently been shown that *Osterix*/*SP7*-expressing cells can produce Wnts and respond to Wnt signalling to control bone homeostasis, as part of a comprehensive investigation into Wnt expression patterns, whereby they were colocalised with Osx-expressing cells by RNA *in situ* hybridisation (Tan *et al.* 2014). Whereas the erythroid cells are still nucleated and can blur the assessment of Wnt target gene expression in putative stem cell populations, the expression of *SP7* is specific for the osteoblastic lineage and multipotent mesenchymal progenitors (Mizoguchi *et al.* 2014, Nakashima *et al.* 2002). Therefore the expression of *SP7* in STRO-1^+ cells was examined, and the results showed that STRO-1^{bright} cells expressed significantly higher levels of this gene than unsorted BMMNCs and the STRO-1^- fraction.

Alternatively, for future approaches aiming to determine the intrinsic Wnt signalling levels in specific cell populations within the heterogeneous BMMNCs, the Image Stream technology could be applied. Staining for β-catenin in conjunction with population specific markers and a nuclear stain would allow determination of cell subsets with various levels of active Wnt signalling, after assessment of nuclear

localisation of β-catenin. The STRO-1 marker in this setting could be used with the negative selection marker GPA and other putative skeletal stem cell markers, allowing for a more accurate identification of skeletal stem cells and assessment of their active β-catenin levels. Wnt signalling levels could be compared in this way in samples from scheduled surgeries with samples following trauma, to determine which populations are likely to be the most responsive. However, one must bear in mind that this technology requires very large sample volumes to accurately assess small populations and, due to inter-donor variability, would require a substantial number of samples to be tested.

Nevertheless, these data indicate that BMMNCs expressing high levels of STRO-1 antigen have higher Wnt signalling activity than those that do not. High levels of Wnt signalling have been linked to the adult stem and progenitor cell populations previously (Reya and Clevers 2005) and an increase in expression of genes involved in the Wnt signalling pathway was reported several times at the site of bone fracture (Chen *et al.* 2007, Hadjiargyrou *et al.* 2002, Kim *et al.* 2007). As the bone marrow samples used in these experiments were mostly from trauma surgeries, Wnt signalling was expected to be increased as well. Further work is required to establish the connection between skeletal stem cell marker expression and the level of Wnt signalling, possibly linking the best marker for these cells with highest Wnt activity following bone fracture.

Unfortunately, no consensus has yet been reached with regards to what might be the best marker for skeletal stem cells, and there is confusing documentation of where this population is localised *in vivo* and how it contributes to maintenance of bone homeostasis (Bianco *et al.* 2013, Boxall and Jones 2012, Lv *et al.* 2014).
In view of this knowledge gap, a considerable amount of study has been done in animal models, which have been employed to lineage trace rare cells that might be the putative skeletal stem cells, to then translate the findings into human biology (Mendez-Ferrer *et al.* 2015). Despite extensive investigation, the studies were not transferable into the human system and the identity of skeletal stem cells and their progeny has remained elusive.

However, recent advances allowed for the introduction of a new technology, the next-generation mass cytometry platform, Time of Flight Mass Cytometry (CyTOF) (Bandura *et al.* 2009), which has the potential to fill the knowledge gap surrounding skeletal stem cells. The dominance of fluorescence-based flow cytometry for analytical cellular biology may change, as measurement of multiple parameters of single cells by flow and mass cytometry combined in this new technique has more diverse uses in understanding cellular differentiation and intracellular signalling cascades, immunophenotyping, identifying rare stem cell populations and drug targeting using intracellular markers. This technique has been used to detect 38 surface and intracellular markers so far (Becher *et al.* 2014), and can theoretically detect up to 200, as it utilises transition element isotopes to label antibodies. The quantities of isotopes bound to each cell are then analysed by a time-of-flight mass spectrometer (Bendall *et al.* 2012). Therefore, there is no requirement for compensation and autofluorescence of cells is not an issue - common limitations of conventional flow cytometry. These technological advances in acquiring an increasing number of parameters per single cell, have led to discovery of novel methods for analysing multidimensional single-cell data, such as the spanning-tree progression analysis of density-normalised events (SPADE) algorithm (Qiu *et al.* 2011), which has allowed for accurate determination of haematopoietic cellular hierarchy, with automated non-user-biased gating and clustering. Therefore CyTOF has the potential to be the technique of choice in stem cell research, enabling study of the continuity of phenotypes, which is inherent in cellular differentiation. It could be the tool of choice for studying the human putative skeletal stem cells in bone marrow explants, enabling the use of the range of currently known positive and negative skeletal stem cell markers.

3.4 Conclusion

The aim of the research presented in this chapter was to characterise the bone marrow isolates and their stromal cell and skeletal stem cell content. The main findings showed that:

- ~1 - 2 ml of fresh bone marrow isolates yielded ~140 x 10^6 mononuclear cells, of which ~8.85 % express the STRO-1 marker;

- to specifically analyse the skeletal stem cell population in STRO-1-enriched fresh bone marrow isolates, co-staining with a negative selection marker, GPA, is necessary;
- mononuclear cell populations with the highest expression of the STRO-1 antigen contain stem cells, with intrinsically elevated levels of Wnt signalling.

These experiments provide a basis for further experiments which will aim to determine whether the STRO-1^+ population might also be responsive to external Wnt cues and what the effects of this Wnt signalling induction might be.

Chapter 4

Effects of Wnt signalling induction on putative skeletal stem cell populations of human bone marrow

4.1 Introduction

The main purpose of this chapter was to test whether induction of the Wnt signalling pathway could stimulate skeletal stem cells in human bone marrow to subsequently form bone. In addition, the aim was to determine how differences in temporal stimulation might affect osteogenesis in SSCs.

As discussed in Section 1.3, the Wnt signalling pathway plays a crucial role in developmental biology, stem cell fate and tissue patterning. It has also been shown to play a role in human skeletal stem cell fate, hence it has become an attractive therapeutic target in the fields of bone tissue engineering and regenerative medicine (Baron and Kneissel 2013, Kim *et al.* 2013). Preclinical and clinical trials using drugs that elevate Wnt signalling have showed promising results, augmenting bone formation in both animal models (Jin et al. 2015, Li et al. 2011, Ominsky et al. 2010) and in humans (Iyer et al. 2014, McClung et al. 2014, Padhi et al. 2011). However, the exact mechanism of their action is poorly understood, and the varying requirements for stimulation of the Wnt signalling pathway in osteoporotic patients or during different phases of fracture healing are not well known. From *in vitro* studies, there is data supporting the notion that Wnts can both stimulate or inhibit the differentiation and/or proliferation of SSCs (reviewed in Section 1.3.2), involved in sustaining bone homeostasis as well as in bone healing following trauma (Taguchi *et al.* 2005). However, these studies were performed mostly on adherent cultures of passaged SSCs. Thus, little is understood about the involvement of Wnts in supporting the maintenance, growth and maturation of SSCs in the bone marrow. Another shortcoming of *in vitro* studies conducted so far is the fact that Wnt signalling has often been induced with unpurified conditioned media, by transfection to overexpress either β-catenin or Wnts, or with the use of GSK3 inhibitors. All of these methods can result in non-specific effects, for example, overexpression can result in over-activation of the pathway far beyond natural levels. Therefore, in this thesis, activation of Wnt signalling was achieved with purified Wnt3A protein, known to activate the canonical pathway (Miller 2002). Furthermore, Wnt exposure experiments were conducted on freshly isolated BMMNCs, in suspension culture, to recapitulate the marrow cellular environment. To the best of the author's knowledge, there appears to be only one

instance in the literature of this type of study in a bioreactor, however, in this paper, Wnt signalling activation was achieved with the use of unpurified Wnt-conditioned media of unknown concentration (Baksh and Tuan 2007).

The STRO-1 marker is known to enrich heterogeneous bone marrow populations for SSCs (as mentioned in the Chapter 3 and discussed in Section 1.1.3) but little is known about the STRO-1 antigen itself, if it is indeed a protein, as the gene coding for STRO-1 has not yet been identified. STRO-1 has originally been described as a cell surface trypsin-resistant antigen expressed by CFU-Fs (Gronthos *et al.* 1994). More recently, it has been suggested that it is a 75kDa endothelial antigen, with its presence on SSCs being an induced event during culture in endothelial growth media (Ning *et al.* 2011). STRO-1 protein expression was also subsequently found in a population of CD34 cells (initially used during the STRO-1 antibody production process, CD34 now being a negative marker for SSC selection), casting doubt on the use of STRO-1 as a true SSC marker (Lin *et al.* 2011). Although the identity of the STRO-1 antigen remains uncertain, the body of evidence regarding other potential markers effective in enriching the skeletal stem cell population is also incomplete. Nonetheless, STRO-1 selection in combination with other markers identifies a population rich in CFU-F potential (Gronthos *et al.* 2003, Simmons and Torok-Storb 1991, Zannettino *et al.* 2007). For this reason, STRO-1 was chosen as the most suitable marker to study the stromal/skeletal stem/precursor cells in fresh bone marrow isolates. To date, no studies have been published examining the effects of Wnt signalling induction specifically in skeletal stem cell populations, as characterised by expression of any of the proposed markers (see 1.1.3 for characterisation of SSCs). Therefore, flow cytometry was employed to examine any possible effects on STRO-1^+ cells within BMMNCs after 24 hours of Wnt induction. To determine whether any observed effects were direct or indirect, MACS enrichment was used to examine STRO-1-selected populations alone in the same experimental system.

CFU-Fs are a common feature among different stem cell populations and are used to quantify functional SSCs and give information regarding their clonogenic potential. As mentioned in Section 1.2.3, CFU-Fs are rare, comprising 0.01 - 0.2 % of BMMNCs (Friedenstein *et al.* 1970, Gronthos and Simmons 1996), this number declining with

age (Stolzing *et al.* 2008). CFU-Fs may be important contributors to fracture repair, so finding a therapeutic intervention to augment them is of great importance from a regenerative medicine perspective. Therefore, the effect of Wnt on CFU efficiency was measured in cells which were stimulated transiently with Wnt, followed by plating at limited dilutions and culture for 14 days.

Osteogenic differentiation (maturation of SSCs into osteoblasts) is pivotal in bone growth, the general bone turnover process as well as in fracture healing. The differentiation of osteoblasts from their progenitors and stem cells is regulated by a number of key factors and signalling pathways, one of the most important being the Wnt signalling pathway (Hayrapetyan *et al.* 2015); described in detail in Section 1.3.2. Some of these factors are also commonly used as markers of osteoblast differentiation, at both gene and protein level. For example, RUNX2, a transcription factor which plays a key role in skeletal development as it is a master gene for osteoblast differentiation, and SP7, which works downstream of RUNX2, are both necessary for skeletal formation, driving the early steps of SSC commitment toward the pre-osteoblast phenotype (Deng *et al.* 2008, Ducy *et al.* 2000). Confirming the initiation of differentiation, ALP is responsible for the mineralisation of the ECM, and is often assessed both at the mRNA and protein level, when the activity of this enzyme is measured (Marom *et al.* 2005). Furthermore, osteonectin, osteopontin and osteocalcin are commonly used as late markers of osteogenic differentiation (Aubin 2001). Staining calcium deposits in the ECM is a histological technique also used for late osteogenic differentiation visualisation, involving the use of Alizarin Red S dye, which can subsequently be extracted and quantified (Gregory *et al.* 2004). Although these markers are commonly used as indicators of osteogenic differentiation, the majority of them cannot be considered purely as bone lineage-specific. Also, the described time-dependent expression of these osteogenic markers (see Figure 1.3 for a schematic of SSC commitment) is somewhat an artificial classification. To date, no perfect marker panel exists, which in a similar way to that used for undifferentiated SSCs, can clearly define a population - in this case separate between various stages of commitment of progenitor cells differentiating towards the osteogenic lineage. However, it is advantageous that extensive knowledge of general markers of differentiation exists, allowing for tracking osteogenesis. In this chapter, the influence of Wnt signalling

induction on the osteogenic commitment of SSCs was therefore measured by assessing the presumed markers of early, medium and late stages of differentiation towards bone cells.

In summary, the aim of the work in this chapter was to:

- identify the effect of Wnt signalling induction on the putative skeletal stem cell population in fresh BMMNC samples;
- enrich this population and determine whether the effects of Wnt signalling induction in SSCs occur directly, or are mediated by other cell populations within the bone marrow;
- measure colony forming and osteogenic differentiation capabilities of bone marrow cells exposed to Wnt.

These studies were performed to test the hypothesis that skeletal stem cells are responsive to external Wnt cues, and whether induction of Wnt signalling in fresh bone marrow isolates leads to increased proliferation and osteogenic differentiation of these stem cells.

A pictorial summary of the experimental protocols is shown in Figure 4.1.

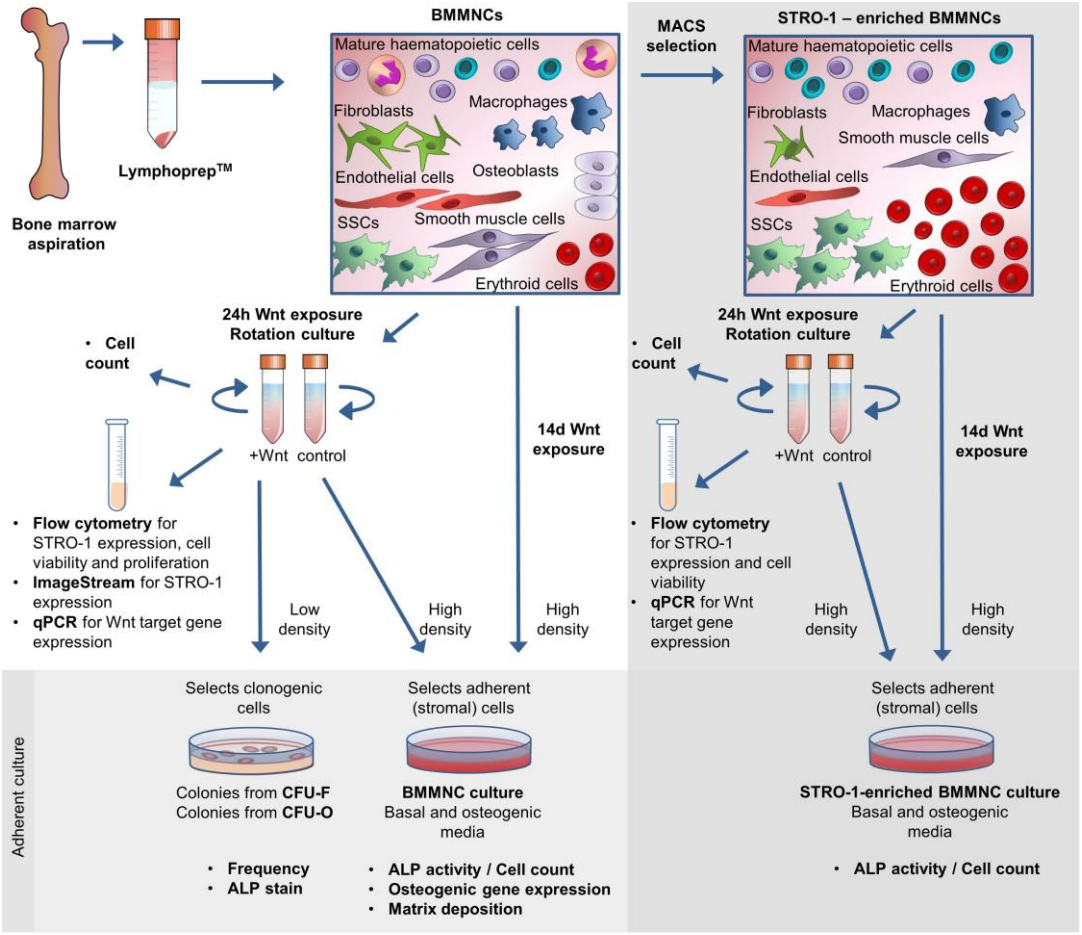

Figure 4.1 Overview of methodologies used and described in this chapter for measurement of the effects of exposure to Wnt protein on bone marrow isolates.

BMMNCs were isolated from bone marrow aspirates by Lymphoprep™, and a subset of samples was further enriched by MACS selection for the STRO-1 antigen, before being exposed to Wnt protein either for 24 hours in suspension or for 14 days in adherent culture. Flow cytometry enabled comparison of STRO-1 expression between BMMNCs and STRO-1-enriched samples after the 24 hour exposure to Wnt. These populations were also assayed for Wnt pathway activation by measuring the expression of Wnt target genes. Adherent cell cultures allowed for quantification of CFU capacity as well as osteogenic differentiation of Wnt-exposed bone marrow isolates. BMMNCs, bone marrow mononuclear cells; MACS, magnetic activated cell sorting; FACS, fluorescence-activated cell sorting; SSCs, skeletal stem cells.

4.2 Results

4.2.1 Wnt protein activity

For the experiments involving the use of Wnt3A protein, initially murine Wnt3A was used, subsequently exchanged for human Wnt3A upon availability. To compare the activity of murine *vs.* human Wnt3A protein in inducing Wnt signalling, a murine 3T3 Wnt reporter cell line was used. The dose response curves from the luciferase assay are depicted in Figure 4.2A, and compare murine *vs.* human Wnt3A activity. A well-known non-specific Wnt pathway inducer, lithium chloride (LiCl), was also tested for comparison of maximum induction levels (Figure 4.2B).

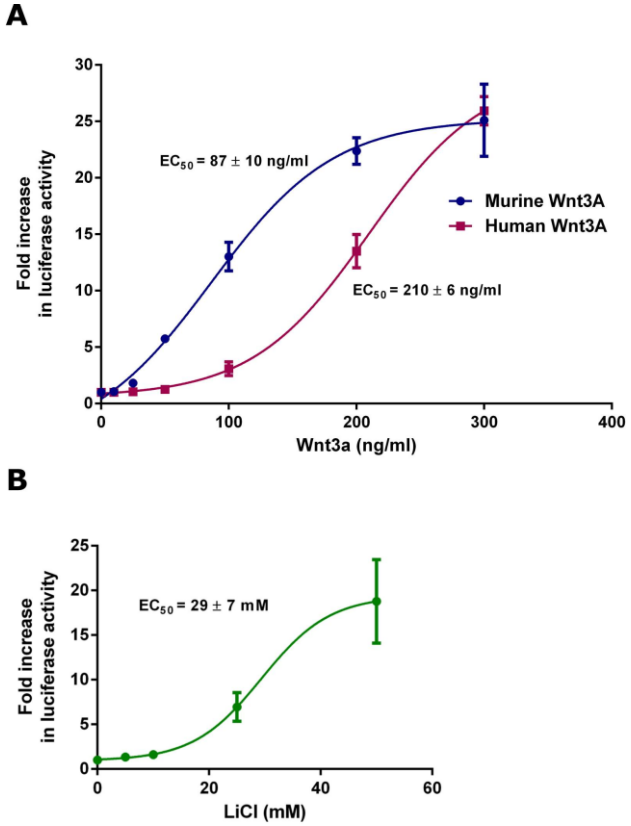

Figure 4.2 Wnt pathway activation by murine *vs.* human Wnt3A protein and LiCl.

A: A comparison between murine and human Wnt3A protein activity, based on a luciferase assay conducted on a murine Wnt-responsive cell line. The EC_{50} for the human protein is ~2 fold higher than for the murine protein. B: Activation of Wnt pathway by LiCl. Maximum induction measured as fold increase in luciferase activity was lower for LiCl than for Wnt3A protein. All data points were normalised to controls without the addition of Wnt3A or for LiCl to NaCl, as well as to cell number.

As the dose response was tested on a murine cell line, it was accepted that a murine Wnt3A could have a lower EC_{50}. For consistency throughout the experiments on

human cells, 100 ng/ml of either murine or human Wnt3A protein was used, unless stated otherwise.

4.2.2 Wnt pathway activation during short-term suspension culture

To study the effects of Wnt signalling induction by the Wnt3A protein in fresh isolates of BMMNCs or in their STRO-1-enriched subset, a 24 hour suspension rotation culture was initially employed. To assess whether Wnt signalling was induced during this short-term incubation, expression of Wnt target genes was measured. For this purpose, both BMMNCs and STRO-1-enriched cells were cultured for 24 hours with the addition of Wnt3A, Dkk1 (Wnt signalling inhibitor) or a carrier control. Subsequently, the expression of *AXIN2, CMYC* and *CCND1* was measured by qPCR (Figure 4.3).

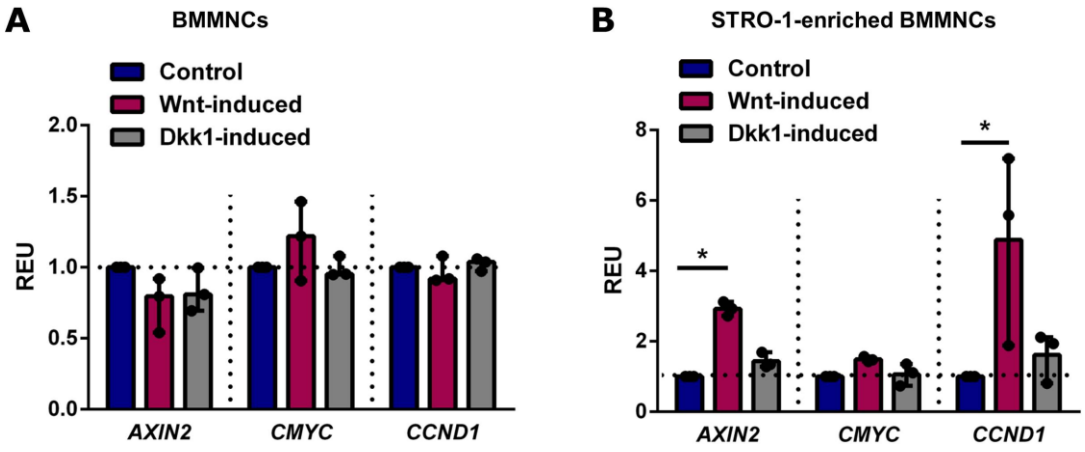

Figure 4.3 Wnt target gene expression after a 24 hour suspension culture of BMMNCs and STRO-1-enriched BMMNCs.

A: mRNA expression of *AXIN2*, *CMYC* and *CCND1* in BMMNCs. No statistical significance between the groups was observed. B: mRNA expression of *AXIN2*, *CMYC* and *CCND1* in STRO-1-enriched BMMNCs. *AXIN2* and *CCND1* expression levels were significantly upregulated compared to controls. Gene expression was normalised to *ACTB* and then normalised to expression in BMMNCs or STRO-1-enriched BMMNCs in the same donor sample. n = 3, data presented as median ± range, statistical significance assessed by Kruskal-Wallis test with Dunn's correction, *$p<0.05$. REU, relative expression units.

No differences were found in Wnt target gene expression within the BMMNC populations, but *AXIN2* and *CCND1* expression were significantly upregulated after a 24 hour incubation with Wnt3A in the STRO-1-enriched fraction of BMMNCs, indicating that the STRO-1^+ cells are responsive to stimulation with Wnt. This short-

term exposure to Wnt3A protein was used in further experiments to study the effects of Wnt signalling induction on skeletal stem cells in fresh bone marrow isolates.

4.2.3 Effects of short-term Wnt exposure on cells in suspension

4.2.3.1 Effects on skeletal stem cell marker expression

As the STRO-1$^+$ population was responsive to Wnt3A protein within 24 hours of suspension culture, an examination was carried out into whether this short, transient, canonical Wnt stimulus could induce an increase in the frequency of the SSC-containing STRO-1$^+$ population. For this reason, flow cytometry was used to study the expression of this marker, following Wnt exposure. 11 different donor BMMNC samples were analysed (see Appendix, Table A.11), and cells were assayed immediately after the short-term incubation in suspension with or without the Wnt3A protein. Figure 4.4 depicts gating applied during analysis, highlighting "monocytic/stromal" gating on the FSC *vs.* SSC dot plot (in order to limit the analysis as close as possible to SSCs, where this population localises (see Chapter 3, Figure 3.8)), and marker setting based on isotype control applied to the histogram showing STRO-1 expression, consistent between control and Wnt-induced samples.

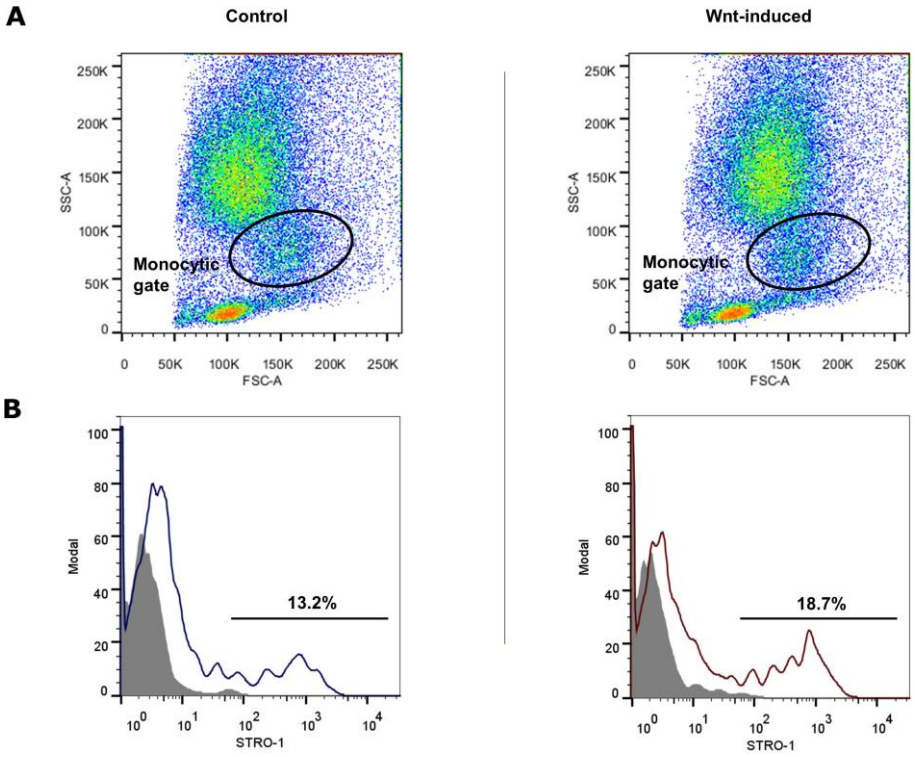

Figure 4.4 Gating strategy for quantification of STRO-1 expression.

BMMNCs were cultured with Wnt3A protein or vehicle control for 24 hours in a suspension rotation culture, after which staining for STRO-1 and flow cytometry were conducted. A: FSC *vs.* SSC dot plots of control and Wnt-induced samples of BMMNCs, with the region colocalising with the "monocytic" gate containing the putative skeletal stem cells highlighted. B: Representative histograms of STRO-1 expression in control and Wnt-induced samples. Markers on histograms were set to the reactivity levels obtained with the isotype-matched control antibodies, and all cells gated as positive showed a fluorescence intensity greater than that detected on 99 % of the cells labelled with the isotype-matched control. FSC, forward scatter; SSC, side scatter.

Short-term Wnt induction in BMMNCs significantly increased STRO-1 expression in the "monocytic/stromal" gate, as compared to a vehicle control (from 9.33 ± 4.59 % to 12.4 ± 6.12 %, Figure 4.5A and Appendix, Table A.11). STRO-1 is a non-specific marker of SSCs, and its expression can be found in other regions of the FSC *vs.* SSC dot plot depicting all BMMNCs in addition to the "monocytic/stromal" gate. However, the differences between the Wnt-induced samples and controls were non-significant when compared within the lymphocytic and granulocytic gates (Figure 4.5B and C). A significant increase in STRO-1 expression in the Wnt-induced samples was also observed when the BMMNC population was analysed as a whole, albeit to a lower degree (Figure 4.5D), suggesting that the effects of Wnt on the increase in STRO-1

frequency was confined to cells with light scattering properties comparable to monocytes, which include stromal cells and putative SSCs.

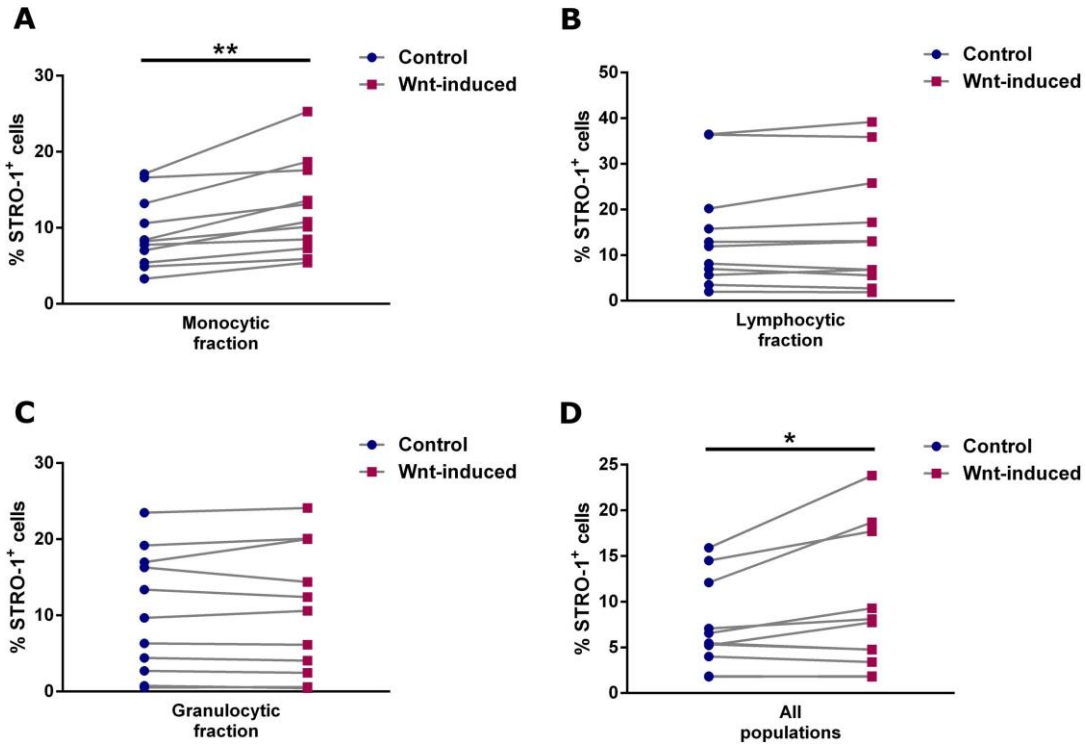

Figure 4.5 STRO-1 expression in BMMNCs after short-term Wnt induction.

BMMNCs were cultured with Wnt3A protein or vehicle control for 24 hours in a suspension rotation culture, after which staining for STRO-1 and flow cytometry were conducted. A: An increase in the expression of STRO-1 in Wnt-induced samples *vs.* control was observed within the "monocytic/stromal" gate based on light scattering. Gating on this region allowed for a more accurate analysis of the STRO-1 expression on skeletal stem cells. B and C: No differences in the expression of STRO-1 were observed within the lymphocytic (contains STRO-1$^+$ erythroid cells) and granulocytic regions. D: An increase in the expression of STRO-1 in Wnt-induced samples *vs.* control was also observed when the entire BMMNC population was analysed. Statistical significance was assessed by paired t-test, n = 11, *$p<0.05$, **$p<0.01$.

Next, to try and exclude a possible indirect role for Wnt3A, for example, inducing a paracrine signal in another non-stromal cell population, STRO-1 expression was assessed on STRO-1 MACS-selected samples (with reduced haematopoietic lineage cells) from 3 donors, immediately after short-term incubation with Wnt in suspension. When stained solely with the STRO-1 antibody (Figure 4.6A), no difference could be seen between the Wnt-induced and control samples, as reasoned in the previous chapter, possibly due to the low specificity of the hybridoma antibody. As shown in the previous chapter, in order to assess the putative skeletal stem cell population accurately in MACS-

selected samples, the STRO-1 marker is best used in conjunction with the negative selection marker for erythroid cells, GPA (Figure 4.6B and C). A 5.63 ± 1.15 % increase in the GPA$^-$/STRO-1$^+$ cells was seen and a 0.91 ± 0.09 % increase in the GPA$^-$/STRO-1^{bright} cells was seen in the "monocytic/stromal" fraction (based on light scattering properties) of the STRO-1-enriched BMMNC population.

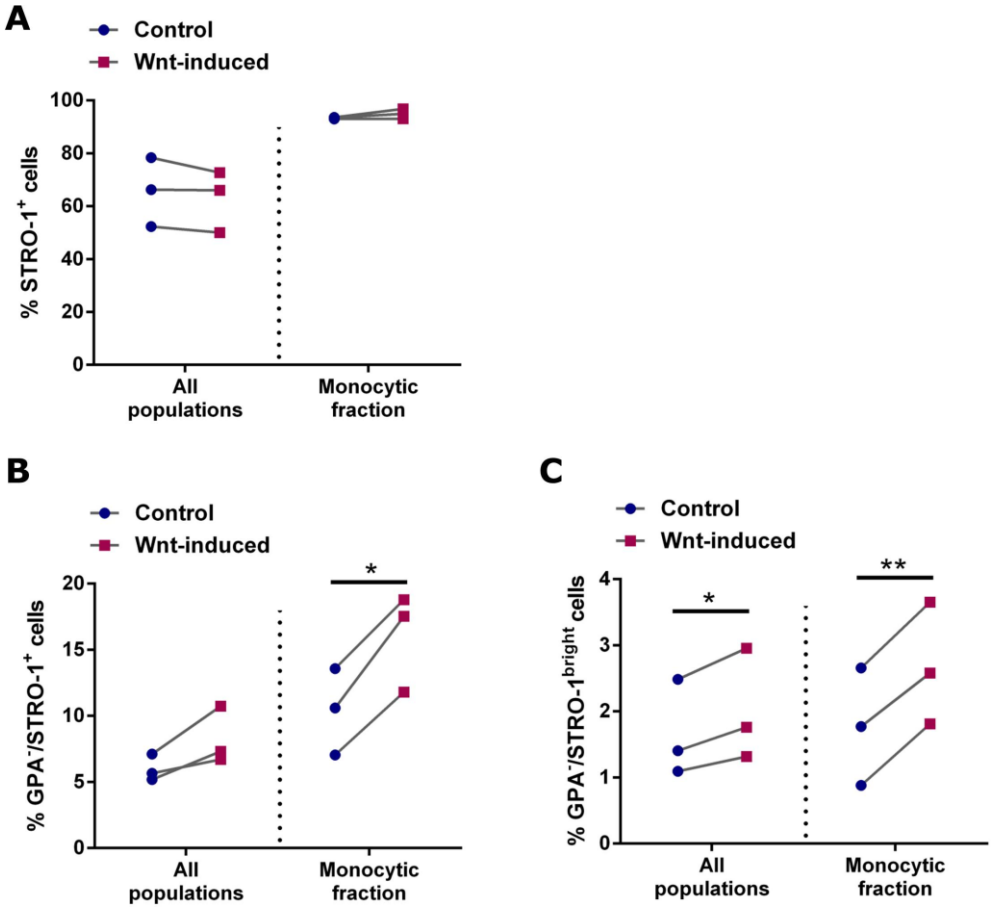

Figure 4.6 STRO-1 expression in STRO-1-enriched BMMNCs after short-term Wnt induction.

MACS STRO-1-enriched cells were cultured with Wnt3A protein or vehicle control for 24 hours in a suspension rotation culture, after which staining for STRO-1 and GPA and flow cytometry were conducted. A: There was no difference in the percentages of STRO-1$^+$ cells within the MACS STRO-1-enriched BMMNCs between the control and the Wnt-induced samples when staining was conducted with the STRO-1 hybridoma antibody alone. B: Addition of the negative selection marker GPA allowed for more accurate analysis of the the skeletal stem cell population. An increase in STRO-1 expression was noted within the "monocytic/stromal" gate after Wnt induction. C: An increase in STRO-1 expression after Wnt induction was noted within the entire population and also the "monocytic/stromal" subset, when the GPA$^-$/STRO-1^{bright} cells were analysed. Statistical significance was assessed by paired t-test, but for ease of interpretation is presented in grouped graphs, n = 3, *$p<0.05$, **$p<0.01$.

Together, these results showed that the STRO-1-expressing putative skeletal stem cell population increases after short-term stimulation with Wnt3A, both within the entire BMMNC population, and within its STRO-1-enriched subset.

Next, Image Stream cytometry was used to confirm that the increased STRO-1 expression observed by flow cytometry was due to a higher percentage of cells expressing this marker as well as its increased expression. By implementing an algorithm differentiating between whole cell expression and specific cell surface expression, Image Stream offers a substantial advantage in analysis of STRO-1 expression (Figure 4.7A). The distribution of the marker within a cell was also calculated (Figure 4.7B), to see whether the response to Wnt signalling might have polarised STRO-1 expression, as little is known about this marker itself and how it is expressed. The results confirmed previous observations of an increased number of STRO-1$^+$ events after Wnt stimulation, and also showed an increased total and surface intensity of the STRO-1 staining, with no difference in its distribution (Figure 4.7C).

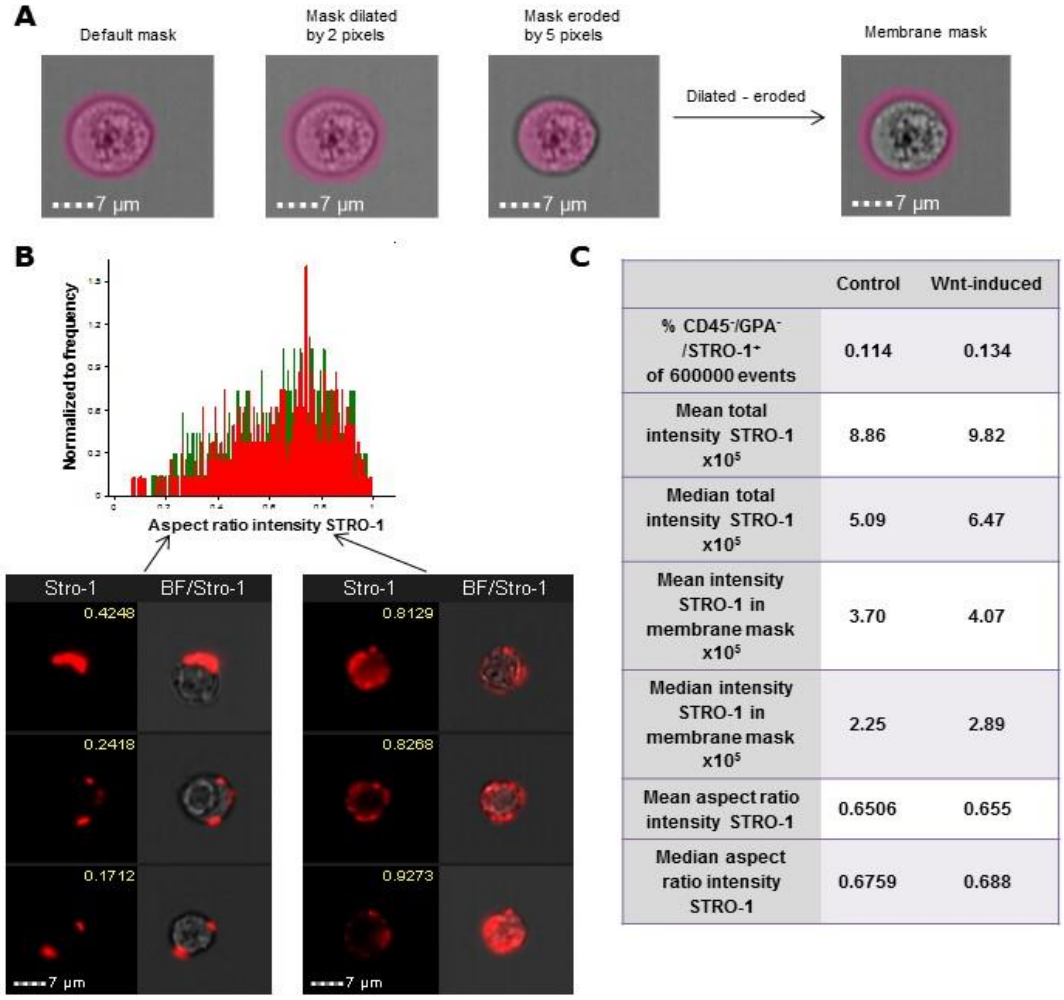

C

	Control	Wnt-induced
% CD45⁻/GPA⁻ /STRO-1⁺ of 600000 events	0.114	0.134
Mean total intensity STRO-1 x10⁵	8.86	9.82
Median total intensity STRO-1 x10⁵	5.09	6.47
Mean intensity STRO-1 in membrane mask x10⁵	3.70	4.07
Median intensity STRO-1 in membrane mask x10⁵	2.25	2.89
Mean aspect ratio intensity STRO-1	0.6506	0.655
Median aspect ratio intensity STRO-1	0.6759	0.688

Figure 4.7 Image Stream analysis of STRO-1 expression in BMMNCs after short-term Wnt induction.
BMMNCs were cultured with Wnt3A protein or vehicle control for 24 hours in a suspension rotation culture, after which staining for CD45, STRO-1 and GPA and Image Stream analysis were conducted. A: A schematic illustrating the default mask setting and derivation of the membrane mask, allowing for the measurement of the STRO-1 expression intensity in the entire cell or only on its surface, respectively, using Image Stream. B: A histogram showing the distribution of STRO-1 staining on Wnt-stimulated (green) *vs.* control cells (red). Cells with an even distribution will have a value near 1, and those that have more of the stain on one side will be nearer 0. C: Table summarising the Image Stream analysis, showing an increased number of $CD45^-/GPA^-/STRO\text{-}1^+$ events in the Wnt-induced group, as well as an increase in the STRO-1 intensity, both in the entire cell as well as the membrane mask. However, Wnt induction did not have an effect on the distribution of STRO-1 expression. A minimum of 600 events of interest were analysed. BF, brightfield.

4.2.3.2 Effects on skeletal stem cell viability and proliferation

Since the increase in $STRO\text{-}1^+$ cells after Wnt stimulation was consistent, and considering that Wnt3A may exert its effect by providing mitogenic or cell survival signals for stem cell/stromal populations, work was performed to assess whether this

effect was due to increased viability or proliferation of STRO-1^+ cells within BMMNC and STRO-1-enriched cells.

Initially, cell numbers were counted using the trypan blue exclusion method following 24 hour rotation suspension culture. Wnt3A caused no significant change in the number of viable BMMNCs (Figure 4.8A; 97.51 ± 33.13 % of starting population after 24 hours) or in the total number of cells present after incubation. However, a widespread death of cells (62.78 ± 15.80 %) within the STRO-1-enriched fraction was observed (Figure 4.8B), although this was the case regardless of whether Wnt3A was present or not.

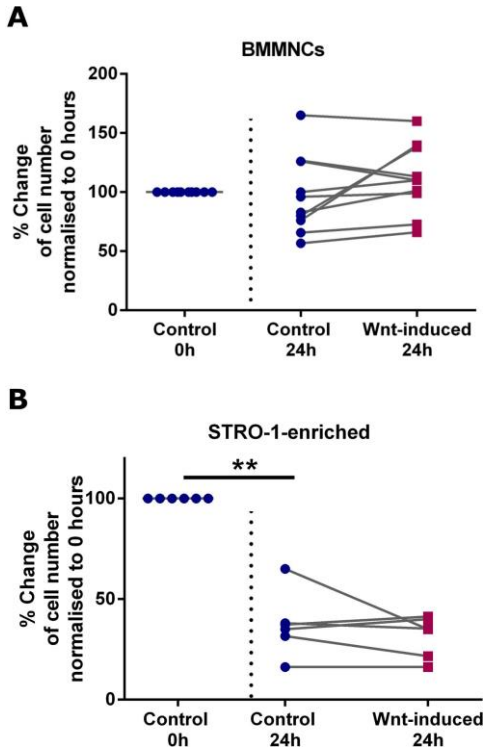

Figure 4.8 Percent change in overall cell numbers after short-term Wnt induction.

BMMNCs and STRO-1-enriched cells were cultured with Wnt3A protein or vehicle control for 24 hours in a suspension rotation culture, after which cell numbers were counted using trypan blue exclusion, and compared to the number of cells before suspension culture. A: BMMNC number did not change significantly when cultured for 24 hours in suspension, and there were no differences observed between the control and the Wnt-induced samples. B: STRO-1-enriched cell number decreased significantly when cultured for 24 hours in suspension, but there were no differences observed between the control and the Wnt-induced samples. Statistical significance between the 0 hour and 24 hour controls and 24 hour comparison between control and Wnt-induced samples for BMMNCs (n = 10) and for STRO-1-enriched BMMNCs (n = 6) was assessed by repeated measures ANOVA with Sidak's correction; **$p<0.01$.

To measure the effects on STRO-1$^+$ cell viability specifically, BMMNCs and STRO-1-enriched BMMNCs were exposed to Wnt3A or a vehicle control during short-term 24 hour suspension culture and subsequently assayed by flow cytometry in conjunction with Annexin V and 7AAD staining. This allowed for detailed analysis of the proportions of viable, apoptotic and necrotic cells within these populations. As depicted in Figure 4.9A, within the STRO-1-enriched fraction *vs.* BMMNCs a smaller proportion of cells was viable, and a higher proportion was undergoing apoptosis, as marked by positive Annexin V staining, consistent with the previous finding with the trypan blue exclusion cell count. Thus, the analysis of STRO-1$^+$ cell viability was restricted to the BMMNC population alone. After gating on cells with "monocytic/stromal" light scattering properties and subsequently on the STRO-1$^+$ subset within that gate (Figure 4.9B), percentages of viable, apoptotic and necrotic cells were calculated, and are presented as a relative change from control (Figure 4.9C). A ~3-fold Wnt3A-dependent increase in the number of viable STRO-1$^+$ cells was observed as well as decreases in the apoptotic and necrotic cells.

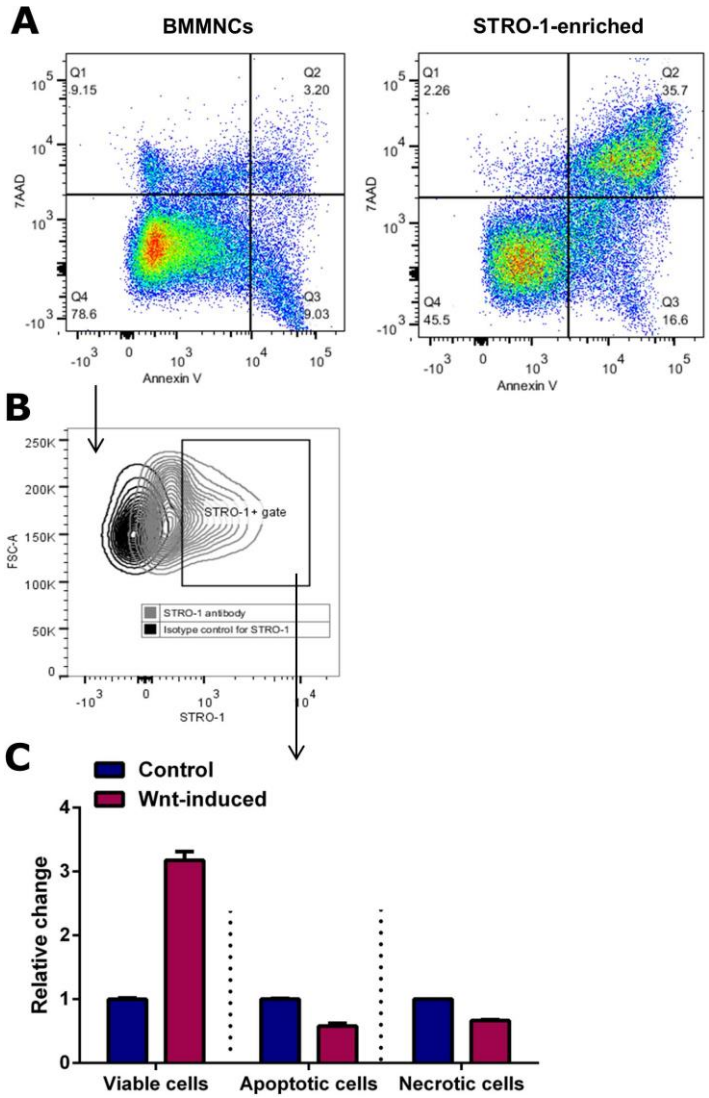

Figure 4.9 Cell viability after short-term Wnt induction.

BMMNCs and STRO-1-enriched BMMNCs were exposed to Wnt3A or a vehicle control during short-term 24 hour suspension culture and subsequently assayed by flow cytometry for STRO-1 staining in conjunction with Annexin V and 7AAD staining. A: Flow cytometry dot plots from BMMNCs and STRO-1-enriched BMMNCs depicting the distribution of viable (AnnexinV$^-$/7AAD$^-$, Q4), apoptotic (AnnexinV$^+$/7AAD$^-$, Q3), late apoptotic (AnnexinV$^+$/7AAD$^+$, Q2) and necrotic (AnnexinV$^-$/7AAD$^+$, Q1) cells within these populations. The STRO-1-enriched subset when cultured in suspension for 24 hours had fewer viable cells than non-selected BMMNCs. B: Due to high cell death in the STRO-1-enriched samples, only BMMNCs were analysed further. STRO-1$^+$ cells were gated within the "stromal" fraction of BMMNCs. C: Within the STRO-1$^+$ gate, percentages of viable, apoptotic (early and late) and necrotic cells were quantified and presented for the Wnt-induced samples as a relative change *vs.* control. n = 1, data from 3 technical replicates, presented as mean ± SD. 7AAD, 7-Aminoactinomycin D.

Subsequently, EdU incorporation, indicative of cell proliferation, was assayed by flow cytometry in the STRO-1$^+$ cells within the "stromal" gate of the BMMNC fraction

(Figure 4.10). A ~2.2 fold Wnt3A-dependent increase in the number of proliferating cells in the STRO-1$^+$ population was observed.

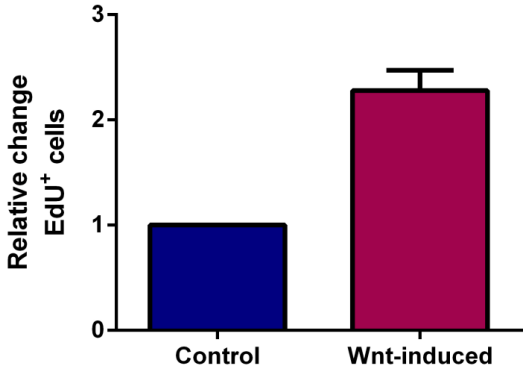

Figure 4.10 STRO-1$^+$ cell proliferation after short-term Wnt induction.

BMMNCs were exposed to Wnt3A or a vehicle control during short-term 24 hour suspension culture, where the EdU reagent was added to the cells for the last 6 hours of culture. The samples were subsequently assayed by flow cytometry for STRO-1 staining in conjunction with detention of the EdU reagent. Within the STRO-1$^+$ cell gate (from the fraction of BMMNCs with "stromal" light scattering properties), the percentage of proliferating cells was quantified based on EdU incorporation, and presented for the Wnt-induced samples as relative change *vs.* control. n = 1, data from 3 technical replicates, presented as mean ± SD.

Taken together, these results indicate that a short, transient exposure to a canonical Wnt ligand increases the frequency of cells expressing the STRO-1 surface marker which is known to enrich BMMNC populations for skeletal stem cells. This increase is likely due to both increased viability and proliferation of Wnt-exposed cells.

4.2.3.3 Effects on blood cell lineages

Next, to test whether Wnt3A stimulation had effects on white blood cell lineages, the effects of short-term, canonical Wnt stimulation were assessed on granulocytes, lymphocytes and monocytes within the BMMNC population. Wnt3A treatment did not induce changes in the relative numbers of haematopoietic lineages, assessed by flow cytometry measurements within gates of specific light scattering (Figure 4.11A). Furthermore, there was no indication of its effects when bone marrow isolates were assayed for viability and proliferation (Figure 4.11B and C), although no blood lineage-specific markers were used for this analysis, only gating based on light scatter, and only one donor sample for each was analysed.

A

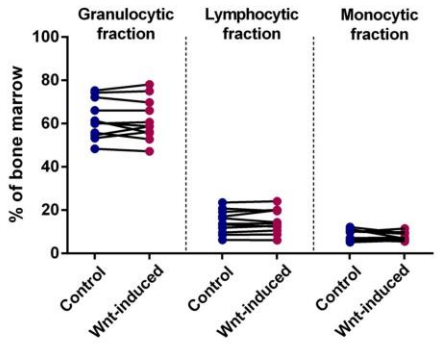

B

	Control	Wnt-induced
Viable cells		
Granulocytic fraction	77.27 ± 2.00 %	75.43 ± 1.25 %
Lymphocytic fraction	87.07 ± 2.76 %	85.03 ± 4.60 %
Monocytic fraction	81.17 ± 1.04 %	81.07 ± 0.90 %
Apoptotic cells		
Granulocytic fraction	14.12 ± 1.15 %	14.90 ± 0.55 %
Lymphocytic fraction	8.09 ± 0.4 %	9.53 ± 1.06 %
Monocytic fraction	14.07 ± 1.00 %	14.70 ± 1.08 %
Necrotic cells		
Granulocytic fraction	9.22 ± 1.13 %	10.49 ± 0.97 %
Lymphocytic fraction	3.17 ± 0.37 %	3.71 ± 0.77 %
Monocytic fraction	4.01 ± 0.22 %	3.81 ± 0.90 %

C

Proliferating cells	Control	Wnt-induced
Granulocytic fraction	17.07 ± 0.15 %	16.37 ± 0.32 %
Lymphocytic fraction	0.63 ± 0.02 %	0.52 ± 0.03 %
Monocytic fraction	13.10 ± 0.20 %	16.13 ± 0.25 %

Figure 4.11 Viability and proliferation of blood lineage cells after short-term Wnt induction.

BMMNCs were cultured with Wnt3A protein or vehicle control for 24 hours in a suspension rotation culture, after which the blood lineage fractions were assessed based on gating, Annexin V and 7AAD and EdU assays. A: 24 hour suspension culture stimulation with Wnt3A protein exerted no effect on the percentages of granulocytic, lymphocytic and monocytic fractions of BMMNCs, gated based on measurements of light scattering by flow cytometry (n = 11). B: Percentages of viable, apoptotic and necrotic cells were also similar between Wnt-induced and control samples, as assessed by flow cytometric staining for Annexin V and 7AAD and gating based on light scatter; n = 1, data from 3 technical replicates, presented as mean ± SD. C: Percentages of proliferating cells, measured by EdU incorporation, were similar between Wnt-induced and control samples, with the exception of a small increase in the "monocytic/stromal" fraction, gated based on light scatter; n = 1, data from 3 technical replicates, presented as mean ± SD.

Therefore, quantification of cells using markers for the blood lineages (CD3 for T cells, CD19 for B cells, CD56 for NK cells, CD14 for monocytes and CD66b for granulocytes) was conducted by flow cytometry. The expression patterns for these markers in the control and Wnt-induced samples were very similar (Figure 4.12), indicating no Wnt3A effect on blood cell lineages in this experimental system.

A

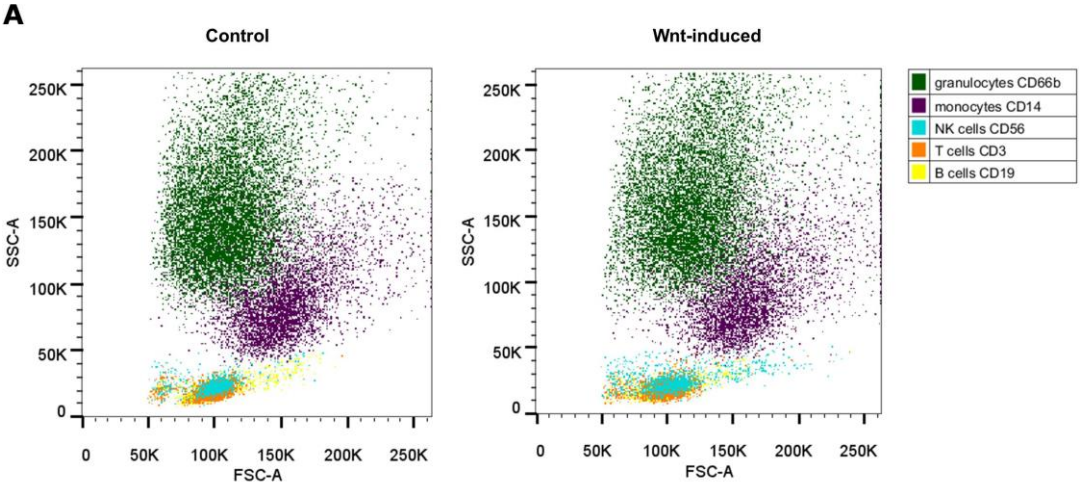

B

	Control	Wnt-induced
CD66b$^+$ (Granulocytes)	59.53 ± 3.64 %	58.07 ± 3.81 %
CD3$^+$ (T cells)	5.73 ± 2.04 %	5.65 ± 2.06 %
CD56$^+$ (NK cells)	1.96 ± 0.91 %	2.74 ± 0.95 %
CD19$^+$ (B cells)	3.87 ± 1.06 %	4.16 ± 1.02 %
CD14$^+$ (Monocytes)	11.17 ± 2.38 %	10.73 ± 2.25 %

Figure 4.12 Expression of blood cell markers after short-term Wnt induction.

BMMNCs were cultured with Wnt3A protein or vehicle control for 24 hours in a suspension rotation culture, after which flow cytometry staining was conducted for CD66b, CD3, CD56, CD19 and CD14. A: Overlays of positively stained bone marrow cell populations on the FSC *vs.* SSC dot plots of control and Wnt-induced samples. Antibodies against markers of granulocytes (CD66b), monocytes (CD14) and lymphocytes (CD56 for NK cells, CD3 for T cells and CD19 for B cells) were used. Gating strategy is detailed in the Appendix, Figure A.1. B: Percentages of granulocytes, monocytes and lymphocytes within the BMMNCs; n = 3, data presented as mean ± SD. A minor non-significant increase in expression of the NK cell marker and the distribution of the population on the FSC *vs.* SSC dot plot after Wnt stimulation were observed.

4.2.4 Effects of short-term Wnt exposure on CFU efficiency

Since STRO-1$^+$ cells contain all of the multipotent CFU-F activity of BMMNCs and are enriched in Wnt-stimulated BMMNCs, assessment of CFU-F formation was carried out.

After short-term suspension culture exposure to Wnt3A, unsorted BMMNCs were plated for 14 days in basal media and assayed for CFU-F with or without ALP (osteoblast precursor marker) staining (Figure 4.13). Purple ALP staining was more visible in colonies formed from cells incubated with Wnt, whereas colonies which arose from cells not treated with Wnt were mostly stained with the haematoxylin

counterstain (blue nuclei). Quantification of the CFU-F formation efficiency and ALP stain is presented in Figure 4.14. No increase in the frequency of CFU-Fs was observed. However, colonies that formed from Wnt3A-stimulated cells had significantly increased ALP activity under basal medium conditions.

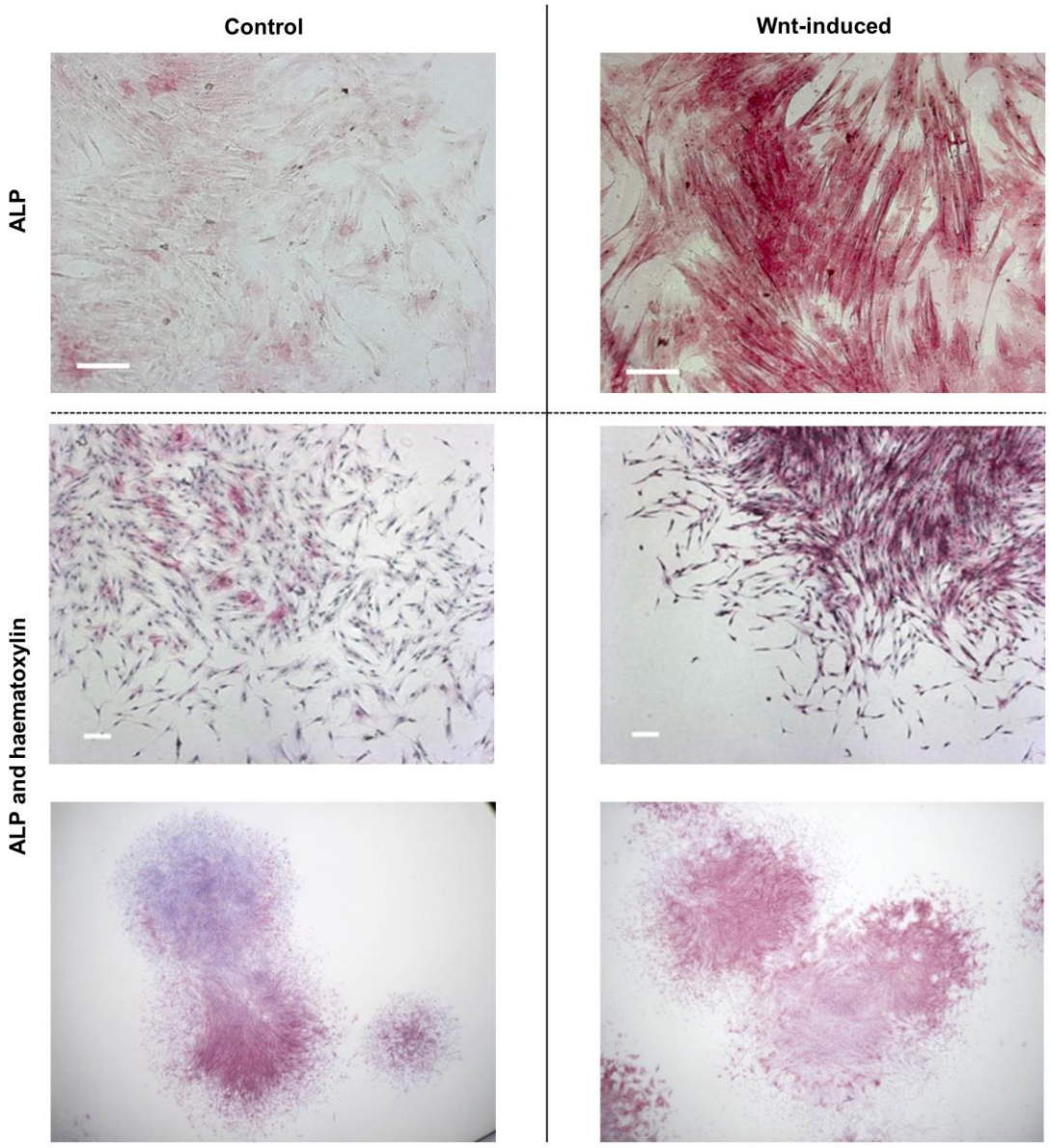

Figure 4.13 CFU-F assay with ALP staining 14 days after short-term Wnt induction.

The CFU-F assay was conducted on 24 hour suspension culture of Wnt-induced samples and controls. Representative images of colonies stained with ALP (purple/magenta) in the first row, and with ALP and haematoxylin used as a counterstain (dark blue nuclei) in subsequent images. Scale bars = 200 μm.

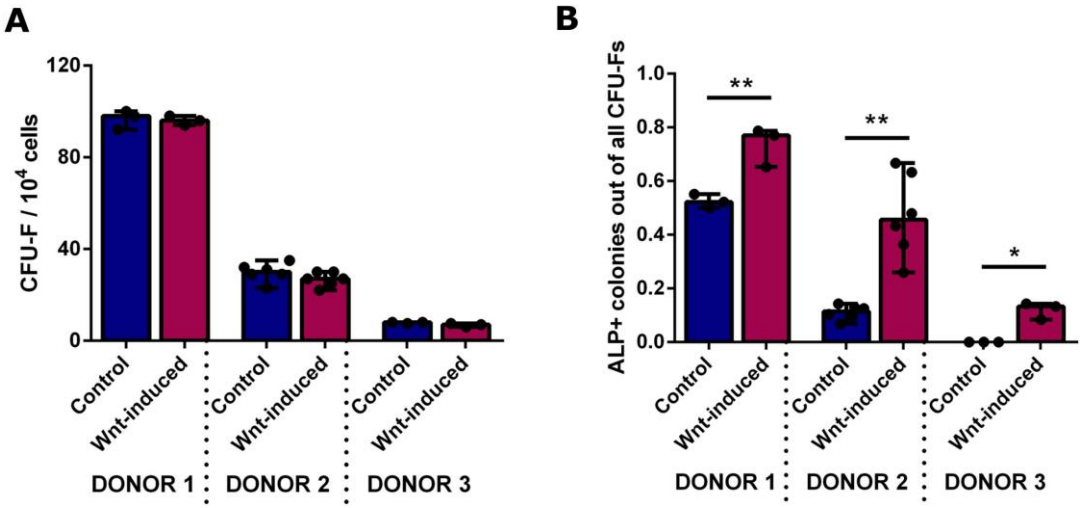

Figure 4.14 CFU-F formation efficiency and ALP staining in basal media.

A: Number of colonies per 10^4 plated BMMNCs at 14 days arising from 24 hour Wnt-treated and control samples. B: Ratios of ALP^+ CFU-Fs at 14 days arising from 24 hour Wnt-treated and control samples. Data from 3 donor samples, presented as median ± range on technical replicates. No statistically significant differences in CFU-F efficiency were observed between two experimental groups (control *vs.* Wnt-induced). However, an increase in ALP-expressing colonies was consistent among all 3 donors after Wnt-induction. Due to high variability between donors, normalisation would be inappropriate, thus data is presented from each donor separately and was analysed separately by Mann-Whitney test. *$p<0.05$; **$p<0.01$. CFU-F, colony-forming unit fibroblastic.

Next, colony formation was assayed in the presence of osteogenic medium (CFU-O assay). Again, purple ALP staining was more visible in colonies formed from cells incubated with Wnt whereas colonies which arose from cells not treated with Wnt were mostly stained with the haematoxylin counterstain (blue nuclei, Figure 4.15). Colonies in the Wnt-induced group were bigger and denser. When quantified, a significant increase in the number of CFU-O and a greater proportion of ALP^+ CFU-Os was present in Wnt-induced samples compared to controls from 2 donors (Figure 4.16). The third donor sample appeared to be highly osteogenic with an overall high colony number and nearly all colonies stained positive for ALP, with no significant difference between Wnt3A-treated or untreated groups.

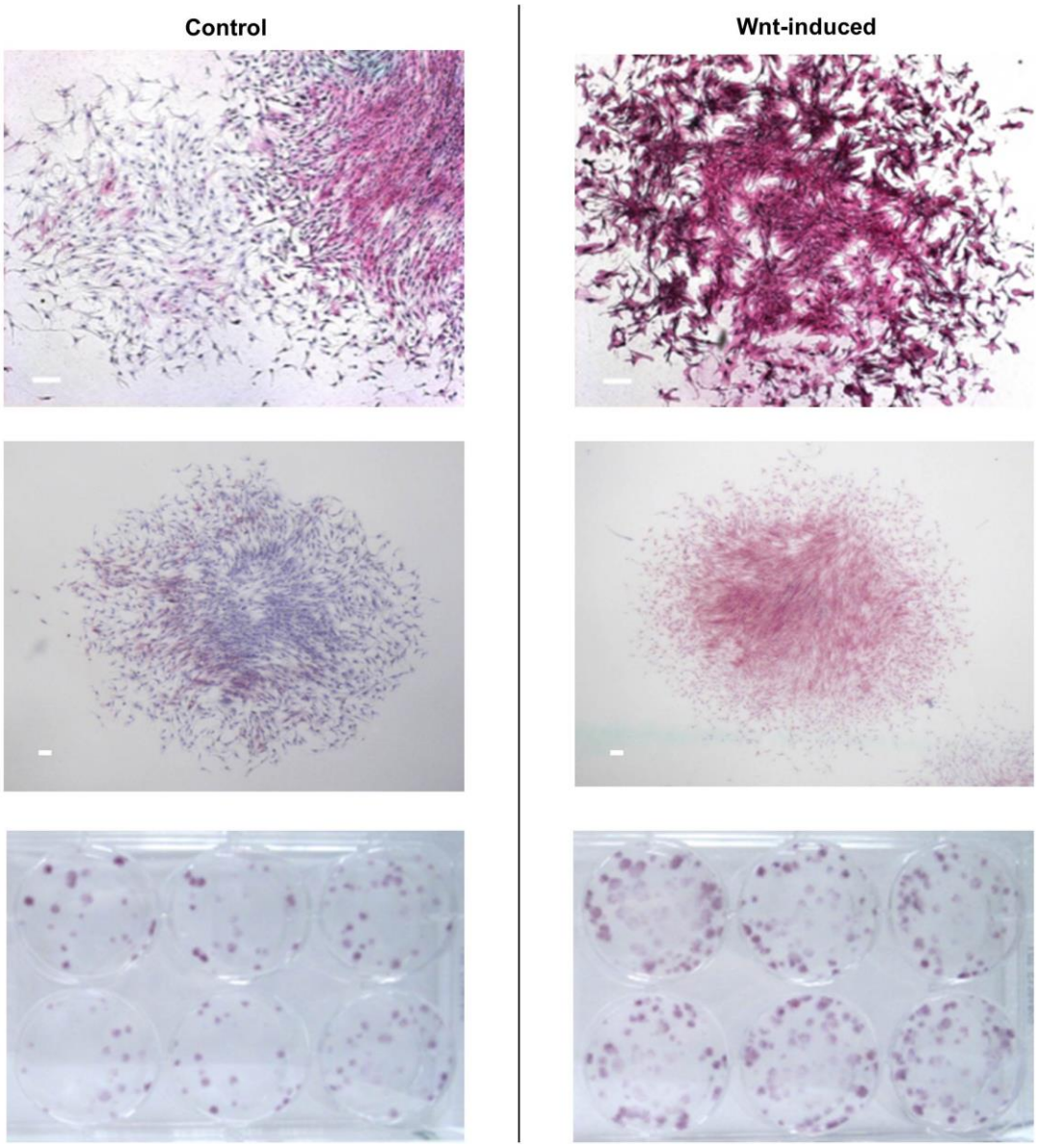

Figure 4.15 CFU-O assay with ALP staining 14 days after short-term Wnt induction.

The CFU-O assay was conducted on 24 hour suspension culture of Wnt-induced samples and controls. Representative images of colonies stained with ALP (purple/magenta) and haematoxylin used as a counterstain (dark blue nuclei) are presented. Scale bars = 200 μm.

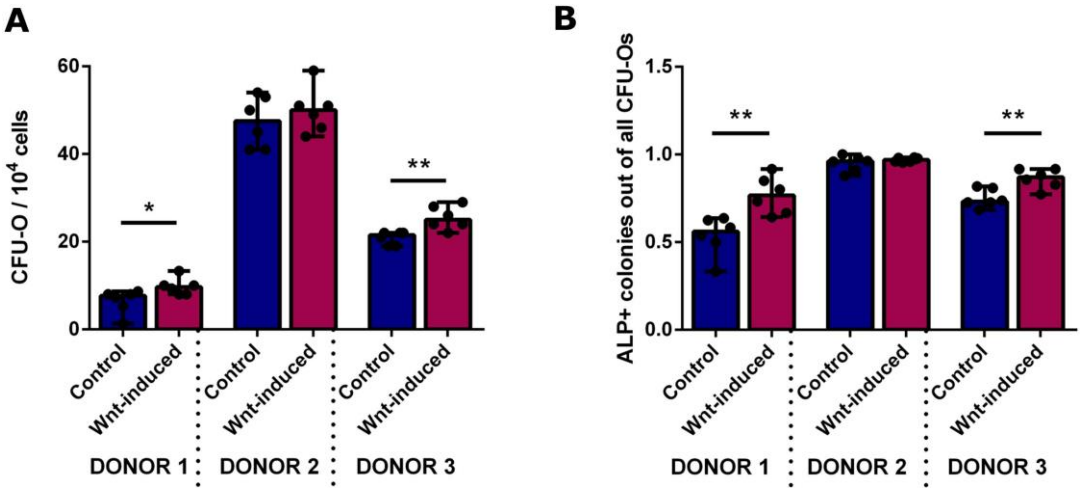

Figure 4.16 CFU-O formation efficiency and ALP staining in osteogenic media.

A: Number of colonies per 10^4 plated BMMNCs at 14 days arising from 24 hour Wnt-treated and control samples. B: Ratios of ALP^+ CFU-Fs at 14 days arising from 24 hour Wnt-treated and control samples. Data from 3 donor samples, presented as median ± range on technical replicates. Statistically significant differences in CFU-O efficiency were observed in 2 donors between the two experimental groups (control *vs.* Wnt-induced). Furthermore, an increase in ALP-expressing colonies was consistent in these 2 donors after Wnt-induction. Due to high variability between donors, normalisation would be inappropriate, thus data is presented from each donor separately and was analysed separately by Mann-Whitney test. *p<0.05; **p<0.01. CFU-O, colony-forming unit osteoblastic.

Overall, these results suggest that Wnt3A stimulation does not increase the frequency of CFU-Fs recovered from BMMNC populations, but rather expands a subset of BMMNCs primed for osteogenesis. This subset, marked by STRO-1^+, STRO-1^+/GPA^- and STRO-1^{bright}, may therefore consist of cells with osteoprogenitor potential.

4.2.5 Osteogenic potential of cells after short and long-term Wnt exposure

4.2.5.1 ALP activity and cell number

The effects of short-term Wnt3A stimulation were measured on cells plated in high density in both basal and osteogenic media. For ease of visualisation, Figure 4.17 presents data on ALP activity from 3 donors normalised to controls (detailed graphs for each donor can be found in the Appendix, Figure A.14). Transient, early stimulation of BMMNCs and STRO-1-enriched cells with Wnt3A resulted in significant increases in the expression of ALP in SSC cultures in osteogenic conditions

(Figure 4.17A). Due to donor-specific differences in the magnitude of the response, results in basal media conditions did not reach significance, however the trend was similar for all donors. Cell number quantification resulted in non-significant trends towards increases after Wnt stimulation, apart from the BMMNCs cultured in basal conditions, for which a significant increase in cell number was measured (Figure 4.17B).

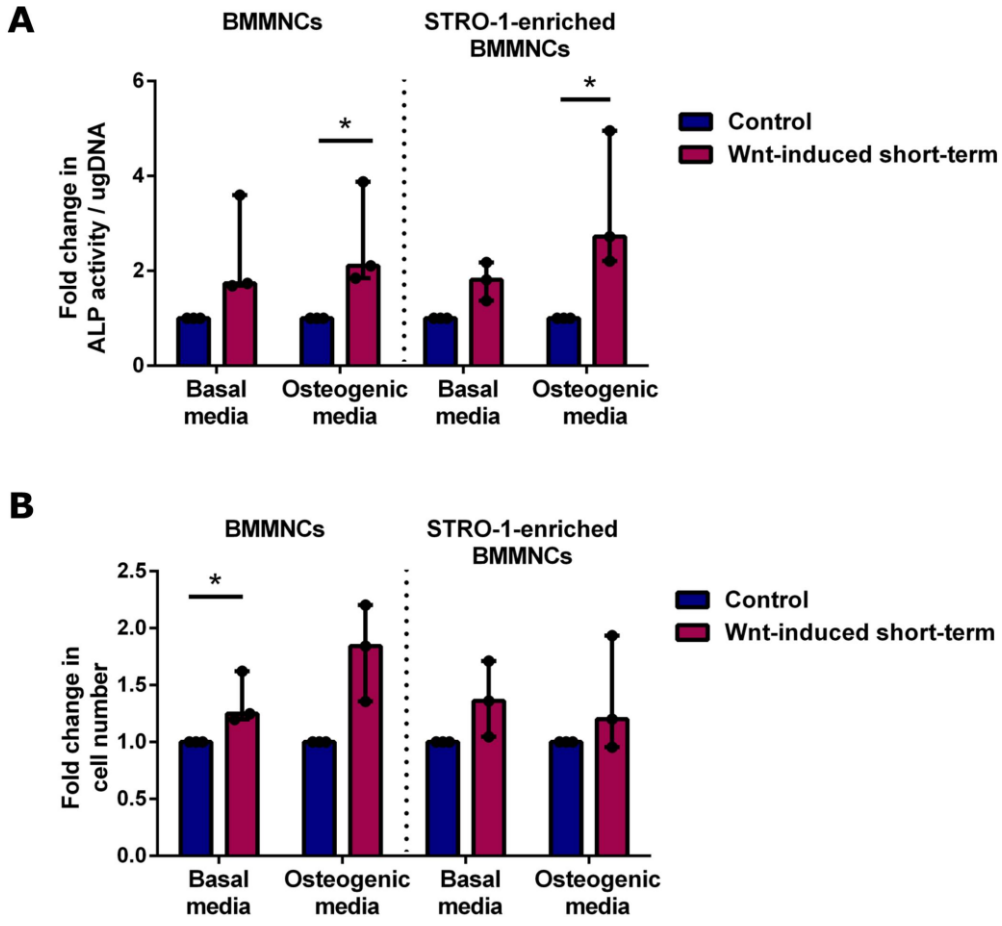

Figure 4.17 ALP activity and cell number in BMMNCs and STRO-1-enriched BMMNCs after short-term Wnt induction.

Cells were cultured in monolayer for 14 days in basal or osteogenic media following a 24 hour treatment with Wnt *vs.* control and assayed for ALP activity (A) and cell number (B). Data presented as median ± range from n = 3 donors, normalised to control. Statistical significance assessed by Friedman's test with Dunn's correction, *$p<0.05$.

Secondly, as the length of Wnt-signalling induction in SSCs in the published literature varies between studies and hence might be the reason for different outcomes, the effects of long-term Wnt3A stimulation (ongoing for 14 days) were measured on cells plated

using the same setup as above (in high density in both basal and osteogenic media) and analysed accordingly. In contrast to the effects of short-term stimulation, ongoing stimulation of BMMNCs and STRO-1-enriched cells with Wnt3A resulted in a significant decrease in the expression of ALP in SSC cultures in both basal and osteogenic conditions (Figure 4.18A). Cell number quantification resulted in non-significant trends towards increases after Wnt stimulation (Figure 4.18B). Detailed graphs for each donor can be found in the Appendix, Figure A.15. These results indicated a significant reduction in osteogenesis following long-term Wnt treatment. This observation was not due to the concentration of Wnt, as a concentration-dependent inhibition was observed at lower Wnt3A concentrations (25 and 50 ng/ml; Appendix, Figure A.16).

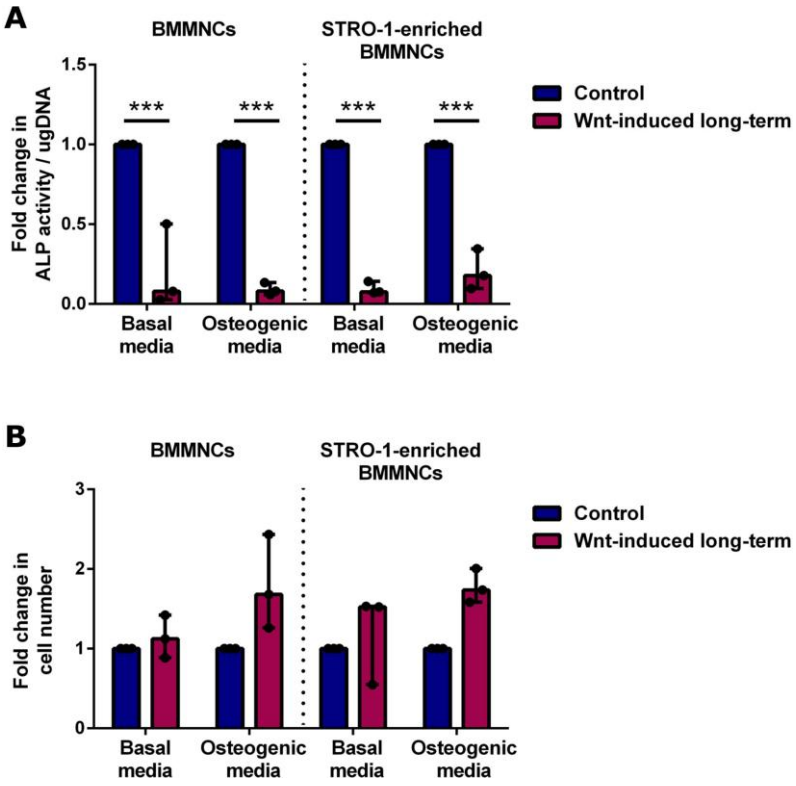

Figure 4.18 ALP activity and cell number in BMMNCs and STRO-1-enriched BMMNCs after long-term Wnt induction.

Cells were cultured in monolayer for 14 days in basal or osteogenic media with Wnt *vs.* control and assayed for ALP activity (A) and cell number (B). Data presented as medina ± range from n = 3 donors, normalised to control. Statistical significance assessed by Friedman's test with Dunn's correction, ***$p<0.001$.

4.2.5.2 Osteogenic gene expression

Next, the effects of Wnt stimulation on the expression of osteogenic genes was measured. The effect of osteogenic media alone on the expression of early osteogenic markers (*RUNX2* and *SP7* transcription factors), early and medium (*ALP*) and markers expressed late in the differentiation process (osteonectin gene - *SPARC* and osteocalcin gene - *BGLAP*), as well as *AXIN2* as a control for Wnt pathway induction in further experiments, are shown in Figure 4.19. As expected, osteogenic media stimulated the expression of osteogenic genes, and had no effect on *AXIN2* expression.

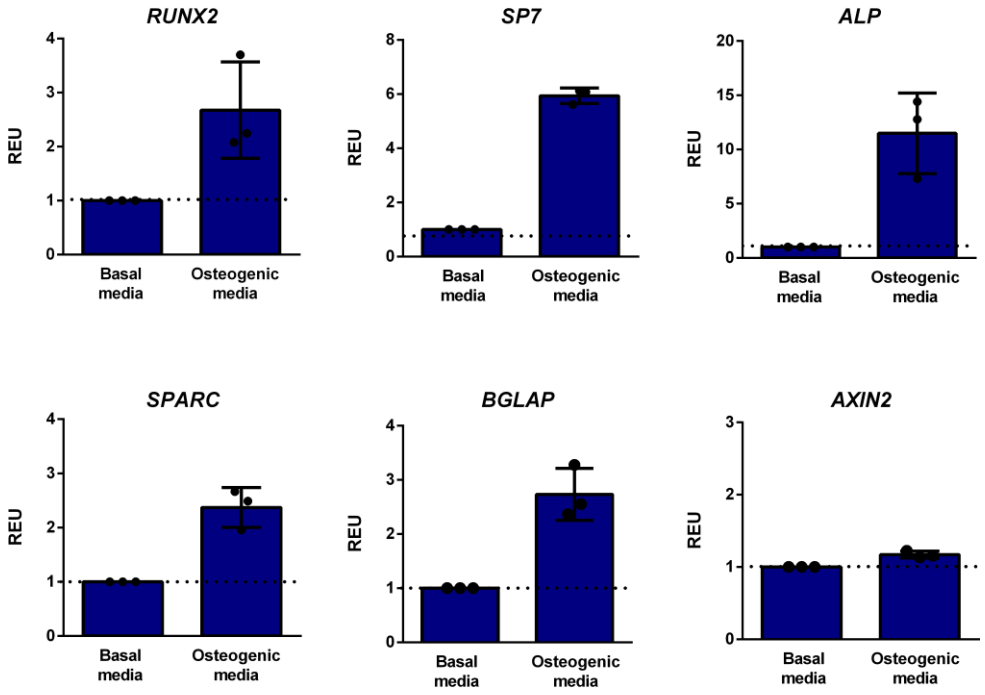

Figure 4.19 Expression of osteogenic genes in BMMNCs cultured in osteogenic media.

A 14-day adherent cell culture in osteogenic media resulted in increased osteogenic gene expression (*RUNX2, SP7, ALP, SPARC, BGLAP*) compared to basal conditions. Expression of *AXIN2* (a Wnt target gene), remained unaffected by culture conditions. n = 1, mean ± SD on 3 technical replicates. Gene expression was normalised to *ACTB* and then normalised to expression in basal media.

Next, the expression of these osteogenic genes was measured in BMMNCs exposed to Wnt for short- or long-term, and cultured as adherent cells for 14 days, in basal and osteogenic conditions. The results are normalised in each case to control, but failed to show a consistent pattern (Figure 4.20). Instead, only trends were observed, with *ALP* expression confirming previous findings, and *RUNX2*, *SPARC* and *BGLAP* showing a similar pattern of upregulation after short-term exposure and downregulation after long-term exposure. *AXIN2* expression, assayed as a control for Wnt pathway activation,

was upregulated by both short-term Wnt exposure and, to a greater extent, by long-term Wnt exposure.

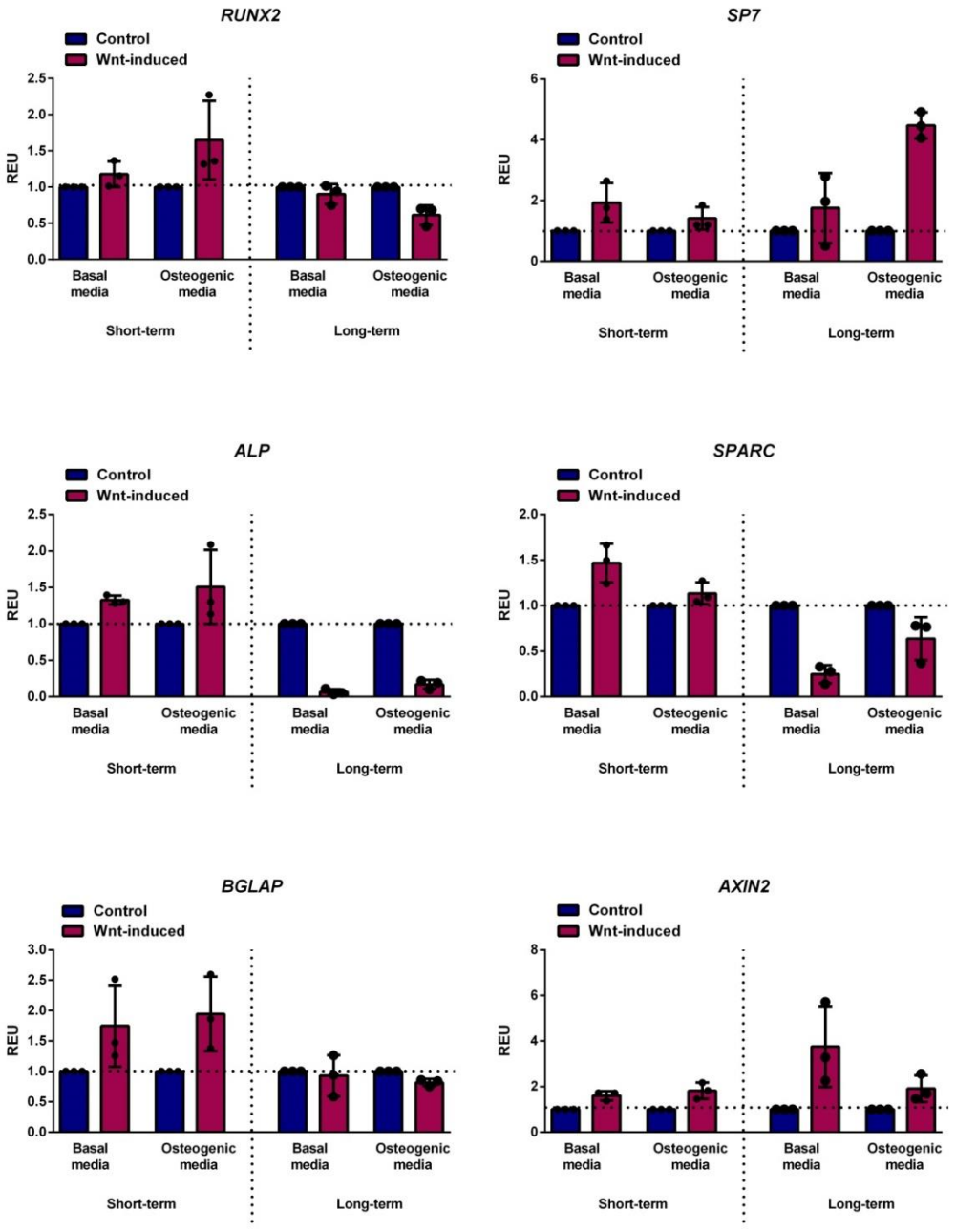

Figure 4.20 Expression of osteogenic genes in BMMNCs cultured in basal and osteogenic media after short- and long-term Wnt stimulation.

Cells were cultured in monolayer for 14 days in basal or osteogenic media following a 24 hour or ongoing treatment with Wnt *vs.* control and assayed by qPCR for osteogenic gene expression (*RUNX2, SP7, ALP, SPARC, BGLAP*). Expression of *AXIN2* (a Wnt target gene) was assayed as a control for Wnt pathway activation. n = 1, mean ± SD on 3 technical replicates. Gene expression was normalised to *ACTB* and then to normalised expression in control basal or osteogenic media.

4.2.5.3 Bone matrix deposition

To test possible effects of Wnt stimulation on late/terminal osteogenic differentiation, as suggested by the gene expression data, Osteopontin expression was measured by immunocytochemistry and calcium deposition by histological Alizarin Red S stain.

Osteopontin expression, indicative of matrix maturation and mineralisation by mature osteoblasts, in short- and long-term Wnt-stimulated BMMNCs followed the pattern previously seen for ALP activity (Figure 4.21).

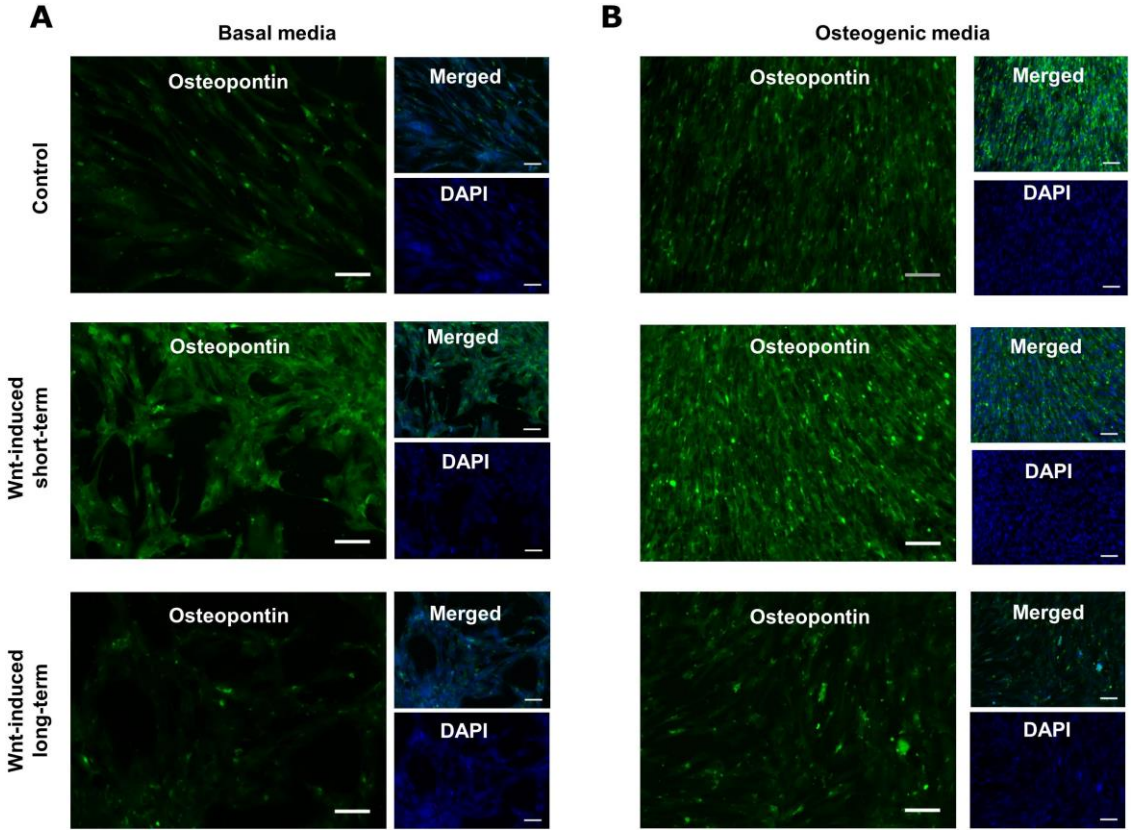

Figure 4.21 Osteopontin expression in BMMNCs cultured in basal and osteogenic media after short- and long-term Wnt stimulation.

Immunocytochemistry staining for Osteopontin (green) and cell nuclei (DAPI, blue) was conducted on cells cultured in monolayer for 14 days in basal or osteogenic media following a 24 hour or ongoing treatment with Wnt *vs.* control. Scale bars = 100 μm.

Alizarin Red S staining for calcium deposits, characteristic of bone matrix mineralisation, mirrored the data for ALP activity as well. Significantly increased Ca^{2+} deposition was seen in cultures stimulated transiently and decreased Ca^{2+} deposition was observed in cells stimulated long-term (Figure 4.22).

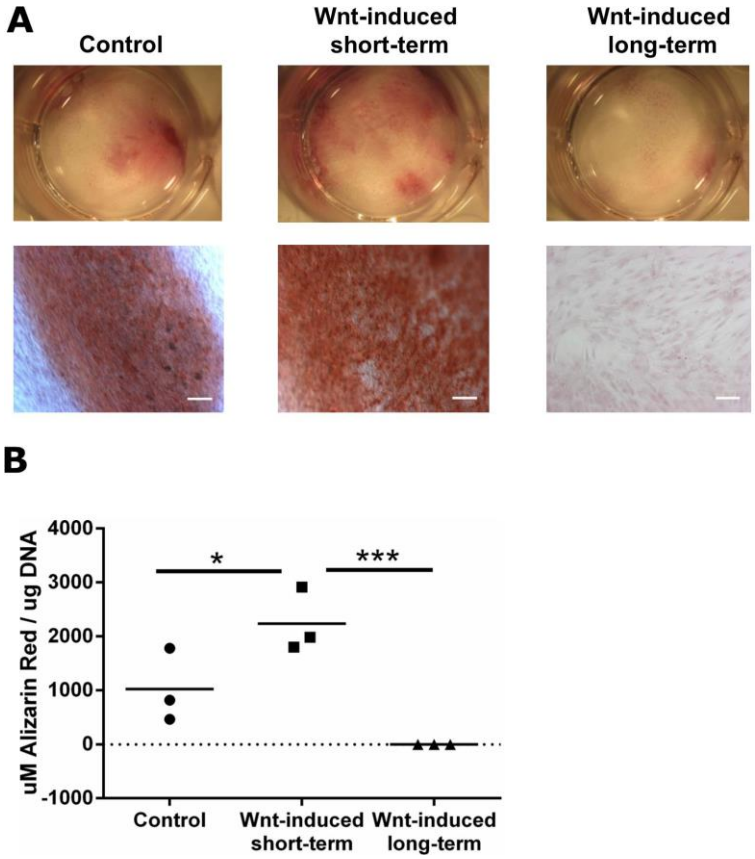

Figure 4.22 Calcium deposition in BMMNCs cultured in osteogenic media after short- and long-term Wnt stimulation.

A: Representative images of Alizarin Red S staining on cells cultured in monolayer for 14 days in osteogenic media following a 24 hour or ongoing treatment with Wnt *vs.* control. Cells in each well had the same level of confluency. Scale bars = 200 μm. B: Quantification of extracted Alizarin Red S dye was achieved by a spectrophotometric measurement. Calcium deposition in wells induced with Wnt for long-term was below detection limit. n = 1, mean on 3 technical replicates, statistical significance assessed by ANOVA with Tukey's correction, *$p<0.05$, ***$p<0.001$.

These results indicate that transient, early Wnt stimulation augments the osteogenic potential of SSCs derived from bone marrow isolates. Sustained Wnt3A activation has the converse effect, markedly inhibiting osteogenesis.

4.3 Discussion

Putative skeletal stem cell populations in murine marrow have recently been shown to express high levels of Wnt ligands and their cognate Frizzled receptors, providing evidence that skeletal stem cell niches may be modulated by Wnt growth factors (Chan *et al.* 2015). This modulation of the Wnt signalling pathway is an attractive target for therapies that augment bone formation, and preclinical and clinical trials on drugs which induce Wnt signalling have shown promising results in the treatment of chronic diseases, such as osteoporosis, and in acute bone injury (Iyer *et al.* 2014, Jin *et al.* 2015, Li *et al.* 2011, McClung *et al.* 2014, Ominsky *et al.* 2010, Padhi *et al.* 2011). However, the mechanism of action of these Wnt-inducing drugs on the biology of SSCs, which are involved in both sustaining bone homeostasis and bone healing following trauma, requires further comprehensive studies into the bone marrow niche, both *in vivo* but also in simplified *in vitro* settings. This chapter aimed to assess the effects of Wnt signalling induction *via* external Wnt cues on SSCs within fresh bone marrow isolates.

As Wnt proteins are highly evolutionarily conserved in animals (Nusse and Varmus 2012), with murine and human Wnt3A sharing 96 % homology according to the Basic Local Alignment Search Tool (BLAST) database, both murine and human Wnt3A were used in this work at 100 ng/ml (unless stated otherwise). This concentration was sufficient to induce an effect in the population of interest within 24 hours of incubation of fresh bone marrow isolates with Wnt3A, as evidenced by the upregulation of Wnt target genes *AXIN2* and *CCND1*. However, it is important to note that the conventional "on" or "off" linear view of the Wnt signalling pathway underemphasises the fact that key outputs, such as the level of β-catenin/TCF-dependent transcription, can be modulated by over four orders of magnitude, and the level of activity determines biological outcomes (Buchert *et al.* 2010). It is difficult to compare the 100 ng/ml concentration to the literature, as the great majority of publications use Wnt3A-conditioned media of unknown concentration (from a stably transfected murine L1 cell line) for between 4 to 28 days, on established human SSC cultures, often after multiple passages (Baksh and Tuan 2007, Boland *et al.* 2004, de Boer *et al.* 2004, De Boer *et al.* 2004, Liu *et al.* 2009). Upregulation of *CCND1* has been shown after 8 days of adherent culture with Wnt3A-conditioned medium, but no earlier time points have been tested (Baksh and Tuan 2007). There is one example

where 100 ng/ml of purified Wnt3A has been used on established human SSC cultures for ongoing 21 day exposure (Liu *et al.* 2009). As previously noted, there appears to be only one instance of fresh bone marrow isolate exposure in suspension, but that was conducted with Wnt3A-conditioned media, and the effects of exposure were measured at 7 days at earliest by plating cells for CFU-F assays (Baksh and Tuan 2007). As such, the present work is the first study of BMMNC exposure to purified Wnt3A (Miller 2002), which activates the canonical signalling pathway, in a culture system which recapitulates the bone marrow cellular environment.

In this system, Wnt stimulation resulted in expansion of the SSC-containing STRO-1$^+$ fraction after only 24 hours of exposure, and this effect was attributable to increased cell proliferation and viability after Wnt treatment. While significant inter-donor variability in STRO-1 frequency was observed (range: 3.32 - 17.10 % in control *vs.* 5.43 - 25.3 % after Wnt treatment), an increase in STRO-1 frequency was observed in every case. One of the study limitations was that the medication status of donors was unknown. Therefore, the high inter-donor variability of the responses to Wnt within the first 24 hours of treatment might be a result of medication use. On the other hand, working with samples from patients affected by bone diseases can increase the clinical relevance of the study, as bone diseases are frequently the underlying cause of failed bone fracture healing. However, in this study, positive effects of Wnt were observed regardless of the donor disease status. Future studies may seek to stratify the effects of drug intervention based on patient age, disease or medication status.

Further experiments aiming to delineate whether the effect of Wnt on STRO-1$^+$ cells was direct or indirect, showed significant increases in the GPA$^-$/STRO-1$^+$ and GPA$^-$/STRO-1^{bright} cells, when the STRO-1-enriched population alone was examined. However, both BMMNC and STRO-1-enriched populations are heterogeneous, as MACS-selection is permissive to blood cell populations (although the number of granulocytes is reduced), so it cannot be definitively asserted that the effect of Wnt on putative SSCs is direct in nature. Implementing FACS for GPA$^-$/STRO-1^{bright} cells and their subsequent 24 hour exposure would be unfeasible due to the insufficient number of cells for suspension culture, limited due to the volume of donor sample available for

the research in this thesis. Therefore to study the directness of Wnt stimulus on sorted SSCs, larger sample volumes should ideally be obtained.

In addition to the increase in the STRO-1^+ cell numbers, the expression of this surface antigen was higher after Wnt induction solely on GPA^-/STRO-1^+ cells as assessed on a cell-by-cell basis on Image Stream. STRO-1 remains an enigmatic marker, a product of an unknown gene, with its expression shown on a variety of adherent cell types, and confirmed by a Western blot on primary skeletal stem cells from adipose tissue and on endothelial cells (Ning *et al.* 2011). The authors suggested that STRO-1 is an endothelial marker, however, it is also found to be expressed in various prostate and breast cancer cell lines, and these two types of cancer most commonly metastasise to bone (Li *et al.* 2012). The lack of evidence of other Western blot/immunoprecipitation of the STRO-1 antigen, despite recognition since 1991 (Simmons and Torok-Storb 1991), highlights the challenge in studying it. Indeed, the antigen itself might be a glycoprotein, or present in lipid rafts, or the attempts may have been unsuccessful due to the pentameric structure of the IgM STRO-1 antibody itself. Therefore, the reason for the Wnt-induced increase in expression of the STRO-1 antigen remains unknown. Although the biological role of this marker is unidentified, as is the case with many stem cell markers, for example CD34 in haematopoietic stem cells (Sutherland *et al.* 1989), STRO-1^+/GPA^- cells have the property of being enriched in cells with trilineage and CFU-F potential (Gronthos *et al.* 2003, Simmons and Torok-Storb 1991, Zannettino *et al.* 2007), and as such, STRO-1-expressing cells are interesting subjects to study.

Overall, CFU-F efficiency was similar to that published previously (Friedenstein *et al.* 1970, Gronthos and Simmons 1996), although these assays vary considerably in the literature, with different seeding densities, culture vessels, and media and supplements used. CFU assays on BMMNCs exposed to Wnt during 24 hour suspension culture showed that Wnt stimulation expands a subset of osteoprogenitors, as it increased the frequency of colony formation after 14 days in osteogenic media (CFU-O). No difference was seen in the frequency of CFU-F, hence under CFU-F culture conditions (in basal media), the growth of these cells primed for osteogenesis might not be promoted. However, all colonies from cells exposed to Wnt showed an increase

in ALP expression, marking osteogenic differentiation. These data, along with the augmented incidence of STRO-1$^+$, GPA$^-$/STRO-1$^+$ and STRO^{bright} cells after 24 hours incubation with Wnt3A, and the measurements of elevated *SP7* from the previous chapter, indicated that these cells (with increased STRO-1 expression and ALP$^+$) truly represented an intermediate preosteoblastic stage of development (Gronthos *et al.* 1999).

These results are in contrast to those previously published on freshly plated human BMMNCs (Baksh and Tuan 2007). Those authors showed that induction with Wnt3A-conditioned media rapidly and efficiently affected recruitment of CFU-F from bone marrow after just 2 days of exposure. However, experiments with conditioned media should be interpreted with caution, as the murine cell line producing Wnt3A might be reactive to it, and produce inhibitors of Wnt signalling if the pathway is over-activated. In this case, the use of conditioned medium from cells which do not stably express Wnt3A would only control for, as an example, depleted glucose, glutamine, serum, or secreted cytokines.

Assays measuring ALP activity in high density adherent cultures showed that transient stimulation with Wnt3A increased the osteogenic differentiation of both BMMNCs and STRO-1-enriched fractions in osteogenic media, with a similar trend in basal conditions. It also influenced BMMNC proliferation in basal conditions with modest trends noticeable in other setups. Continuous Wnt exposure experiments conducted on both BMMNC heterogeneous populations and cells selected on the basis of STRO-1 expression, showed inhibition of differentiation marked by a decrease in ALP activity, with non-significant trends observed towards an increase in proliferation. Therefore, long-term Wnt signalling induction prevents these cells from following the osteoblastic lineage of differentiation, in direct contrast to short-term Wnt exposure. Osteogenic gene expression data and staining for bone matrix deposition followed similar patterns to ALP, underlining the effects of transient *vs.* continuous Wnt exposure on SSCs. In the literature, an increase in ALP activity after 48 hour incubation with Wnt has been reported in the C2C12 cell line (Lu *et al.* 2008) and after 72 hour incubation in ST2 and C3H10T1/2 cell lines (Gong *et al.* 2001). Furthermore, transfection of these cell lines with Wnt3A has yielded similar results (Rawadi *et al.*

2003). Exposure to Wnt conditioned media for 12 days has resulted in increased ALP expression in human SSCs but transfection with Wnt3A had the opposite effect, simultaneously increasing proliferation (Boland *et al.* 2004), similar to 5 day treatment with Wnt3A-conditioned media in another study (de Boer *et al.* 2004). When human adipose-derived stromal cells (hADSC) were exposed to Wnt3A conditioned media for 14 days, osteogenic differentiation was inhibited in favour of cell proliferation (Cho *et al.* 2006). Other studies showed that short-term exposure to Wnt3A promotes osteogenesis, whereas long term exposure inhibits osteogenic differentiation (Eijken *et al.* 2008, Liu *et al.* 2009), although these results depended on the concentration of Wnt3A used, as well as which osteogenic markers were used as a readout. These discordant findings regarding Wnt signalling as either promoting SSC proliferation or differentiation might arise from the variety of cell lines used in the experiments, or the maturity of cells in the case of primary cells, as well as the duration of exposure to Wnt and concentrations used, and the use of conditioned media of unknown concentrations.

From these listed variables, different requirements for Wnt stimulation during a lifecourse of an osteoprogenitor are perhaps most important as several studies have shown that the stimulatory effect of Wnt signalling is dependent on the stage of commitment of the progenitor cell/osteoblast (Cook *et al.* 2014, Liu *et al.* 2009, Quarto *et al.* 2010). In particular, Cook *et al.* have shown, with the use of ALP activity and mineralisation assays, that continuous induction of Wnt signalling by the small molecule AR28 inhibited ALP activity but had no effect on mineralisation, marked by Alizarin red stain. However, when osteogenic medium was used without the addition of dexamethasone, for assessment of early osteogenesis, enhancement of early osteogenesis and formation of precursor cells was detected when a low dose of the inducer was used. This was in contrast to a high dose, which led to a decrease in ALP activity. These results are in agreement with findings presented in this thesis, where induction of Wnt signalling in early progenitors, achieved by short-term stimulation, enhanced the osteoprogenitor pool and induced higher ALP expression and activity compared to control conditions, possibly accelerating the cells through the osteoblast precursor stage. However, as ALP levels decrease in later stages of differentiation, the

correlation of decreased expression of this marker with inhibition *vs.* acceleration of osteogenesis should also be performed using other differentiation markers.

One of the study limitations was that a limited number of assays was used to determine osteogenic differentiation, with most of the assays relying on ALP. For further studies, additional assays could be used to evaluate osteogenic markers at the protein level as well as phosphate deposition using von Kossa staining. Moreover, examining differentiation also towards adipogenic lineage simultaneously with osteogenic lineage would be of great interest, considering the crosstalk between these commitment pathways (Takada *et al.* 2009). The lack of *in vivo* readout for bone formation is another limitation of the study presented here. Several studies have shown that the identified predictive markers *in vitro* often do not translate into *in vivo* bone formation (Kuznetsov *et al.* 1997, Mendes *et al.* 2004, Sacchetti *et al.* 2007, Satomura *et al.* 2000). The heterotopic ossicle formation assay dates back to seminal experiments that paved the way towards identifying SSCs, their bone forming potential, and role as a haematopoietic microenvironment (Bianco *et al.* 2013). Nowadays, subcutaneous transplantation of stem cells of varying purity, often with hydrogel-deposited growth factors, is the most commonly used readout for *in vivo* bone formation. These studies usually aim to evaluate the suitability of different transplanted cell populations for clinical applications. Therefore, comparison of the bone formation potential of the Wnt-exposed and non-exposed $GPA^-/STRO\text{-}1^+$ cells could be considered in the future. This model offers a simple readout, however it does not take into account the signalling in the bone marrow niche and the influence of inflammation present at the fracture site (Kolar *et al.* 2010), nor the fact that human *vs.* murine skeletal stem cell populations are identified by different markers, the murine model lacking the expression of STRO-1, which is a strictly human antigen. Therefore, the true potential of Wnt as a therapeutic should be examined in a murine bone fracture model, followed by a thorough analysis of affected cell populations, using markers reported for murine SSCs. For this study, however, a delivery technology for Wnt should be established, which would ensure its spatiotemporal actions.

In summary, the results presented here showed that transient stimulation with Wnt-primed SSCs towards the osteogenic differentiation pathway, whereas prolonged

overstimulation negatively affected the already committed progeny of SSCs. Hence, the timing of Wnt exposure is crucial in promoting osteogenic differentiation and this complexity of Wnt signalling requirements should be considered for therapeutic approaches, for successful differentiation of osteoblasts from progenitors present at injury sites.

4.4 Conclusion

The aim of the research presented in this chapter was to assess the effects of Wnt signalling induction *via* external Wnt cues on SSCs within fresh bone marrow isolates. This *in vitro* experimental system, although a simplification of the *in vivo* situation, provided results which aided understanding of what the effects might be when the Wnt signalling pathway is induced in the bone marrow niche, as the SSCs were exposed to Wnt while still surrounded by components of the niche. The main findings showed that:

- transient, 24 hour Wnt3A stimulation activates Wnt signalling pathway activity in stromal/skeletal stem cell populations within bone marrow isolates, and promotes their expansion, by increasing their proliferation and protecting them from cell death;
- transient Wnt exposure primes uncommitted stromal/skeletal stem cells in BMMNC isolates to an osteogenic fate and increases the frequency of CFU-Os;
- osteogenic differentiation in BMMNCs and STRO-1-selected populations is promoted by early transient Wnt exposure but is abrogated by continuous Wnt stimulation.

These data shed more light on the time-dependent responses to Wnt signalling within skeletal stem cells and how Wnts can alter the osteoprogenitor populations. Short, transient stimulation of bone marrow populations with Wnt protein might therefore positively influence bone repair upon injury, directing more stem cells towards the osteoblastic lineage. Therefore, further experiments presented in the following chapter aimed to investigate a suitable delivery method for the Wnt protein for therapeutic purposes.

Chapter 5

Liposomes for Wnt3A protein delivery to bone fracture sites

5.1 Introduction

In the previous chapter, Wnt protein was shown to increase the frequency and osteogenic differentiation of progenitor fractions, meaning that it could potentially be used for therapeutic purposes in bone fracture healing. As the timing of action of Wnt signalling is critical to its effect on osteoprogenitors/stem cells, there is a need to ensure that Wnt stimulation acts in a spatiotemporally-controlled manner. Nanoparticles, such as liposomes, can promote controlled drug release in a spatiotemporally defined manner. Therefore, the aim of this chapter was to assess the suitability of liposomes as a nanoparticle delivery system for Wnt3A protein.

Due to the hydrophobic nature of Wnt proteins, attributable to their posttranslational modification with fatty acids, their extracellular transport requires the presence of other molecules. Wnts have been shown to associate with various lipid-rich vesicles for this purpose (see Section 1.3.4 for Wnt structure and biology). This makes liposomes an attractive delivery technology, and in *in vitro* situations it has already been suggested, though not proven, that Wnt proteins potentially associate with the lipid bilayer of the liposomes (Dhamdhere *et al.* 2014, Morrell *et al.* 2008). In this formulation, the Wnt3A protein has been shown to have extended activity, up to 72 hours in comparison to free protein, which is only active for ~24 hours (Morrell *et al.* 2008).

Liposomes are used extensively by the pharmaceutical and cosmetics industry as delivery systems for hydrophobic agents. Liposomal drug formulations have been shown to offer considerable advantages, such as superior therapeutic efficacy and safety (see Section 1.4 for description of liposomes and their use in drug delivery). These particles can be designed to passively or actively localise to desired target areas or cell populations *in vivo*, and therefore are an attractive tool for delivering therapeutic agents to stem cells for regenerative medicine purposes. Lipid nanoparticles of ~100 nm in size have the potential to extravasate from the vasculature at sites of increased permeability, such as during inflammation or from leaky blood vessels surrounding tumours (Jia *et al.* 2015, Yuan *et al.* 1994). Some liposome preparations have also been shown to localise to the bone marrow (Section 1.4.6; (Sou *et al.* 2011)). By modifying the lipid composition of the liposomal membrane, the fluidity,

permeability, surface characteristics and structural integrity (important for cargo release) of a liposome can be controlled. When liposomes are coated with 5 – 10 molar % polyethylene glycol (PEG), the so called "stealth" or "sterically stabilised" preparations evade uptake by the reticuloendothelial system (RES), thus exhibiting longevity in circulation (Veronese and Pasut 2005). Therefore, the liposomes produced for the experiments in this thesis were initially composed of various lipids for optimisation purposes, were PEGylated, and designed to be ~100 nm in size.

In general, within a broad range of industry sectors, the analysis of nanoparticles is a requirement, for both routine quality control and from a research and development standpoint. A variety of methods were also used within this thesis for assessment and characterisation of the liposome preparations, as they could potentially serve as a drug delivery method for regenerative medicine strategies.

The formation efficiency and, most importantly, degree of PEGylation of liposome preparations was assessed here by gas chromatography (GC). The main principle underlying the separation of fatty acids by GC is that they differ in the temperature at which they become volatile. This depends upon carbon chain length, and the number and position of carbon-carbon double bonds. Increasing chain length increases the temperature at which fatty acids enter the vapour phase. Hence various peaks of the chromatogram and their area give information regarding the type and concentration of the fatty acid, as long as a suitable internal standard is used. Therefore, as PEG is attached to lipid, and GC provides information about the acyl portion of the compound, an indirect quantification was possible (Berenholz and Lasic 1995). Other techniques commonly used for liposome characterisation, include electron microscopy (EM), dynamic light scattering (DLS) and recently also scanning ion occlusion sensing (SIOS) and nanoparticle tracking analysis (NTA).

EM is regularly used for assessment of size, morphology and lamellarity of liposome preparations. Resolution of the structure of vesicles ≤100 nm in size requires the use of transmission electron microscopy (TEM). However, negative stains used for visualisation and subsequent vacuum-forming processes can cause structural changes in the vesicles. More popular techniques, such as cryo-TEM and freeze-fracture TEM,

keep the sample at cryogenic temperatures without the need for staining, but the instrumentation is not easily accessible, the specimen preparation is time-consuming, and can nonetheless still interfere with the structure of the liposome. EM techniques do not meet the requirements of batch analysis, and a statistically representative profile of liposome populations cannot be generated (Bibi *et al.* 2011).

DLS, also known as photon correlation spectroscopy, is used to determine the size distribution of particles in suspension, moving under Brownian motion and subject to light scattering (Selser *et al.* 1976). This technique measures fluctuations in scattered light intensity due to diffusing particles, and allows determination of the mean diameter of the particles or, in the case of a multi-angle instrument, the full particle size distribution. This measurement depends on the size of the particle core, the size of surface structures, particle concentration, and the ionic species in the medium. The main shortcomings of DLS include low resolution and "multiple" light scattering, where the scattered light from one particle is scattered by another before reaching the detector, compromising the accuracy of the readout for polydisperse samples.

SIOS, commercialised by Izon Science, is a nanopore-based technology similar in principle to the conventional Coulter Counter, allowing for analysis of particles in solution on a particle-by-particle basis (Yang *et al.* 2012). Particles, passing through a tuneable (for size selectivity) nanopore, cause a reduction in electrical current as a result of an increase in electrical resistance. The magnitude of this reduction and the frequency of the pulses are then related to the particle size and concentration, respectively. This method offers a higher resolution than DLS, due to a lower contamination with large particles. However, the choice of a suitable elastic pore and adjustment of the pore diameter is problematic when a sample of particles is highly polydisperse, as ensuring complete detection and avoiding the detection of several particles at the same time is an issue.

NTA, commercialised by Nanosight, is another technology which tracks and measures nanoparticles moving under Brownian motion in solution, on individual basis (Malloy and Carr 2006, Saveyn *et al.* 2010). The moving paths of nanoparticles are recorded under a microscope, using conventional CCD cameras, alongside the analysis of

scattered light, which together give information about the size distribution of particles and their type, if their size is equal but light scattering properties differ. The advantage of this system over DLS is the additional information on particle concentration, as the aperture allows for analysis in a microfluidic device with a syringe pump, without the drawbacks of SIOS. The potential shortcoming of this technique, however, is the 2D plane of the tracking, whereas naturally the particles move in three dimensions, which means the particles with a greater degree of movement in the z-plane relative to the x-y plane will be misinterpreted as larger particles during a short detection period. The microscope can also be fitted with different lasers, allowing for analysis of differently labelled particles, although it is not sensitive enough to detect differentially labelled compounds encapsulated or tethered to the nanoparticle surface.

As it was important to study the interaction of the encapsulated Wnt with the liposome nanoparticles, spectroscopy methods were used to characterise this interaction at a single molecule level. The techniques employed for this purpose comprised of total internal reflection fluorescence microscopy (TIRFM), and two-colour coincidence detection (TCCD). Both these techniques require the molecules under examination to be differentially fluorescently-labelled. TIRFM is a wide-field technique that uses expanded beams to excite fluorophore molecules, but it restricts the illumination volume to ~200 nm from the surface, enabling resolution of single molecule fluorescence. This technique is of particular use for studying proteins in the cellular membranes (James *et al.* 2007). TCCD is a confocal microscopy technique, which uses two focused laser beams to illuminate the sample in a microfluidics chamber in a probe volume of <1fl, while working at picomolar concentrations. This technique is often used to study protein aggregation (Orte *et al.* 2008).

Reporter cells have been used extensively in biology to provide a readout for specific gene activation, as a tool for screening drugs and their influence on intracellular pathways. In the case of the Wnt signalling pathway, reporter genes encoding fluorescent proteins or luciferase are usually transcribed under the control of TCF/LEF promoters, which are active in cells in which this pathway has been induced (Biechele *et al.* 2009). Therefore, to test whether the various liposomal Wnt

preparations, whose design has been documented in this chapter, were biologically active, a reporter cell line expressing luciferase gene was used.

Nanoparticles have been shown to enter the intracellular environment by a variety of different mechanisms, including phagocytosis, macropinocytosis, caveolar endocytosis or clathrin-mediated endocytosis (Canton and Battaglia 2012, Petros and DeSimone 2010). These routes are highly dependent on the size of the nanoparticles as well as their composition and surface properties, and are an important consideration when designing liposomes whose uptake is undesirable, or which aim to target specifically various intracellular compartments (see Section 1.4.3). As the-time frame and mechanism of uptake of liposomal formulations designed to deliver Wnt is unknown, it was studied here *in vitro* on cultured BMMNCs by means of flow cytometry and confocal microscopy. As a system recapitulating the bone marrow microenvironment, fresh BMMNCs, the target of therapeutic Wnt delivery, were exposed to the nanoparticles, and their localisation in phagocytic cells as well as skeletal stem cells was assessed.

The ability of the nanoparticles to accumulate in the bone is of utmost importance, as they are aimed at influencing skeletal stem cell subsets within the bone marrow niche. Under normal circumstances, accumulation of nanoparticles occurs primarily in the liver, the spleen and the bone marrow (due to the involvement of RES in their clearance). However, because of their different characteristics, such as surface chemistry and size, their biodistribution can vary widely. In addition, as discussed earlier, inflammation present at injury sites can also influence nanoparticle localisation (see Section 1.4.6). An *in vivo* imaging system (IVIS) was used here to determine the biodistribution of liposomes over time following a systemic injection in a murine bone fracture model.

In summary, the aim of the work in this chapter was to:

- characterise the liposome formulations on the basis of their size, stability, concentration, and formation efficiency;
- determine the optimal formulation for Wnt delivery;
- measure the uptake of liposomes *in vitro* and assess their distribution *in vivo*.

These studies were performed to test the hypothesis that liposomes can be used as delivery vesicles for Wnt3A protein and that due to their formulation and size, they preferentially localise at the bone fracture site *in vivo*.

A pictorial summary of the experimental protocols is shown in Figure 5.1.

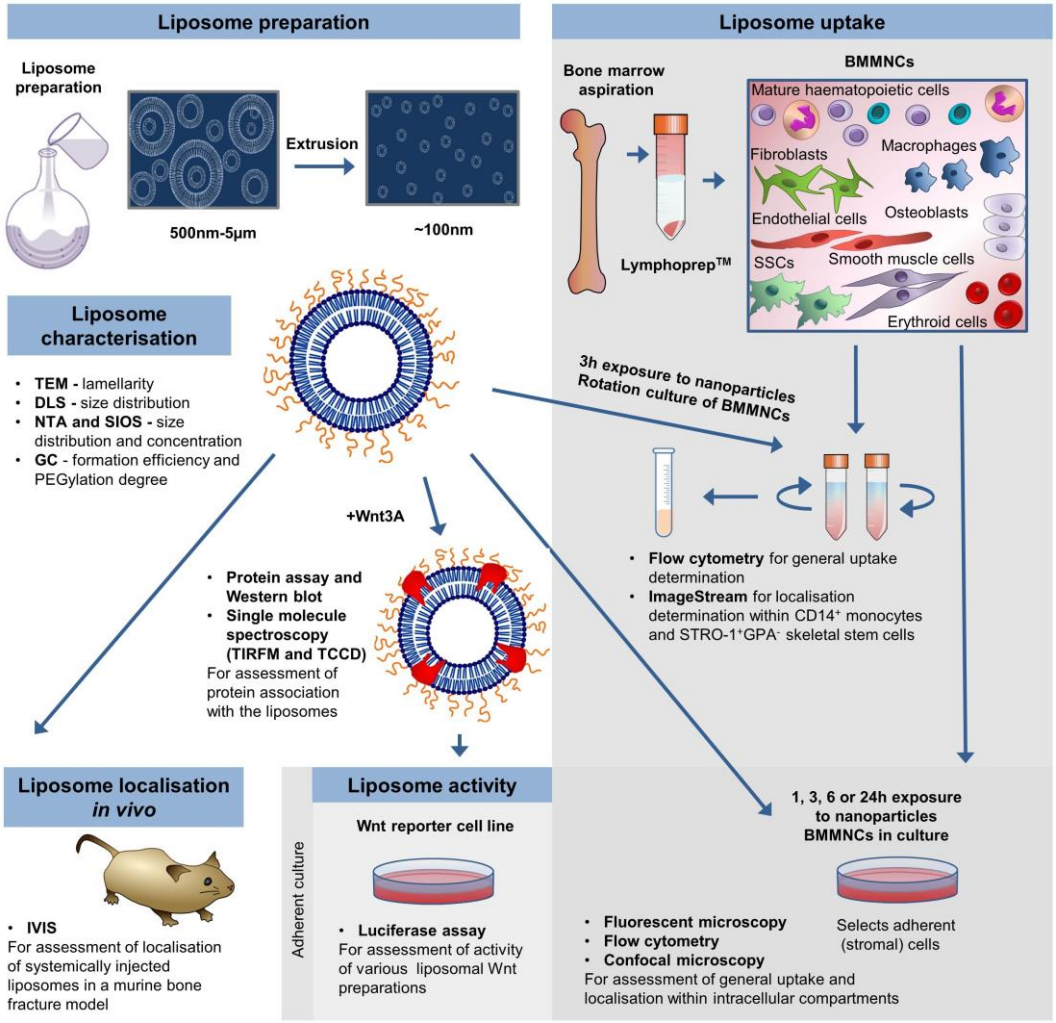

Figure 5.1 Overview of methodologies used and described in this chapter for assessment of liposomes as a delivery system for Wnt3A protein for therapeutic purposes.

Liposomes were prepared *via* extrusion, and characterised by TEM, DLS, NTA, SIOS and GC. Wnt3A protein association with the liposomes was studied by protein assay, Western blot and at a single molecule spectroscopy level by TIRFM and TCCD. The activity of liposomal Wnt preparations was assayed on a Wnt reporter cell line. Flow cytometry, Image Stream, fluorescence microscopy and confocal microscopy allowed to study nanoparticle uptake in fresh or cultured BMMNCs, initially isolated from bone marrow aspirates by Lymphoprep™. *In vivo* localisation of the nanoparticles was studied by IVIS, in a murine bone fracture model after systemic injection. BMMNCs, bone marrow mononuclear cells; DLS, dynamic light scattering; GC, gas chromatography; IVIS, *in vivo* imaging system; NTA, nanoparticle tracking analysis; SIOS, scanning ion occlusion sensing; SSCs, skeletal stem cells; TCCD, two-colour coincidence detection; TEM, transmission electron microscopy; TIRFM, total internal reflection fluorescence microscopy.

5.2 Results

5.2.1 Characterisation of liposome preparations

Initially, different lipid compositions of the liposome preparations were tested, before the incorporation of Wnt3A. A list of the lipids used in the experiments and detailed molar % composition of the liposomes can be found in the Appendix, Table A.12 and Table A.13. Apart from cholesterol, all the lipids used for making liposomes were synthetic, to ensure increased stability and purity, as guaranteed by the manufacturer. Lipids chosen for liposome preparations varied in length and saturation of their fatty acid chains, which allowed for the study of liposomes composed of lipids with different properties. Characterisation of the liposome preparations with techniques such as TEM, DLS, NTA, SIOS and GC is described below. This allowed further studies to focus on the liposome preparation giving the desired properties for Wnt3A delivery to a bone fracture site.

5.2.1.1 Size distribution, stability and concentration of liposomes

Firstly, liposomes were produced *via* extrusion through a 100 nm filter membrane and imaged under TEM, to assess the lamellarity of the preparations and to obtain an approximation of their size. It was impossible to image the liposomes with this technique without prior fixation. After applying glutaraldehyde fixation, the procedure was still difficult, as the liposomes broke apart rapidly due to exposure to vacuum and high energy electron beam. Figure 5.2 depicts representative images of liposome preparations seen under TEM, confirming their unilamellarity. Suspected PEG polymer structures were observed under higher magnification in "stealth" preparations.

As shown on the micrograph, the liposomes were <150 nm in size. However, due to the nature of this technique, the size of nanoparticles can only be an approximation. Therefore more accurate measurements were conducted with the use of DLS and NTA technologies. Figure 5.3A shows the that the liposome preparations were 100 ± 20 nm in size according to DLS analysis. A more accurate measurement offered by the NTA technique (Figure 5.3B), provided information on the spread of the nanoparticle populations and their concentration, which was ~10^{14} particles/ml. This confirmed the

calculations made for estimation of liposome concentration (see Appendix, Figure A.17), based on lipid concentrations and approximation of particle size.

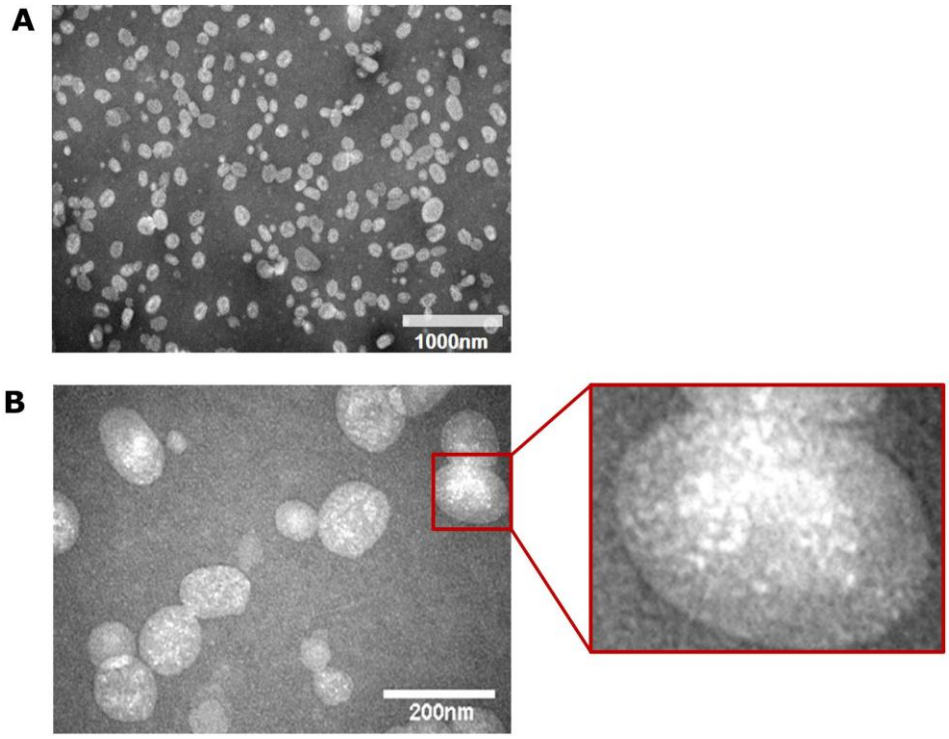

Figure 5.2 Liposomes under TEM.

TEM micrograph showing fixed and negatively stained liposome preparations. A: Representative image of DMPC/DSPE-PEG liposomes at 20 000x magnification. Liposomes are uniform and unilamellar. B: At 80 000x magnification, uneven structures are visible in the "stealth" (PEGylated) preparations, which can be attributed to "mushroom-like" or "brush-like" polymer conformations of PEG.

Both "stealth" (PEGylated) and unPEGylated preparations were examined, to compare the possible effects on liposome size and dispersity of the incorporation of this polymer within liposomes. It is important to note that the PEG polymer in all preparations was tethered to DSPE lipid added during mixing of the lipids, rather than after liposome formation; hence the polymer could be incorporated on both inner and outer surfaces of the liposome. Despite this, the size distribution of the PEGylated preparations was similar to that of unPEGylated preparations, close to the desired ~100 nm, and all the samples were of very low polydispersity (Figure 5.3C).

Because the "stealth" preparations offer considerable advantages when considered for *in vivo* applications, research in this thesis focused on PEGylated preparations, and liposomes without PEG are used as controls for most of the experiments. However,

for assessing the stability of the preparations during storage at 4°C, only PEGylated preparations of various lipid compositions were examined (Figure 5.4). This analysis provided data on the optimal lipid composition for use in further experiments.

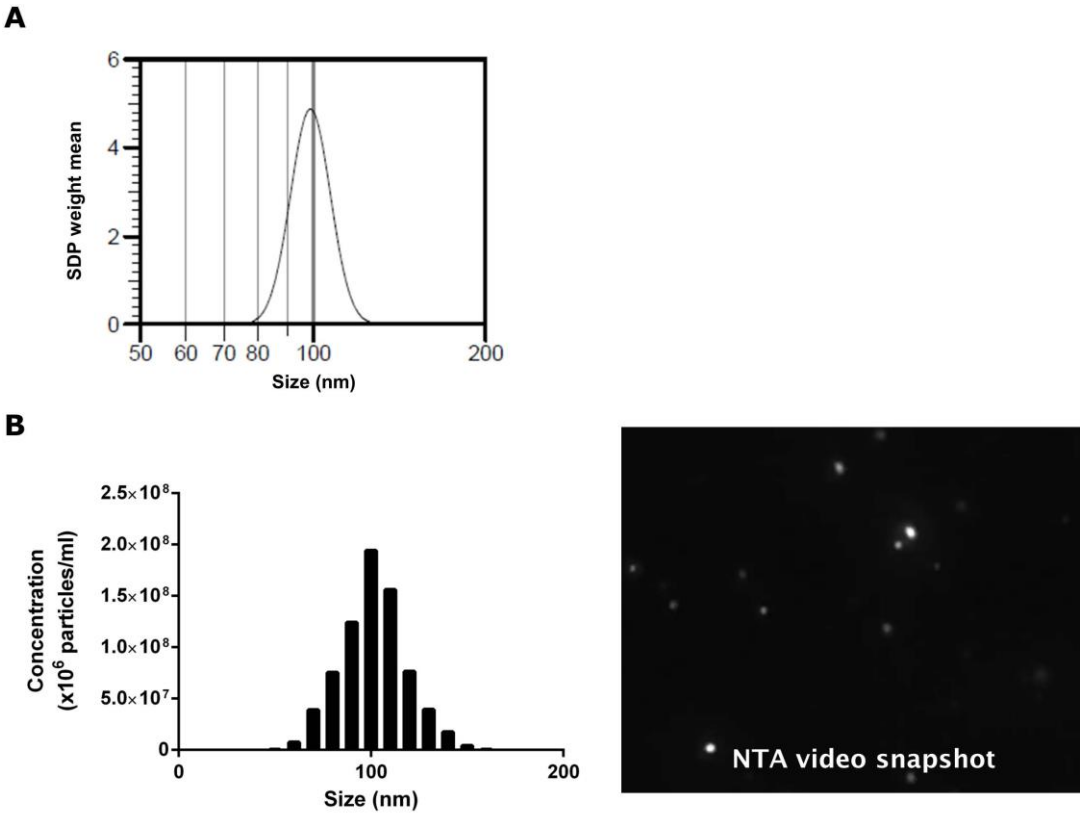

C

Preparation	DMPC	DMPC/DPSE-PEG	DOPC	DOPC/DSPE-PEG
Mean (size)	98.6 nm	98.7 nm	110.1 nm	102 nm
Mode (size)	104.4 nm	91.3 nm	112.1 nm	109.8 nm
SD (size)	21.7 nm	25.4 nm	26.3 nm	23.1 nm
d10	69.0 nm	68.0 nm	74.7 nm	71.0 nm
d50	93.1 nm	90.9 nm	102.7 nm	96.4 nm
d90	116.4 nm	117.9 nm	135.9 nm	118.8 nm
Concentration (particles/ml)	9.40×10^{13}	1.44×10^{14}	1.19×10^{14}	1.66×10^{14}
PI	0.058	0.084	0.071	0.051

Figure 5.3 Size and concentration of liposome preparations measured by DLS and NTA.

A: Representative histogram from DLS, showing narrow distribution of the liposome preparation, 100 ± 20 nm in size. B: Size and concentration measurement histogram from NTA, based on analysis of the recorded video. C: Summary of size, concentration and polydispersity index (PI) of the 4 tested liposome preparations. d10, d50, d90 - % levels below which the sample population falls, giving an indication of the overall spread of size, *i.e.* 50 % of DMPC liposomes are ≤ 93.1 nm.

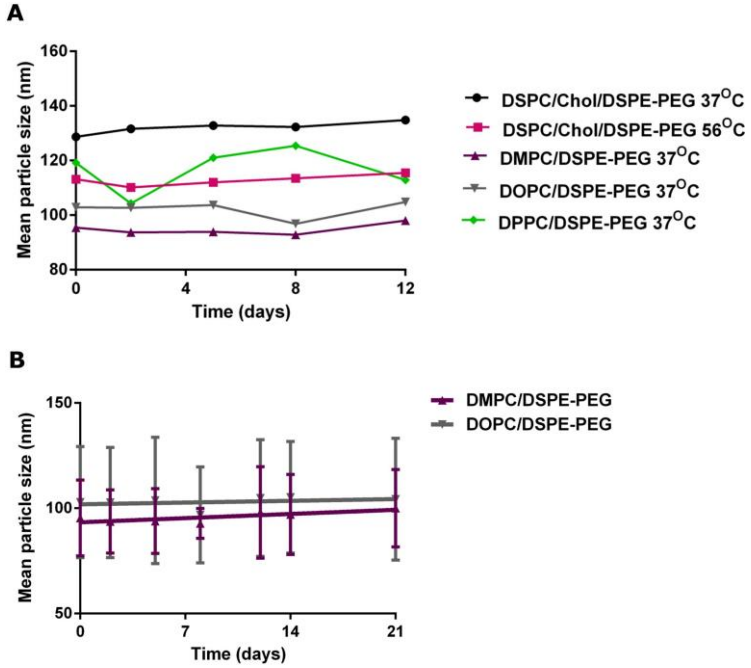

Figure 5.4 Liposome particle stability measured by DLS.

A: Mean particle size of different liposome preparations over a period of 12 days while stored at 4°C. Different lines represent different lipid content and extrusion temperature. B: Two preparations nearest the desired 100 nm size (PEGylated DMPC and DOPC) were analysed further, for a total of 21 days. Data presented as mean ± SD, n = 3. Chol, cholesterol.

Liposomes consisting of lipids with high transition temperatures (Tc) which were extruded below this temperature formed vesicles larger than intended (DSPC at 37°C *vs.* 56°C extrusion). Liposome preparations consisting mainly of DMPC or DOPC were examined in further experiments as potential delivery vesicles, due to their desirable narrow size distribution, and reproducibility of this size distribution between repeat preparations. All formulations were stable over the test period.

SIOS technology was applied to assess liposome fusion during prolonged storage (> 1.5 months, Figure 5.5), as it enables examination of the size distribution of highly polydisperse samples more accurately than DLS or NTA, within a certain window of analysis, due to the pore size applied.

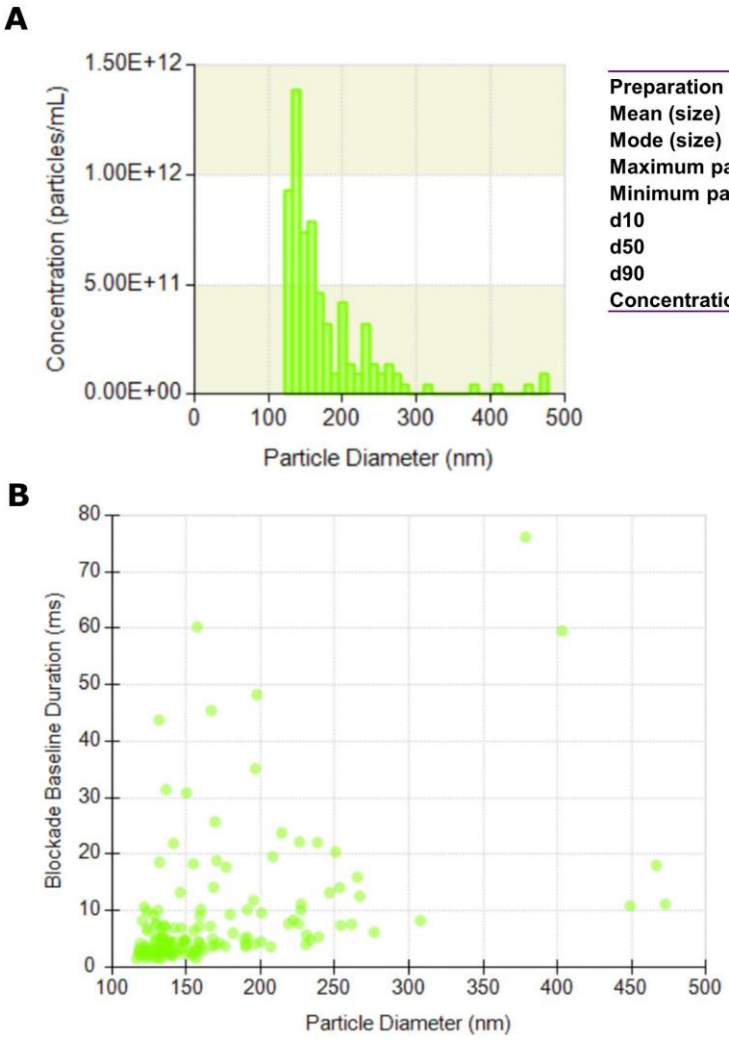

Preparation	DOPC/DSPE-PEG
Mean (size)	172.3 nm
Mode (size)	132.1 nm
Maximum particle diameter	472.9 nm
Minimum particle diameter	116.4 nm
d10	123.2 nm
d50	149.0 nm
d90	239.0 nm
Concentration (particles/ml)	6.5E+12

Figure 5.5 Size and concentration of liposome preparations measured by SIOS.

SIOS technology was applied to DOPC/PEG liposome preparations stored for > 1.5 months at 4°C, showing substantial "fusing" of the particles within the sample and formation of liposomes of a size larger than that desired. A 500 nm pore was used. A: Size and concentration measurement histogram. B: Population view of the sample. A discrete blockade event signal is recorded by the system each time a particle traverses the nanopore. The magnitude of the measured blockade signal is proportional to the particle size. Blockade duration (translocation time / time-of-flight) relates to the surface charge of the particles. E+n = multiplied by 10^n.

During this prolonged storage, liposome concentration dropped and mean size increased, possibly due to fusion of liposomes and formation of particles of a size larger than desired. Therefore, all liposomes in this thesis were used for experiments within a period of 21 days from formation.

It is noteworthy that the size of liposome formulations containing Wnt3A protein was no different to the size of empty liposomes. Also, preparations that were labelled with lipophilic dyes (3,3'-dioctadecyloxacarbocyanine perchlorate, DiO; 1,1'-dioctadecyl-

3,3,3',3'-tetramethylindocarbocyanine perchlorate, DiI; or 1,1'-dioctadecyl-3,3,3',3'-tetramethylindotricarbocyanine iodide, DiR), used for imaging purposes, were of ~100 nm size. The only exception was for liposomes with a DSPE-conjugated biotinyl cap, extending slightly from the liposome surface due to a short linker, used for labelling with a fluorescent AF647-streptavidin. These liposomes, a control for membrane-bound protein, were 175 ± 25 nm in size (n = 3; see Appendix for Wnt3A-incorporating, dye-labelled and biotinylated liposome size, Figure A.18).

5.2.1.2 Liposome lipid composition and formation efficiency

As a low degree of liposome PEGylation offers substantial advantages with regards to *in vivo* applications, as well as to the general stability of the preparations, GC was used to assess whether the PEG molar % after formation of the nanoparticles was as desired (~5 molar %). The GC technique also allowed for the estimation of liposome formation efficiency. Representative gas chromatograms and a summary of the analysis is shown in Figure 5.6. Substantial loss of lipid during the preparation steps can be attributed to the extrusion step. Nonetheless, the formulations of interest were indeed ~4.6 - 4.8 molar % PEGylated, and the DOPC PEGylated liposomes formed with highest efficiency (~68 %). This analysis also provided evidence of the purity of lipids used for making nanoparticles.

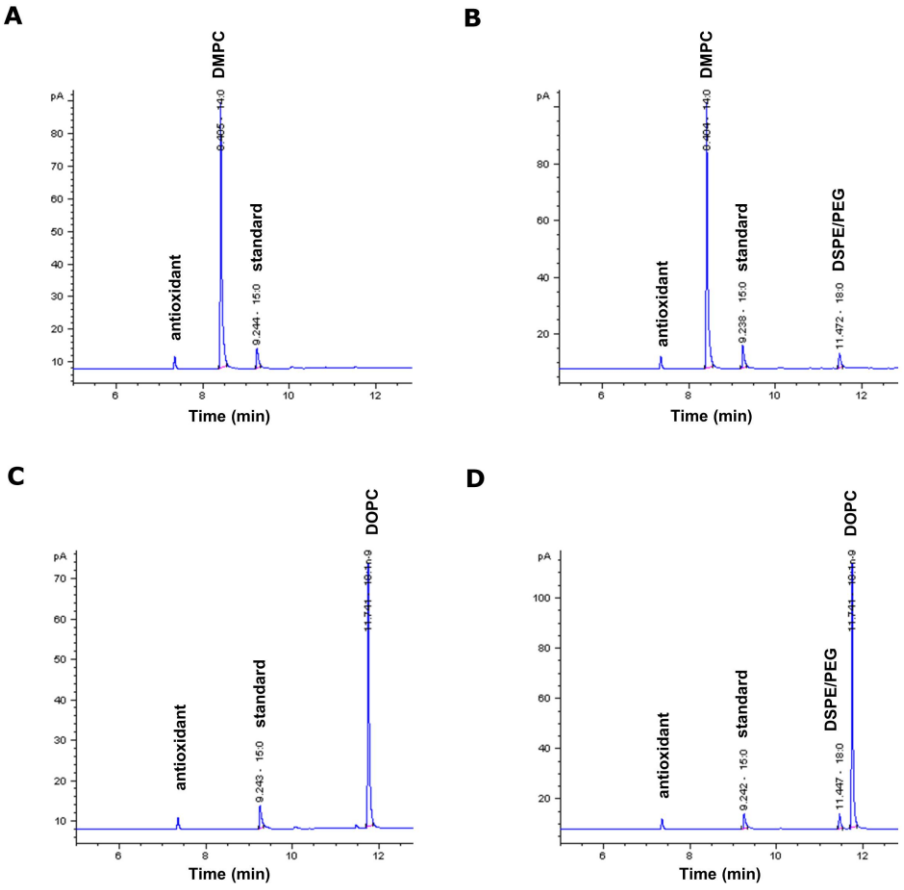

E

Preparation	DMPC	DMPC/DPSE-PEG	DOPC	DOPC/DSPE-PEG
% lipid content out of total used for preparation	49.5 %	47.3 %	48.1 %	68.6 %
PEGylation	0 mol %	4.8 mol %	0 mol %	4.6 mol %

Figure 5.6 Lipid composition and PEGylation assessment by GC.

Gas chromatograms for A: DMPC, B: DMPC/DSPE-PEG, C: DOPC and D: DOPC/DSPE-PEG liposome preparations. Standard lipid of 15:0 (1,2-dipentadecanoyl-sn-glycero-3-phosphocholine, PC) was used as it had a different elution time from the 14:0 (DMPC), 18:0 (DSPE) and 18:1 (DOPC) lipids used in the preparations. E: Total lipid mass, formation efficiency and degree of PEGylation were calculated.

5.2.2 Functionality of Wnt in liposome preparations

A Wnt responsive murine 3T3 cell line, which expresses a luciferase reporter gene under the control of Wnt-responsive promoters (TCF/LEF), was used to assess the activity of liposomal Wnt preparations. First, the response of the cell line was tested on neat murine and human Wnt3A proteins used in this thesis (see Section 4.2.1 for Figure 4.2 in previous chapter). Wnt3A protein activity readout can vary depending on

the cell line expression of its surface receptor, Frizzled, hence an intracellular small molecule inducer of the Wnt signalling pathway, the GSK3 inhibitor 6-bromoindirubin-3'-oxime (BIO), was used as an internal test control for the cell line (Figure 5.7). For all assays testing Wnt3A protein activity, 5 μm BIO was used (inducing the maximum response), and fold increase in luciferase activity after its addition is stated in each figure legend. As cell proliferation may change upon addition of Wnt pathway inducing agents, following the luminometric readout cell lysates were also analysed for dsDNA content as a control for cell number.

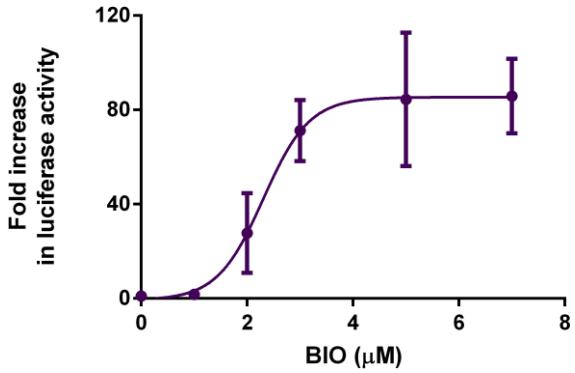

Figure 5.7 Responsiveness of the Wnt reporter cell line to Wnt agonist, BIO.

BIO, a very potent Wnt signalling inducer, markedly activated the Wnt pathway at micromolar concentrations. 5 μM concentration of BIO was used for future assay controls. Data presented as mean ± SD, n = 3 separate experiments. All data points were normalised to controls without the addition of BIO, as well as to cell number.

Initially, in liposomal Wnt preparations, the Wnt3A protein was added during the rehydration of the lipid cake/liposome formation step, before extrusion of the liposome formulation (see Methods Section 2.2.5.9). Figure 5.8 shows the activity of these preparations.

The activity of the DMPC liposome-incorporated Wnt3A was similar to that of the neat, unincorporated protein, whereas other preparations had lower activity, with DMPC lipid preparations with cholesterol being completely inactive. To increase the activity of liposomes, another preparation method was applied, whereby the protein was incubated with the liposomes after their formation. This greatly increased the activity of liposomal preparations composed of DOPC lipid and DOPC and PEG (Figure 5.9).

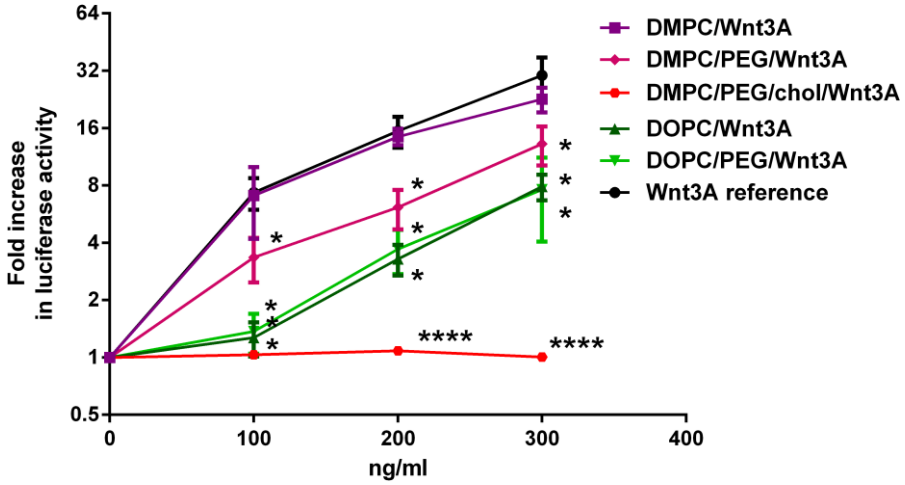

Figure 5.8 Activity of liposomes with Wnt3A protein added before extrusion.

Wnt3A activity in PEGylated and unPEGylated DMPC and DOPC liposomes was tested after ultracentrifugation. Data from reconstituted liposomal pellets shown. Supernatants had no detectable activity. Concentration is expressed in ng/ml, assuming 100 % Wnt3A encapsulation efficiency. Neat Wnt3A protein was used as a reference. 5 μM concentration of BIO resulted in 95 ± 28 fold increase in luciferase activity. Data presented as mean ± SD, n = 3 separate experiments. All data points were normalised to appropriate controls (for liposomes, these were the liposome preparations without the addition of Wnt3A), as well as to cell number. *p<0.05, ****p<0.0001 for liposome preparations *vs.* Wnt3A reference. Data presented as mean ± SD. Statistical significance assessed by two-way ANOVA with Tukey's correction. Chol, cholesterol.

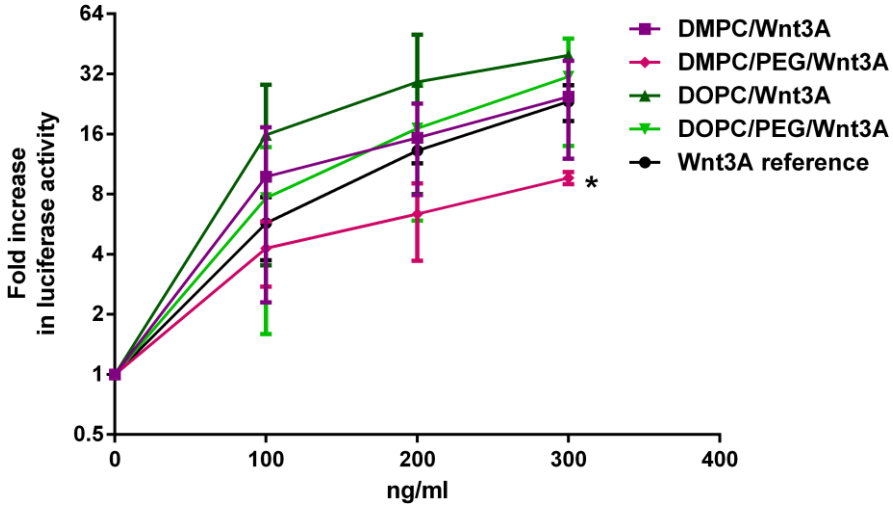

Figure 5.9 Activity of liposomes with Wnt3A protein added after formation.

Wnt3A activity in PEGylated and unPEGylated DMPC and DOPC liposomes was tested after 24 hours of incubation with the particles at room temperature and subsequent ultracentrifugation. Data from reconstituted liposomal pellets shown. Concentration is expressed in ng/ml, assuming 100 % Wnt3A incorporation efficiency. Neat Wnt3A protein was used as a reference. 5 μM concentration of BIO resulted in 92 ± 33 fold increase in luciferase activity. Data presented as mean ± SD, n = 3 separate experiments. All data points were normalised to appropriate controls (for liposomes, these were the liposome preparations without the addition of Wnt3A), as well as to cell number. *p<0.05, for liposome preparation *vs.* Wnt3A reference. Data presented as mean ± SD. Statistical significance assessed by two-way ANOVA with Tukey's correction.

Data from various incubation time points of liposomes with the Wnt3A protein, and the activity of reconstituted liposomal pellets and supernatants, can be found in the Appendix, Figure A.19. For most of the liposomal preparations, incubation with Wnt3A for 6 to 24 hours was sufficient. Also, additional time points for the luciferase assay readout can be found in Appendix, Figure A.20. The cellular response to liposome-encapsulated Wnt, tested on the murine cell line, was seen to be optimal at 18 hours.

5.2.3 Wnt assosiation with liposomes

5.2.3.1 Protein content analysis of liposomes

The results showed that Wnt3A protein activity was highly dependent on the incorporation technique used, and, to an even greater extent, on the type of lipids used in different liposome formulations, indicating there are differences in how the protein interacts with the liposomal bilayer. Therefore, the Wnt3A protein content of the various liposomes was measured (Figure 5.10). Biochemical measurements of proteins in the liposome pellet and supernatant post-formation, confirmed that the majority of the protein was found in the liposome pellet after ultracentrifugation, with a small amount in the supernatant (compare dark green bars to light grey bars in Figure 5.10A). However, the concentration results showed that Wnt3A incorporation efficiency varied between liposomal preparations (71.5 - 90.0 %), and was higher for the DMPC than DOPC lipid-based formulations.

Western blot analysis conducted on the pellets and supernatants of samples ultracentrifuged after 24 hours and 5 days of storage at 4°C showed that Wnt3A protein associated more strongly with liposomes formed of DMPC, DMPC/PEG and DOPC/PEG lipids, rather than DOPC, as the amount of Wnt in the supernatant after ultracentrifugation was lower in these cases, 24 hour after formation (compare left and right upper panels in Figure 5.10B). However, after 5 days of storage, the association of Wnt3A with DOPC/PEG liposomes became weaker, as more protein was found in the supernatant, in comparison to the 24 hour time point (compare right lower and upper panels in Figure 5.10B). Because of this observation, for assays involving liposomal-Wnt, liposomes were used within 3 days of incubation with this protein.

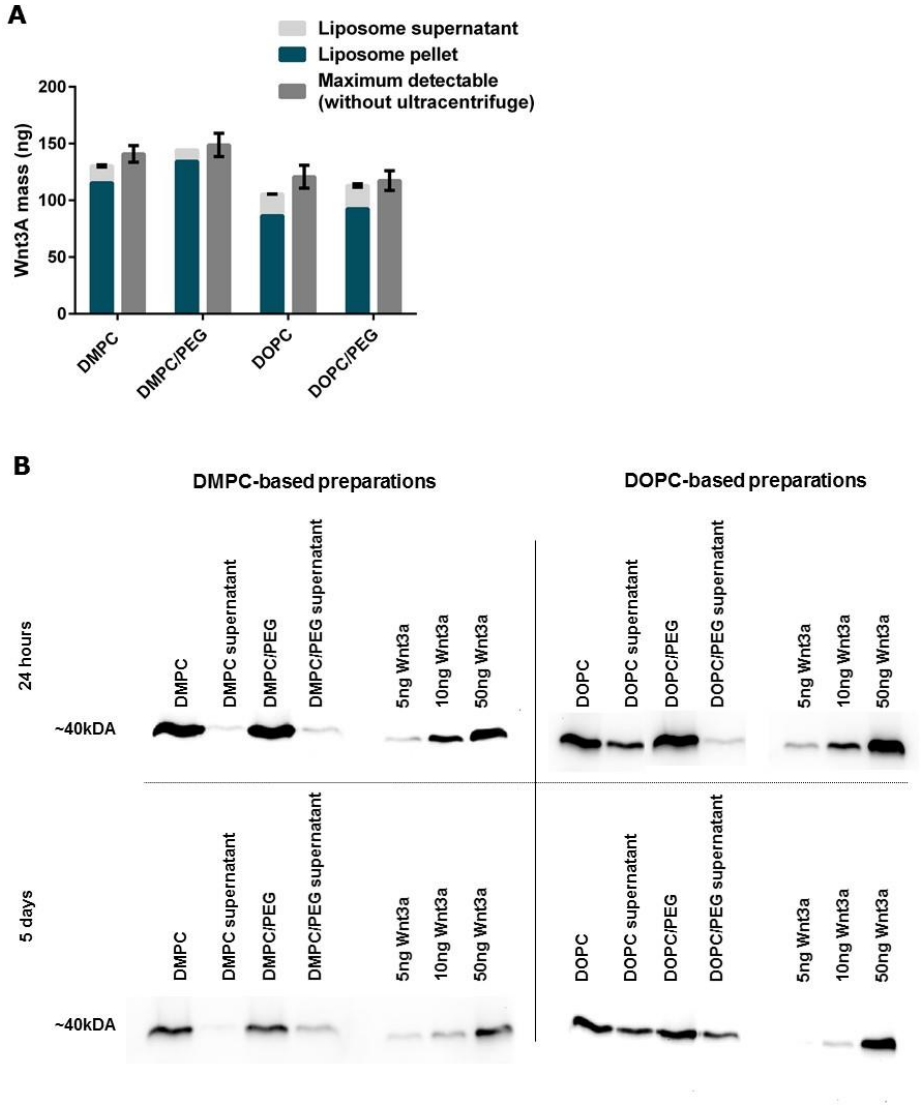

Figure 5.10 Association of Wnt3A protein with liposomes.

A: Protein concentration in pellets and supernatants after liposome ultracentrifugation was assessed immediately following preparation, *vs.* non-centrifuged preparations, with the use of a commercial CBQCA fluorescent assay. 150 ng of liposomal Wnt3A (assuming 100 % incorporation efficiency) associated with DMPC and DOPC, PEGylated and unPEGylated preparations was assessed. Neat, unincorporated Wnt3A was used for construction of the standard curve. Data presented as mean ± SD, n = 3. Efficiency of incorporation was calculated based on the Wnt3A mass associated with the liposomal pellet out of total detectable by assay and was: 82 %, 90 %, 71 % and 79 % for DMPC, DMPC/PEG, DOPC and DOPC/PEG, respectively. B: Western blot analysis for Wnt3A protein content of liposome pellets and supernatants after ultracentrifugation 24 hours and 5 days after formation. DMPC and DOPC, PEGylated and unPEGylated preparations were assessed. 50 ng of liposomal Wnt3A (assuming 100 % incorporation efficiency) was loaded onto an SDS-PAGE gel. 5, 10 and 50 ng of neat Wnt3A was used as a reference for each blot.

5.2.3.2 Single molecule spectroscopy measurements of liposomes and Wnt3A

Furthermore, Wnt3A protein association with liposomes was examined at the single molecule level. To be able to visualise the liposomes, a lipophilic fluorescent dye, DiO, was incorporated after formation of the liposomes, simply by incubation with the lipid particles. To enable visualisation of Wnt3A protein, conjugation with various fluorescent dyes was carried out, using a dye containing either a maleimide group or an NHS group, to enable the attachment of the dye to different amino acid residues of the Wnt3A protein. More detailed results of conjugation with the AF647-maleimide dye, Atto680-maleimide and Atto680-NHS dyes are found in the Appendix, Figure A.22-Figure A.24. As the Wnt3A protein used in the experiments was a commercially available recombinant protein, and bovine serum albumin (BSA) is typically added to such preparations, a "carrier free" version (>75 % purity) was used was purchased for the tagging experiments. Unfortunately, this preparation also contained a substantial amount of BSA, which was unavoidable due to the nature of Wnt3A purification protocols. A costly "pure" Wnt3A (>95 % purity) was assayed as well, but the majority of this protein was lost in the chromatography column purification step following dye conjugation, and therefore was not used further. Figure 5.11 shows the efficiency of "carrier free" Wnt3A labelling with fluorescent dyes, and an approximation of the total protein load by silver staining. Loading of the tagged protein onto SDS-PAGE gels accounts for the ~50 % protein loss during the column purification step, which was also an issue for the "carrier free" Wnt3A (see Appendix, Figure A.21). The results clearly show contamination of Wnt3A preparations with BSA protein. This is a major concern due to the fact that the BSA contaminating each Wnt3A preparation clearly conjugates with the fluorescent labels as well, indeed to an even higher degree than Wnt3A in the case of NHS conjugation. Therefore for the single molecule studies of Wnt3A association with liposomes, fluorescently-labelled BSA protein was used as a control.

After conjugation with the fluorescent dye, the activity of tagged proteins was measured using a Wnt-responsive cell line (Figure 5.12). Atto680-NHS-tagged Wnt3A failed to induce a response on the Wnt-responsive cell line, whereas both Atto680-maleimide and AF647-maleimide were active. This indicated that conjugation *via* NHS

affected amino acid residues which were important for Wnt3A binding to its receptor, and therefore this method was not used further.

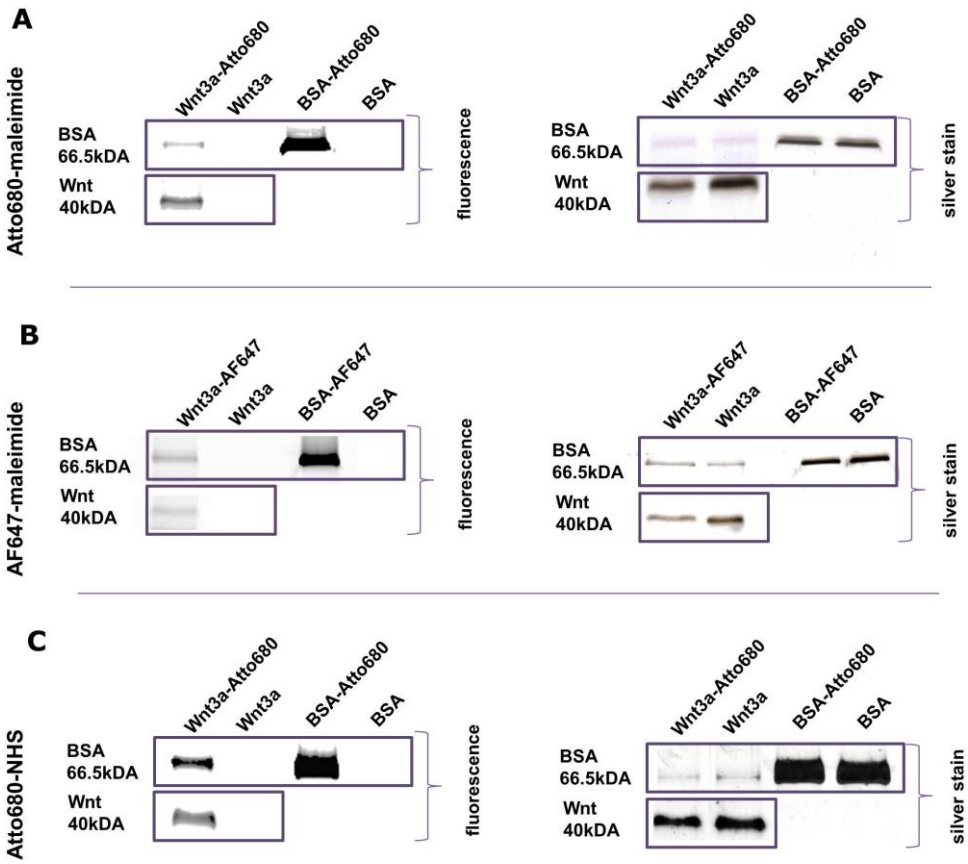

Figure 5.11 SDS-PAGE of tagged Wnt3A protein.

Wnt3A protein was tagged with Atto680-maleimide (A) or AF647-maleimide (B) or Atto680-NHS (C) and the SDS-PAGE gels were photographed in a fluorescent reader to visualise the tag and subsequently stained with a silver stain kit for total protein visualisation. BSA protein, contaminating commercial Wnt3A preparations, was used as control. Size of band was determined based on a protein ladder (see Appendix Figure A.22 - Figure A.24).

Furthermore, liposomal preparations with fluorescently-labelled Wnt3A were assayed for activity. Wnt3A conjugated with AF647-maleimide was not active in the liposomal environment (see Appendix, Figure A.25), as opposed to Atto680-maleimide-conjugated Wnt3A, which showed activity within all the liposomal preparations, although with DMPC/PEG liposomes this activity was significantly diminished (Figure 5.13).

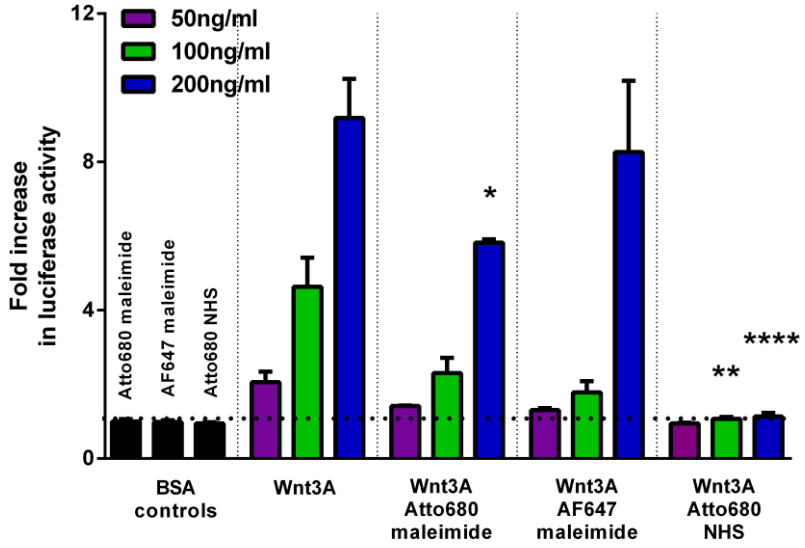

Figure 5.12 Wnt3A protein activity on a Wnt-responsive cell line after tagging with fluorescent dyes.

Wnt3A protein conjugated with Atto680-NHS dye was inactive, as opposed to Wnt3A tagged with Atto680-maleimide or AF647-maileimide dyes. Data presented as mean ± SD, n = 3 separate experiments. 5 μM concentration of BIO resulted in 90 ± 25 fold increase in luciferase activity. All data points were normalised to controls without the addition of fluorescent proteins, as well as to cell number. *p<0.05, **p<0.01, ****p<0.0001 *vs.* equivalent concentration of Wnt3A control sample. Statistical significance assessed by one-way ANOVA with Tukey's correction.

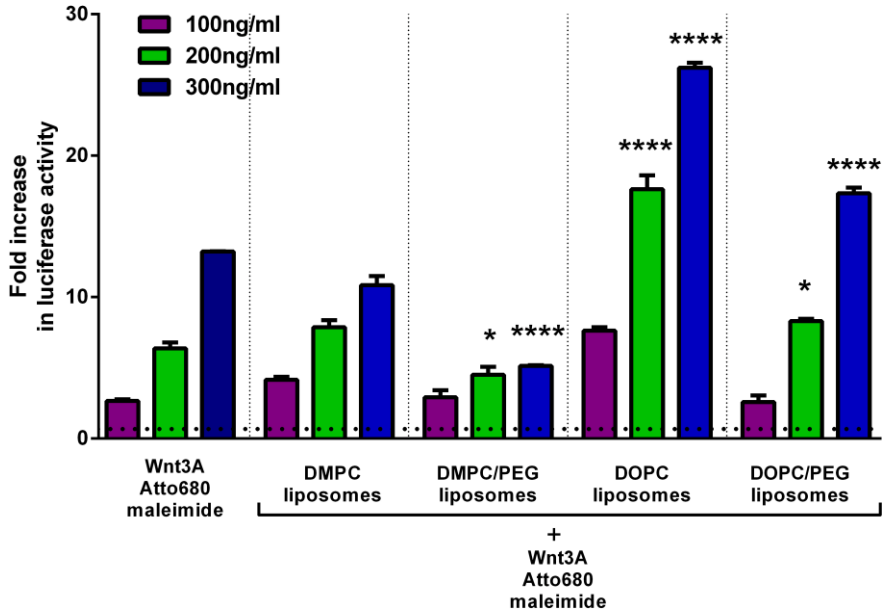

Figure 5.13 Liposome activity with labelled Wnt3A protein.

Wnt3A protein conjugated with Atto680-maleimide dye was active in DMPC and DOPC liposomal preparations. Data presented as mean ± SD, n = 3 separate experiments. 5 μM concentration of BIO resulted in 89 ± 29 fold increase in luciferase activity. All data points were normalised to controls without the addition of fluorescent proteins, as well as to cell number. *p<0.05, **p<0.01, ****p<0.0001 *vs.* equivalent concentration of Wnt3A non-liposomal sample. Statistical significance assessed by one-way ANOVA with Tukey's correction.

As a positive control for a protein associated with the liposomal bilayer, biotinylated liposomes incubated with AF647-labelled streptavidin were prepared. Biotin binds to streptavidin with high affinity (Weber *et al.* 1989) and therefore this method acted as a positive control for protein in the proximity of the lipid bilayer. BSA conjugated with Atto680-maleimide, as previously mentioned, was used as negative control; BSA is a protein soluble in aqueous solutions, and therefore does not associate specifically with membranes.

Firstly, TIRFM was used to study the colocalisation of both fluorescent tags (on liposomes and protein; see Methods, Section 2.2.5.14). The proteins and liposomes were incubated for 5 minutes before imaging. Results are depicted in Figure 5.14, and show coincidence between Wnt3A and liposomes. The degree of colocalisation of labelled Wnt3A protein with DiO-labelled liposomes was 24 % compared with 34 % for labelled streptavidin and 7 % for BSA. Labelled BSA was used at the same concentration as Wnt, but due to more efficient labelling, this concentration was too high to act as an appropriate control; hence the chance of the coincidence was high as well.

Secondly, the level of colocalisation of Wnt3A protein and liposomes was studied by TCCD (see Methods, Section 2.2.5.14). Results from this confocal microfluidic method are presented in Figure 5.15. The maximum detectable coincidence level for this technique reached 15.7 %, as measured on a DNA duplex. This was due to the capacity of the microscope setup and the overlaying of the two lasers within the small confocal volume used in this method to assure analysis at a single molecule level. The coincidence was 9.2 % for the positive control streptavidin sample, and 2.2 % and 0.2 % for Wnt3A and BSA, respectively.

Similar results were obtained when this TCCD experiment was repeated twice more on DMPC liposomes, as well as on DMPC/PEG, DOPC and DOPC/PEG liposomes.

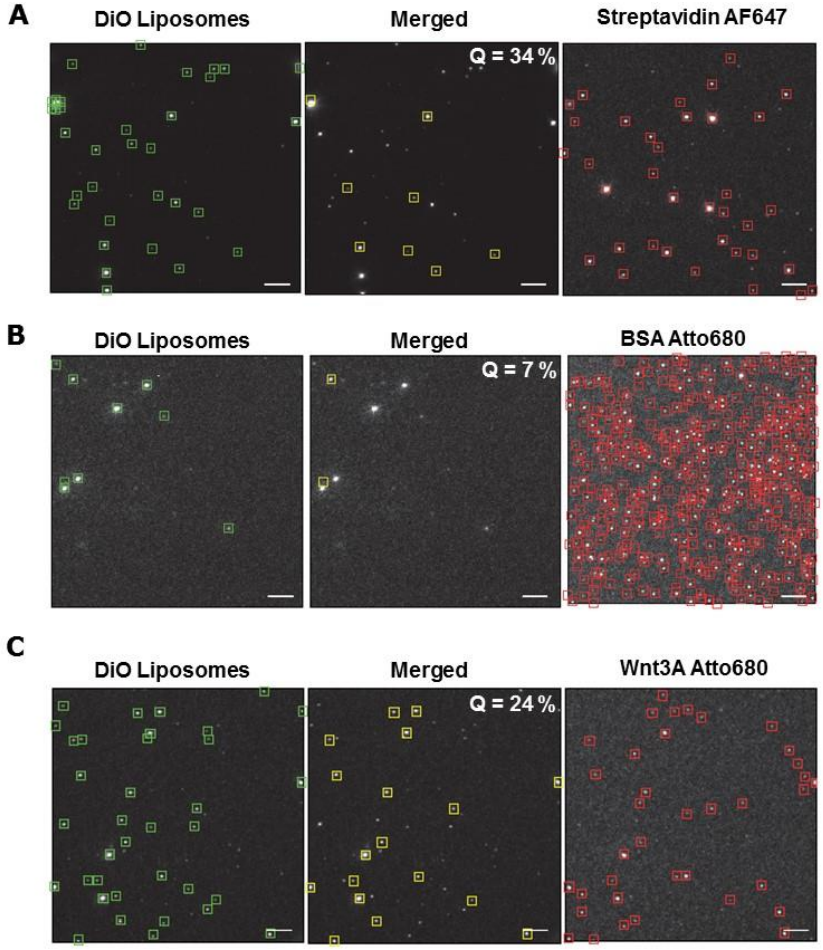

Figure 5.14 TIRFM images of protein colocalisation with liposomes.

A: DiO-labelled DMPC liposomes with biotin (left) and AF647-labelled streptavidin (right). The level of coincidence reached 34 % (centre). B: DiO-labelled DMPC liposomes (left) and Atto680-labelled BSA (right). The level of coincidence reached 7 % (centre). C: DiO-labelled DMPC liposomes (left) and Atto680-labelled Wnt3A (right). The level of coincidence reached 24 % (centre). Coincident spots were measured for the liposome channel. Scale bars = 5 μm.

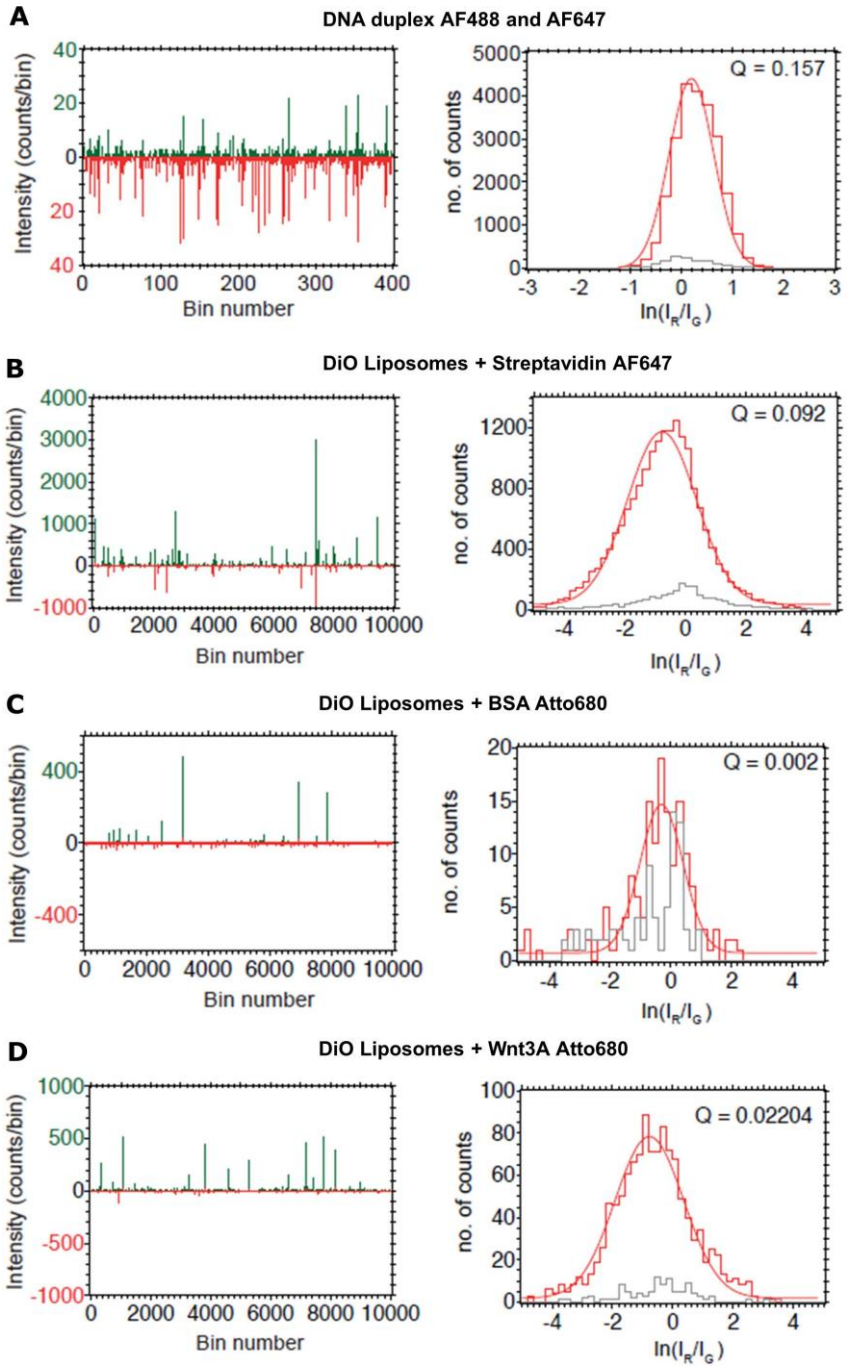

Figure 5.15 TCCD results of protein colocalisation with liposomes.

As a control for the TCCD experiment and for defining the maximum detectable level of coincidence, double labelled (green and red) DNA duplex was assayed. The representative diagram with photon bursts (left), shows both the green and the red channel (A) with coincident bursts shown on the Z-parameter histogram (right) and indicated by the association quotient (Q). Red histogram represents real events, whereas grey histogram represents chance events. Representative diagrams with photon bursts from TCCD experiment (left), showing both the green (DMPC liposomes) and the red (protein) channel for liposomes with streptavidin, BSA and Wnt3A, (B, C, D, respectively). Very few bursts are coincident in both channels for BSA, as shown on the Z-parameter histogram (right) and indicated by the association quotient (Q), and most of them were due to chance coincidence as indicated by the grey line.

In summary, the described results showed that Wnt3A does indeed associate with the liposomes and is active in these preparations. Depending on lipid composition, the activity of Wnt3A incorporated within liposomes can exceed that of the neat protein. Because of this and the "stealth" characteristics, as well as narrow size distribution, the DOPC PEGylated preparations were of particular interest.

5.2.4 Uptake of liposomes *in vitro* and *in vivo*

As the overall aim of the nanoparticle production and characterisation was for drug delivery purposes, their uptake was studied both *in vitro* and *in vivo*.

5.2.4.1 Uptake of liposomes by cultured BMMNCs

Initially, adherent BMMNCs were exposed to liposomes. To visualise the nanoparticles, the liposomal bilayer was stained with lipophilic dyes, whereas the inner core incorporated sodium fluorescein, which is self-quenching at the high concentrations found inside the liposomes, but fluorescent upon release in the cell cytosol. Examination by simple fluorescence microscopy is hindered by nanoparticle size (100 nm), which means that the liposomes are not visible unless "clumped" on the cell surface or in the cellular compartments. After 24 hours of incubation with double labelled sodium fluorescein/DiI liposomes, only occasional positive cells could be imaged (Figure 5.16). However, flow cytometry was sensitive enough to detect these nanoparticles within BMMNCs, when the same preparations were examined over various time points (Figure 5.17). Quantification of the percentage of positive cells from these experiments is shown in Figure 4.18A and B, and mean fluorescence intensity (MFI) for both dyes is shown in Figure 5.18C and D. The uptake of the nanoparticles was rapid, and within 3 hours of incubation ~50 % of cells stained positive. This percentage began to increase more slowly at later time points, eventually reaching a maximum of ~70 % for the 24 hour time point. The difference in uptake between various liposome compositions was not significant after 1, 3 and 6 hours of incubation, but at 24 hours a significant increase in uptake of DOPC/PEG liposomes was noticed.

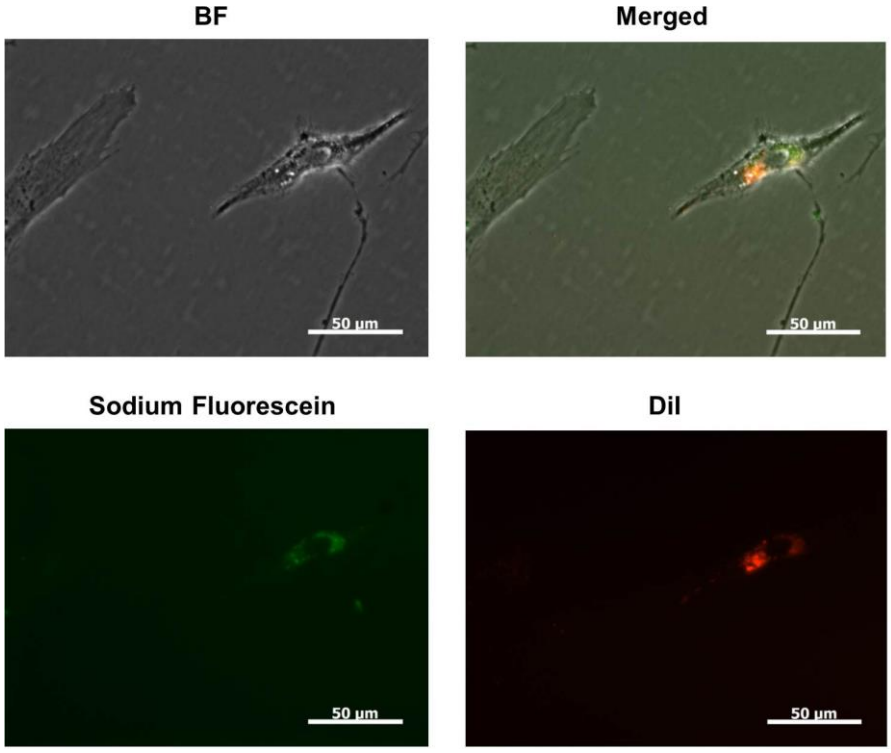

Figure 5.16 Uptake of dual-labelled liposomes by cultured BMMNCs – fluorescence microscopy.

Sodium fluorescein and DiI double-labelled liposome preparations were incubated with seeded BMMNCs for 24 hours. Only occasional positive signals were found in a minority of the cells imaged by this technique. BF, brightfield.

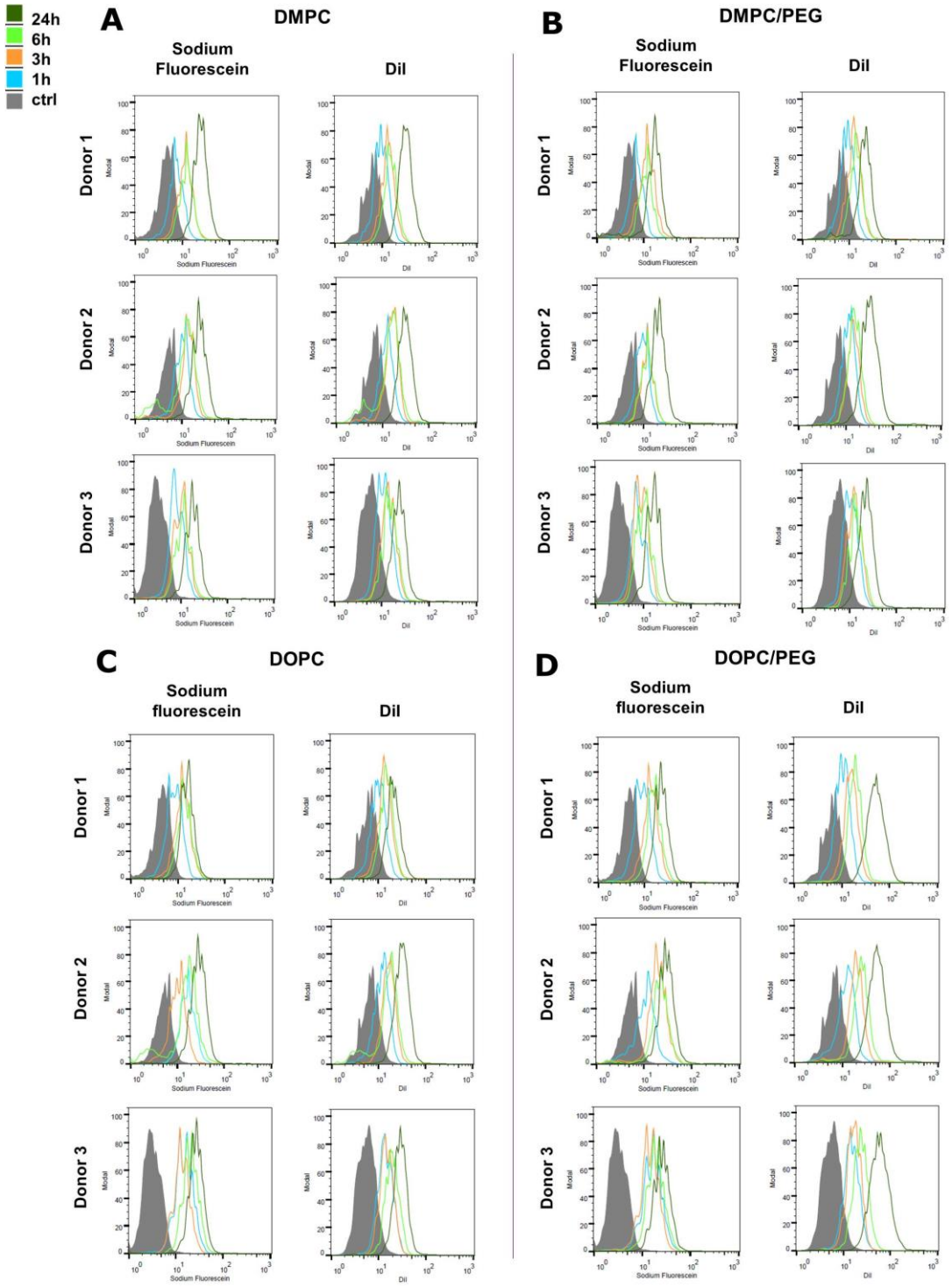

Figure 5.17 Uptake of dual-labelled liposomes by cultured BMMNCs, measured using flow cytometry.

Flow cytometry analysis of BMMNCs incubated with sodium fluorescein and DiI double-labelled liposomes for 1, 3, 6 and 24 hours. Clear shifts in the histograms representing cells exposed to nanoparticles (coloured) *vs.* control cells (grey, ctrl) are visible in all donor samples (n = 3) examined.

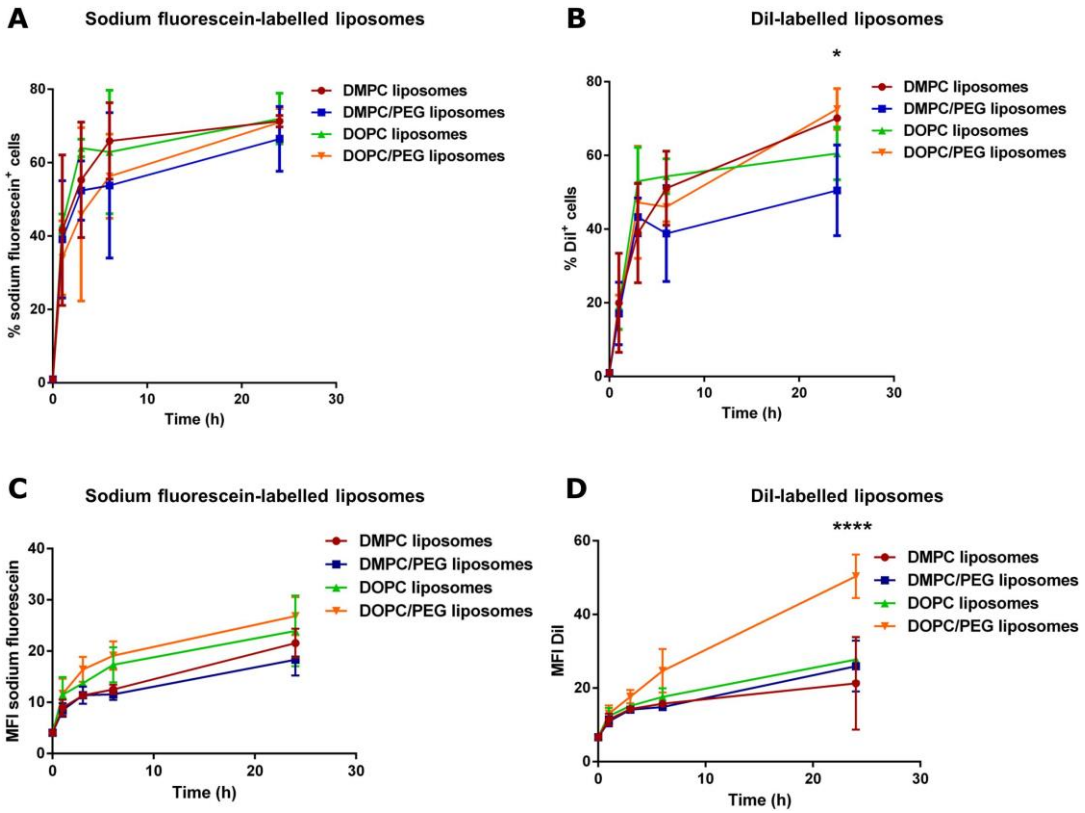

Figure 5.18 Uptake of dual-labelled liposomes by cultured BMMNCs – analysis of flow cytometry results.

Quantification of the uptake of sodium fluorescein and DiI double-labelled liposomes by BMMNCs after 1, 3, 6 and 24 hour incubation. A and B: All cells gated as positive showed a fluorescence intensity greater than that detected on 99 % of the cells not incubated with the particles. All liposome preparations were taken up rapidly by cells, resulting in 40 % and 20 % of the cells positively stained with sodium fluorescein and DiI dyes, respectively, within an hour of incubation. *$p<0.05$ for DOPC/PEG liposomes *vs.* DMPC/PEG liposomes. C and D: MFI of the geometric mean for sodium fluorescein and DiI. ****$p<0.0001$ for DOPC/PEG *vs.* all other preparations. Data presented as mean ± SD. Statistical significance assessed by two-way ANOVA with Tukey's correction. MFI, mean fluorescence intensity.

No cytotoxicity was observed with liposomal preparations over the course of 48 hours (see Appendix, Figure A.26). Next, cells exposed to liposomes labelled by other methods were examined. These methods included using the biotinylated liposomes labelled with AF647-streptavidin, or incorporation of the DiO dye during the lipid film formation step while drying under the nitrogen stream (see Methods, Section 2.2.5.9). This allowed for the use of a higher concentration of this lipophilic dye within liposomes and improved detection, as measured by flow cytometry (Figure 5.19). ~80 % of adherent BMMNCs took up DiO-labelled DOPC/PEG liposomes within 3

hours of incubation. DOPC/PEG liposomes labelled with AF647 stained ~21 % of BMMNCs.

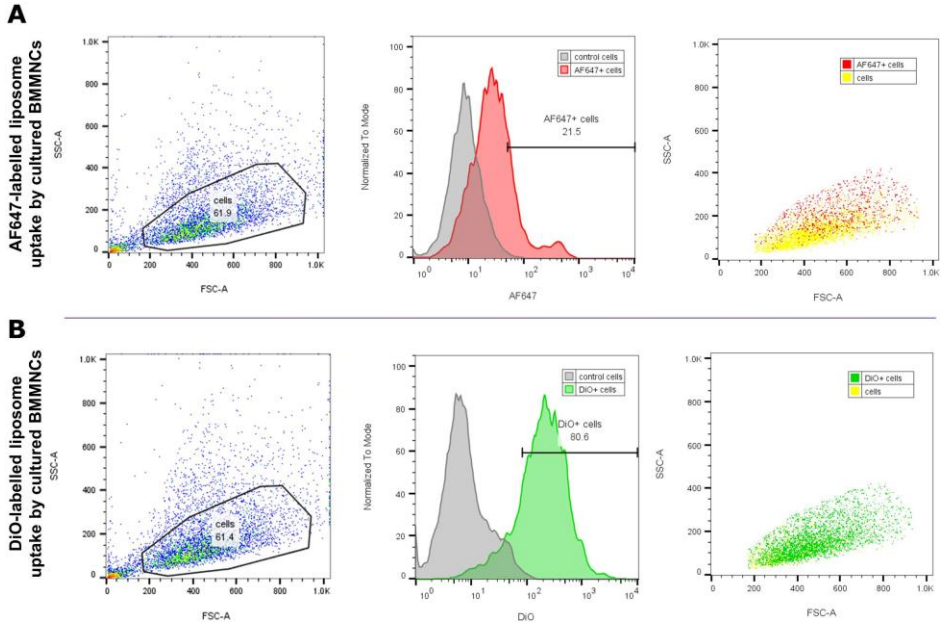

Figure 5.19 Uptake of AF647 or DiO labelled liposomes by cultured BMMNCs – flow cytometry.

Flow cytometry FSC *vs.* SSC dot plots (left) showing the examined populations, with representative histograms (centre), and subsequent overlays of positively stained cells on top of the entire population (right) for AF647 (A) and DiO (B) labelled DMPC/PEG liposomes. Cell were incubated with the liposomes for 3 hours, and all cells gated as positive showed a fluorescence intensity greater than that detected on 99% of the cells not incubated with the particles (grey histograms). 21.5 % and 80.6 % of BMMNCs stained with AF647- and DiO-labelled liposomes, respectively.

5.2.4.2 Uptake of liposomes by fresh BMMNC isolates

To test for representative uptake in primary cell populations likely to be present *in vivo* at injury sites, liposome uptake was next measured in fresh BMMNCs by flow cytometry and Image Stream (Figure 5.20 and Figure 5.21).

A small proportion of nanoparticles localised to cells with "monocytic/stromal" light scattering properties, which encompasses monocytes and skeletal/stromal stem/progenitor populations (see Chapter 3, Section 3.2.2.3). Nanoparticles labelled with AF647-streptavidin colocalised more selectively with these fractions than did the DiO-labelled nanoparticles, of which a high proportion was also visible within the granulocytic fraction, based on light scattering characteristics (Figure 5.20). Overall, only a small proportion of the entire BMMNC fraction was positive for these particles (5.81 % and 2.12 % for the AF647-streptavidin and DiO liposomes, respectively).

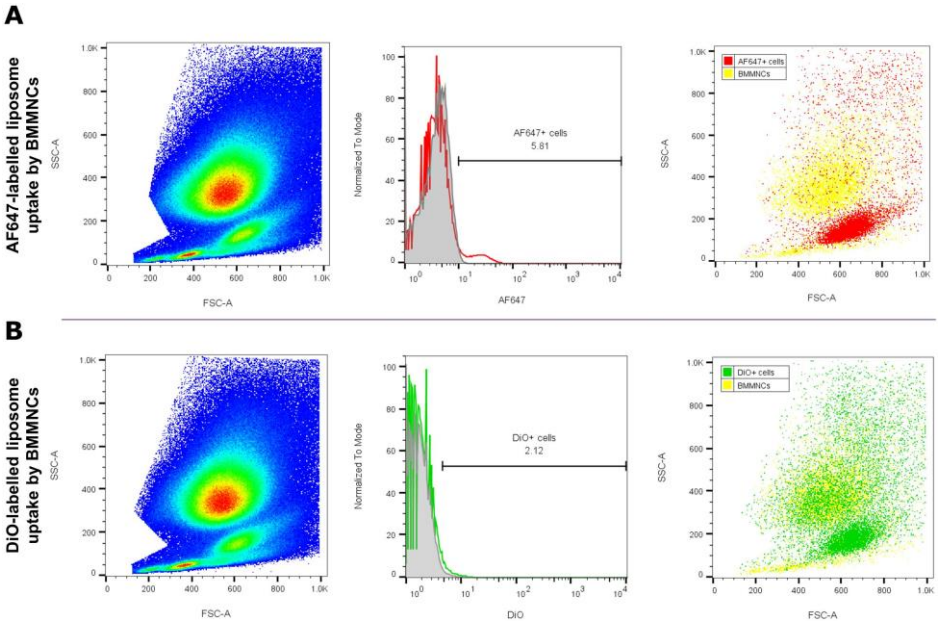

Figure 5.20 Uptake of AF647 or DiO labelled liposomes by fresh BMMNCs – flow cytometry.

Flow cytometry FSC *vs.* SSC dot plots (left) showing the examined populations, with representative histograms (centre), and subsequent overlays of positively stained cells on top of the entire population (right) for AF647 (A) and DiO (B) labelled DMPC/PEG liposomes. Cell were incubated with the liposomes for 3 hours, and all cells gated as positive showed a fluorescence intensity greater than that detected on 99 % of the cells not incubated with the particles (grey histograms). 5.81 % and 2.12 % of BMMNCs stained with AF647- and DiO-labelled liposomes, respectively, and most of the positive cells localised within the "monocytic/stromal" region, based on light scattering properties.

To determine whether the liposomes had an intracellular localisation, or were adhered to the cellular membrane, resulting in cell staining without liposome uptake, samples were examined using Image Stream flow cytometry. The results showed that the AF647-streptavidin liposomes localised predominantly on the cell surface of $CD14^+$ monocytes (Figure 5.21A). Unfortunately, the $STRO\text{-}1^+/GPA^-$, skeletal stem cell-containing fraction, could not be examined in this instance due to suboptimal staining cause by expired antibody. However, the DiO liposomes examined in both the monocytes and putative skeletal stem cell fractions showed uptake, with punctate intracellular localisation within these cell populations (Figure 5.21B and C).

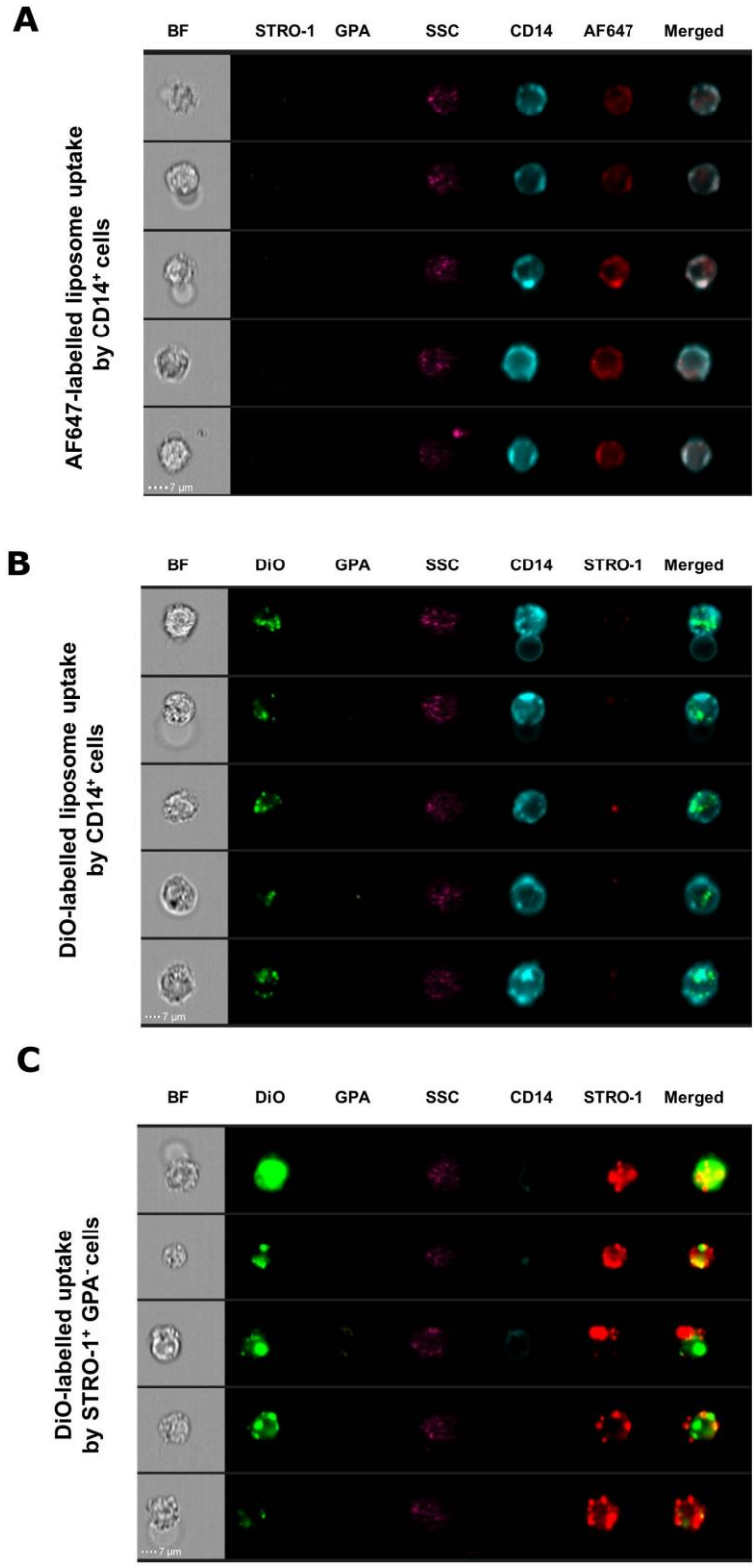

Figure 5.21 Uptake of AF647 or DiO labelled liposomes by fresh BMMNCs – Image Stream.

Freshly isolated BMMNCs were incubated with liposomes for 3 hours, prior to staining with CD14, STRO-1 and GPA antibodies. A and B show intracellular localisation of the particles within $CD14^+$ cells, whereas C shows their uptake by the $STRO\text{-}1^+/GPA^-$ population. BF, brightfield.

To try to define which cellular compartments they were likely occupying after uptake, the intracellular localisation of these DiO-labelled nanoparticles was further examined by confocal microscopy. Cultured BMMNCs were exposed to these liposomes for 1, 3 or 24 hours, fixed, and imaged after staining with endosomal or lysosomal markers (Figure 5.22). The results showed increased intracellular localisation of DiO liposomes with longer incubation periods. At the earlier time point, more cells presented with membrane staining, compared with later time points. Furthermore, there was no indication that these nanoparticles colocalised with any of the stained cellular compartments (endosomes or lysosomes). However, any interpretation of these initial results requires caution because, as previously mentioned, the liposomes needed to be accumulating in the same areas in order to be visible, due to detection limits of confocal microscopy (the resolution does not surpass ~200 nm). Therefore, it is possible that not all of the particles were detected.

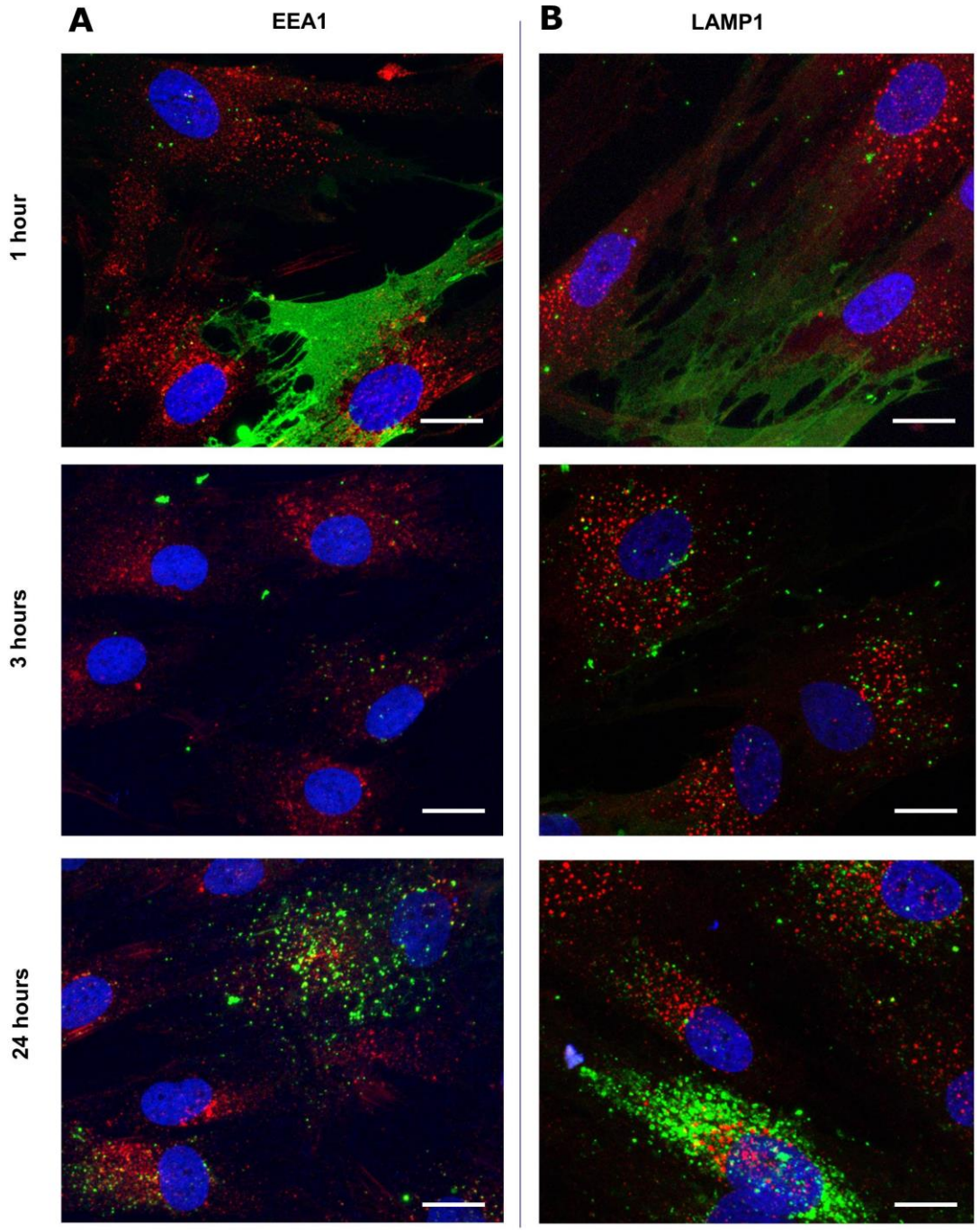

Figure 5.22 Confocal imaging of liposomes and the endosomal and lysosomal cellular compartments.

Confocal micrographs representing the cellular uptake by cultured BMMNCs of DiO-stained liposomes (green) over the course of 1, 3 and 24 hours. Cells were co-stained with DAPI (blue), and the endosomal marker EEA1 (red, A) or the lysosomal marker LAMP1 (red, B). Magnification 63x, scale bars = 20 μm.

5.2.4.3 Biodistribution of liposomes

Finally, because the nanoparticles were examined in relation to their potential use as a drug delivery method for bone fractures, preliminary data was acquired for their localisation and potential toxicity in an *in vivo* fracture model. For this purpose, nanoparticles were labelled with a near infra-red fluorescent dye, to enable transmission of excitation and emission light through mouse tissues. Femur drill defects were created in the left hind leg, and nanoparticles were injected systemically *via* the tail vein in 3 mice (one with unlabelled liposomes, two with DiR-labelled liposomes) within 30 minutes of the drilling procedure, and imaged immediately, and also after 24 and 48 hours (Figure 5.23). Liposomes preferentially localised at the bone defect site 24 and 48 hours after the fracture (see Appendix for additional ventral and contralateral views, Figure A.27). There was no apparent sign of toxicity, and the animals recovered as expected after the operation and injection procedures.

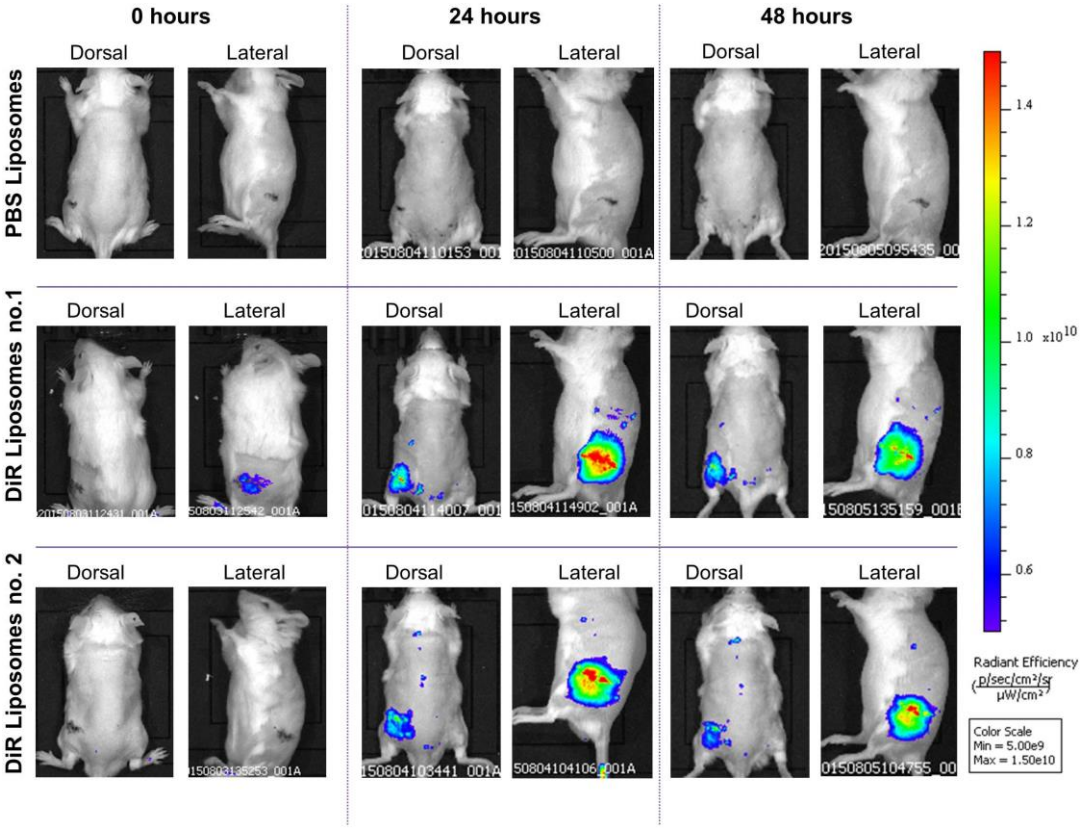

Figure 5.23 IVIS whole animal imaging of liposome localisation after systemic injection in a murine bone fracture model.

DiR-labelled DOPC/PEG liposome nanoparticles (not containing Wnt3A) were injected systemically *via* tail vein within 30 minutes of left femur drill defect formation. The fluorescent signal imaged at 24 and 48 hour time points localised in the bone fracture area.

Furthermore, for more accurate determination of the localisation of the particles within the fracture site, femurs were extracted after 48 hours and imaged (Figure 5.24A). Surprisingly, femurs from only one of the DiR liposome-receiving mice exhibited fluorescence, with a greater degree of the fluorescent signal localising at the drill defect spot. As femurs from the other mouse showed no degree of fluorescence, the fluorescence signal recorded during whole body imaging might have been attributable to the soft/muscle tissues surrounding the femur, as these bone were imaged stripped of these tissues. Moreover, individual organs, possible targets of nanoparticles due to degradation/excretion or toxic effects, were also imaged 48 hours post injection (Figure 5.24B). A substantial localisation in the liver and spleen of the animals was detected. These imaged organs were fixed for further toxicity analysis, although such work is beyond the scope of this thesis.

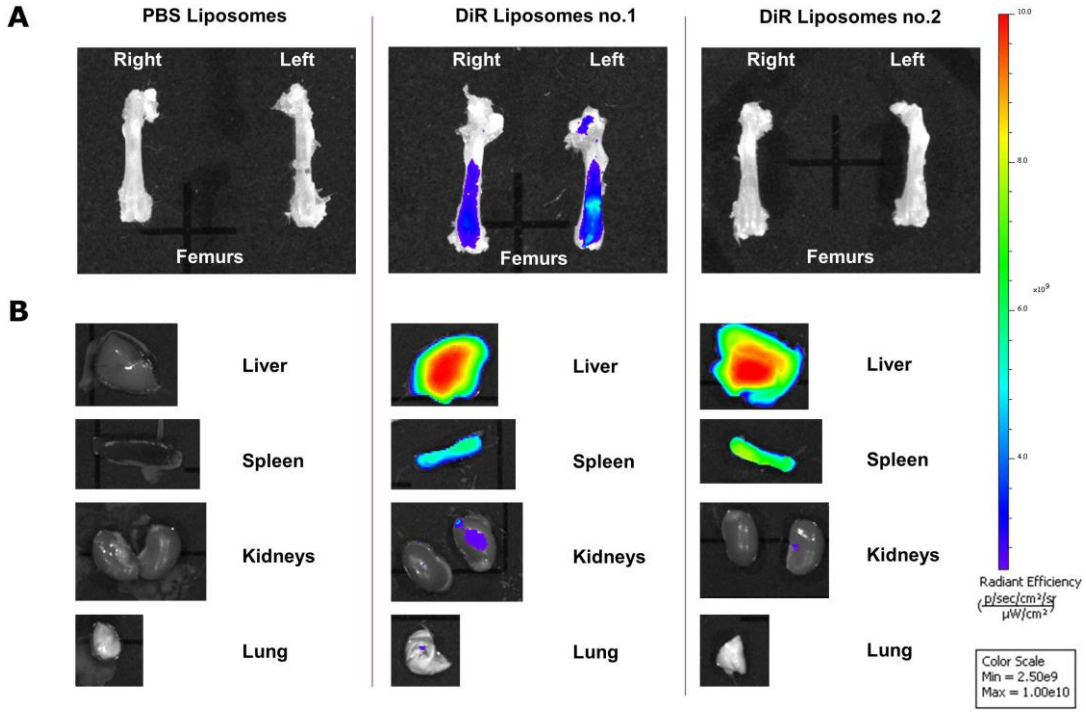

Figure 5.24 IVIS imaging of organs after 48 hours after systemic liposome injection in a murine bone fracture model.

DiR-labelled liposome nanoparticles were injected systemically *via* the tail vein within 30 minutes of left femur drill defect formation. 48 hours after the procedure, a fluorescent signal was detected in the organs of studied animals. A: Femurs were extracted and stripped of the surrounding soft tissues. A high degree of localisation in the femur drill defect (left leg), as well as in the opposite leg was recorded in 1 of the 2 mice receiving the labelled liposomes. B: A lobe of the liver, the spleen, kidneys and a lobe of a lung were extracted. Liposomes localised to a high degree to the liver and spleen. Exposure time was equivalent for all organs and was matching the exposure time used for whole animal imaging.

5.3 Discussion

As shown in Chapter 4, Wnt protein stimulation augments the frequency of stem cells in bone marrow and their subsequent differentiation to the osteoblastic lineage. Therefore Wnt protein could potentially be used for therapeutic purposes in bone fracture healing. To exert its beneficial effects, however, it needs to be delivered at the correct place and at the correct time. Nanoparticles, such as liposomes, are attractive delivery vesicles for hydrophobic agents, and therefore, the aim of this chapter was to assess their suitability as a delivery system for Wnt3A protein.

Various lipid compositions were investigated for the stability and size distribution of the resultant liposomes. Preparations of greatest interest included 5 molar % PEG, as this molecule acts as a stabilising agent for *in vivo* applications. For experiments involving the encapsulation of Wnt into liposomal membranes, DMPC (Tc = 23°C) and DOPC (Tc = -20°C) were chosen due to their low Tc. DMPC/PEG and DOPC/PEG lipids formed unilamellar liposomes averaging 100 nm in size, which were stable for 21 days. DMPC is a 14:0 carbon chain lipid which was previously shown to be the most promising in tested vesicle preparations (Morrell *et al.* 2008), sustaining the activity of the incorporated protein, and therefore served as a positive control for experiments. DOPC is an 18:1c9 lipid which, due to its unsaturated chain, has a very low Tc and remains in the liquid phase over the physiological temperature range. With larger spaces between lipid heads, it could potentially ease the incorporation of Wnt into the lipid bilayer. However, DOPC might also facilitate the leakage of the protein, hence the increased activity and protein content of stabilised PEGylated DOPC liposomes. Cholesterol was added to DMPC liposomes in order to decrease the Tc, increase the spaces between the lipid heads, and therefore theoretically facilitate the incorporation of Wnt protein. Surprisingly, this effect was not observed, and therefore cholesterol-containing preparations were not considered for Wnt delivery. In future experiments designed to further optimise the liposomal compositions, the use of lipids which increase the spaces between the lipid heads and also fusogenicity, such as DOPA, DOPE or DAG at 5 molar %, can be considered. The protocols for achieving high encapsulation efficiencies for chemically stable molecules often cannot be used with fragile molecules, such as proteins, and often lead

to a decrease in their functionality. It has been shown previously that, in addition to the parameters of the liposome formation protocol, the efficiency of protein encapsulation in the liposome depends on the interaction between the protein and phospholipid bilayer (Colletier *et al.* 2002). Therefore, the optimisation of lipid composition which promotes these interactions is crucial. Indeed, this might be the only tuneable parameter for liposomal Wnt preparation as other tuneable parameters, such as the film hydration and freeze-thaw cycles, which increase the encapsulation efficiency before the extrusion step, cannot be used for labile molecules such as Wnt3A.

It may be the case that larger spaces between the lipid heads accommodate the protein within the liposomal bilayer in a way which facilitates its release, as is the case with DOPC/PEG formulations, thus increasing the activity of these preparations. The way in which Wnt protein interacts with the lipid bilayer of the liposome is, however, unknown. It has been proposed that the lipid modification on Wnt proteins responsible for interactions with the receptor, Frizzled, might also be involved in docking Wnts to lipid bilayers during transport (Lorenowicz and Korswagen 2009). However, Drosophila WntD which lacks the posttranslational lipid modification is also transported by membranous vesicles, as it requires Rab1, a membrane tethering protein, for its secretion (Ching *et al.* 2008). Hence, palmitoylation of Wnts, required for their activity, might be involved in proper folding of these proteins, rather than for transport/membrane-docking purposes. Therefore, optimisation of the liposomal formulation may be important for interaction of the whole protein with the lipid bilayer, not the lipid anchor. This will likely affect the encapsulation efficiency of Wnt protein in the liposome particle and affect the drug to lipid ratio in final commercial compositions. The studies of Wnt protein interaction with the liposomes at a single molecule spectroscopy level confirmed association of the protein with these lipid particles, although there is a need for further optimisation to enable the study of the kinetics of this association. Such work could be performed with the use of TIRFM on adherent liposomal bilayers, as these would also allow for the study of maximal Wnt load which results in liposomal association, as opposed to TCCD which is limited to picomolar concentrations. However, for all single molecule spectroscopy studies, due to issues with insufficient Wnt3A protein tagging, production and use of a

recombinant protein with additional taggable amino acids would be advantageous. Furthermore, maximal purification to remove contaminating BSA protein would be recommended. BSA association with the liposomes was negligible; however, its content in Wnt3A preparations creates issues with defining the correct concentration for the study of the kinetics of protein association with different liposomal preparations.

Studies of liposome stability showed fusion with prolonged storage, alongside varying degrees of leakage of the Wnt protein from the Wnt-containing preparations. It has been noted previously, that liposomes dispersed in aqueous solutions generally exhibit physical and chemical instability after long-term storage, due to hydrolysis and oxidation of phospholipids (Chen *et al.* 2010). As this is a common phenomenon, all commercially available liposome-based drugs are sold as lyophilised products. This would therefore also need to be the case for liposome-loaded Wnts for therapeutic applications.

Flow cytometry, Image Stream and confocal microscopy analyses revealed that liposomes were internalised or interacted with target cells. When dual-labelled liposomes were used (carrying sodium fluorescein as cargo and a hydrophobic dye within their bilayer) different numbers of cells were positive in each case. This might be because of the sensitivity issue, as the flow cytometry machine used in this case was able to only excite and detect a fraction of DiI. Also, the transition of a lipophilic dye between liposomal and cell membranes independently of fusion or uptake cannot be excluded, so these results need to be interpreted with caution. Liposomes single-labelled with AF647, incorporating streptavidin on their surface, generally showed cell surface localisation, whereas DiO single-labelled particles were rapidly internalised, indicating that streptavidin protein prevents uptake of these nanoparticles, at least in the 3 hour time frame tested. Although the streptavidin-labelled liposomes were used here to test for possible uptake of liposomes with proteins tethered to the liposomal bilayer, such as in the case of Wnt protein, one must bear in mind that the streptavidin-biotin bond is of a different nature to that between Wnt and lipids within the liposomal bilayer. Therefore, it is better to think about these systems in terms of which cell populations are likely to interact with a hydrophobic dye- or protein-bearing

nanoparticle in the heterogeneous bone marrow environment, rather than as a definite indicator of whether the particles will or will not be internalised. In the case of Wnt, prolonged exposure of the cell surface to Wnt-carrying liposomes might be advantageous, because of the localisation of its receptor, Frizzled. Conversely, Wnt proteins have been shown to be rapidly endocytosed by clathrin-mediated processes. Interfering with these processes blocks Wnt signalling at the β-catenin level (Blitzer and Nusse 2006). Although the mechanisms of this are still poorly understood, Wnt signalling in similar studies has also been shown to be dependent on protein internalisation *in vivo* (Seto and Bellen 2006). However, this is in contrast to a recent study, where Wnt3A was chemically tethered to 2.8 μm beads (this size is generally unlikely to be internalised even by macropinocytosis), which have been shown to activate signalling at a single cell level in embryonic stem cells, without being internalised (Habib *et al.* 2013). Either way, the liposomal Wnt preparations studied in this thesis showed activity on a reporter cell line, and future studies should look into whether these preparations could induce Wnt pathway activation in populations of interest within fresh human BMMNCs. This could again be studied on Image Stream by analysing nuclear localisation of β-catenin in cells positive for nanoparticles carrying Wnts *vs.* unloaded nanoparticles, ideally using dual-labelled liposomes. However, the cell line data showed the highest response to nanoparticles 18 hours after their addition; hence the pathway activation in BMMNC suspension cultures should also be examined over longer incubation times. Although the initial Image Stream data confirmed nanoparticle localisation in skeletal stem cells after 3 hours of incubation, data from confocal microscopy showed increased uptake of these particles over longer time periods. This observation lends further weight to the suggestion of studying pathway activation in specific populations of BMMNCs over longer incubation periods. Such a time period could be extended up to 24 - 48 hours, since this corresponds to the time period for which liposomes were observed to persist *in vivo* in the murine bone fracture defect model, at least in one of the studied mice.

Confirming this *in vivo* observation, another very recent study on administered PEG-micelle nanoparticles has shown their preferential retention at the bone fracture site, and this phenomenon has been attributed to the presence of a haematoma and leaky vasculature (Jia *et al.* 2015). A clear next step would be to examine liposomal Wnt

preparations in the murine bone fracture model and their influence on bone regeneration. This would also involve studying the possible therapeutic benefits in animals with known difficulties in bone fracture healing, such as in aged mice or mice chronically exposed to glucocorticoids, as opposed to young animals. If a positive influence on bone fracture healing were to be noticed, a murine set of markers could be used to delineate which cell populations are most affected by this treatment at early time points (24 – 48 hours). This would include investigations into nestin^{+} cells, which contain all the CFU-F activity in mice (Mendez-Ferrer *et al.* 2010), either by Image Stream or histological analysis. Ideally, this type of study would, however, be carried out in a mouse reporter model for Wnt signalling, such as those expressing GFP or LacZ under the control of Axin2 (Jho *et al.* 2002, Lustig *et al.* 2002).

The *in vivo* study also confirmed nanoparticle localisation at the likely sites of their degradation and highly occupied by cells of the RES, such as the liver and spleen (Sou *et al.* 2011). In a therapeutic scenario for humans however, the nanoparticles would ideally be injected locally to the site of bone injury. Therefore, injection to the bone fracture site, or the fracture haematoma, and examination of nanoparticle retention, is another possibility to consider for further investigations in the animal model. This approach might also limit the exposure of other organs to nanoparticles; however any possible toxic effects still need to be verified by further histological examination. The clearance mechanisms of nanoparticle material by the endothelium of bone marrow sinusoids require more study (Moghimi 1995).

Future approaches, which aim to increase the retention of liposomes at the fracture site, may utilise some of the technologies used for delivery of therapeutics to the bone marrow in studies published so far. For example, active targeting of particles to the sinusoidal epithelia of the bone marrow might be the most promising approach to targeted deposition of delivery systems in the bone (Mann *et al.* 2011). It relies on the fact that E-selectin, a cell adhesion molecule expressed on the endothelial cells in response to inflammatory stimuli only, is constitutively expressed in the bone marrow. ESTA aptamers have been developed, that bind E-selectin with high affinity and selectivity *in vitro* and *in vivo*, and when conjugated to porous silicon particles, increased their biodistribution to the bone marrow. Other studies have evaluated the use of

bone-binding molecules, such as bisphosphonic acid moieties, targeting hydroxyapatite (Hengst *et al.* 2007). Lipid particles tethered with $(AspSerSer)_6$, for interaction with calcium-rich bone surfaces, showed selectivity for bone forming surfaces, as opposed to sites of bone resorption, which could be useful in early phases of bone fracture healing (Zhang et al. 2012). These liposomes, even in untargeted formulation, localised preferentially to bone, liver and kidney. However the targeting moiety, as expected, dramatically increased bone retention and decreased localisation to liver and kidney. Accumulation of liposomes in bone marrow, without the use of specific targeting, has been previously suggested, as the bone marrow macrophages supposedly have a role in the delivery of lipids to the bone marrow (Sou *et al.* 2011). Succinic acid dihexadecyl ester lipid-based particles have also been show to lead to rapid phagocytosis by the bone marrow macrophages. However, the liposomes in these studies were negatively charged, and the biodistribution of liposomes to the bone was species specific and in fact lower in rodents than in primates (Sou 2012). Also, low doses of liposomes have been shown to preferentially localise to bone marrow, whereas high doses presented with no such specificity and bone marrow, liver and spleen localisation was observed, due to saturation of phagocytic cells. These observations underline the importance of studying nanoparticle distribution in multiple animal species. In addition, several studies have shown that reduction in size of the nanoparticles improved passive as well as active targeting to the bone marrow (Harris *et al.* 2010, Porter *et al.* 1992, Schettini *et al.* 2006). Recently, multiple preliminary studies have investigated the use of magnetic iron oxide particles, conjugated with growth factors (BMP2), bisphosphonates or coated with calcium phosphate and a bioactive peptide (YRGDSPC) and showed significant increases in osteoblast proliferation (Balasundaram and Webster 2007, Pareta *et al.* 2008). Moreover, use of a 100 nm magnet implanted upon surgery aided the localisation of magnetic liposomes encapsulating BMP2 in a rat segmental bone defects (Matsuo *et al.* 2003). Discovery of receptors or bone specific molecules expressed in the bone marrow tissue would facilitate the development of novel drug carriers targeting bone marrow in the future.

Various therapeutics are under investigation for modulating the Wnt signalling pathway (Rudge and Dale 2014). However, there are several advantages to the use of protein therapeutics over small-molecule drugs (Leader *et al.* 2008). Proteins often

serve a highly specific and complex set of functions that cannot be mimicked by simple chemical compounds, and because the action of proteins is highly specific, there is often less potential for protein therapeutics to cause adverse side-effects. Whereas nanoparticles can be used for delivery of proteins intracellularly (Shah *et al.* 2011), and in that way induce pathway activation, the use of proteins acting specifically on surface receptors is beneficial. In the case of Wnt protein, its action upon the surface Frizzled receptor leads to specific pathway activation, as opposed to small molecule GSK3 inhibitors, which can interfere with other pathways, in which this enzyme is involved, or elicit non-specific effects. For example, although BIO is highly specific for GSK3β (Meijer et al. 2003), the parent molecule, indirubin monooxime has been shown to inhibit cyclin dependent kinases at high concentrations (Damiens et al. 2001). High doses of BIO have been shown to lead to cell cycle arrest similar to that of heavily contact-inhibited cells, arresting mitosis (Krause et al. 2010). As Wnt3A is a protein naturally produced in the body, its use offers an advantage over antibodies modulating the Wnt pathway, which can elicit unwanted immune responses. Therefore liposomal Wnt therapeutics merit further study.

5.4 Conclusion

The aim of the research presented in this chapter was to assess the suitability of PEGylated liposome formulations for Wnt3A protein delivery to SSCs *in vitro* and to the bone fracture site *in vivo*.

The main findings showed that:

- Wnt3A protein is active in several different PEGylated liposome formulations;
- liposomes are rapidly taken up by SSC cultures *in vitro* as well as by SSCs within the fresh, heterogeneous bone marrow populations;
- liposomes localise at the bone fracture site 24 and 48 hours after systemic injection in a murine model of bone injury.

Therefore PEGylated liposomes are an attractive delivery method for Wnt3A protein to the bone fracture site. As a therapeutic, it has the potential to positively influence bone fracture healing. However, further research needs to address the safety and efficacy of such an approach.

Chapter 6

Discussion and Future Directions for Research

6.1 Discussion

6.1.1 Achievements of the study

The main aim of this thesis was to determine the effect of Wnt stimulation on the osteogenic response of populations of cells in human bone marrow and to establish a technology for the delivery of active Wnt proteins selectively at the bone fracture site. This project is part of a longer-term strategy to develop novel therapeutics which can be administered systemically to stimulate, augment or expedite fracture healing and to address the burgeoning, debilitating and expensive problem of bone fracture morbidity. In doing so, the project tested the hypotheses that temporal control of Wnt stimulation promotes osteogenesis in human SSCs, that Wnt proteins associate with liposomes and retain their activity, and finally that this technology could be used for spatiotemporal delivery of Wnts (and other therapeutics) in fracture healing.

This thesis achieved these aims by:

- the development of flow cytometric methods and *ex vivo* cultivation protocols to study the effects of Wnt stimulation on human marrow samples;
- the demonstration that timing of Wnt stimulation is critical in the potency of this signalling pathway in promoting osteogenesis in SSCs;
- the development of Wnt tagging protocols and utilisation of single molecule spectroscopy (TIRFM and TCCD) to study protein-liposome association;
- the optimisation of liposome formulation for maintaining Wnt activity for delivery to SSCs *in vitro* and to the fracture site *in vivo*.

6.1.2 Summary of main findings

The main findings of this study in relation to the aims and hypotheses of the thesis are summarised as follows:

- transient (24 hour) activation of the Wnt signalling pathway in human BMMNCs cultivated *ex vivo* in suspension culture results in (a) an increase in the frequency of cells expressing known stem cell markers and (b) an increase in their subsequent differentiation to the osteoblastic lineage;

- sustained (14 day) Wnt stimulation dramatically inhibits both early and late osteogenesis in these same cells;
- Wnt protein was shown to associate with liposomes and retain its activity in the PEGylated liposomal formulations;
- 3 hour incubation of nanoparticles with fresh BMMNC isolates resulted in liposome uptake by SSC-enriched populations and also by monocytes;
- 24 and 48 hours after systemic administration in a murine bone fracture model, liposomes preferentially localised to the bone fracture site.

In Chapter 3, FACS and Image Stream cytometry protocols were developed as tools to assess the different cell populations present in human bone samples. Staining panels based on recognised SSC markers were designed to specifically analyse the skeletal stem cell population within fresh bone marrow isolates. Co-staining with a negative selection marker, GPA, in STRO-1-enriched fresh bone marrow isolates allowed further enrichment of samples for SSCs. Moreover, mononuclear cell populations with the highest expression of the STRO-1 antigen had intrinsically elevated levels of Wnt signalling, suggesting that they likely contain SSCs.

In Chapter 4, it was found that bone marrow cell populations identified in Chapter 3 with high intrinsic Wnt signalling, and marked by the expression of a putative skeletal stem cell marker, STRO-1, were responsive to external Wnt stimulation, showing marked increases in the expression of genetic markers of the Wnt signalling pathway following stimulation. Transient stimulation promoted the expansion of cells expressing the STRO-1^+ marker by increasing their proliferation and protecting them from cell death. It also primed stem cells within the bone marrow towards an osteogenic fate, increasing the frequency of CFU-Os. Moreover, transient Wnt signalling induction by Wnt3A enhanced early and late osteogenic differentiation of bone marrow isolates. However, in striking contrast to these effects, sustained Wnt stimulation completely abrogated osteodifferentiation. These studies demonstrate that the timing of Wnt3A stimulation is critical in its osteogenic effects and illustrate that the use of Wnt-stimulating drugs in bone fracture healing must take into account such temporal patterns of responsiveness.

In Chapter 5, it was found that liposomes of defined size could be fabricated by hydration and extrusion of various lipids in aqueous solution. These liposomes retained their size over prolonged periods of time. By testing the incorporation of Wnt3A protein at different stages of the fabrication of liposomes, it was found that liposomes could be produced with high levels of Wnt incorporation by adding the protein after extrusion. In doing so, this study showed that various PEGylated lipids could be used to make active liposomes, where previously in the literature only the use of a single unPEGylated lipid has been successful. The association of protein with the liposomes was thoroughly tested using a number of techniques, in particular TCCD and TIRFM. These single molecule spectroscopy techniques have never been used previously to assess protein/liposomal interactions for drug delivery purposes. Moreover, liposome uptake by fresh and adherent BMMNCs was studied by FACS, Image Stream cytometry and confocal microscopy, over the time course of 1 – 24 hours. The liposomes were readily taken up by cell populations of interest, such as SSCs and monocytes, and studies evaluating nanoparticle uptake by fresh bone marrow populations using Image Stream cytometry are novel for bone marrow-targeted nanotherapeutics. In addition, preliminary findings from the small animal study of bone injury indicated that liposomes localised at the bone fracture site 24 and 48 hours after systemic injection. After analysing the fractured femurs *ex vivo*, liposomes were visible in the bone drill defect. These studies demonstrate that Wnt3A protein can be incorporated into the liposomal preparations while still retaining its activity. Liposomes can target tissue at the fracture site and thus liposomal Wnt formulations have the potential to enhance bone regeneration.

6.1.3 A discussion of the main findings and their context

The work which constitutes this thesis contributes to the field of regenerative medicine of the bone in a number of ways. Most importantly, it furthers knowledge of the effects of Wnt signalling on SSCs of the human bone marrow. The finding that Wnt increases the osteoprogenitor populations within the bone marrow and enhances their osteogenic differentiation, but only when the stimulation of the Wnt signalling pathway is transient, has clinical implications. A pictorial summary of the findings, how they relate to what is known about bone fracture healing, and potential

applications of liposomal Wnt therapeutics is shown in Figure 6.1. The disparate roles of Wnts in different phases of fracture healing have been postulated before and should be considered in the future development of therapeutic strategies (Xu *et al.* 2014). The results presented in this thesis suggest that a short, transient Wnt stimulus in the initial phase of bone fracture healing may be beneficial, and a decrease in Wnt signalling following the initial stimulus is necessary for osteodifferentiation to occur. This is supported by other work, where constitutive activation of the pathway caused a delay in bone regeneration as cells were maintained in a proliferative state and their differentiation was abrogated (Kim *et al.* 2007). Evidence from other studies also indicates that increased Wnt signalling during later stages of fracture healing could be useful in bone remodelling. For example, increased Lrp5 expression persists throughout the later stages of osteoblastic differentiation, suggesting its role as a receptor during terminal differentiation (Gong *et al.* 2001) and dramatically enhanced bone healing occurs in mice expressing a stabilised form of β-catenin, but only when restricted to osteoblasts (Chen *et al.* 2007). Therefore, a double injection approach, in the initial inflammatory and later remodelling stages of fracture healing, might be considered for a time-controlled delivery of bone-targeted Wnt inducing therapeutics. An additional injection of Wnt signalling inhibitors during the repair phase of healing might be another attractive possibility. Interestingly, a similar requirement for time-controlled Wnt delivery has been implicated in the regeneration of other tissues, with skin being one example where increased β-catenin activity during the proliferative phase has been shown to be crucial for successful wound repair. However the prolonged activity of β-catenin beyond the normal time frame of healing contributes to excessive fibrosis and scar formation (Sato 2006).

In addition, as a novel approach, in the present work fresh bone marrow isolates were studied which were sourced from patients who would likely be the recipients of the therapy under investigation. Moreover, the effects of Wnt signalling were investigated in the presence of haematopoietic cell lineages, which is advantageous since bone homeostasis has been shown to be greatly affected by immune cells (Kolar *et al.* 2010).

In this study an exogenous, purified protein was used to stimulate Wnt signalling, as opposed to conditioned media or as a result of cell transfection or transduction. The

weaknesses of the latter approaches are discussed in Section 4.1, but to summarise, these techniques can result in non-specific effects, or over-activation of the pathway far beyond endogenous levels. In this study, purified protein was used, which circumvents many of these problems. The approach presented in this thesis ultimately has more relevance to clinical studies.

Drugs including bisphosphonates, PTH and denosumab (discussed in Section 1.2.2) are used widely in the clinic to augment bone mass and prevent fracture in osteoporosis, but their efficacy in fracture healing is unclear (Goldhahn *et al.* 2012). For example, the anti-resorptive bisphosphonates are efficacious only in reduction of vertebral fractures, due to higher content of cortical *vs.* trabecular bone and therefore even a small decrease in resorption makes a difference. For non-vertebral long bone defects, anabolic therapies are better suited due to the greater content of trabecular bone. Furthermore, while systemically administered PTH might have its therapeutic window during most stages of fracture healing, it is more likely to accelerate normal fracture healing in healthy individuals than to prevent non-unions in difficult cases. Wnts offer an advantage over PTH as they possess the potential to influence the first stages of fracture healing by increasing proliferation and osteogenic differentiation of SSCs homing to the fracture haematoma. PTH lacks this role and it mainly increases the longevity of osteoblasts (Aspenberg 2013). In addition, it is the quality of SSCs (measured by their potential to differentiate) that is influenced by Wnts, rather than the number of SSCs, that is crucial for successful fracture healing, as concentration of poor quality SSCs fails to prevent non-unions (Hernigou *et al.* 2005).

Clinical trials on the SOST Ab, Romosozumab, have shown that it induced both bone formation and reduced bone resorption (the mechanism of this uncoupling is unknown), which would hugely benefit osteoporotic patients by affecting bone remodelling. However, clinical trials on Romosozumab on fracture healing have been suspended after Phase II (ClinicalTrials.gov identifier: NCT01081678), for reasons that are unclear. One speculative reason might be low efficacy of the treatment, as it has been shown that the very rapid bone formation slows down after administering multiple doses of the antibody. As mentioned before, during fracture healing Wnt signalling decreases during the intermediate phases of osteogenic differentiation and

artificial overstimulation can be detrimental to the fracture healing (Kim *et al.* 2007). The cell types or combinations of cell types affected by SOST Abs are as yet unknown – their identification will be key to understanding SOST Abs' mechanism of action. For example, a recent study showed that the fractures in SOST-KO mice healed to the same extent as in the wild-type mice, only faster. This observation is very similar to those observed following the administration of PTH (Kakar *et al.* 2007). This may indicate that SOST Ab might predominantly affect osteoblasts, rather than SSCs. Furthermore, although the SOST Ab is humanised, some patients developed neutralising antibodies against it, which might limit the efficacy of the therapy after continuous dosing. Concerns with safety on cardiovascular health have also been raised, as high levels of SOST have been reported for calcifying vascular tissues, where it might exert anti-mineralization effects (Brandenburg *et al.* 2013, Zhu *et al.* 2011), raising the issue of non-bone-related side effects.

Nanomaterials, such as nanostructured particles and scaffolds, have been widely studied for treatment of bone diseases and for bone regeneration. Bone-targeted delivery of nanoparticles may increase the efficacy of treatment, lowering its side effects and reducing the dose of drug required (Gu *et al.* 2013). Materials with high affinity to bone, such as particles with tethered bisphosphonates or repeated aspartate sequences for interaction with the mineralised tissue have been used to better localise drugs to bone for anti-cancer or anti-osteoporotic treatment (Luhmann *et al.* 2012, Swami *et al.* 2014). However, the use of nanoparticles for bone fracture healing is still in its infancy.

Due to the advantages of spatiotemporal delivery of Wnt modulators, this work focused on a liposome delivery system for Wnt3A to the bone fracture site. The findings confirmed that liposomal encapsulation enhances Wnt activity and that the protein does indeed associate with the nanoparticles. Crucially, however, it showed for the first time, that the protein is also active in PEGylated formulations of liposomes. This has great implications with regards to its delivery as a therapeutic *in vivo*, as "stealth" formulations offer significant advantages in delivery of therapeutics (Klibanov *et al.* 1990).
In addition, liposomes are rapidly taken up by cells in fresh bone marrow isolates, not only by monocytes but also by putative SSCs. Most importantly, the finding that

liposomes localise at the bone fracture site after systemic injection and persist in the injury area, underlines the suitability of 100 nm PEGylated liposomes as delivery vesicles for therapeutics enhancing the healing of bone fractures. This has implications for other studies beyond those investigated in this thesis. For example, liposomal formulations may be a useful delivery method for antibiotics in high-energy trauma leading to open fractures, which are particularly susceptible to infections and often require additional surgical procedures to clean out the infection and allow for placement of special drains to remove pus (Zalavras and Patzakis 2003). Infections in orthopaedic and reconstructive surgery can be devastating and very difficult to treat, and are associated with significant morbidity and poor functional outcomes (Haddad *et al.* 2000). Therefore, localising therapeutics at the fracture site after systemic administration could offer potential advantages over locally administered antibiotics. As the fluorescent tag on the particles was also visible, although to a lower extent, in the non-fractured femur, liposomes of the studied formulation may represent a potential delivery vesicle for localisation in bone marrow in general (see Section 5.3), for example for diagnostics or for treatment of bone metastasis. Bone-targeted delivery of drug-loaded nanoparticles is a rapidly growing field for the treatment of cancer, as bone metastases are a huge clinical burden (Mundy 2002).

In summary, liposomes, although nano-sized, have a gigantic potential. They are suitable for a variety of biological applications, from acting as carriers of Wnts for regenerative medicine purposes, to delivery of diagnostic tools or antibiotics specifically to the bone, and as cytotoxic drug carriers for bone cancer. Therefore, 40 years since their discovery, they are still highly attractive molecules to study in biomedical research.

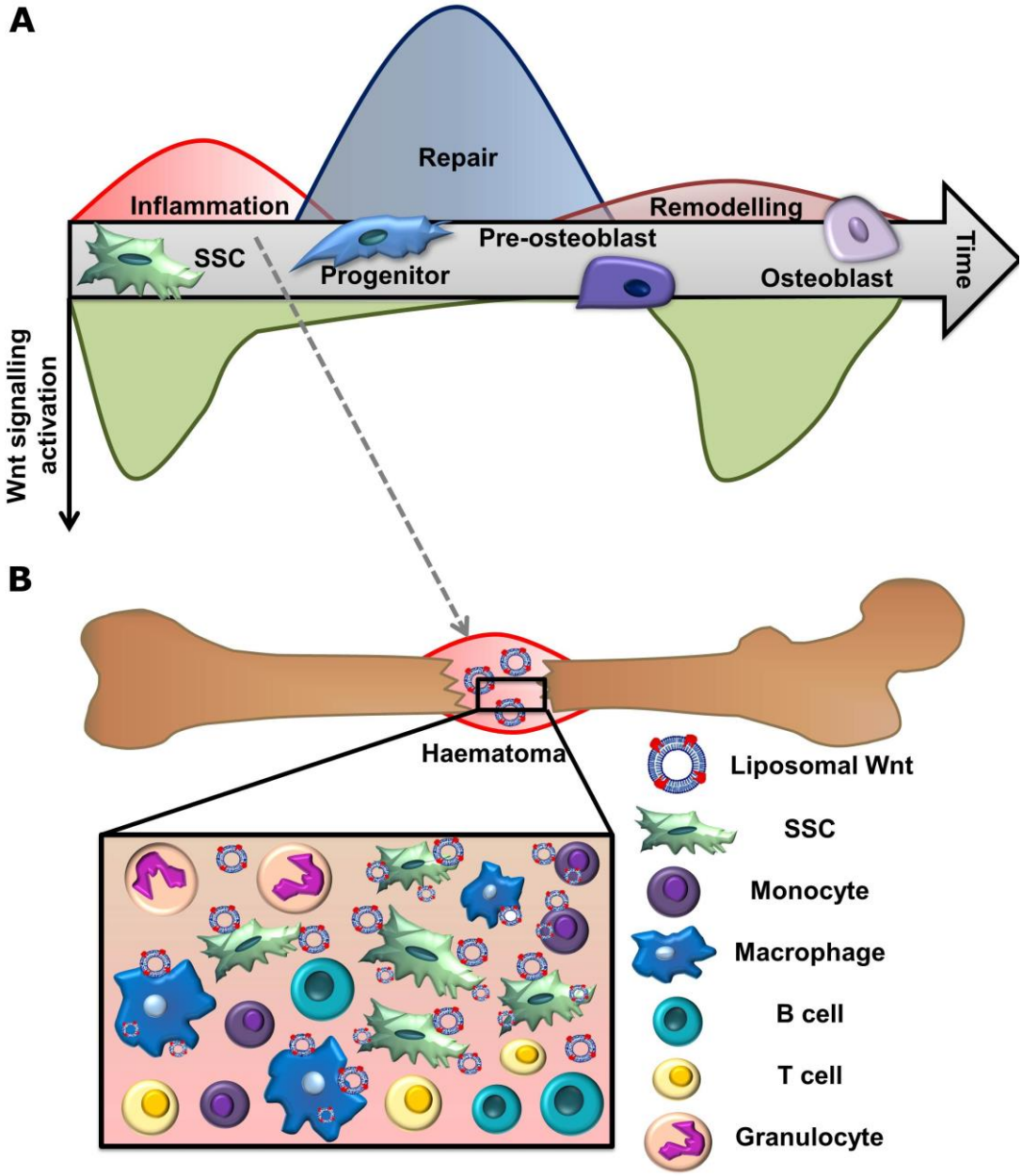

Figure 6.1 Suggested effects of Wnt signalling within the bone marrow niche in tissue homeostasis and following a bone fracture.

A: Phases of bone fracture healing (inflammation, repair and remodelling), osteogenic differentiation of SSC and Wnt signalling pathway activation at these different stages of healing and osteogenic commitment. Wnt signalling is crucial for appropriate healing of bone fractures, especially in the initial inflammatory phase as well as in the remodelling phase. B: Targeting the inflammatory phase of bone fracture healing with liposomal Wnt may enhance the healing process. Various cell types are present in the haematoma; liposomes are taken up SSCs as well as by phagocytic cells. SSC, skeletal stem cell. Based on own findings and: (Baron and Kneissel 2013, Einhorn and Gerstenfeld 2015, Kawai *et al.* 2011)

6.1.4 Limitations of the study

A major advantage of the study was the use of fresh, human bone marrow samples from patients undergoing hip replacement surgery. However, this also brought some limitations. The marrow samples were isolated by a number of different surgeons in Southampton General Hospital and so it was not possible to accurately control the isolation techniques. In addition, aside from sex differences, the patients vary considerably in factors such as their age, medication status, weight and height. As a result, marrow samples varied considerably in their volume and marrow *vs.* fat/bone content, making it very difficult to compare between some of the results. To try and overcome this limitation, a large number of samples were incorporated in our experimental results (for example, 11 donors in the STRO-1 expression experiments described in Chapter 4, Section 4.2.3.1) but nevertheless the standard deviations were usually very high. Despite this limitation, statistically significant, valuable results about the efficacy of Wnt in promoting skeletal stem cell expansion were obtained (Chapters 3 and 4).

The use of a protein as a therapeutic may be seen as a weakness in the study, as the number of potential protein therapies that have failed outnumbers those which have been successful (Leader *et al.* 2008). This is due to the challenges facing protein therapeutics during their development and use, which include stability, solubility, route of administration and distribution, as their half-life *in vivo* is affected by enzymes and clearance mechanisms. Moreover, the cost of developing protein therapies is high. In addition, large-scale production and storage systems may present several issues which are not experienced during the production of the protein therapeutic for animal testing or clinical trials. For instance, stability of the protein, its folding and tendency to aggregate may all be affected by mass production. Furthermore, the approach using a protein to activate the Wnt signalling pathway is highly dependent on the level of the Frizzled receptor on the target cell surface. The *in vivo* level of Frizzled receptors on SSCs in the human bone marrow at the bone fracture site has yet to be assessed. However, in an animal model, the overall gene expression at the femoral fracture site indicates a significant upregulation of the Frizzled receptor (Hadjiargyrou *et al.* 2002). Despite these limitations, there is a precedent for the use of protein therapeutics in humans. For example, insulin is one of the most successful drugs of the 20th Century

and is used by many millions of patients (Berenson *et al.* 2011). In addition, monoclonal antibodies are used successfully for a range of conditions, including cancer and chronic autoimmune diseases (Chames *et al.* 2009), and growth factors, like Wnt, are indicated clinically for conditions as diverse as skin wound healing, bone repair and myocardial infarction (Whyte *et al.* 2012).

This study focused on the use of Wnt3A ligand, as this was the first Wnt protein to be purified (Willert *et al.* 2003) and in fact the first human Wnt commercially available at the time of starting this research. Some animal studies have shown that this ligand is broadly expressed at the bone injury site (Kim *et al.* 2007), and shows greatest downregulation upon aging. Although brief *ex vivo* incubation of grafts from aged animals with liposomal Wnt3A re-established their osteogenic competence (Jing *et al.* 2015, Leucht *et al.* 2013), a different Wnt ligand may be a more potent alternative for specific regulation of skeletal stem cells. Indeed, several animal studies have suggested Wnt10b as regulator of bone formation that acts specifically on skeletal precursors (Cawthorn *et al.* 2012, Stevens *et al.* 2010). Overall however, the involvement of various Wnt ligands in human bone fracture healing is not yet well known and requires further examination in order to determine the most therapeutically potent Wnt ligand(s).

Another potential limitation is that Wnt ligands are ubiquitously expressed within all tissues, and can exert their effects not only on normal cells but also neoplastic cells. Although aberrant Wnt signalling leading to carcinogenesis is mainly caused by mutations, rather than being induced exogenously (Clevers and Nusse 2012), there are reports which have shown that Wnt ligands are up-regulated in some cancers, and that their expression often correlates with aggressiveness and metastasis, such as in the case of prostate cancer (Valkenburg *et al.* 2011). For these reasons, it is likely that ultimately any Wnt ligands will be administered in the recognition of contraindications, for example early-stage cancer or high cancer risk. It is important to note that several monoclonal antibodies, that agonise Wnt signalling, such as Romosozumab, have passed phase I safety trials and are now in phase III. In addition, the study presented here provides an extra layer of control in Wnt delivery: by ensuring spatiotemporal

delivery of Wnt proteins, the site of action of the drug can be controlled to a greater degree.

Additionally, the current study did not investigate the potential toxic effects of systemic liposome delivery. The use of nanotechnology in medicine, and more specifically in drug delivery, is advancing rapidly, but the short- and long-term toxicity of nanoparticles is an understudied issue (De Jong and Borm 2008). Despite this, it is encouraging that the "nanotechnology" of liposomes has been employed successfully in the cancer therapeutic field for ~30 years (Torchilin 2014). In addition, the efficacy of liposomal Wnt delivery in bone fracture healing was not investigated due to time limitations. These issues will need addressing in future studies.

6.2 Indications for further experiments and future directions for research

While this research provided evidence for the possibility of using Wnts to fine tune SSC lineage commitment and osteogenic differentiation for bone regeneration purposes, the effects of Wnt on other differentiation pathways of SSCs, such as adipogenesis and chondrogenesis, also merit investigation. Interestingly, although Wnt signalling activation has been shown to supress chondrogenesis in the majority of the studies (Chun *et al.* 2008), it has also been indicated that a low level of Wnt signalling can favour chondrogenic differentiation over osteogenesis (Day *et al.* 2005). Taking into consideration the involvement of chondrocytes in bone fracture healing, as well as the need to develop therapeutics for bone fractures which also cause cartilage defects, the potential effects of Wnt on SSCs and on chondrocytes merit further study.

Furthermore, it is unclear whether the results on SSCs obtained after Wnt stimulation are due to direct effects on the SSC population, or indirect effects through another cell population. Provided that larger volumes of the bone marrow samples could be obtained, it might be possible to isolate "higher purity" populations of SSCs by FACS, using a combination of CD106, CD146 and STRO-1 selection markers (Bakopoulou *et al.* 2013, Gronthos *et al.* 2003), followed by exposure to Wnt. Incubation of these cells with Wnt and study of their behaviour in the presence or absence of other bone marrow populations may aid understanding of the specificity of Wnt stimulus by determining which population is truly susceptible to changes in Wnt signalling levels.

However, as the current study noted beneficial effects of transient Wnt stimulation and at the same time could not exclude the nonspecific effects of Wnt3A on other bone marrow stem cell populations, it may be sensible to direct therapeutic Wnts to the bone marrow niche, without the requirement for them to be targeted to specific stem cell populations.

As discussed in Section 5.3, several studies have addressed the issue of bone marrow-specific targeting of particles, and there have been diverse approaches to increase their retention in the bone marrow at the fracture site. These studies may serve as guidance when designing novel Wnt nanocarriers.

Further work is required to establish a truly spatiotemporal liposomal release system within the bone marrow. Whereas liposomes were shown in this study to deliver therapeutics within the bone marrow niche, and more specifically at the bone fracture site, further work is necessary to determine whether Wnt proteins retain their activity at the target site. Also, further studies are needed to assess the efficacy of liposomal Wnts in bone fracture healing. Although it has been postulated that the native Wnt protein denatures within minutes at 37°C, and that the liposomal formulation extends its stability (Dhamdhere *et al.* 2014), a rapid release of Wnt from liposomes at the fracture site and its quick serum clearance would be undesirable. A reporter mouse study of the myxovirus resistance-1 (Mx1) promoter has been shown to label osteolineage-restricted stem/progenitor population, and suggested that this population has been fully responsible for bone regeneration at the fracture site (Park *et al.* 2012). Interestingly, these osteogenic progenitors have been shown to appear at the site of injury 2 days after injury and proliferate, with the cells close to the fracture site differentiating into functional osteoblasts. Thus, the release of the protein *in vivo,* with the potential of extending its activity for 48 hours to affect the osteogenic progenitors, should be subject to future study.

It is still not known whether Wnt liposomes will be effective in fracture healing. To test this, the small animal study reported in this thesis could be extended to determine the efficacy of the administered liposomes during fracture healing. The timing of injection could be varied, and the bone fracture healing rate could be measured *in vivo* by μCT over a time course of 3 weeks. This would allow for determination of the ideal

therapeutic window for liposomal Wnt administration. As the liposomes are labelled with fluorescent dyes, the bone fracture site, as well as the organs responsible for liposome degradation, could be histologically studied. A longer animal study would also allow for the assessment of the toxic effects of these nanoparticles, and could include histopathological studies of the organs and their weight, as well as testing the blood of the animals for elevated cytokine levels (such as IL-6 and TNFα) by ELISA (Knudsen *et al.* 2015). In addition, the uptake and effects of the nanoparticles in specific bone marrow populations after a systemic injection could be studied by Image Stream cytometry. Identification of fluorescently labelled nanoparticles in haematopoietic lineage and SSC populations, with additional identification of cells with active β-catenin, would aid understanding of which of the populations are targeted by the nanoparticles and which are targeted by Wnt stimulation, as well as providing quantitative measurements of nanoparticle uptake.

Furthermore, recent developments in 4D *in vivo* imaging of the bone marrow niche can be used to better assess the liposome delivery system. This technology would enable real-time monitoring after nanoparticle injection in a murine or rat bone fracture model (Lo Celso *et al.* 2011). The interaction of populations of SSCs, stromal cells and other niche components, such as osteoblasts, collagen or vasculature could be studied, although this would require the use of appropriate reporter mice.

To address possible issues with rapid Wnt release, and considering that the injection of therapeutic Wnt formulations for the application in human fractures would be local, rather than systemic, investigations into localising "depot" sources of liposomes may be sound. For this purpose, lipogels or hydrogel-embedded liposomes could potentially be tested (Alinaghi *et al.* 2014, Jensen *et al.* 2013).

Furthermore, investigation of the use of other biodegradable particle types would be interesting, especially if they could localise to the bone marrow and induce Wnt signalling specifically at the receptor level. Recently, the peptide UM206(S-S), derived from the primary sequence of Wnt3 (Patent number: EP 2226080 A1), has been shown to induce Wnt signalling when covalently bound to magnetic particles (Rotherham *et al.* 2015), acting on the Frizzled receptor. A similar technology could be used to attach this peptide to smaller nanoparticles, of 100 nm size (as opposed to 250

nm), made from more biocompatible materials, such as polymers. This could ensure delivery of more stable particles and inducers of Wnt signalling pathway, without compromising their specificity.

6.3 Concluding remarks

No previous study has addressed how Wnt proteins affect the proliferation and differentiation of human skeletal stem cells, identified by known surface markers. This study provides evidence to suggest that a temporal activation leads to a large increase in osteogenesis. In addition, before a therapeutic can be developed, a stable nanoparticle incorporation technique is needed. In this study it has been shown that a number of "stealth" liposomal formulations retain Wnt activity *in vitro* and may be used in the future as delivery agents. Finally, the studies reported in this thesis show that liposomes accumulate at the fracture site post injury, which gives further encouragement that this technology could be used in future studies to allow systemic administration of anabolic bone therapies for promoting fracture repair in patients. Future studies of this nature will be informed by the research presented in this thesis.

References

1. Alinaghi A, Rouini MR, Johari Daha F, Moghimi HR. The influence of lipid composition and surface charge on biodistribution of intact liposomes releasing from hydrogel-embedded vesicles. International Journal of Pharmaceutics. 2014;459(1-2):30-9.

2. Allen TM, Cullis PR. Liposomal drug delivery systems: from concept to clinical applications. Adv Drug Deliv Rev. 2013;65(1):36-48.

3. Alshaer W, Hillaireau H, Vergnaud J, Ismail S, Fattal E. Functionalizing Liposomes with anti-CD44 Aptamer for Selective Targeting of Cancer Cells. Bioconjugate Chemistry. 2015;26(7):1307-13.

4. Andersen DC, Kortesidis A, Zannettino AC, Kratchmarova I, Chen L, Jensen ON, et al. Development of novel monoclonal antibodies that define differentiation stages of human stromal (mesenchymal) stem cells. Molecules and Cells. 2011;32(2):133-42.

5. Aro HT, Govender S, Patel AD, Hernigou P, Perera de Gregorio A, Popescu GI, et al. Recombinant human bone morphogenetic protein-2: a randomized trial in open tibial fractures treated with reamed nail fixation. Journal of Bone and Joint Surgery (American Volume). 2011;93(9):801-8.

6. Aspenberg P. Annotation: parathyroid hormone and fracture healing. Acta Orthopaedica. 2013;84(1):4-6.

7. Aubin JE. Regulation of osteoblast formation and function. Reviews in Endocrine & Metabolic Disorders. 2001;2(1):81-94.

8. Babij P, Zhao W, Small C, Kharode Y, Yaworsky PJ, Bouxsein ML, et al. High bone mass in mice expressing a mutant LRP5 gene. Journal of Bone and Mineral Research. 2003;18(6):960-74.

9. Baek SE, Lee KH, Park YS, Oh DK, Oh S, Kim KS, et al. RNA aptamer-conjugated liposome as an efficient anticancer drug delivery vehicle targeting cancer cells in vivo. Journal of Controlled Release. 2014;196:234-42.

10. Bain G, Muller T, Wang X, Papkoff J. Activated beta-catenin induces osteoblast differentiation of C3H10T1/2 cells and participates in BMP2 mediated signal transduction. Biochemical and Biophysical Research Communications. 2003;301(1):84-91.

11. Baker NE. Molecular cloning of sequences from wingless, a segment polarity gene in Drosophila: the spatial distribution of a transcript in embryos. EMBO Journal. 1987;6(6):1765-73.

12. Bakopoulou A, Leyhausen G, Volk J, Koidis P, Geurtsen W. Comparative characterization of STRO-1(neg)/CD146(pos) and STRO-1(pos)/CD146(pos) apical papilla stem cells enriched with flow cytometry. Archives of Oral Biology. 2013;58(10):1556-68.

13. Baksh D, Boland GM, Tuan RS. Cross-talk between Wnt signaling pathways in human mesenchymal stem cells leads to functional antagonism during osteogenic differentiation. Journal of Cellular Biochemistry. 2007;101(5):1109-24.

14. Baksh D, Tuan RS. Canonical and non-canonical Wnts differentially affect the development potential of primary isolate of human bone marrow mesenchymal stem cells. Journal of Cellular Physiology. 2007;212(3):817-26.

15. Balasundaram G, Webster TJ. Applications of magnetic nanoparticles for the treatment of osteoporosis. Mater Res Soc Symp Proc. 2007:1019:-FF02-06.

16. Balemans W, Ebeling M, Patel N, Van Hul E, Olson P, Dioszegi M, et al. Increased bone density in sclerosteosis is due to the deficiency of a novel secreted protein (SOST). Human Molecular Genetics. 2001;10(5):537-43.

17. Bandura DR, Baranov VI, Ornatsky OI, Antonov A, Kinach R, Lou X, et al. Mass cytometry: technique for real time single cell multitarget immunoassay based on inductively coupled plasma time-of-flight mass spectrometry. Analytical Chemistry. 2009;81(16):6813-22.

18. Bangham AD, Horne RW. Negative Staining of Phospholipids and Their Structural Modification by Surface-Active Agents as Observed in the Electron Microscope. Journal of Molecular Biology. 1964;8:660-8.

19. Baron R, Kneissel M. WNT signaling in bone homeostasis and disease: from human mutations to treatments. Nature Medicine. 2013;19(2):179-92.

20. Battula VL, Treml S, Bareiss PM, Gieseke F, Roelofs H, de Zwart P, et al. Isolation of functionally distinct mesenchymal stem cell subsets using antibodies against CD56, CD271, and mesenchymal stem cell antigen-1. Haematologica. 2009;94(2):173-84.

21. Becher B, Schlitzer A, Chen J, Mair F, Sumatoh HR, Teng KW, et al. High-dimensional analysis of the murine myeloid cell system. Nature Immunology. 2014;15(12):1181-9.

22. Bendall SC, Nolan GP, Roederer M, Chattopadhyay PK. A deep profiler's guide to cytometry. Trends in Immunology. 2012;33(7):323-32.

23. Bennett CN, Longo KA, Wright WS, Suva LJ, Lane TF, Hankenson KD, et al. Regulation of osteoblastogenesis and bone mass by Wnt10b. Proceedings of the National Academy of Sciences of the United States of America. 2005;102(9):3324-9.

24. Benzinger P, Martiny-Baron G, Reusch P, Siemeister G, Kley JT, Marme D, et al. Targeting of endothelial KDR receptors with 3G2 immunoliposomes in vitro. Biochimica et Biophysica Acta. 2000;1466(1-2):71-8.

25. Berendsen AD, Fisher LW, Kilts TM, Owens RT, Robey PG, Gutkind JS, et al. Modulation of canonical Wnt signaling by the extracellular matrix component biglycan. Proceedings of the National Academy of Sciences of the United States of America. 2011;108(41):17022-7.

26. Berenholz Y, Lasic D. Gas chromatography. In: Barenholz Y, Lasic D, editors. Handbook of Nonmedical Applications of Liposomes. 3. Florida, USA: CRC Press; 1995. p. 8-10.

27. Berenson DF, Weiss AR, Wan ZL, Weiss MA. Insulin analogs for the treatment of diabetes mellitus: therapeutic applications of protein engineering. Annals of the New York Academy of Sciences. 2011;1243:E40-E54.

28. Beresford JN. Osteogenic stem cells and the stromal system of bone and marrow. Clinical Orthopaedics and Related Research. 1989(240):270-80.

29. Bertoncello I, Bradley TR, Hodgson GS. The concentration and resolution of primitive hemopoietic cells from normal mouse bone marrow by negative selection using monoclonal antibodies and Dynabead monodisperse magnetic microspheres. Experimental Hematology. 1989;17(2):171-6.

30. Bianco P, Robey PG, Simmons PJ. Mesenchymal stem cells: revisiting history, concepts, and assays. Cell Stem Cell. 2008;2(4):313-9.

31. Bianco P, Cao X, Frenette PS, Mao JJ, Robey PG, Simmons PJ, et al. The meaning, the sense and the significance: translating the science of mesenchymal stem cells into medicine. Nature Medicine. 2013;19(1):35-42.

32. Bibi S, Kaur R, Henriksen-Lacey M, McNeil SE, Wilkhu J, Lattmann E, et al. Microscopy imaging of liposomes: from coverslips to environmental SEM. International Journal of Pharmaceutics. 2011;417(1-2):138-50.

33. Bibi S, Lattmann E, Mohammed AR, Perrie Y. Trigger release liposome systems: local and remote controlled delivery? Journal of Microencapsulation. 2012;29(3):262-76.

34. Biechele TL, Adams AM, Moon RT. Transcription-based reporters of Wnt/beta-catenin signaling. Cold Spring Harb Protoc. 2009;2009(6):pdb prot5223.

35. Bilezikian JP, Raisz LG, Martin TJ. Principles of bone biology. 3rd ed. San Diego, Calif.: Academic Press/Elsevier; 2008.

36. Blitzer JT, Nusse R. A critical role for endocytosis in Wnt signaling. BMC Cell Biology. 2006;7:28.

37. Boland GM, Perkins G, Hall DJ, Tuan RS. Wnt 3a promotes proliferation and suppresses osteogenic differentiation of adult human mesenchymal stem cells. Journal of Cellular Biochemistry. 2004;93(6):1210-30.

38. Bolland MJ, Avenell A, Baron JA, Grey A, MacLennan GS, Gamble GD, et al. Effect of calcium supplements on risk of myocardial infarction and cardiovascular events: meta-analysis. BMJ. 2010;341:c3691.

39. Bossuyt X, Marti GE, Fleisher TA. Comparative analysis of whole blood lysis methods for flow cytometry. Cytometry. 1997;30(3):124-33.

40. Boxall SA, Jones E. Markers for characterization of bone marrow multipotential stromal cells. Stem Cells Int. 2012;2012:975871.

41. Boyden LM, Mao J, Belsky J, Mitzner L, Farhi A, Mitnick MA, et al. High bone density due to a mutation in LDL-receptor-related protein 5. New England Journal of Medicine. 2002;346(20):1513-21.

42. Boyum A. Separation of leukocytes from blood and bone marrow. Introduction. Scandinavian Journal of Clinical and Laboratory Investigation Supplement. 1968;97:7.

43. Brandenburg VM, Kramann R, Koos R, Kruger T, Schurgers L, Muhlenbruch G, et al. Relationship between sclerostin and cardiovascular calcification in hemodialysis patients: a cross-sectional study. BMC Nephrology. 2013;14:219.

44. Brincat M, Gambin J, Brincat M, Calleja-Agius J. The role of vitamin D in osteoporosis. Maturitas. 2015;80(3):329-32.

45. Buchert M, Athineos D, Abud HE, Burke ZD, Faux MC, Samuel MS, et al. Genetic dissection of differential signaling threshold requirements for the Wnt/beta-catenin pathway in vivo. PLoS Genetics. 2010;6(1):e1000816.

46. Buck DW, 2nd, Dumanian GA. Bone biology and physiology: Part II. Clinical correlates. Plastic and Reconstructive Surgery. 2012;129(6):950e-6e.

47. Buck DW, 2nd, Dumanian GA. Bone biology and physiology: Part I. The fundamentals. Plastic and Reconstructive Surgery. 2012;129(6):1314-20.

48. Burge R, Worley D, Johansen A, Bhattacharyya S, Bose U. The cost of osteoporotic fractures in the UK: projections for 2000–2020. Journal of Medical Economics. 2001;4(1-4):51-62.

49. Burge R, Dawson-Hughes B, Solomon DH, Wong JB, King A, Tosteson A. Incidence and economic burden of osteoporosis-related fractures in the United States, 2005-2025. Journal of Bone and Mineral Research. 2007;22(3):465-75.

50. Canton I, Battaglia G. Endocytosis at the nanoscale. Chemical Society Reviews. 2012;41(7):2718-39.

51. Caplan AI. Mesenchymal stem cells. Journal of Orthopaedic Research. 1991;9(5):641-50.

52. Caplan AI, Bruder SP. Mesenchymal stem cells: building blocks for molecular medicine in the 21st century. Trends in Molecular Medicine. 2001;7(6):259-64.

53. Caplan AI, Correa D. The MSC: an injury drugstore. Cell Stem Cell. 2011;9(1):11-5.

54. Capurro MI, Shi W, Sandal S, Filmus J. Processing by convertases is not required for glypican-3-induced stimulation of hepatocellular carcinoma growth. Journal of Biological Chemistry. 2005;280(50):41201-6.

55. Cawthorn WP, Bree AJ, Yao Y, Du B, Hemati N, Martinez-Santibanez G, et al. Wnt6, Wnt10a and Wnt10b inhibit adipogenesis and stimulate osteoblastogenesis through a beta-catenin-dependent mechanism. Bone. 2012;50(2):477-89.

56. Chames P, Van Regenmortel M, Weiss E, Baty D. Therapeutic antibodies: successes, limitations and hopes for the future. British Journal of Pharmacology. 2009;157(2):220-33.

57. Chan CK, Seo EY, Chen JY, Lo D, McArdle A, Sinha R, et al. Identification and specification of the mouse skeletal stem cell. Cell. 2015;160(1-2):285-98.

58. Chen C, Han D, Cai C, Tang X. An overview of liposome lyophilization and its future potential. Journal of Controlled Release. 2010;142(3):299-311.

59. Chen Y, Whetstone HC, Lin AC, Nadesan P, Wei Q, Poon R, et al. Beta-catenin signaling plays a disparate role in different phases of fracture repair: implications for therapy to improve bone healing. PLoS Medicine. 2007;4(7):e249.

60. Cheng WW, Allen TM. Targeted delivery of anti-CD19 liposomal doxorubicin in B-cell lymphoma: a comparison of whole monoclonal antibody, Fab' fragments and single chain Fv. Journal of Controlled Release. 2008;126(1):50-8.

61. Ching W, Hang HC, Nusse R. Lipid-independent secretion of a Drosophila Wnt protein. Journal of Biological Chemistry. 2008;283(25):17092-8.

62. Cho H, Magid R, Danila DC, Hunsaker T, Pinkhassik E, Hasty KA. Theranostic Immunoliposomes for Osteoarthritis. Nanomedicine: Nanotechnology, Biology, and Medicine. 2013.

63. Cho HH, Kim YJ, Kim SJ, Kim JH, Bae YC, Ba B, et al. Endogenous Wnt signaling promotes proliferation and suppresses osteogenic differentiation in human adipose derived stromal cells. Tissue Engineering. 2006;12(1):111-21.

64. Christodoulides C, Lagathu C, Sethi JK, Vidal-Puig A. Adipogenesis and WNT signalling. Trends in Endocrinology and Metabolism. 2009;20(1):16-24.

65. Christodoulou C, Cooper C. What is osteoporosis? Postgraduate Medical Journal. 2003;79(929):133-8.

66. Chun JS, Oh H, Yang S, Park M. Wnt signaling in cartilage development and degeneration. BMB Rep. 2008;41(7):485-94.

67. Churchman SM, Ponchel F, Boxall SA, Cuthbert R, Kouroupis D, Roshdy T, et al. Transcriptional profile of native CD271+ multipotential stromal cells: evidence for multiple

fates, with prominent osteogenic and Wnt pathway signaling activity. Arthritis and Rheumatism. 2012;64(8):2632-43.

68. Clarke B. Normal bone anatomy and physiology. Clinical Journal of the American Society of Nephrology. 2008;3 Suppl 3:S131-9.

69. Clevers H, Nusse R. Wnt/beta-Catenin Signaling and Disease. Cell. 2012;149(6):1192-205.

70. Colletier JP, Chaize B, Winterhalter M, Fournier D. Protein encapsulation in liposomes: efficiency depends on interactions between protein and phospholipid bilayer. BMC Biotechnology. 2002;2:9.

71. Cook DA, Fellgett SW, Pownall ME, O'Shea PJ, Genever PG. Wnt-dependent osteogenic commitment of bone marrow stromal cells using a novel GSK3beta inhibitor. Stem Cell Res. 2014;12(2):415-27.

72. Coulter WH. High speed automatic blood cell counter and cell size analyzer. Proc Natl Electronics Conf. 1956;12:1034-42.

73. Covas DT, Panepucci RA, Fontes AM, Silva WA, Orellana MD, Freitas MCC, et al. Multipotent mesenchymal stromal cells obtained from diverse human tissues share functional properties and gene-expression profile with CD146(+) perivascular cells and fibroblasts. Experimental Hematology. 2008;36(5):642-54.

74. Crisan M, Yap S, Casteilla L, Chen CW, Corselli M, Park TS, et al. A perivascular origin for mesenchymal stem cells in multiple human organs. Cell Stem Cell. 2008;3(3):301-13.

75. Cullis PR. Lateral diffusion rates of phosphatidylcholine in vesicle membranes: effects of cholesterol and hydrocarbon phase transitions. FEBS Letters. 1976;70(1):223-8.

76. Cummings SR, San Martin J, McClung MR, Siris ES, Eastell R, Reid IR, et al. Denosumab for prevention of fractures in postmenopausal women with osteoporosis. New England Journal of Medicine. 2009;361(8):756-65.

77. da Silva Meirelles L, Chagastelles PC, Nardi NB. Mesenchymal stem cells reside in virtually all post-natal organs and tissues. Journal of Cell Science. 2006;119(Pt 11):2204-13.

78. Dawson JI, Oreffo RO. Clay: new opportunities for tissue regeneration and biomaterial design. Advanced Materials. 2013;25(30):4069-86.

79. Day TF, Guo X, Garrett-Beal L, Yang Y. Wnt/beta-catenin signaling in mesenchymal progenitors controls osteoblast and chondrocyte differentiation during vertebrate skeletogenesis. Developmental Cell. 2005;8(5):739-50.

80. de Boer J, Siddappa R, Gaspar C, van Apeldoorn A, Fodde R, van Blitterswijk C. Wnt signaling inhibits osteogenic differentiation of human mesenchymal stem cells. Bone. 2004;34(5):818-26.

81. De Boer J, Wang HJ, Van Blitterswijk C. Effects of Wnt signaling on proliferation and differentiation of human mesenchymal stem cells. Tissue Engineering. 2004;10(3-4):393-401.
82. De Jong WH, Borm PJ. Drug delivery and nanoparticles:applications and hazards. Int J Nanomedicine. 2008;3(2):133-49.
83. Deng ZL, Sharff KA, Tang N, Song WX, Luo J, Luo X, et al. Regulation of osteogenic differentiation during skeletal development. Frontiers in Bioscience. 2008;13:2001-21.
84. Dhamdhere GR, Fang MY, Jiang J, Lee K, Cheng D, Olveda RC, et al. Drugging a stem cell compartment using wnt3a protein as a therapeutic. PloS One. 2014;9(1):e83650.
85. Ding L, Saunders TL, Enikolopov G, Morrison SJ. Endothelial and perivascular cells maintain haematopoietic stem cells. Nature. 2012;481(7382):457-62.
86. Ding VM, Ling L, Natarajan S, Yap MG, Cool SM, Choo AB. FGF-2 modulates Wnt signaling in undifferentiated hESC and iPS cells through activated PI3-K/GSK3beta signaling. Journal of Cellular Physiology. 2010;225(2):417-28.
87. Dittrich W, Gohde W. Impulsfluorometrie bei Einzelzellen in Suspensionen. Z Naturforsch. 1969;24b:360-1.
88. Dominici M, Le Blanc K, Mueller I, Slaper-Cortenbach I, Marini F, Krause D, et al. Minimal criteria for defining multipotent mesenchymal stromal cells. The International Society for Cellular Therapy position statement. Cytotherapy. 2006;8(4):315-7.
89. Ducy P, Schinke T, Karsenty G. The osteoblast: a sophisticated fibroblast under central surveillance. Science. 2000;289(5484):1501-4.
90. Ducy P, Karsenty G. The two faces of serotonin in bone biology. Journal of Cell Biology. 2010;191(1):7-13.
91. Ehninger A, Trumpp A. The bone marrow stem cell niche grows up: mesenchymal stem cells and macrophages move in. Journal of Experimental Medicine. 2011;208(3):421-8.
92. Eijken M, Meijer IM, Westbroek I, Koedam M, Chiba H, Uitterlinden AG, et al. Wnt signaling acts and is regulated in a human osteoblast differentiation dependent manner. Journal of Cellular Biochemistry. 2008;104(2):568-79.
93. Einhorn TA, Gerstenfeld LC. Fracture healing: mechanisms and interventions. Nat Rev Rheumatol. 2015;11(1):45-54.
94. Enochson L, Stenberg J, Brittberg M, Lindahl A. GDF5 reduces MMP13 expression in human chondrocytes via DKK1 mediated canonical Wnt signaling inhibition. Osteoarthritis and Cartilage. 2014;22(4):566-77.
95. Erickson HP. Size and shape of protein molecules at the nanometer level determined by sedimentation, gel filtration, and electron microscopy. Biological Procedures Online. 2009;11:32-51.

96. Etheridge SL, Spencer GJ, Heath DJ, Genever PG. Expression profiling and functional analysis of wnt signaling mechanisms in mesenchymal stem cells. Stem Cells. 2004;22(5):849-60.

97. Ettinger B, Black DM, Mitlak BH, Knickerbocker RK, Nickelsen T, Genant HK, et al. Reduction of vertebral fracture risk in postmenopausal women with osteoporosis treated with raloxifene: results from a 3-year randomized clinical trial. Multiple Outcomes of Raloxifene Evaluation (MORE) Investigators. JAMA. 1999;282(7):637-45.

98. Eugster C, Panakova D, Mahmoud A, Eaton S. Lipoprotein-heparan sulfate interactions in the Hh pathway. Developmental Cell. 2007;13(1):57-71.

99. Friedenstein AJ, Chailakhjan RK, Lalykina KS. The development of fibroblast colonies in monolayer cultures of guinea-pig bone marrow and spleen cells. Cell and Tissue Kinetics. 1970;3(4):393-403.

100. Friedenstein AJ, Gorskaja JF, Kulagina NN. Fibroblast precursors in normal and irradiated mouse hematopoietic organs. Experimental Hematology. 1976;4(5):267-74.

101. Fuchs E, Chen T. A matter of life and death: self-renewal in stem cells. EMBO Rep. 2013;14(1):39-48.

102. Fuerer C, Habib SJ, Nusse R. A study on the interactions between heparan sulfate proteoglycans and Wnt proteins. Developmental Dynamics. 2010;239(1):184-90.

103. Gaipa G, Dassi M, Perseghin P, Venturi N, Corti P, Bonanomi S, et al. Allogeneic bone marrow stem cell transplantation following CD34+ immunomagnetic enrichment in patients with inherited metabolic storage diseases. Bone Marrow Transplantation. 2003;31(10):857-60.

104. Gambardella A, Nagaraju CK, O'Shea PJ, Mohanty ST, Kottam L, Pilling J, et al. Glycogen synthase kinase-3alpha/beta inhibition promotes in vivo amplification of endogenous mesenchymal progenitors with osteogenic and adipogenic potential and their differentiation to the osteogenic lineage. Journal of Bone and Mineral Research. 2011;26(4):811-21.

105. Gao X, Hannoush RN. Single-cell imaging of Wnt palmitoylation by the acyltransferase porcupine. Nature Chemical Biology. 2014;10(1):61-8.

106. Gao Y, Jheon A, Nourkeyhani H, Kobayashi H, Ganss B. Molecular cloning, structure, expression, and chromosomal localization of the human Osterix (SP7) gene. Gene. 2004;341:101-10.

107. Gao Y, Xie J, Chen H, Gu S, Zhao R, Shao J, et al. Nanotechnology-based intelligent drug design for cancer metastasis treatment. Biotechnology Advances. 2014;32(4):761-77.

108. George TC, Basiji DA, Hall BE, Lynch DH, Ortyn WE, Perry DJ, et al. Distinguishing modes of cell death using the ImageStream multispectral imaging flow cytometer. Cytometry A. 2004;59(2):237-45.

109. Glinka A, Wu W, Delius H, Monaghan AP, Blumenstock C, Niehrs C. Dickkopf-1 is a member of a new family of secreted proteins and functions in head induction. Nature. 1998;391(6665):357-62.

110. Goldhahn J, Feron JM, Kanis J, Papapoulos S, Reginster JY, Rizzoli R, et al. Implications for fracture healing of current and new osteoporosis treatments: an ESCEO consensus paper. Calcified Tissue International. 2012;90(5):343-53.

111. Gomez-Barrena E, Rosset P, Lozano D, Stanovici J, Ermthaller C, Gerbhard F. Bone fracture healing: cell therapy in delayed unions and nonunions. Bone. 2015;70:93-101.

112. Gong Y, Slee RB, Fukai N, Rawadi G, Roman-Roman S, Reginato AM, et al. LDL receptor-related protein 5 (LRP5) affects bone accrual and eye development. Cell. 2001;107(4):513-23.

113. Goren D, Horowitz AT, Zalipsky S, Woodle MC, Yarden Y, Gabizon A. Targeting of stealth liposomes to erbB-2 (Her/2) receptor: in vitro and in vivo studies. British Journal of Cancer. 1996;74(11):1749-56.

114. Gosk S, Gottstein C, Bendas G. Targeting of immunoliposomes to endothelial cells expressing VCAM: a future strategy in cancer therapy. International Journal of Clinical Pharmacology and Therapeutics. 2005;43(12):581-2.

115. Goulet JA, Senunas LE, DeSilva GL, Greenfield ML. Autogenous iliac crest bone graft. Complications and functional assessment. Clinical Orthopaedics and Related Research. 1997(339):76-81.

116. Greco V, Hannus M, Eaton S. Argosomes: a potential vehicle for the spread of morphogens through epithelia. Cell. 2001;106(5):633-45.

117. Greenbaum A, Hsu YM, Day RB, Schuettpelz LG, Christopher MJ, Borgerding JN, et al. CXCL12 in early mesenchymal progenitors is required for haematopoietic stem-cell maintenance. Nature. 2013;495(7440):227-30.

118. Gregoriadis G. The carrier potential of liposomes in biology and medicine (first of two parts). New England Journal of Medicine. 1976;295(13):704-10.

119. Gregoriadis G. Engineering liposomes for drug delivery: progress and problems. Trends in Biotechnology. 1995;13(12):527-37.

120. Gregory CA, Gunn WG, Peister A, Prockop DJ. An Alizarin red-based assay of mineralization by adherent cells in culture: comparison with cetylpyridinium chloride extraction. Analytical Biochemistry. 2004;329(1):77-84.

121. Gregory CA, Gunn WG, Reyes E, Smolarz AJ, Munoz J, Spees JL, et al. How Wnt signaling affects bone repair by mesenchymal stem cells from the bone marrow. Annals of the New York Academy of Sciences. 2005;1049:97-106.

122. Griffith JF, Yeung DK, Ma HT, Leung JC, Kwok TC, Leung PC. Bone marrow fat content in the elderly: a reversal of sex difference seen in younger subjects. Journal of Magnetic Resonance Imaging. 2012;36(1):225-30.

123. Gronthos S, Graves SE, Ohta S, Simmons PJ. The STRO-1+ fraction of adult human bone marrow contains the osteogenic precursors. Blood. 1994;84(12):4164-73.

124. Gronthos S, Simmons PJ. The biology and application of human bone marrow stromal cell precursors. Journal of Hematotherapy. 1996;5(1):15-23.

125. Gronthos S, Zannettino AC, Graves SE, Ohta S, Hay SJ, Simmons PJ. Differential cell surface expression of the STRO-1 and alkaline phosphatase antigens on discrete developmental stages in primary cultures of human bone cells. Journal of Bone and Mineral Research. 1999;14(1):47-56.

126. Gronthos S, Zannettino AC, Hay SJ, Shi S, Graves SE, Kortesidis A, et al. Molecular and cellular characterisation of highly purified stromal stem cells derived from human bone marrow. Journal of Cell Science. 2003;116(Pt 9):1827-35.

127. Gu W, Wu C, Chen J, Xiao Y. Nanotechnology in the targeted drug delivery for bone diseases and bone regeneration. Int J Nanomedicine. 2013;8:2305-17.

128. Guo J, Liu M, Yang D, Bouxsein ML, Saito H, Galvin RJ, et al. Suppression of Wnt signaling by Dkk1 attenuates PTH-mediated stromal cell response and new bone formation. Cell Metab. 2010;11(2):161-71.

129. Habib SJ, Chen BC, Tsai FC, Anastassiadis K, Meyer T, Betzig E, et al. A localized Wnt signal orients asymmetric stem cell division in vitro. Science. 2013;339(6126):1445-8.

130. Hacker U, Lin X, Perrimon N. The Drosophila sugarless gene modulates Wingless signaling and encodes an enzyme involved in polysaccharide biosynthesis. Development. 1997;124(18):3565-73.

131. Haddad FS, Muirhead-Allwood SK, Manktelow AR, Bacarese-Hamilton I. Two-stage uncemented revision hip arthroplasty for infection. Journal of Bone and Joint Surgery (British Volume). 2000;82(5):689-94.

132. Hadjiargyrou M, Lombardo F, Zhao S, Ahrens W, Joo J, Ahn H, et al. Transcriptional profiling of bone regeneration. Insight into the molecular complexity of wound repair. Journal of Biological Chemistry. 2002;277(33):30177-82.

133. Hak DJ. Management of aseptic tibial nonunion. Journal of the American Academy of Orthopaedic Surgeons. 2011;19(9):563-73.

134. Harichandan A, Buhring HJ. Prospective isolation of human MSC. Best Practice & Research: Clinical Haematology. 2011;24(1):25-36.

135. Harris TJ, Green JJ, Fung PW, Langer R, Anderson DG, Bhatia SN. Tissue-specific gene delivery via nanoparticle coating. Biomaterials. 2010;31(5):998-1006.

136. Hatakeyama H, Akita H, Maruyama K, Suhara T, Harashima H. Factors governing the in vivo tissue uptake of transferrin-coupled polyethylene glycol liposomes in vivo. International Journal of Pharmaceutics. 2004;281(1-2):25-33.

137. Hayrapetyan A, Jansen JA, van den Beucken JJ. Signaling pathways involved in osteogenesis and their application for bone regenerative medicine. Tissue Eng Part B Rev. 2015;21(1):75-87.

138. Heino TJ, Hentunen TA. Differentiation of osteoblasts and osteocytes from mesenchymal stem cells. Current Stem Cell Research & Therapy. 2008;3(2):131-45.

139. Hengst V, Oussoren C, Kissel T, Storm G. Bone targeting potential of bisphosphonate-targeted liposomes. Preparation, characterization and hydroxyapatite binding in vitro. International Journal of Pharmaceutics. 2007;331(2):224-7.

140. Hernigou P, Poignard A, Beaujean F, Rouard H. Percutaneous autologous bone-marrow grafting for nonunions. Influence of the number and concentration of progenitor cells. Journal of Bone and Joint Surgery (American Volume). 2005;87(7):1430-7.

141. Herzenberg LA, Sweet RG, Herzenberg LA. Fluorescence-activated cell sorting. Scientific American. 1976;234(3):108-17.

142. Hiyama A, Sakai D, Arai F, Nakajima D, Yokoyama K, Mochida J. Effects of a Glycogen Synthase Kinase-3 beta Inhibitor (LiCl) on c-myc Protein in Intervertebral Disc Cells. Journal of Cellular Biochemistry. 2011;112(10):2974-86.

143. Hodsman AB, Bauer DC, Dempster DW, Dian L, Hanley DA, Harris ST, et al. Parathyroid hormone and teriparatide for the treatment of osteoporosis: a review of the evidence and suggested guidelines for its use. Endocrine Reviews. 2005;26(5):688-703.

144. Hofmann A, Ritz U, Hessmann MH, Schmid C, Tresch A, Rompe JD, et al. Cell viability, osteoblast differentiation, and gene expression are altered in human osteoblasts from hypertrophic fracture non-unions. Bone. 2008;42(5):894-906.

145. Hofmann K. A superfamily of membrane-bound O-acyltransferases with implications for wnt signaling. Trends in Biochemical Sciences. 2000;25(3):111-2.

146. Holroyd C, Cooper C, Dennison E. Epidemiology of osteoporosis. Best Practice & Research: Clinical Endocrinology & Metabolism. 2008;22(5):671-85.

147. Hovanes K, Li TW, Munguia JE, Truong T, Milovanovic T, Lawrence Marsh J, et al. Beta-catenin-sensitive isoforms of lymphoid enhancer factor-1 are selectively expressed in colon cancer. Nature Genetics. 2001;28(1):53-7.

148. Ishitani T, Kishida S, Hyodo-Miura J, Ueno N, Yasuda J, Waterman M, et al. The TAK1-NLK mitogen-activated protein kinase cascade functions in the Wnt-5a/Ca(2+) pathway to antagonize Wnt/beta-catenin signaling. Molecular and Cellular Biology. 2003;23(1):131-9.

149. Iyer SP, Beck JT, Stewart AK, Shah J, Kelly KR, Isaacs R, et al. A Phase IB multicentre dose-determination study of BHQ880 in combination with anti-myeloma therapy and zoledronic acid in patients with relapsed or refractory multiple myeloma and prior skeletal-related events. British Journal of Haematology. 2014;167(3):366-75.

150. James JR, White SS, Clarke RW, Johansen AM, Dunne PD, Sleep DL, et al. Single-molecule level analysis of the subunit composition of the T cell receptor on live T cells. Proceedings of the National Academy of Sciences of the United States of America. 2007;104(45):17662-7.

151. Janda CY, Waghray D, Levin AM, Thomas C, Garcia KC. Structural basis of Wnt recognition by Frizzled. Science. 2012;337(6090):59-64.

152. Janeczek AA, Scarpa E, Newman TA, Oreffo ROC, Tare RS, Evans ND. Skeletal Stem Cell Niche of the Bone Marrow. In: Turksen K, editor. Tissue-Specific Stem Cell Niche. Stem Cell Biology and Regenerative Medicine: Springer International Publishing; 2015. p. 245-79.

153. Jensen BE, Hosta-Rigau L, Spycher PR, Reimhult E, Stadler B, Zelikin AN. Lipogels: surface-adherent composite hydrogels assembled from poly(vinyl alcohol) and liposomes. Nanoscale. 2013;5(15):6758-66.

154. Jho EH, Zhang T, Domon C, Joo CK, Freund JN, Costantini F. Wnt/beta-catenin/Tcf signaling induces the transcription of Axin2, a negative regulator of the signaling pathway. Molecular and Cellular Biology. 2002;22(4):1172-83.

155. Jia Z, Zhang Y, Chen YH, Dusad A, Yuan H, Ren K, et al. Simvastatin prodrug micelles target fracture and improve healing. Journal of Controlled Release. 2015;200:23-34.

156. Jin H, Wang B, Li J, Xie W, Mao Q, Li S, et al. Anti-DKK1 antibody promotes bone fracture healing through activation of beta-catenin signaling. Bone. 2015;71:63-75.

157. Jing W, Smith AA, Liu B, Li J, Hunter DJ, Dhamdhere G, et al. Reengineering autologous bone grafts with the stem cell activator WNT3A. Biomaterials. 2015;47:29-40.

158. Joseph C, Quach JM, Walkley CR, Lane SW, Lo Celso C, Purton LE. Deciphering hematopoietic stem cells in their niches: a critical appraisal of genetic models, lineage tracing, and imaging strategies. Cell Stem Cell. 2013;13(5):520-33.

159. Juliano RL, Stamp D. Pharmacokinetics of liposome-encapsulated anti-tumor drugs. Studies with vinblastine, actinomycin D, cytosine arabinoside, and daunomycin. Biochemical Pharmacology. 1978;27(1):21-7.

160. Kakar S, Einhorn TA, Vora S, Miara LJ, Hon G, Wigner NA, et al. Enhanced chondrogenesis and Wnt signaling in PTH-treated fractures. Journal of Bone and Mineral Research. 2007;22(12):1903-12.

161. Kang S, Bennett CN, Gerin I, Rapp LA, Hankenson KD, Macdougald OA. Wnt signaling stimulates osteoblastogenesis of mesenchymal precursors by suppressing CCAAT/enhancer-binding protein alpha and peroxisome proliferator-activated receptor gamma. Journal of Biological Chemistry. 2007;282(19):14515-24.

162. Kanis J. Assessment of Osteoporosis at the Primary Health-care Level. Technical report. . World Health Organization Collaborating Centre for Metabolic Bone Diseases. 2007.

163. Karsenty G. The complexities of skeletal biology. Nature. 2003;423(6937):316-8.

164. Kato M, Patel MS, Levasseur R, Lobov I, Chang BH, Glass DA, 2nd, et al. Cbfa1-independent decrease in osteoblast proliferation, osteopenia, and persistent embryonic eye vascularization in mice deficient in Lrp5, a Wnt coreceptor. Journal of Cell Biology. 2002;157(2):303-14.

165. Kawai M, Modder UI, Khosla S, Rosen CJ. Emerging therapeutic opportunities for skeletal restoration. Nature Reviews: Drug Discovery. 2011;10(2):141-56.

166. Kelly C, Jefferies C, Cryan SA. Targeted liposomal drug delivery to monocytes and macrophages. J Drug Deliv. 2011;2011:727241.

167. Kim JA, Choi HK, Kim TM, Leem SH, Oh IH. Regulation of mesenchymal stromal cells through fine tuning of canonical Wnt signaling. Stem Cell Res. 2015;14(3):356-68.

168. Kim JB, Leucht P, Lam K, Luppen C, Ten Berge D, Nusse R, et al. Bone regeneration is regulated by wnt signaling. Journal of Bone and Mineral Research. 2007;22(12):1913-23.

169. Kim JH, Liu X, Wang J, Chen X, Zhang H, Kim SH, et al. Wnt signaling in bone formation and its therapeutic potential for bone diseases. Therapeutic Advances in Musculoskeletal Disease. 2013;5(1):13-31.

170. Klibanov AL, Maruyama K, Torchilin VP, Huang L. Amphipathic polyethyleneglycols effectively prolong the circulation time of liposomes. FEBS Letters. 1990;268(1):235-7.

171. Knight MN, Hankenson KD. R-spondins: novel matricellular regulators of the skeleton. Matrix Biology. 2014;37:157-61.

172. Knudsen KB, Northeved H, Kumar PE, Permin A, Gjetting T, Andresen TL, et al. In vivo toxicity of cationic micelles and liposomes. Nanomedicine: Nanotechnology, Biology, and Medicine. 2015;11(2):467-77.

173. Kohler G, Milstein C. Continuous cultures of fused cells secreting antibody of predefined specificity. Nature. 1975;256(5517):495-7.

174. Kolar P, Schmidt-Bleek K, Schell H, Gaber T, Toben D, Schmidmaier G, et al. The early fracture hematoma and its potential role in fracture healing. Tissue Eng Part B Rev. 2010;16(4):427-34.

175. Korkut C, Ataman B, Ramachandran P, Ashley J, Barria R, Gherbesi N, et al. Trans-synaptic transmission of vesicular Wnt signals through Evi/Wntless. Cell. 2009;139(2):393-404.

176. Kuhl M, Sheldahl LC, Park M, Miller JR, Moon RT. The Wnt/Ca2+ pathway - a new vertebrate Wnt signaling pathway takes shape. Trends in Genetics. 2000;16(7):279-83.

177. Kunisaki Y, Bruns I, Scheiermann C, Ahmed J, Pinho S, Zhang D, et al. Arteriolar niches maintain haematopoietic stem cell quiescence. Nature. 2013;502(7473):637-43.

178. Kuznetsov SA, Krebsbach PH, Satomura K, Kerr J, Riminucci M, Benayahu D, et al. Single-colony derived strains of human marrow stromal fibroblasts form bone after transplantation in vivo. Journal of Bone and Mineral Research. 1997;12(9):1335-47.

179. Larsen KH, Frederiksen CM, Burns JS, Abdallah BM, Kassem M. Identifying a molecular phenotype for bone marrow stromal cells with in vivo bone-forming capacity. Journal of Bone and Mineral Research. 2010;25(4):796-808.

180. Lasic DD. Liposomes : from physics to applications. Amsterdam ; New York: Elsevier; 1993. xviii, 575 p. p.

181. Laurencin C, Khan Y, El-Amin SF. Bone graft substitutes. Expert Review of Medical Devices. 2006;3(1):49-57.

182. Leader B, Baca QJ, Golan DE. Protein therapeutics: a summary and pharmacological classification. Nature Reviews: Drug Discovery. 2008;7(1):21-39.

183. Leucht P, Jiang J, Cheng D, Liu B, Dhamdhere G, Fang MY, et al. Wnt3a reestablishes osteogenic capacity to bone grafts from aged animals. Journal of Bone and Joint Surgery (American Volume). 2013;95(14):1278-88.

184. Leupin O, Kramer I, Collette NM, Loots GG, Natt F, Kneissel M, et al. Control of the SOST bone enhancer by PTH using MEF2 transcription factors. Journal of Bone and Mineral Research. 2007;22(12):1957-67.

185. Li L, Clevers H. Coexistence of quiescent and active adult stem cells in mammals. Science. 2010;327(5965):542-5.

186. Li S, Peng Y, Weinhandl ED, Blaes AH, Cetin K, Chia VM, et al. Estimated number of prevalent cases of metastatic bone disease in the US adult population. Clinical Epidemiology. 2012;4:87-93.

187. Li X, Zhang Y, Kang H, Liu W, Liu P, Zhang J, et al. Sclerostin binds to LRP5/6 and antagonizes canonical Wnt signaling. Journal of Biological Chemistry. 2005;280(20):19883-7.

188. Li X, Grisanti M, Fan W, Asuncion FJ, Tan HL, Dwyer D, et al. Dickkopf-1 regulates bone formation in young growing rodents and upon traumatic injury. Journal of Bone and Mineral Research. 2011;26(11):2610-21.

189. Lin G, Liu G, Banie L, Wang G, Ning H, Lue TF, et al. Tissue distribution of mesenchymal stem cell marker Stro-1. Stem Cells Dev. 2011;20(10):1747-52.

190. Ling L, Nurcombe V, Cool SM. Wnt signaling controls the fate of mesenchymal stem cells. Gene. 2009;433(1-2):1-7.

191. Lissenberg-Thunnissen SN, de Gorter DJ, Sier CF, Schipper IB. Use and efficacy of bone morphogenetic proteins in fracture healing. International Orthopaedics. 2011;35(9):1271-80.

192. Liu G, Vijayakumar S, Grumolato L, Arroyave R, Qiao H, Akiri G, et al. Canonical Wnts function as potent regulators of osteogenesis by human mesenchymal stem cells. Journal of Cell Biology. 2009;185(1):67-75.

193. Lo Celso C, Lin CP, Scadden DT. In vivo imaging of transplanted hematopoietic stem and progenitor cells in mouse calvarium bone marrow. Nature Protocols. 2011;6(1):1-14.

194. Lodewyckx L, Lories RJ. WNT Signaling in osteoarthritis and osteoporosis: what is the biological significance for the clinician? Curr Rheumatol Rep. 2009;11(1):23-30.

195. Loomis K, Smith B, Feng Y, Garg H, Yavlovich A, Campbell-Massa R, et al. Specific targeting to B cells by lipid-based nanoparticles conjugated with a novel CD22-ScFv. Experimental and Molecular Pathology. 2010;88(2):238-49.

196. Lorenowicz MJ, Korswagen HC. Sailing with the Wnt: charting the Wnt processing and secretion route. Experimental Cell Research. 2009;315(16):2683-9.

197. Lu W, Kim KA, Liu J, Abo A, Feng X, Cao X, et al. R-spondin1 synergizes with Wnt3A in inducing osteoblast differentiation and osteoprotegerin expression. FEBS Letters. 2008;582(5):643-50.

198. Luhmann T, Germershaus O, Groll J, Meinel L. Bone targeting for the treatment of osteoporosis. Journal of Controlled Release. 2012;161(2):198-213.

199. Lum L, Clevers H. Cell biology. The unusual case of Porcupine. Science. 2012;337(6097):922-3.

200. Luria EA, Panasyuk AF, Friedenstein AY. Fibroblast colony formation from monolayer cultures of blood cells. Transfusion. 1971;11(6):345-9.

201. Lustig B, Jerchow B, Sachs M, Weiler S, Pietsch T, Karsten U, et al. Negative feedback loop of Wnt signaling through upregulation of conductin/axin2 in colorectal and liver tumors. Molecular and Cellular Biology. 2002;22(4):1184-93.

202. Lv FJ, Tuan RS, Cheung KM, Leung VY. Concise review: the surface markers and identity of human mesenchymal stem cells. Stem Cells. 2014;32(6):1408-19.

203. Lyon T, Scheele W, Bhandari M, Koval KJ, Sanchez EG, Christensen J, et al. Efficacy and safety of recombinant human bone morphogenetic protein-2/calcium phosphate matrix for closed tibial diaphyseal fracture: a double-blind, randomized, controlled phase-II/III trial. Journal of Bone and Joint Surgery (American Volume). 2013;95(23):2088-96.

204. Malloy A, Carr B. NanoParticle Tracking Analysis – The Halo™ System. Particle and Particle Systems Characterization. 2006;23:197–204.

205. Mamot C, Drummond DC, Noble CO, Kallab V, Guo Z, Hong K, et al. Epidermal growth factor receptor-targeted immunoliposomes significantly enhance the efficacy of multiple anticancer drugs in vivo. Cancer Research. 2005;65(24):11631-8.

206. Mann AP, Tanaka T, Somasunderam A, Liu X, Gorenstein DG, Ferrari M. E-selectin-targeted porous silicon particle for nanoparticle delivery to the bone marrow. Advanced Materials. 2011;23(36):H278-82.

207. Manolagas SC. From estrogen-centric to aging and oxidative stress: a revised perspective of the pathogenesis of osteoporosis. Endocrine Reviews. 2010;31(3):266-300.

208. Marieb EN. Essentials of human anatomy & physiology. 10th ed. San Francisco, CA: Benjamin Cummings; 2012. xxiv, 632 p. p.

209. Marom R, Shur I, Solomon R, Benayahu D. Characterization of adhesion and differentiation markers of osteogenic marrow stromal cells. Journal of Cellular Physiology. 2005;202(1):41-8.

210. Marsell R, Einhorn TA. The biology of fracture healing. Injury. 2011;42(6):551-5.

211. Marson A, Foreman R, Chevalier B, Bilodeau S, Kahn M, Young RA, et al. Wnt signaling promotes reprogramming of somatic cells to pluripotency. Cell Stem Cell. 2008;3(2):132-5.

212. Matsuo T, Sugita T, Kubo T, Yasunaga Y, Ochi M, Murakami T. Injectable magnetic liposomes as a novel carrier of recombinant human BMP-2 for bone formation in a rat bone-defect model. Journal of Biomedical Materials Research, Part A. 2003;66(4):747-54.

213. Mbalaviele G, Sheikh S, Stains JP, Salazar VS, Cheng SL, Chen D, et al. Beta-catenin and BMP-2 synergize to promote osteoblast differentiation and new bone formation. Journal of Cellular Biochemistry. 2005;94(2):403-18.

214. McCarthy TL, Centrella M. Novel links among Wnt and TGF-beta signaling and Runx2. Molecular Endocrinology. 2010;24(3):587-97.

215. McClung MR, Grauer A, Boonen S, Bolognese MA, Brown JP, Diez-Perez A, et al. Romosozumab in postmenopausal women with low bone mineral density. New England Journal of Medicine. 2014;370(5):412-20.

216. McGreevy C, Williams D. Safety of drugs used in the treatment of osteoporosis. Ther Adv Drug Saf. 2011;2(4):159-72.

217. McKibbin B. The biology of fracture healing in long bones. Journal of Bone and Joint Surgery (British Volume). 1978;60-B(2):150-62.

218. Megas P. Classification of non-union. Injury. 2005;36 Suppl 4:S30-7.

219. Melton LJ, 3rd, Gabriel SE, Crowson CS, Tosteson AN, Johnell O, Kanis JA. Cost-equivalence of different osteoporotic fractures. Osteoporosis International. 2003;14(5):383-8.

220. Mendes SC, Tibbe JM, Veenhof M, Both S, Oner FC, van Blitterswijk CA, et al. Relation between in vitro and in vivo osteogenic potential of cultured human bone marrow stromal cells. Journal of Materials Science: Materials in Medicine. 2004;15(10):1123-8.

221. Mendez-Ferrer S, Michurina TV, Ferraro F, Mazloom AR, Macarthur BD, Lira SA, et al. Mesenchymal and haematopoietic stem cells form a unique bone marrow niche. Nature. 2010;466(7308):829-34.

222. Mendez-Ferrer S, Scadden DT, Sanchez-Aguilera A. Bone marrow stem cells: current and emerging concepts. Annals of the New York Academy of Sciences. 2015;1335(1):32-44.

223. Miki T, Yasuda SY, Kahn M. Wnt/beta-catenin Signaling in Embryonic Stem Cell Self-renewal and Somatic Cell Reprogramming. Stem Cell Reviews and Reports. 2011;7(4):836-46.

224. Miller J, Chan BK, Nelson HD. Postmenopausal estrogen replacement and risk for venous thromboembolism: a systematic review and meta-analysis for the U.S. Preventive Services Task Force. Annals of Internal Medicine. 2002;136(9):680-90.

225. Miller JR. The Wnts. Genome Biology. 2002;3(1):REVIEWS3001.

226. Mills JK, Needham D. Targeted drug delivery. Expert Opin Ther Patents. 1999(9):1499 - 513.

227. Min JK, Park H, Choi HJ, Kim Y, Pyun BJ, Agrawal V, et al. The WNT antagonist Dickkopf2 promotes angiogenesis in rodent and human endothelial cells. Journal of Clinical Investigation. 2011;121(5):1882-93.

228. Minear S, Leucht P, Jiang J, Liu B, Zeng A, Fuerer C, et al. Wnt proteins promote bone regeneration. Science Translational Medicine. 2010;2(29):29ra30.

229. Mizoguchi T, Pinho S, Ahmed J, Kunisaki Y, Hanoun M, Mendelson A, et al. Osterix marks distinct waves of primitive and definitive stromal progenitors during bone marrow development. Developmental Cell. 2014;29(3):340-9.

230. Moghimi SM. Exploiting bone marrow microvascular structure for drug delivery and future therapies. 1995.

231. Morrell NT, Leucht P, Zhao L, Kim JB, ten Berge D, Ponnusamy K, et al. Liposomal packaging generates Wnt protein with in vivo biological activity. PloS One. 2008;3(8):e2930.

232. Morrison SL, Johnson MJ, Herzenberg LA, Oi VT. Chimeric human antibody molecules: mouse antigen-binding domains with human constant region domains. Proceedings of the National Academy of Sciences of the United States of America. 1984;81(21):6851-5.
233. Mundy GR. Metastasis to bone: causes, consequences and therapeutic opportunities. Nature Reviews: Cancer. 2002;2(8):584-93.
234. Nakashima K, Zhou X, Kunkel G, Zhang Z, Deng JM, Behringer RR, et al. The novel zinc finger-containing transcription factor osterix is required for osteoblast differentiation and bone formation. Cell. 2002;108(1):17-29.
235. Nellis DF, Giardina SL, Janini GM, Shenoy SR, Marks JD, Tsai R, et al. Preclinical manufacture of anti-HER2 liposome-inserting, scFv-PEG-lipid conjugate. 2. Conjugate micelle identity, purity, stability, and potency analysis. Biotechnology Progress. 2005;21(1):221-32.
236. Neumann S, Coudreuse DY, van der Westhuyzen DR, Eckhardt ER, Korswagen HC, Schmitz G, et al. Mammalian Wnt3a is released on lipoprotein particles. Traffic. 2009;10(3):334-43.
237. Ning HX, Lin GT, Lue T, Lin CS. Mesenchymal stem cell marker Stro-1 is a 75kd endothelial antigen. Biochemical and Biophysical Research Communications. 2011;413(2):353-7.
238. Nusse R, Varmus HE. Many tumors induced by the mouse mammary tumor virus contain a provirus integrated in the same region of the host genome. Cell. 1982;31(1):99-109.
239. Nusse R, Varmus H. Three decades of Wnts: a personal perspective on how a scientific field developed. EMBO Journal. 2012;31(12):2670-84.
240. Ominsky MS, Vlasseros F, Jolette J, Smith SY, Stouch B, Doellgast G, et al. Two doses of sclerostin antibody in cynomolgus monkeys increases bone formation, bone mineral density, and bone strength. Journal of Bone and Mineral Research. 2010;25(5):948-59.
241. Orte A, Birkett NR, Clarke RW, Devlin GL, Dobson CM, Klenerman D. Direct characterization of amyloidogenic oligomers by single-molecule fluorescence. Proceedings of the National Academy of Sciences of the United States of America. 2008;105(38):14424-9.
242. Owen M, Friedenstein AJ. Stromal stem cells: marrow-derived osteogenic precursors. Ciba Foundation Symposium. 1988;136:42-60.
243. Padhi D, Jang G, Stouch B, Fang L, Posvar E. Single-dose, placebo-controlled, randomized study of AMG 785, a sclerostin monoclonal antibody. Journal of Bone and Mineral Research. 2011;26(1):19-26.
244. Palumbo C, Palazzini S, Zaffe D, Marotti G. Osteocyte differentiation in the tibia of newborn rabbit: an ultrastructural study of the formation of cytoplasmic processes. Acta Anatomica. 1990;137(4):350-8.

245. Panakova D, Sprong H, Marois E, Thiele C, Eaton S. Lipoprotein particles are required for Hedgehog and Wingless signalling. Nature. 2005;435(7038):58-65.

246. Pareta RA, Taylor E, Webster TJ. Increased osteoblast density in the presence of novel calcium phosphate coated magnetic nanoparticles. Nanotechnology. 2008;19(26):265101.

247. Park D, Spencer JA, Koh BI, Kobayashi T, Fujisaki J, Clemens TL, et al. Endogenous bone marrow MSCs are dynamic, fate-restricted participants in bone maintenance and regeneration. Cell Stem Cell. 2012;10(3):259-72.

248. Park JW, Hong K, Kirpotin DB, Colbern G, Shalaby R, Baselga J, et al. Anti-HER2 immunoliposomes: enhanced efficacy attributable to targeted delivery. Clinical Cancer Research. 2002;8(4):1172-81.

249. Pernicova I, Middleton ET, Aye M. Rash, strontium ranelate and DRESS syndrome put into perspective. European Medicine Agency on the alert. Osteoporosis International. 2008;19(12):1811-2.

250. Petros RA, DeSimone JM. Strategies in the design of nanoparticles for therapeutic applications. Nature Reviews: Drug Discovery. 2010;9(8):615-27.

251. Pierelli L, Bonanno G, Rutella S, Marone M, Scambia G, Leone G. CD105 (endoglin) expression on hematopoietic stem/progenitor cells. Leukemia and Lymphoma. 2001;42(6):1195-206.

252. Pinzone JJ, Hall BM, Thudi NK, Vonau M, Qiang YW, Rosol TJ, et al. The role of Dickkopf-1 in bone development, homeostasis, and disease. Blood. 2009;113(3):517-25.

253. Platt VM, Szoka FC, Jr. Anticancer therapeutics: targeting macromolecules and nanocarriers to hyaluronan or CD44, a hyaluronan receptor. Molecular Pharmaceutics. 2008;5(4):474-86.

254. Popelut A, Rooker SM, Leucht P, Medio M, Brunski JB, Helms JA. The acceleration of implant osseointegration by liposomal Wnt3a. Biomaterials. 2010;31(35):9173-81.

255. Porter CJ, Moghimi SM, Illum L, Davis SS. The polyoxyethylene/polyoxypropylene block co-polymer poloxamer-407 selectively redirects intravenously injected microspheres to sinusoidal endothelial cells of rabbit bone marrow. FEBS Letters. 1992;305(1):62-6.

256. Prockop DJ. Marrow stromal cells as stem cells for nonhematopoietic tissues. Science. 1997;276(5309):71-4.

257. Puchtler H, Meloan SN, Terry MS. On the history and mechanism of alizarin and alizarin red S stains for calcium. Journal of Histochemistry and Cytochemistry. 1969;17(2):110-24.

258. Qian H, Le Blanc K, Sigvardsson M. Primary mesenchymal stem and progenitor cells from bone marrow lack expression of CD44 protein. Journal of Biological Chemistry. 2012;287(31):25795-807.

259. Qiu P, Simonds EF, Bendall SC, Gibbs KD, Jr., Bruggner RV, Linderman MD, et al. Extracting a cellular hierarchy from high-dimensional cytometry data with SPADE. Nature Biotechnology. 2011;29(10):886-91.

260. Qiu W, Andersen TE, Bollerslev J, Mandrup S, Abdallah BM, Kassem M. Patients with high bone mass phenotype exhibit enhanced osteoblast differentiation and inhibition of adipogenesis of human mesenchymal stem cells. Journal of Bone and Mineral Research. 2007;22(11):1720-31.

261. Quarto N, Behr B, Longaker MT. Opposite spectrum of activity of canonical Wnt signaling in the osteogenic context of undifferentiated and differentiated mesenchymal cells: implications for tissue engineering. Tissue Eng Part A. 2010;16(10):3185-97.

262. Quirici N, Soligo D, Bossolasco P, Servida F, Lumini C, Deliliers GL. Isolation of bone marrow mesenchymal stem cells by anti-nerve growth factor receptor antibodies. Experimental Hematology. 2002;30(7):783-91.

263. Raffaghello L, Pagnan G, Pastorino F, Cosimo E, Brignole C, Marimpietri D, et al. In vitro and in vivo antitumor activity of liposomal Fenretinide targeted to human neuroblastoma. International Journal of Cancer. 2003;104(5):559-67.

264. Raisz LG. Pathogenesis of osteoporosis: concepts, conflicts, and prospects. Journal of Clinical Investigation. 2005;115(12):3318-25.

265. Ramachandran M. Basic Orthopaedic Sciences: Hodder Arnold; 2007. p. 36-9

266. Rawadi G, Vayssiere B, Dunn F, Baron R, Roman-Roman S. BMP-2 controls alkaline phosphatase expression and osteoblast mineralization by a Wnt autocrine loop. Journal of Bone and Mineral Research. 2003;18(10):1842-53.

267. Rey JP, Ellies DL. Wnt modulators in the biotech pipeline. Developmental Dynamics. 2010;239(1):102-14.

268. Reya T, Duncan AW, Ailles L, Domen J, Scherer DC, Willert K, et al. A role for Wnt signalling in self-renewal of haematopoietic stem cells. Nature. 2003;423(6938):409-14.

269. Reya T, Clevers H. Wnt signalling in stem cells and cancer. Nature. 2005;434(7035):843-50.

270. Rodriguez-Merchan EC, Forriol F. Nonunion: general principles and experimental data. Clinical Orthopaedics and Related Research. 2004(419):4-12.

271. Ross AC. The 2011 report on dietary reference intakes for calcium and vitamin D. Public Health Nutrition. 2011;14(5):938-9.

272. Rossouw JE, Anderson GL, Prentice RL, LaCroix AZ, Kooperberg C, Stefanick ML, et al. Risks and benefits of estrogen plus progestin in healthy postmenopausal women: principal results From the Women's Health Initiative randomized controlled trial. JAMA. 2002;288(3):321-33.

273. Rot C, Stern T, Blecher R, Friesem B, Zelzer E. A Mechanical Jack-like Mechanism Drives Spontaneous Fracture Healing in Neonatal Mice. Developmental Cell. 2014;31(2):159-70.

274. Rotherham M, Henstock JR, Qutachi O, Shakesheff K, El Haj AJ. Regulation of Wnt signalling and promotion of bone mineralisation using peptide-conjugated magnetic nanoparticles. European Cells and Materials. 2015;29(3):95.

275. Rucci N. Molecular biology of bone remodelling. Clin Cases Miner Bone Metab. 2008;5(1):49-56.

276. Rudge F, Dale T. Therapeutic Targetingof the Wnt Signaling Network. Wnt Signaling in Development and Disease: John Wiley & Sons, Inc; 2014. p. 421-44.

277. Sacchetti B, Funari A, Michienzi S, Di Cesare S, Piersanti S, Saggio I, et al. Self-renewing osteoprogenitors in bone marrow sinusoids can organize a hematopoietic microenvironment. Cell. 2007;131(2):324-36.

278. Sakaguchi Y, Sekiya I, Yagishita K, Ichinose S, Shinomiya K, Muneta T. Suspended cells from trabecular bone by collagenase digestion become virtually identical to mesenchymal stem cells obtained from marrow aspirates. Blood. 2004;104(9):2728-35.

279. Salari Sharif P, Abdollahi M, Larijani B. Current, new and future treatments of osteoporosis. Rheumatology International. 2011;31(3):289-300.

280. Sanchez-Freire V, Ebert AD, Kalisky T, Quake SR, Wu JC. Microfluidic single-cell real-time PCR for comparative analysis of gene expression patterns. Nature Protocols. 2012;7(5):829-38.

281. Sato M. Upregulation of the Wnt/beta-catenin pathway induced by transforming growth factor-beta in hypertrophic scars and keloids. Acta Dermato-Venereologica. 2006;86(4):300-7.

282. Satomura K, Krebsbach P, Bianco P, Gehron Robey P. Osteogenic imprinting upstream of marrow stromal cell differentiation. Journal of Cellular Biochemistry. 2000;78(3):391-403.

283. Saveyn H, De Baets B, Thas O, Hole P, Smith J, Van der Meeren P. Accurate particle size distribution determination by nanoparticle tracking analysis based on 2-D Brownian dynamics simulation. Journal of Colloid and Interface Science. 2010;352(2):593-600.

284. Schettini DA, Ribeiro RR, Demicheli C, Rocha OG, Melo MN, Michalick MS, et al. Improved targeting of antimony to the bone marrow of dogs using liposomes of reduced size. International Journal of Pharmaceutics. 2006;315(1-2):140-7.

285. Secreto FJ, Hoeppner LH, Westendorf JJ. Wnt signaling during fracture repair. Curr Osteoporos Rep. 2009;7(2):64-9.

286. Seeman E, Delmas PD, Hanley DA, Sellmeyer D, Cheung AM, Shane E, et al. Microarchitectural deterioration of cortical and trabecular bone: differing effects of denosumab and alendronate. Journal of Bone and Mineral Research. 2010;25(8):1886-94.

287. Selser JC, Yeh Y, Baskin RJ. A light-scattering characterization of membrane vesicles. Biophysical Journal. 1976;16(4):337-56.

288. Seto ES, Bellen HJ. Internalization is required for proper Wingless signaling in Drosophila melanogaster. Journal of Cell Biology. 2006;173(1):95-106.

289. Shah DA, Kwon SJ, Bale SS, Banerjee A, Dordick JS, Kane RS. Regulation of stem cell signaling by nanoparticle-mediated intracellular protein delivery. Biomaterials. 2011;32(12):3210-9.

290. Sharma A, Sharma US. Liposomes in drug delivery: Progress and limitations. . International Journal of Pharmaceutics. 1997(154):123-40.

291. Shtutman M, Zhurinsky J, Simcha I, Albanese C, D'Amico M, Pestell R, et al. The cyclin D1 gene is a target of the beta-catenin/LEF-1 pathway. Proceedings of the National Academy of Sciences of the United States of America. 1999;96(10):5522-7.

292. Simmons PJ, Torok-Storb B. Identification of stromal cell precursors in human bone marrow by a novel monoclonal antibody, STRO-1. Blood. 1991;78(1):55-62.

293. Sou K, Goins B, Oyajobi BO, Travi BL, Phillips WT. Bone marrow-targeted liposomal carriers. Expert Opin Drug Deliv. 2011;8(3):317-28.

294. Sou K. Advanced Drug Carriers Targeting Bone Marrow. 2012.

295. Spira G, Bargellesi A, Teillaud JL, Scharff MD. The identification of monoclonal class switch variants by sib selection and an ELISA assay. Journal of Immunological Methods. 1984;74(2):307-15.

296. Stanford CM, Jacobson PA, Eanes ED, Lembke LA, Midura RJ. Rapidly forming apatitic mineral in an osteoblastic cell line (UMR 106-01 BSP). Journal of Biological Chemistry. 1995;270(16):9420-8.

297. Stevens JR, Miranda-Carboni GA, Singer MA, Brugger SM, Lyons KM, Lane TF. Wnt10b deficiency results in age-dependent loss of bone mass and progressive reduction of mesenchymal progenitor cells. Journal of Bone and Mineral Research. 2010;25(10):2138-47.

298. Stolzing A, Jones E, McGonagle D, Scutt A. Age-related changes in human bone marrow-derived mesenchymal stem cells: consequences for cell therapies. Mechanisms of Ageing and Development. 2008;129(3):163-73.

299. Strebhardt K, Ullrich A. Paul Ehrlich's magic bullet concept: 100 years of progress. Nature Reviews: Cancer. 2008;8(6):473-80.

300. Sutherland HJ, Eaves CJ, Eaves AC, Dragowska W, Lansdorp PM. Characterization and partial purification of human marrow cells capable of initiating long-term hematopoiesis in vitro. Blood. 1989;74(5):1563-70.

301. Suzuki R, Takizawa T, Kuwata Y, Mutoh M, Ishiguro N, Utoguchi N, et al. Effective anti-tumor activity of oxaliplatin encapsulated in transferrin-PEG-liposome. International Journal of Pharmaceutics. 2008;346(1-2):143-50.

302. Swami A, Reagan MR, Basto P, Mishima Y, Kamaly N, Glavey S, et al. Engineered nanomedicine for myeloma and bone microenvironment targeting. Proceedings of the National Academy of Sciences of the United States of America. 2014;111(28):10287-92.

303. Szoka FC, Jr. The future of liposomal drug delivery. Biotechnology and Applied Biochemistry. 1990;12(5):496-500.

304. Taguchi K, Ogawa R, Migita M, Hanawa H, Ito H, Orimo H. The role of bone marrow-derived cells in bone fracture repair in a green fluorescent protein chimeric mouse model. Biochemical and Biophysical Research Communications. 2005;331(1):31-6.

305. Takada I, Kouzmenko AP, Kato S. Wnt and PPARgamma signaling in osteoblastogenesis and adipogenesis. Nat Rev Rheumatol. 2009;5(8):442-7.

306. Tan SH, Senarath-Yapa K, Chung MT, Longaker MT, Wu JY, Nusse R. Wnts produced by Osterix-expressing osteolineage cells regulate their proliferation and differentiation. Proceedings of the National Academy of Sciences of the United States of America. 2014;111(49):E5262-71.

307. Tare RS, Babister JC, Kanczler J, Oreffo RO. Skeletal stem cells: phenotype, biology and environmental niches informing tissue regeneration. Molecular and Cellular Endocrinology. 2008;288(1-2):11-21.

308. Teitelbaum SL. Bone resorption by osteoclasts. Science. 2000;289(5484):1504-8.

309. Thompson Z, Miclau T, Hu D, Helms JA. A model for intramembranous ossification during fracture healing. Journal of Orthopaedic Research. 2002;20(5):1091-8.

310. Torchilin VP. Recent advances with liposomes as pharmaceutical carriers. Nature Reviews: Drug Discovery. 2005;4(2):145-60.

311. Torchilin VP. Multifunctional, stimuli-sensitive nanoparticulate systems for drug delivery. Nature Reviews: Drug Discovery. 2014;13(11):813-27.

312. Tormin A, Li O, Brune JC, Walsh S, Schutz B, Ehinger M, et al. CD146 expression on primary nonhematopoietic bone marrow stem cells is correlated with in situ localization. Blood. 2011;117(19):5067-77.

313. Tresset G. The multiple faces of self-assembled lipidic systems. PMC Biophys. 2009;2(1):3.

314. Tsaousi A, Mill C, George SJ. The Wnt pathways in vascular disease: lessons from vascular development. Current Opinion in Lipidology. 2011;22(5):350-7.

315. Tseng YL, Liu JJ, Hong RL. Translocation of liposomes into cancer cells by cell-penetrating peptides penetratin and tat: a kinetic and efficacy study. Molecular Pharmacology. 2002;62(4):864-72.

316. Tzioupis C, Giannoudis PV. Prevalence of long-bone non-unions. Injury. 2007;38 Suppl 2:S3-9.

317. Urbinati G, Marsaud V, Renoir JM. Anticancer drugs in liposomal nanodevices: a target delivery for a targeted therapy. Current Topics in Medicinal Chemistry. 2012;12(15):1693-712.

318. Valkenburg KC, Graveel CR, Zylstra-Diegel CR, Zhong Z, Williams BO. Wnt/beta-catenin Signaling in Normal and Cancer Stem Cells. Cancers. 2011;3(2):2050-79.

319. Veeman MT, Axelrod JD, Moon RT. A second canon. Functions and mechanisms of beta-catenin-independent Wnt signaling. Developmental Cell. 2003;5(3):367-77.

320. Veronese FM, Pasut G. PEGylation, successful approach to drug delivery. Drug Discovery Today. 2005;10(21):1451-8.

321. Wang S, Wang X, Draenert FG, Albert O, Schroder HC, Mailander V, et al. Bioactive and biodegradable silica biomaterial for bone regeneration. Bone. 2014;67:292-304.

322. Watson JT, Foo T, Wu J, Moed BR, Thorpe M, Schon L, et al. CD271 as a marker for mesenchymal stem cells in bone marrow versus umbilical cord blood. Cells Tissues Organs. 2013;197(6):496-504.

323. Weber PC, Ohlendorf DH, Wendoloski JJ, Salemme FR. Structural origins of high-affinity biotin binding to streptavidin. Science. 1989;243(4887):85-8.

324. Weinstein JN, Yoshikami S, Henkart P, Blumenthal R, Hagins WA. Liposome-cell interaction: transfer and intracellular release of a trapped fluorescent marker. Science. 1977;195(4277):489-92.

325. Whyte JL, Smith AA, Helms JA. Wnt Signaling and Injury Repair. Cold Spring Harbor Perspectives in Biology. 2012;4(8).

326. Willert K, Brown JD, Danenberg E, Duncan AW, Weissman IL, Reya T, et al. Wnt proteins are lipid-modified and can act as stem cell growth factors. Nature. 2003;423(6938):448-52.

327. Wong AP, Dutly AE, Sacher A, Lee H, Hwang DM, Liu M, et al. Targeted cell replacement with bone marrow cells for airway epithelial regeneration. American Journal of Physiology: Lung Cellular and Molecular Physiology. 2007;293(3):L740-52.

328. Worthley DL, Churchill M, Compton JT, Tailor Y, Rao M, Si Y, et al. Gremlin 1 identifies a skeletal stem cell with bone, cartilage, and reticular stromal potential. Cell. 2015;160(1-2):269-84.

329. Wray J, Hartmann C. WNTing embryonic stem cells. Trends in Cell Biology. 2012;22(3):159-68.

330. Xu H, Duan J, Ning D, Li J, Liu R, Yang R, et al. Role of Wnt signaling in fracture healing. BMB Rep. 2014;47(12):666-72.

331. Xu L, Tang WH, Huang CC, Alexander W, Xiang LM, Pirollo KF, et al. Systemic p53 gene therapy of cancer with immunolipoplexes targeted by anti-transferrin receptor scFv. Molecular Medicine. 2001;7(10):723-34.

332. Yadav VK, Ryu JH, Suda N, Tanaka KF, Gingrich JA, Schutz G, et al. Lrp5 controls bone formation by inhibiting serotonin synthesis in the duodenum. Cell. 2008;135(5):825-37.

333. Yadav VK, Balaji S, Suresh PS, Liu XS, Lu X, Li Z, et al. Pharmacological inhibition of gut-derived serotonin synthesis is a potential bone anabolic treatment for osteoporosis. Nature Medicine. 2010;16(3):308-12.

334. Yang L, Broom MF, Tucker IG. Characterization of a nanoparticulate drug delivery system using scanning ion occlusion sensing. Pharmaceutical Research. 2012;29(9):2578-86.

335. Yeung DK, Griffith JF, Antonio GE, Lee FK, Woo J, Leung PC. Osteoporosis is associated with increased marrow fat content and decreased marrow fat unsaturation: a proton MR spectroscopy study. Journal of Magnetic Resonance Imaging. 2005;22(2):279-85.

336. Young HE, Black AC, Jr. Adult stem cells. Anatomical Record Part A: Discoveries in Molecular, Cellular, and Evolutionary Biology. 2004;276(1):75-102.

337. Yuan F, Leunig M, Huang SK, Berk DA, Papahadjopoulos D, Jain RK. Microvascular permeability and interstitial penetration of sterically stabilized (stealth) liposomes in a human tumor xenograft. Cancer Research. 1994;54(13):3352-6.

338. Zalavras CG, Patzakis MJ. Open fractures: evaluation and management. Journal of the American Academy of Orthopaedic Surgeons. 2003;11(3):212-9.

339. Zannettino AC, Paton S, Kortesidis A, Khor F, Itescu S, Gronthos S. Human mulipotential mesenchymal/stromal stem cells are derived from a discrete subpopulation of STRO-1bright/CD34 /CD45(-)/glycophorin-A-bone marrow cells. Haematologica. 2007;92(12):1707-8.

340. Zhai L, Chaturvedi D, Cumberledge S. Drosophila wnt-1 undergoes a hydrophobic modification and is targeted to lipid rafts, a process that requires porcupine. Journal of Biological Chemistry. 2004;279(32):33220-7.

341. Zhang G, Guo B, Wu H, Tang T, Zhang BT, Zheng L, et al. A delivery system targeting bone formation surfaces to facilitate RNAi-based anabolic therapy. Nature Medicine. 2012;18(2):307-14.

342. Zhang R, Oyajobi BO, Harris SE, Chen D, Tsao C, Deng HW, et al. Wnt/beta-catenin signaling activates bone morphogenetic protein 2 expression in osteoblasts. Bone. 2013;52(1):145-56.

343. Zhang YF, Wang JC, Bian DY, Zhang X, Zhang Q. Targeted delivery of RGD-modified liposomes encapsulating both combretastatin A-4 and doxorubicin for tumor therapy: in vitro and in vivo studies. European Journal of Pharmaceutics and Biopharmaceutics. 2010;74(3):467-73.

344. Zhu D, Mackenzie NC, Millan JL, Farquharson C, MacRae VE. The appearance and modulation of osteocyte marker expression during calcification of vascular smooth muscle cells. PloS One. 2011;6(5):e19595.

Appendix

Reagents

Table A.1 Media composition.

Medium A: BMMNCs isolation medium reagents	
αMEM with 2.2 g of sodium bicarbonate supplemented with:	Gibco
100 U/ml penicillin and 100 µg/ml streptomycin	PAA
Medium B: Wnt signalling induction medium reagents	
αMEM with 2.2 g of sodium bicarbonate supplemented with:	Sigma
5 % FBS	Gibco
100 U/ml penicillin and 100 µg/ml streptomycin	PAA
Additionally, 100 ng/ml Wnt3A protein for 24 hours or solvent (0.5 % BSA in PBS) of Wnt3A protein as a control	R&D
Basal culture medium reagents	
αMEM with 2.2 g of sodium bicarbonate supplemented with:	Gibco
10 % FBS	Gibco
100 U/ml penicillin and 100 µg/ml streptomycin	PAA
Osteogenic medium reagents	
αMEM supplemented with:	Gibco
10 % FBS	Gibco
100 U/ml penicillin and 100 µg/ml streptomycin	PAA
100 µM sodium-2-ascorbate	Sigma
5 mM β-glycerophosphate	Sigma
10 nM dexamethasone	Sigma
MG63 and HaCaT cell lines culture medium reagents	
DMEM supplemented with:	Sigma
10 % FBS	Gibco
100 U/ml penicillin and 100 µg/ml streptomycin	PAA
3T3 Wnt reporter cell line culture medium reagents	
DMEM supplemented with:	Sigma
Growth medium concentrate	Enzo Life Sciences
or 10 % FBS	Gibco

100 U/ml penicillin and 100 µg/ml streptomycin	PAA
3T3 Wnt reporter cell line assay medium reagents	
DMEM supplemented with:	Sigma
Assay medium concentrate	Enzo Life Sciences
or 25 mM HEPES pH=7.2 and 5 % FBS	Fisher, Gibco
50 U/ml penicillin and 50 µg/ml streptomycin	PAA

Table A.2 Staining buffers

Flow cytometry buffer reagents
PBS
1 % BSA (Sigma)
2 mM EDTA (Promega)
Flow cytometry blocking buffer
PBS
1 % BSA
2 mM EDTA (Promega)
3 % goat or rat serum (Sigma)
MACS buffer reagents
PBS
0.5 % BSA
2 mM EDTA
MACS blocking buffer
αMEM
1 % BSA
1 % AB human serum (Sigma)
0.5 % FBS
Alkaline phosphatase assay buffer
5 ml 1.5 M Alkaline buffer solution (Sigma)
10 ml dH2O
30 µl Igepal CA-630 (Sigma)
Blocking and permeabilisation buffer
PBS
1 % BSA
10 % goat serum
0.3 M glycine
0.1 % Tween (Fisher)

Table A.3 Western blot reagents

Resolving gel (10 ml)	
Protogel (National Diagnostics)	3.3 ml
Resolving Buffer (National Diagnostics)	2.6 ml
dH_2O	3.9 ml
TEMED (Sigma)	10 µl
10 % APS (Sigma)	100 µl
Stacking gel (5 ml)	
Protogel (National Diagnostics)	0.65 ml
Stacking Buffer (National Diagnostics)	1.25 ml
dH_2O	3.05 ml
TEMED (Sigma)	5 µl
10 % APS (Sigma)	25 µl
SDS-PAGE running buffer 10x (1L)	
Tris (Fisher)	30.39 g
Glycine (Fisher)	144 g
SDS (Fisher)	10 g
topped up with dH_2O to 1L	
Transfer buffer (1L)	
Running buffer (10x)	80 ml
Methanol (Fisher)	200 ml
Top up with dH_2O to 1L	
Blocking buffer and antibody diluent (30 ml)	
PBS (PAA)	30 ml
Tween (Fisher)	30 µl
dried skimmed milk (Marvel)	1.5 g

Table A.4 Reagents

Reagent	**Supplier**
Annexin V Apoptosis Detection Kit eFluor® 450	eBioscience
Alkaline phosphatase standard	Sigma
Alkaline phosphatase substrate	Sigma
BIO	Sigma
Cholesterol	Sigma
Collagenase IV	Sigma
Easy Lyse Erythrocyte Lysing Reagent	Dako
FAST Violet B salts	Sigma

GeneRuler DNA ladder 50bp	Thermo Fisher
Hematoxylin solution Gill no. 3	Sigma
Lipid DMPC 14:0	Avanti Polar Lipids
Lipid DOPC 18:1	Avanti Polar Lipids
Lipid DSPE-PEG(2000)	Avanti Polar Lipids
Lipid DSPE-PEG(2000) Biotin	Avanti Polar Lipids
Lipid DSPC 18:0	Avanti Polar Lipids
Lipid DPPC 16:0	Avanti Polar Lipids
Luciferase substrate and buffer Steady Glo	Promega
Lymphoprep™ Density Gradient Medium	Axis-Shield
MACS rat anti-mouse IgM microbeads	Miltenyi Biotec
Napthol AS-MX Phosphate Alkaline Solution	Sigma
PicoPure RNA extraction kit	Invitrogen
Protein ladder Fermentas Spectra™ Multicolor Broad Range	Fermentas
Proteo Silver Stain Kit	Sigma
RNeasy Mini Kit	Qiagen
SuperScript® VILO™ cDNA Synthesis Kit	Invitrogen
TMB 1x ELISA Substrate Solution	eBioscience
Trypan blue	Sigma
Trypsin	Lonza
Virkon tablets	DuPont
Wnt3A protein and "carrier-free" Wnt3A (human)	R&D systems
Wnt3A protein (murine)	Gift from Dr Shukry Habib, Stanford

Table A.5 Antibodies

Antibody		**Working dilution**
Primary antibodies		
Mouse anti-human STRO-1 IgM	R&D systems MAB1038	1/100 (Flow cytometry) subsequent 10x dilutions starting from 1/5000 (ELISA)
Hybridoma supernate anti-human STRO-1 IgM	hybridoma cultured "in house"	500 µl undiluted, non-purified (Flow cytometry and FACS) 1 ml undiluted, non-purified (MACS) subsequent 2x dilutions starting from 1/5000 (ELISA)

Mouse Isotype control IgM from murine myeloma	Invitrogen M5909	1/100 (control for flow cytometry with hybridoma supernate STRO-1 antibody) 1/40 (control for flow cytometry with STRO-1 antibody from R&D) subsequent 10x dilutions starting from 1/2000 (ELISA)
Rabbit anti-human Osteopontin	GeneTex GTX28448	1/50 (immunostaining for microscopy)
Rabbit anti-human LAMP1	Abcam Ab24170	1/500 (Immunostaining for confocal microscopy)
Mouse anti-human EEA1	Santa Cruz Sc-53939	1/200 (Immunostaining for confocal microscopy)
Rabbit anti-human Wnt3A	Abcam Ab172612	1/10 000 (Western blot)
Primary conjugated antibodies		
Mouse anti-human CD19 FITC	made "in house" and kindly supplied by Dr Kam Hussain, Cancer Sciences, University of Southampton	1/10 (Flow cytometry)
Mouse Isotype control IgG1 FITC	BioLegend 400110	1/20 (Flow cytometry)
Mouse anti-human CD56 PE	BioLegend 318306	1/20 (Flow cytometry)
Mouse Isotype control IgG1 PE	BioLegend 400112	1/20 (Flow cytometry)
Mouse anti-human CD3 PerCP	BioLegend 344814	1/20 (Flow cytometry)
Mouse Isotype control IgG1 PerCP	BD Biosciences 559425	1/20 (Flow cytometry)
Mouse anti-human CD14 APC	eBioscience 17-0149-41	1/20 (Flow cytometry)
Mouse Isotype control IgG1 APC	BioLegend 400120	1/20 (Flow cytometry)

Mouse anti-human CD14 PE	BioLegend 325606	1/20(Flow cytometry)
Mouse Isotype control IgG1 PE	BioLegend 400114	1/40 (Flow cytometry)
Mouse anti-human CD14 Pacific Blue	BioLegend 325616	1/20 (Flow cytometry)
Mouse Isotype control IgG1 Pacific Blue	BioLegend 400131	1/40 (Flow cytometry)
Mouse anti-human CD66b PECy7	eBioscience 25-0666-41	1/20 (Flow cytometry)
Mouse Isotype control IgG2a PECy7	BioLegend 400231	1/20 (Flow cytometry)
Mouse anti-human GPA APC	BioLegend 306607	1/20 (Flow cytometry)
Mouse Isotype control IgG2b APC	BioLegend 400319	1/20 (Flow cytometry)
Mouse anti-human GPA PE	BioLegend 349106	1/40 (Flow cytometry)
Mouse Isotype control IgG2a PE	BioLegend 400211	1/40 (Flow cytometry)
Mouse anti-human CD45 AF488	BioLegend 304017	1/20 (Flow cytometry)
Mouse Isotype control IgG1 AF488	BioLegend 400129	1/40 (Flow cytometry)
	Secondary antibodies	
Goat anti-mouse IgM AF488	Invitrogen A21042	1/200 (Flow cytometry and FACS)
Goat anti-mouse IgM AF647	Invitrogen A21238	1/200 (Flow cytometry)
Rat anti-mouse IgM PE	BioLegend 406507	1/50 (Flow cytometry)
MACS rat anti-mouse IgM microbeads	Miltenyi Biotec 130-047-301	1/5; 200 µl of beads in 800 µl of MACS buffer (MACS)
Goat anti-mouse IgM polyclonal	Abcam Ab9167	1/100 (ELISA)
Goat anti-mouse IgM peroxidase-conjugate	Sigma A8786	1/15000 (ELISA)
Goat-anti rabbit IgG AF488	Invitrogen A11008	1/100 (immunostaining for microscopy)

Goat anti-mouse IgG AF594	Invitrogen A11005	1/100 (Immunostaining for confocal microscopy)
Goat anti-rabbit IgG AF594	Invitrogen A11037	1/100 (Immunostaining for confocal microscopy)
Goat anti-rabbit IgG HRP	Abcam Ab6721	1/3000 (Western blot)
	Staining kits	
Human Mesenchymal Stem Cell Multi-Color Flow Kit	R&D Systems FMC002	All antibodies used at 1/10 (Flow cytometry)
Human Haematopoietic Stem Cell Flow Kit	R&D Systems Test sample	All antibodies used at 1/10 (Flow cytometry)

Equipment

Table A.6 Equipment

Equipment	
BD FACS Canto II	BD Biosciences
BD FACS Calibur	BD Biosciences
Centrifuge Megafuge 1.0R	Heraeus
Centrifuge 5415R	Eppendorf
Digital camera Power Shot G10	Canon
ELx800 colorimetric microplate reader	Biotek
Extruder	Avanti Polar Lipids
FACS Guava	Millipore
FLx800 fluorescence microplate reader	Biotek
MACSmixTM tube rotator	Miltenyi Biotec
Microscope	Zeiss Axiovert
Microscope	Zeiss Stemi 2000
NanoDrop ND-1000	Thermo Fisher
PCR machine Veriti	Applied Biosystems
Plate heater	Jencons PLS
QuadroMACS magnetic rack	Miltenyi Biotec
Real-Time PCR system 7500	Applied Biosystems
Ultracentrifuge Optima Max	Beckman Coulter
VarioscanFlash luminometric microplate reader	Thermo Scientific

Bone marrow samples

Table A.7 Bone marrow samples.
Abbreviations: M - male; F - female; OA – osteoarthritic; OP – osteoporotic.

No.	Sample ID	Sex	Age	OA/OP	Aspirated	Isolated	Cell no. x10^6
1	M65 090212	M	65	OP	09/02/12	13/02/12	21.6
2	F78 090212	F	78	OP	09/02/12	13/02/12	4.75
3	F89 190212	F	89	OA	19/02/12	20/02/12	87
4	M91 190212	M	91	OA	19/02/12	20/02/12	175
5	F89 010312	F	89	OA	01/03/12	02/03/12	29
6	M68 090312	M	68	OP	09/03/12	12/03/12	12.8
7	F67 090312	F	67	OP	09/03/12	12/03/12	80.6
8	M66 190312	M	66	OP	19/03/12	21/03/12	3
9	M65 250312	M	65	OA	25/03/12	26/03/12	56.4
10	M84 170412	M	84	OP	17/04/12	17/04/12	38.8
11	F87 230412	F	87	OP	23/04/12	24/04/12	4
12	F63 191012	F	63	OP	19/10/12	22/10/12	10
13	F93 191012	F	93	OP	19/10/12	22/10/12	8.5
14	M63 051112	M	63	OP	05/11/12	06/11/12	50
15	M87 100113	M	87	OP	10/01/13	12/01/13	70
16	M83 250113	M	83	OP	25/01/13	26/01/13	103
17	F80 200213	F	80	OP	20/02/13	22/03/13	196
18	F94 030313	F	94	OP	03/03/13	05/03/13	270
19	F96 120813	F	96	OP	12/08/13	15/08/13	159
20	F84 060913	F	84	OA	06/09/13	10/09/13	82.5
21	F70 121013	F	70	OA	12/10/13	15/10/13	125
22	M71 181013	M	71	OP	18/10/13	21/10/13	100
23	F97 241013	F	97	OP	24/10/13	29/10/13	58
24	F75 041113	F	75	OP	04/11/13	05/11/13	75
25	M77 011113	M	77	OP	01/11/13	05/11/13	125
26	F59 141113	F	59	OA	14/11/13	18/11/13	220
27	M71 181113	M	71	OA	18/11/13	21/11/13	67
28	F86 181113	F	86	OP	18/11/13	21/11/13	37
29	F92 221113	F	92	OP	22/11/13	22/11/13	70
30	F57 271113	F	57	OA	27/11/13	28/11/13	171
31	M64 271113	M	64	OP	27/11/13	28/11/13	10.6
32	M66 271113	M	66	OP	27/11/13	28/11/13	132
33	M76 071213	M	76	OP	07/12/13	09/12/13	500
34	F73 170114	F	73	OP	17/01/14	20/01/14	98
35	F80 220114	F	80	OP	22/01/14	23/01/14	6.8

36	M72 220114	M	72	OP	22/01/14	23/01/14	1.8
37	F64 230114	F	64	OA	23/01/14	24/01/14	17.5
38	F84 230114	F	84	OA	23/01/14	24/01/14	22
39	F75 310114	F	75	OP	31/01/14	03/02/14	204
40	M91 300114	M	91	OA	30/01/14	03/02/14	14.3
41	F70 060214	F	70	OA	06/02/14	07/02/14	35
42	M57 060214	M	57	OA	06/02/14	07/02/14	62
43	M76 190214	M	76	OA	19/02/14	21/02/14	85
44	F65 190214	F	65	OA	19/02/14	21/02/14	140
45	F62 140314	F	62	OP	14/03/14	18/03/14	470
46	M68 090513	M	68	OA	09/05/14	11/05/14	221
47	F67 090513	F	67	OP	09/05/14	11/05/14	131
48	M79 130514	M	79	OP	13/05/14	14/05/14	200
49	F54 130514	F	54	OA	13/05/14	14/05/14	1.8
50	F57 190514	F	57	OP	19/05/14	20/05/14	300
51	M59 230514	M	59	OP	23/05/14	24/05/14	630
52	M66 230514	M	66	OP	23/05/14	24/05/14	181
53	M74 230514	M	74	OP	23/05/14	24/05/14	213
54	M58 240614	M	58	OP	24/06/14	25/06/14	383
55	F72 030914	F	72	OP	03/09/14	04/09/14	500
56	F80 030914	F	80	OA	03/09/14	04/09/14	200
57	M53 020914	M	53	OA	02/09/14	04/09/14	200
58	F82 100914	F	82	OA	10/09/14	11/09/14	208
59	F69 100914	F	69	OA	10/09/14	11/09/14	83
60	F78 180914	F	78	OA	18/09/14	19/09/14	125
61	F69 190914	F	69	OP	19/09/14	19/09/14	300
62	F77 220115	F	77	OA	22/01/15	24/01/15	8
63	F68 230115	F	68	OA	23/01/15	24/01/15	147.5
64	F69 230115	F	69	OA	23/01/15	24/01/15	422.5
65	M55 230315	M	55	OP	23/03/15	26/03/15	4
66	M71 230315	M	71	OP	23/03/15	26/03/15	82.5
67	M82 250315	M	82	OP	25/03/15	26/03/15	19
68	F58 010415	F	58	OP	01/04/15	03/04/15	700
69	M61 010415	M	61	OP	01/04/15	03/04/15	473
70	F84 280415	F	84	OA	28/04/15	29/04/15	65.8
71	F64 290415	F	64	OA	29/04/15	29/04/15	107.5
72	F74 300515	F	74	OP	30/05/15	31/05/15	49
73	F57 300515	F	57	OP	30/05/15	31/05/15	220
74	M64 030615	M	64	OP	03/06/15	04/05/15	169

Experiments

Flow cytometry - blood lineage gating strategy

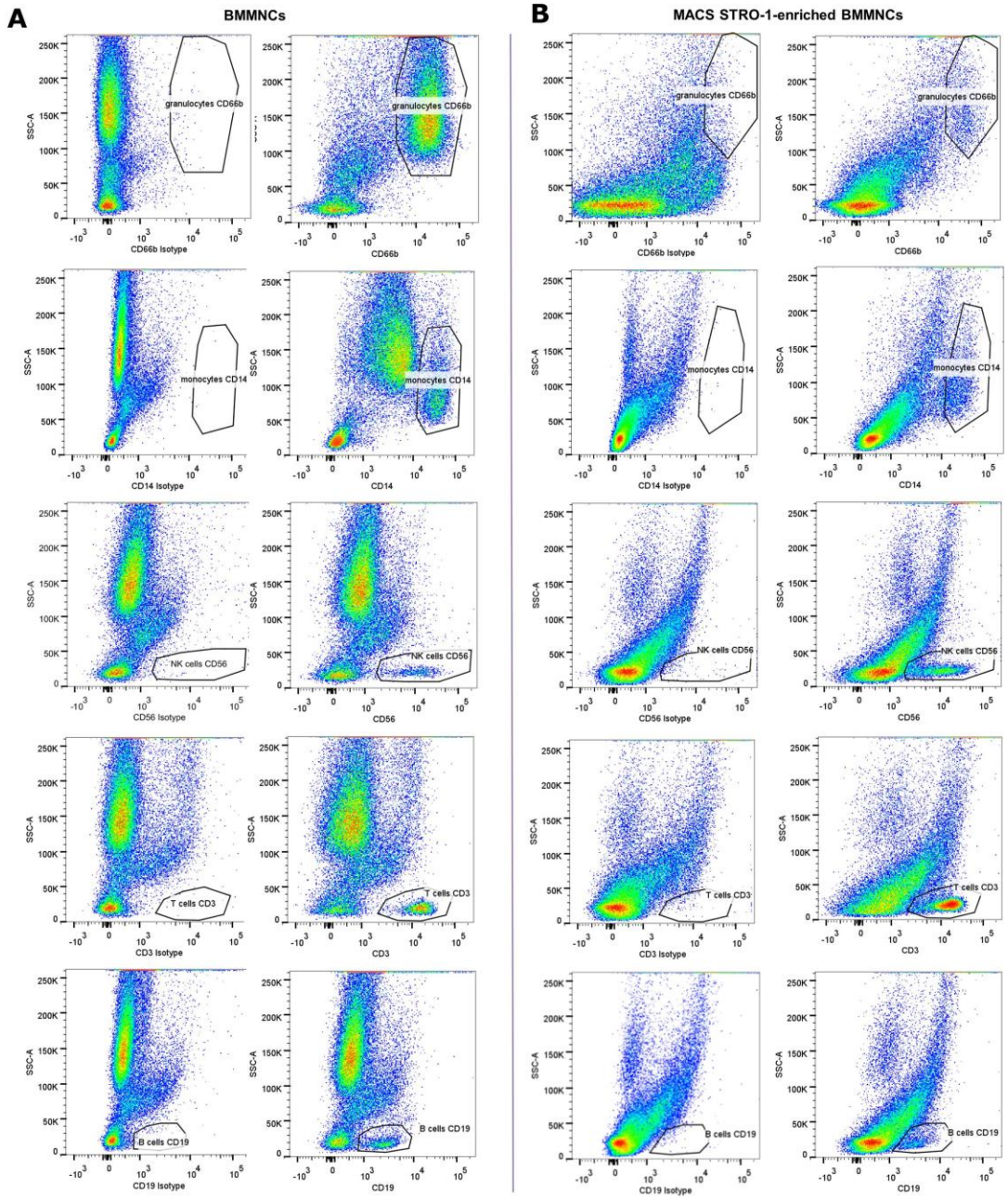

Figure A.1 Gating strategy for blood lineage staining panel.

A: Gating on granulocytes, monocytes, NK cells, T cells and B cells based on staining with isotype-matched control antibodies on BMMNC samples. B: Gating on granulocytes, monocytes, NK cells, T cells and B cells based on staining with isotype-matched control antibodies on STRO-1-enriched BMMNC samples.

Flow cytometry – HSC kit isotype controls

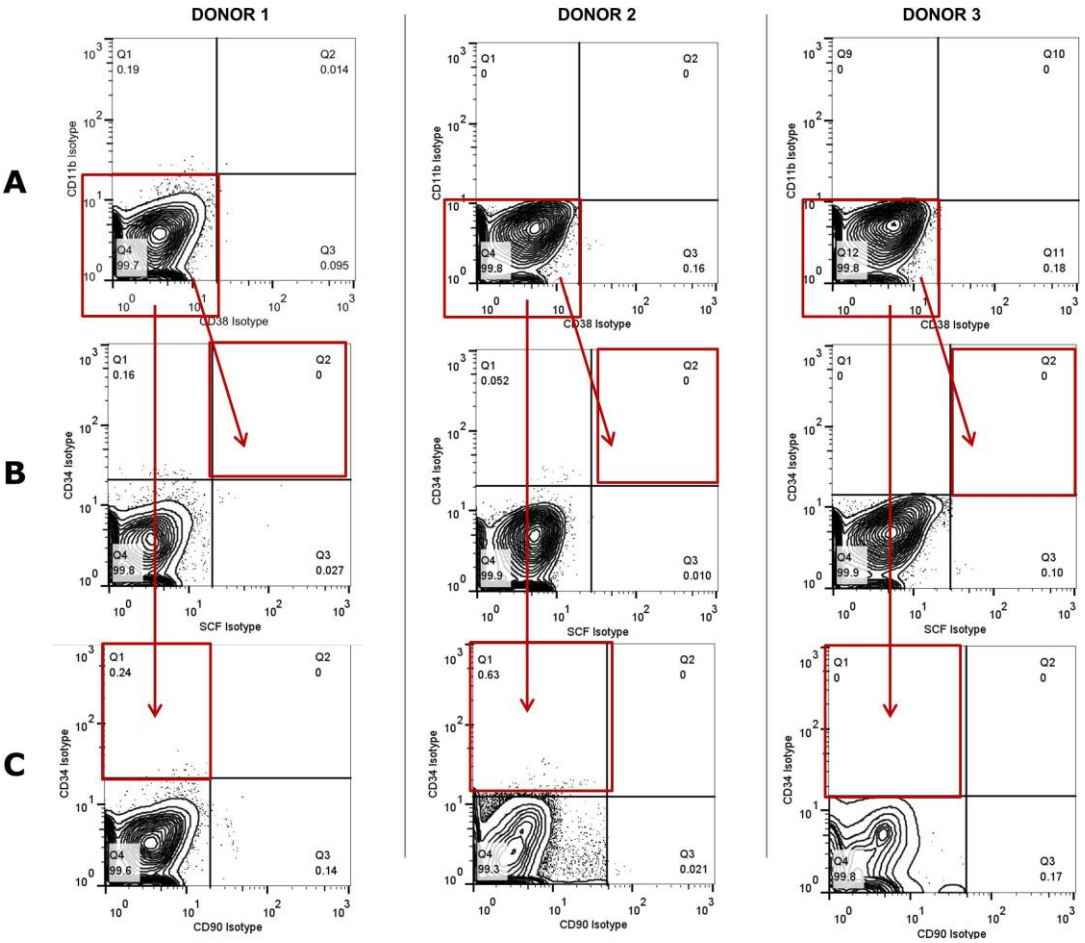

Figure A.2 Isotype controls for HSC staining panel.

Samples from 3 donors were analysed with the haematopoietic stem cell marker panel. Figures in A, B and C show the gating strategy set up based on the isotype-matched controls from the HSC kit.

Flow cytometry – haematopoietic cell staining isotype controls

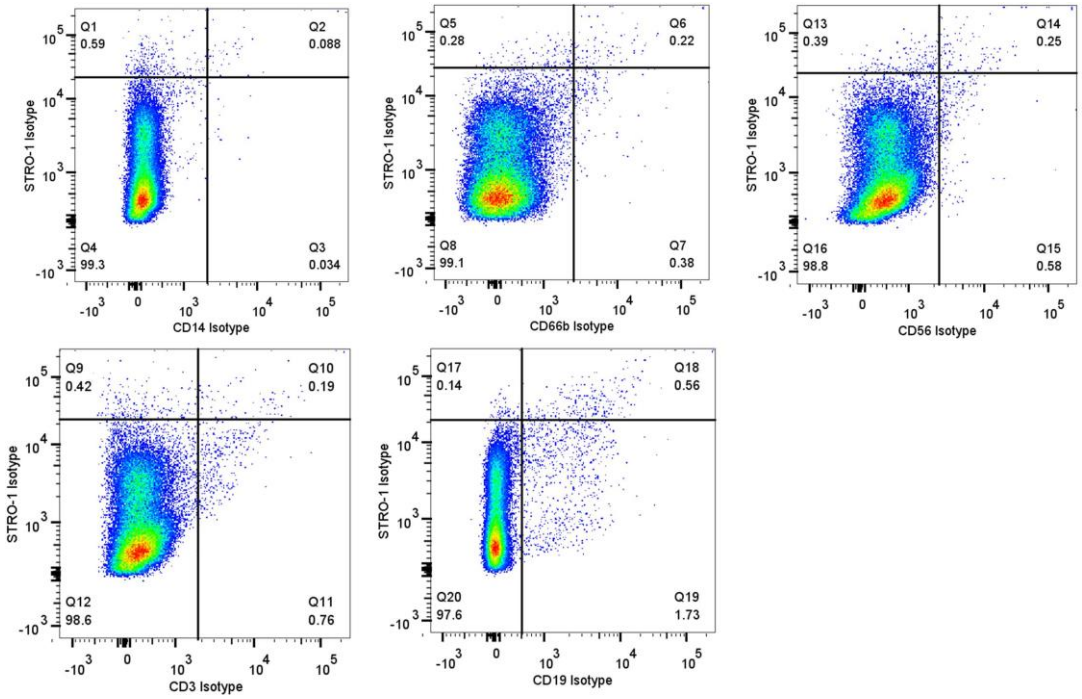

Figure A.3 Isotype controls for haematopoietic staining panel.

Quadrant dot plots depicting colocalisation of STRO-1 with haematopoietic cell markers (CD14, CD66b, CD56, CD3 and CD19) as stained with isotype-matched antibodies for this staining panel.

STRO-1 antibody - positive and negative controls

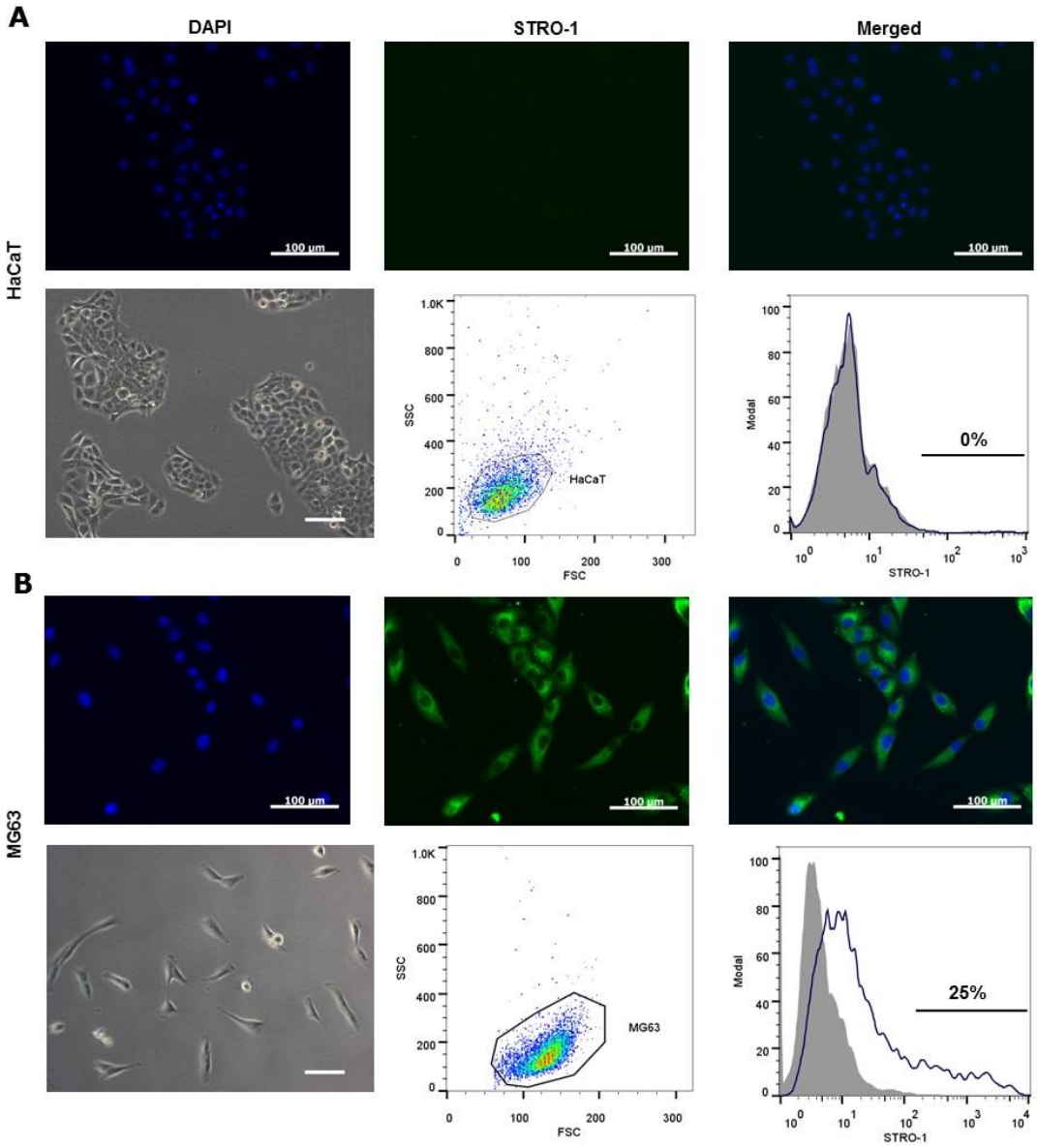

Figure A.4 STRO-1 antibody positive and negative control.

A: Human keratinocyte cell line, HaCaT cells, served as a negative control for the STRO-1 antibody. These cells did not express the STRO-1 antigen, as assessed by flow cytometry. B: Human osteosarcoma cell line, MG63 cells, served as a positive control for the STRO-1 antibody. 25 % of MG63 cells examined by flow cytometry expressed STRO-1.

ELISA – STRO-1 antibody concentration determination

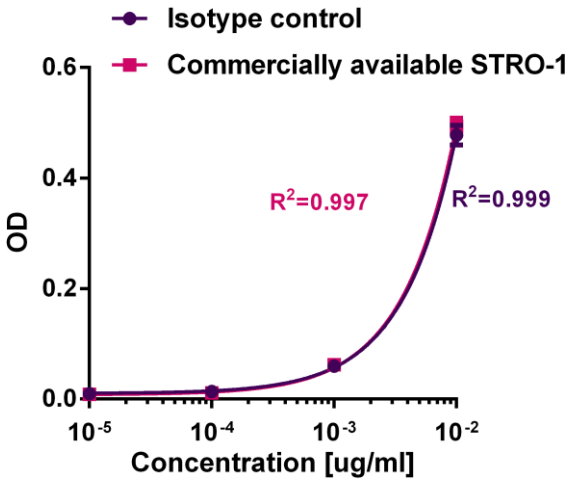

Figure A.5 ELISA standard curves.

Both the isotype antibody and commercially available STRO-1 antibody concentration resulted in very similar standard curves, hence for further testing between batches of the supernatant, only the isotype was used. Logarithmic concentration scale has been used for visualisation; linear curve fit values shown on the graph.

Table A.8 Concentration of STRO-1 antibody in the hybridoma supernatant.

Due to highl antibody content, high dilutions were tested. For future batch to batch testing of the hybridoma supernatant, two dilutions, 1 in 40000 and 1 in 80000, are sufficient to be assessed.

Dilution	Concentration [ng/ml ± SD]	Concentration x dilution [ug/ml]
1 in 20000	34.01 ± 3.63	680.11
1 in 40000	17.58 ± 1.32	703.20
1 in 80000	9.16 ± 1.01	732.54
	average	**~706 ug/ml**

qPCR and primer validation

Table A.9 Reverse transcription reaction

Incubation	25°C, 10 minutes
Reverse transcription	42°C, 120 minutes
Termination	85°C, 5 minutes
Final incubation	4°C ∞

Table A.10 Primer list

Abbreviation	Gene and transcript ID	Gene name	Sequence	Product length
Wnt target genes				
AXIN2	Gene ID: 8313 NM_004655.3	axin-2; axin-like protein; axis inhibition protein 2; conductin	F:5'CAAGGGCCAGGTCACCAA3' R:5'CCCCCAACCCATCTTCG3'	68bp
CMYC	Gene ID: 4609 NM_002467.4	myelocytomatosis viral oncogene homolog;proto-oncogene c-Myc	F:5'CACCACCAGCAGCGACTC3' R:5'GCCTGCCTCTTTTCCACA3'	78bp
CCND1	Gene ID: 595 NM_053056.2	cyclin D1	F:5'CTACCGCCTCACACGCTT3' R:5'CTTGGGGTCCATGTTCTGC3'	130bp
LEF1	Gene ID: 51176 NM_001130714.2	lymphoid enhancer-binding factor 1	F:5'AGCACGGAAAGAAAGACAGC3' R:5'GAGCTTCGTTTTCCACCTGA3'	129bp
TCF4	Gene ID: 6934 NM_001146274.1	TCF7L2 transcription factor 7-like 2	F:5'TTCATATGCAACTGTACCCCG3' R:5'GCTGCTTGTCCCTTTTCCT3'	78bp
Osteogenic genes				
ALP	Gene ID: 249 NM_001177520.1	alkaline phosphatase, liver/bone/ kidney	F:5'GGAACTCCTGACCCTTGACC3' R:5'TCCTGTTCAGCTCGTACTGC3'	86bp

BGLAP	Gene ID: 632 NM_199173.4	Osteocalcin; bone gamma-carboxyglutamate protein (BGLAP)	F:5'GGCAGCGAGGTAGTGAAGAG3' R:5'CTCACACACCTCCCTCCT3'	102bp
SPARC	Gene ID: 6678 NM_003118.3	SPARC; secreted protein, acidic, cysteine-rich (osteonectin)	F:5'GAGGAAACCGAAGAGGAGG3' R:5'GGGGTGTTGTTCTCATCCAG3'	95bp
SP7	Gene ID: 121340 NM_001173467.1	Osterix; Sp7 transcription factor	F:5'ATGGGCTCCTTTCACCTG3' R:5'GGGAAAAGGGAGGGTAATC3'	75bp
RUNX2	Gene ID: 860 NM_001024630.3	runt-related transcription factor 2; CBF-alpha-1	F:5'GTAGATGGACCTCGGGAACC3' R:5'GAGGCGGTCAGAGAACAAAC3'	78bp
Housekeeping genes				
ACTB	Gene ID: 60 NM_001101.3	actin beta	F:5'GGCATCCTCACCCTGAAGTA3' R:5'AGGTGTGGTGCCAGATTTTC3'	82bp
GAPDH	Gene ID: 2597 NM_ 001289745.1	glyceraldehyde-3-phosphate dehydrogenase; G3PD; GAPD	F:5'CCAGGTGGTCTCCTCTGACTTC3' R:5'TCATACCAGGAAATGAGCTTGACA3'	108bp

Primer validation

Figure A.6 shows dissociation curves (also called melting curves) of *ACTB, AXIN2, CCND1, LEF1, TCF4* and *CMYC* amplicons. The primers are specific for the template intended to amplify, as there is only one specific product of the RT-qPCR reaction indicated by one characteristic peak present in each graph. Therefore the newly designed primers, as well as *ACTB* primers, do not form any secondary structures, such as hairpins or primer dimers that could result in additional melting peaks when amplified. As an additional confirmation an agarose gel was run with the products of amplification and only one product was present for each primer set (Figure A.7). Figure A.8 – Figure A.12 show data from primer efficiency analysis. On graph A and B in each figure a slope of the curve resulting from plotting the logarithms of mRNA dilutions against its Ct

value is used to calculate the efficiency of each primer pair. The efficiency of *ACTB* primers assessed on different mRNA samples from STRO-1^+ cells was 116 %; 103 %; 87 %; 106 %; 106 %; respectively, and the differences between this value and the efficiencies calculated for *AXIN2* (117 %), *CCND1* (99 %), *LEF1* (85 %), *TCF4* (105 %), and *CMYC* (105 %), as plotted on graph C of each figure, are less than 0.1 (10 %). This means that the efficiencies are similar enough to use the relative ΔΔCt method for calculations from subsequent RT-qPCR experiments.

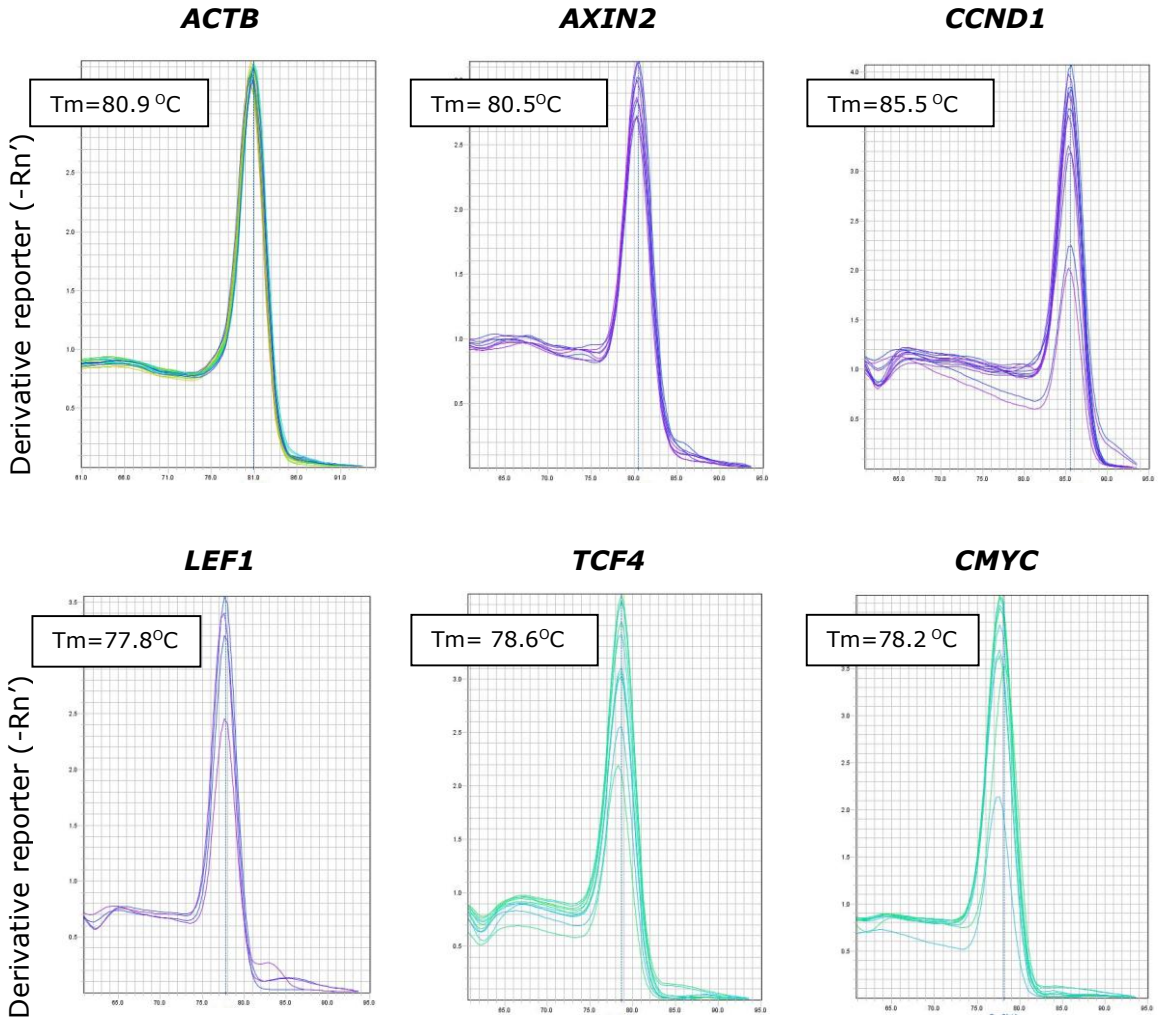

Figure A.6 Primer validation – dissociation curves.
Representative melting curves showing melting temperature (Tm) values of *ACTB*, *AXIN2, CCND1, LEF1, TCF4,* and *CMYC* amplicons from primer validation RT-qPCR experiments.

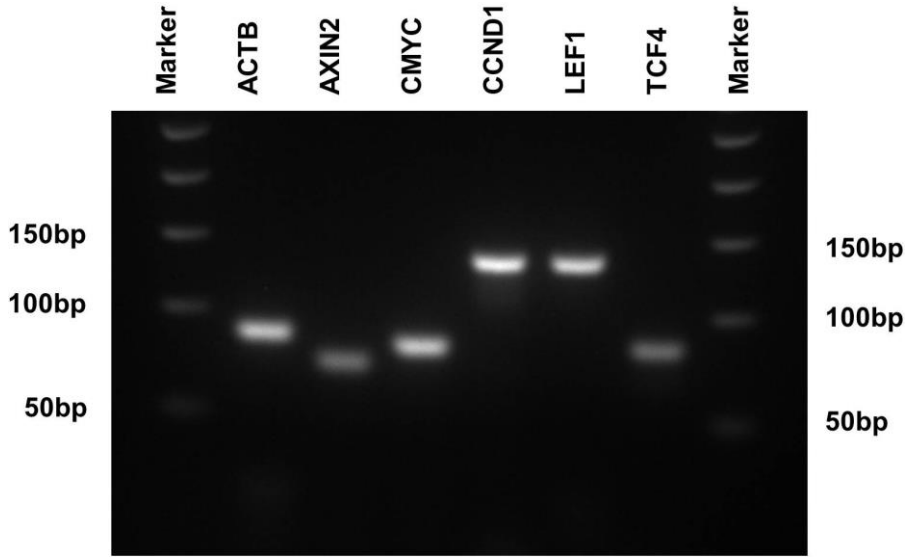

Figure A.7 Primer validation – amplification products.

Amplification products of *ACTB*, *AXIN2, CMYC, CCND1, LEF1* and *TCF4* primers, showing bands specific for the size of intended amplicons from primer validation RT-qPCR experiments.

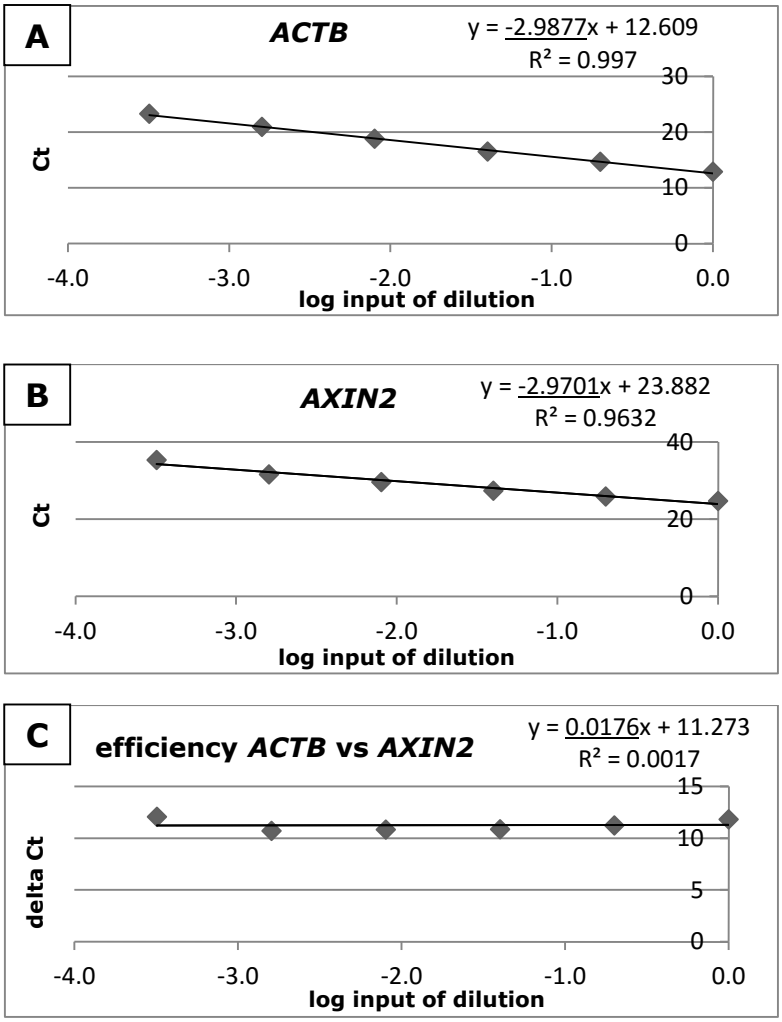

ACTB primers efficiency [%]

$= (10^{\frac{1}{slope}} - 1) * 100\ \%$

$= (10^{\frac{1}{-2.9877}} - 1) * 100\ \%$

$= 116\ \%$

AXIN2 primers efficiency [%]

$= (10^{\frac{1}{slope}} - 1) * 100\ \%$

$= (10^{\frac{1}{-2.9701}} - 1) * 100\ \%$

$= 117\ \%$

Δ Ct = Ct target gene– Ct endogenous control

Slope of Δ Ct for *ACTB* and *AXIN2* = 0.0176

0.0176 <0.1

Figure A.8 *AXIN2* primer validation results.

RT-qPCR efficiencies of *ACTB* (A) and *AXIN2* (B) primers calculated from the gradient of graphs presenting Ct values of 6 10-fold dilutions of cDNA. Ct values shown are a mean of 2 replicates. Differences between Ct values of *ACTB* and *AXIN2* for each dilution are shown in (C) enabling the comparison of RT-qPCR efficiencies between target gene (*AXIN2*) and endogenous control (*ACTB*).

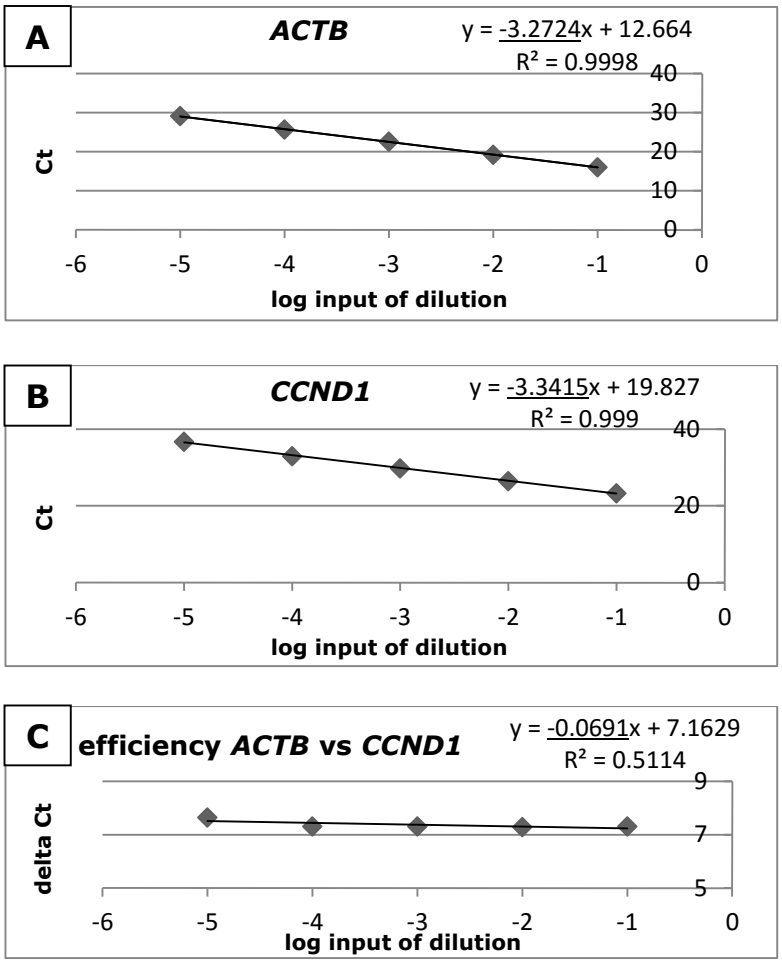

$ACTB$ primers efficiency [%]

$= (10^{\frac{1}{slope}} - 1) * 100\ \%$

$= (10^{\frac{1}{-3.2724}} - 1) * 100\ \%$

$= 103\ \%$

$CCND1$ primers efficiency [%]

$= (10^{\frac{1}{slope}} - 1) * 100\ \%$

$= (10^{\frac{1}{-3.3415}} - 1) * 100\ \%$

$= 99\ \%$

Δ Ct = Ct target gene– Ct endogenous control

Slope of Δ Ct for *ACTB* and *CCND1* = 0.0691

0.0691 <0.1

Figure A.9 *CCND1* primer validation results.

RT-qPCR efficiencies of *ACTB* (A) and *CCND1* (B) primers calculated from the gradient of graphs presenting Ct values of 5 subsequent 10-fold dilutions of cDNA. Ct values shown are a mean of 2 replicates. Differences between Ct values of *ACTB* and *CCND1* for each dilution are shown in (C) enabling the comparison of RT-qPCR efficiencies between target gene (*CCND1*) and endogenous control (*ACTB*).

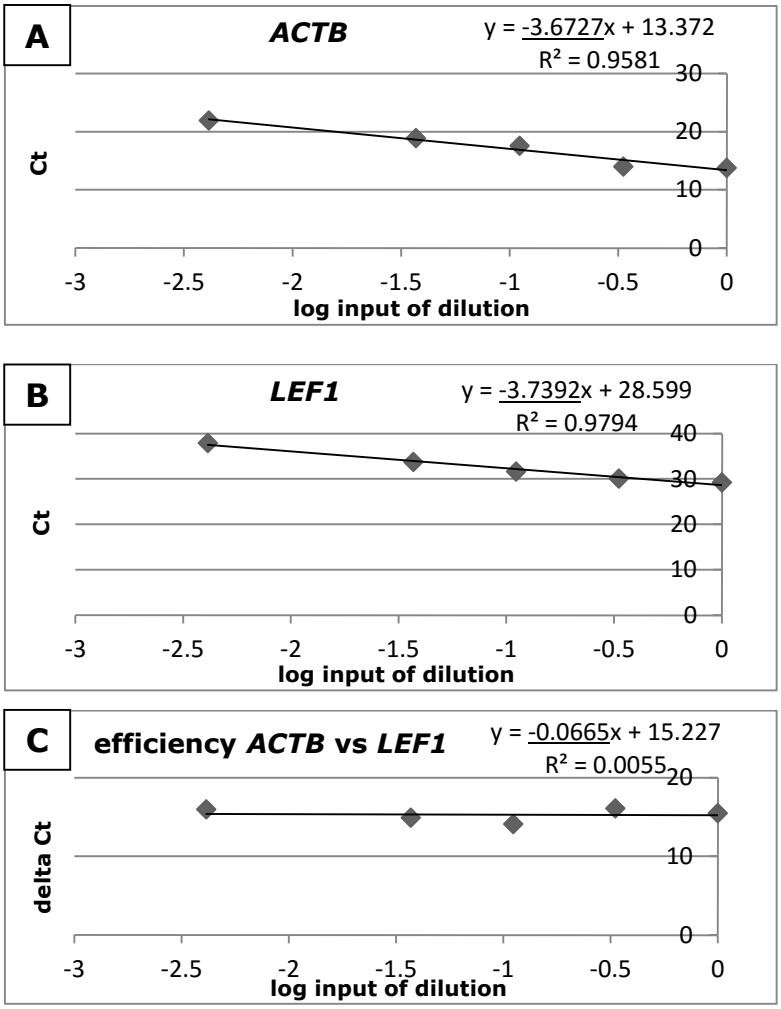

ACTB primers efficiency [%]

$= (10^{\frac{1}{slope}} - 1) * 100\ \%$

$= (10^{\frac{1}{-3.6727}} - 1) * 100\ \%$

$= 87\ \%$

*LEF*1 primers efficiency [%]

$= (10^{\frac{1}{slope}} - 1) * 100\ \%$

$= (10^{\frac{1}{-3.7392}} - 1) * 100\ \%$

$= 85\ \%$

Δ Ct = Ct target gene– Ct endogenous control

Slope of Δ Ct for *ACTB* and *LEF1* = 0.0665

0.0665 <0.1

Figure A.10 *LEF1* primer validation results.

RT-qPCR efficiencies of *ACTB* (A) and *LEF1* (B) primers calculated from the gradient of graphs presenting Ct values of 5 3-fold dilutions of cDNA. Ct values shown are a mean of 2 replicates. Differences between Ct values of *ACTB* and *LEF1* for each dilution are shown in (C) enabling the comparison of RT-qPCR efficiencies between target gene (*LEF1*) and endogenous control (*ACTB*).

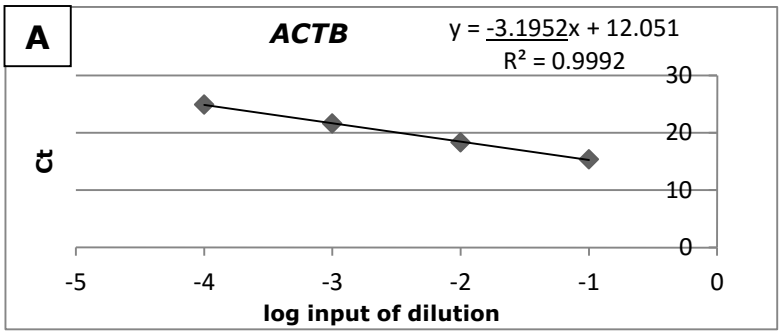

ACTB primers efficiency [%]

$= (10^{\frac{1}{slope}} - 1) * 100\ \%$

$= (10^{\frac{1}{-3.1952}} - 1) * 100\ \%$

$= 106\ \%$

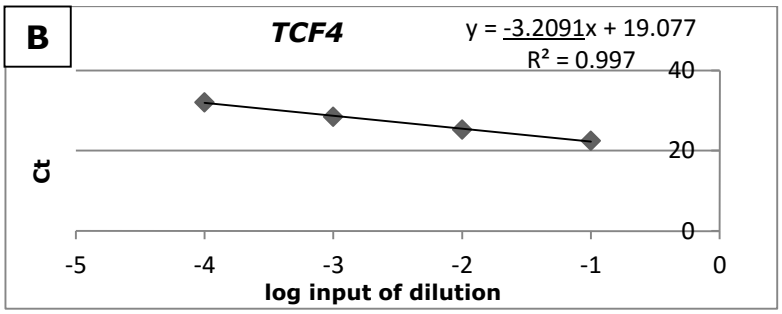

TCF4 primers efficiency [%]

$= (10^{\frac{1}{slope}} - 1) * 100\ \%$

$= (10^{\frac{1}{-3.2091}} - 1) * 100\ \%$

$= 105\ \%$

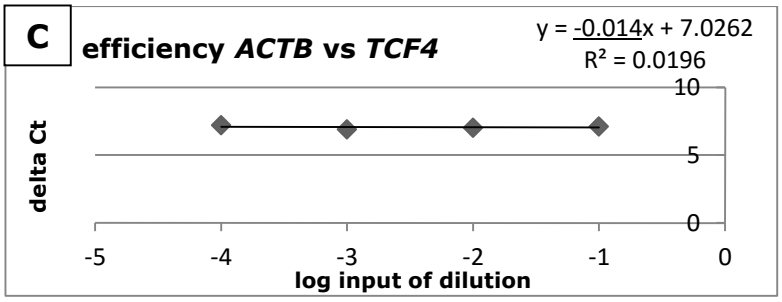

Δ Ct = Ct target gene– Ct endogenous control

Slope of Δ Ct for *ACTB* and *TCF4* = 0.014

0.014 <0.1

Figure A.11 *TCF4* primer validation results.

RT-qPCR efficiencies of *ACTB* (A) and *TCF4* (B) primers calculated from the gradient of graphs presenting Ct values of 4 subsequent 10-fold dilutions of cDNA. Ct values shown are a mean of 2 replicates. Differences between Ct values of *ACTB* and *TCF4* for each dilution are shown in (C) enabling the comparison of RT-qPCR efficiencies between target gene (*TCF4*) and endogenous control (*ACTB*).

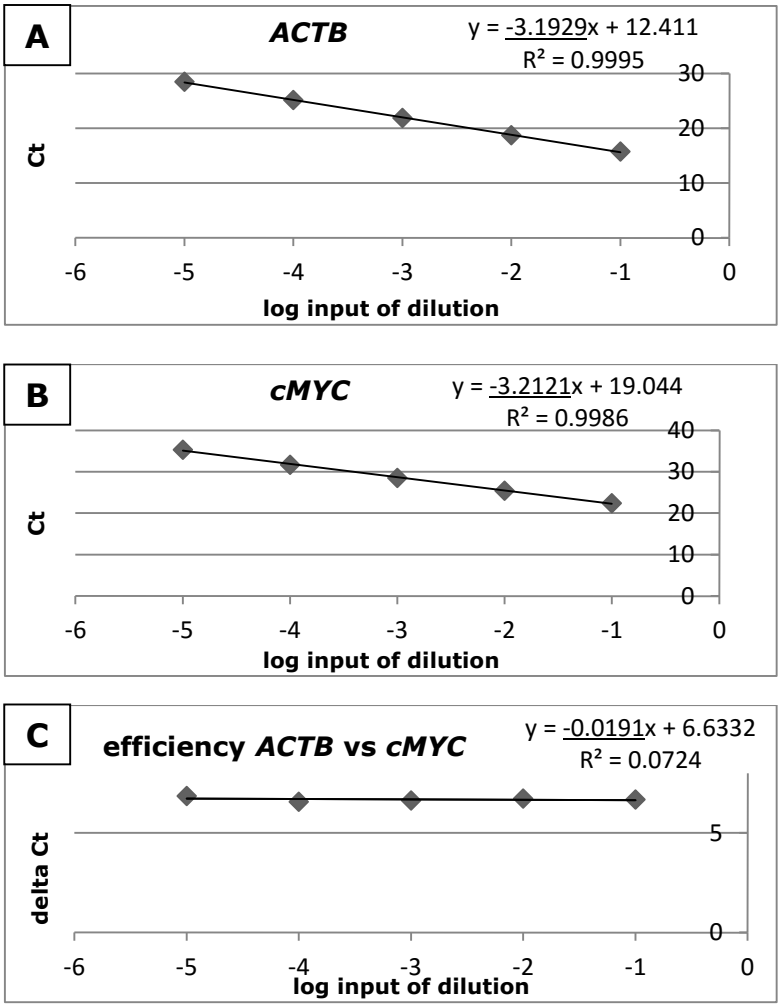

ACTB primers efficiency [%]

$= (10^{\frac{1}{slope}} - 1) * 100\ \%$

$= (10^{\frac{1}{-3.1929}} - 1) * 100\ \%$

$= 106\ \%$

CMYC primers efficiency [%]

$= (10^{\frac{1}{slope}} - 1) * 100\ \%$

$= (10^{\frac{1}{-3.2121}} - 1) * 100\ \%$

$= 105\ \%$

Δ Ct = Ct target gene– Ct endogenous control

Slope of Δ Ct for *ACTB* and *CMYC* = 0.0191

0.0191 <0.1

Figure A.12 *CMYC* primer validation results.

RT-qPCR efficiencies of *ACTB* (A) and *CMYC* (B) primers calculated from the gradient of graphs presenting Ct values of 5 subsequent 10-fold dilutions of cDNA. Ct values shown are a mean of 2 replicates. Differences between Ct values of *ACTB* and *CMYC* for each dilution are shown in (C) enabling the comparison of RT-qPCR efficiencies between target gene (*CMYC*) and endogenous control (*ACTB*).

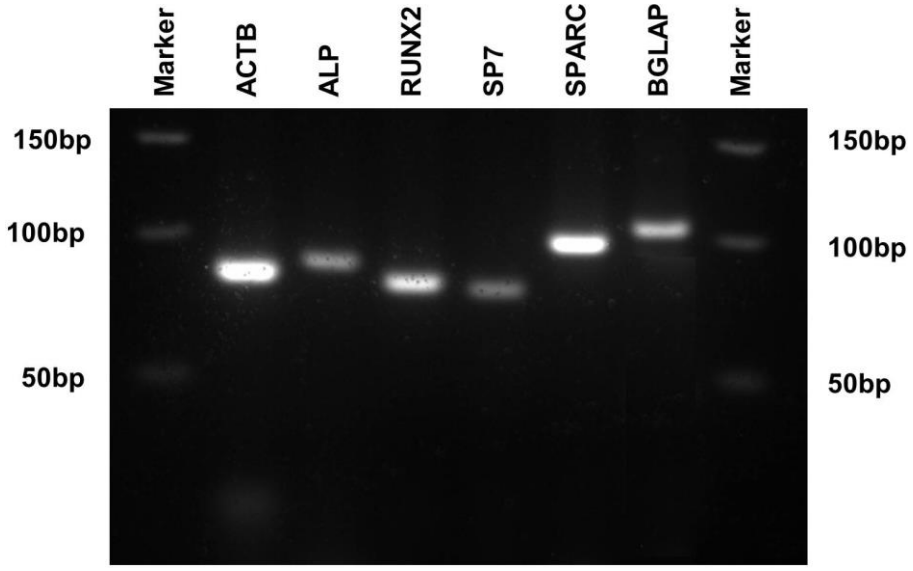

Figure A.13 Osteogenic primer check – amplification products.

Amplification products of *ACTB*, *ALP, RUNX2, SP7, SPARC* and *BGLAP* primers, showing bands specific for the size of intended amplicons from RT-qPCR experiments for osteogenic genes.

STRO-1 expression after 24 hour Wnt induction

Table A.11 STRO-1 expression after Wnt stimulation.

Detailed donor information (sex, age and disease) and percentages of STRO-1 expressing cells in the entire bone marrow and within the "monocytic/stromal" gate, set based on light scattering properties.

STRO-1 expression		In the entire bone marrow		In the monocytic/stromal fraction	
No.	Sample details	Control	Wnt-induced	Control	Wnt-induced
1	F89 OA	15.90 %	23.80 %	17.10 %	25.30 %
2	M91 OA	12.10 %	18.70 %	16.60 %	17.60 %
3	M68 OP	5.23 %	7.75 %	8.24 %	10.14 %
4	F67 OP	5.46 %	4.76 %	7.76 %	8.49 %
5	M84 OP	6.57 %	9.29 %	7.06 %	10.80 %
6	F80 OP	14.50 %	17.70 %	13.20 %	18.70 %
7	F94 OP	7.07 %	8.11 %	10.60 %	13.10 %
8	F57 OP	4.00 %	3.40 %	5.43 %	7.30 %
9	M59 OP	5.34 %	4.78 %	8.42 %	13.60 %
10	F68 OA	1.85 %	1.80 %	4.91 %	5.91 %
11	F69 OA	1.80 %	1.85 %	3.32 %	5.43 %
OA – osteoarthritic; OP – osteoporotic.					

ALP activity or expression and cell number after short-term and long-term Wnt induction

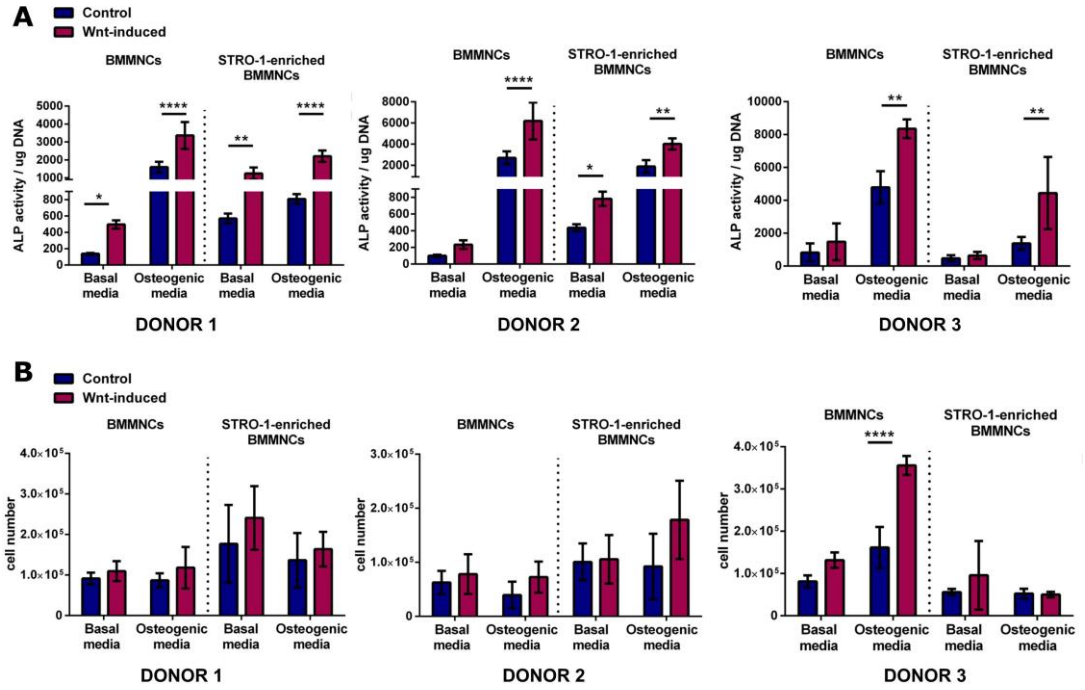

Figure A.14 ALP activity and cell number in BMMNCs and STRO-1-enriched BMMNCs after short-term Wnt induction.

Cells were cultured in monolayer for 14 days in basal or osteogenic media following a 24 hour treatment with Wnt *vs.* control and assayed for ALP activity (A) and cell number (B). Data presented as mean ± SD from n=6 wells. Statistical significance assessed by two-way ANOVA with Sidak's correction: *p<0.05; **p<0.01; ****p<0.0001, on technical replicates. Each donor sample is presented on a separate graph.

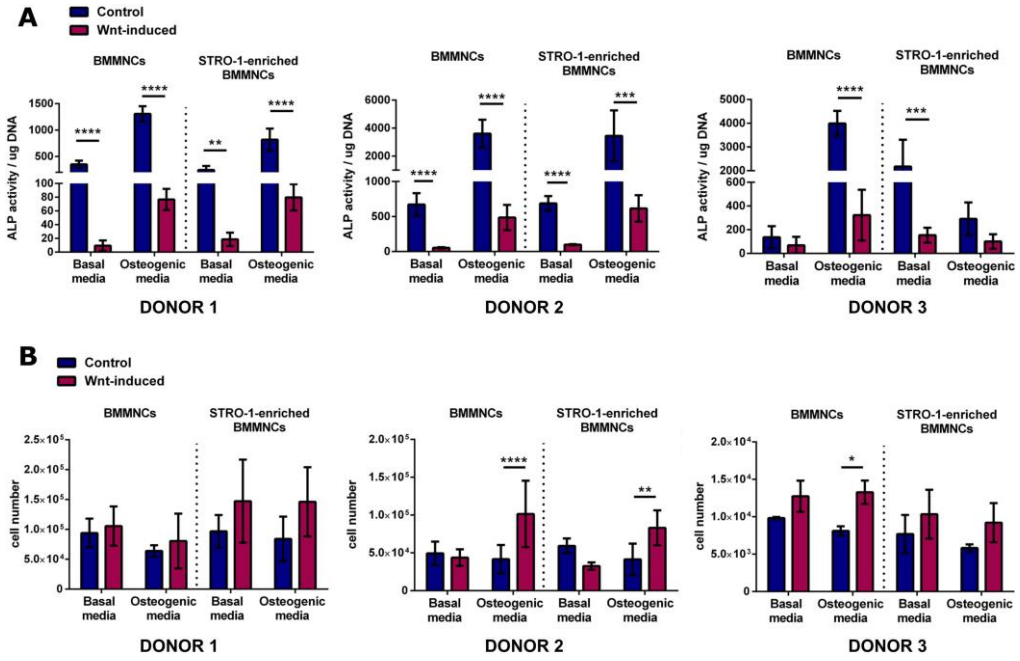

Figure A.15 ALP activity and cell number in BMMNCs and STRO-1-enriched BMMNCs after long-term Wnt induction.

Cells were cultured in monolayer for 14 days in basal or osteogenic media with Wnt vs. control and assayed for ALP activity (A) and cell number (B). Data presented as mean ± SD from n=6 wells. Statistical significance assessed by two-way ANOVA with Sidak's correction: *p<0.05; **p<0.01; ***p<0.001; ****p<0.0001, on technical replicates. Each donor sample is presented on a separate graph.

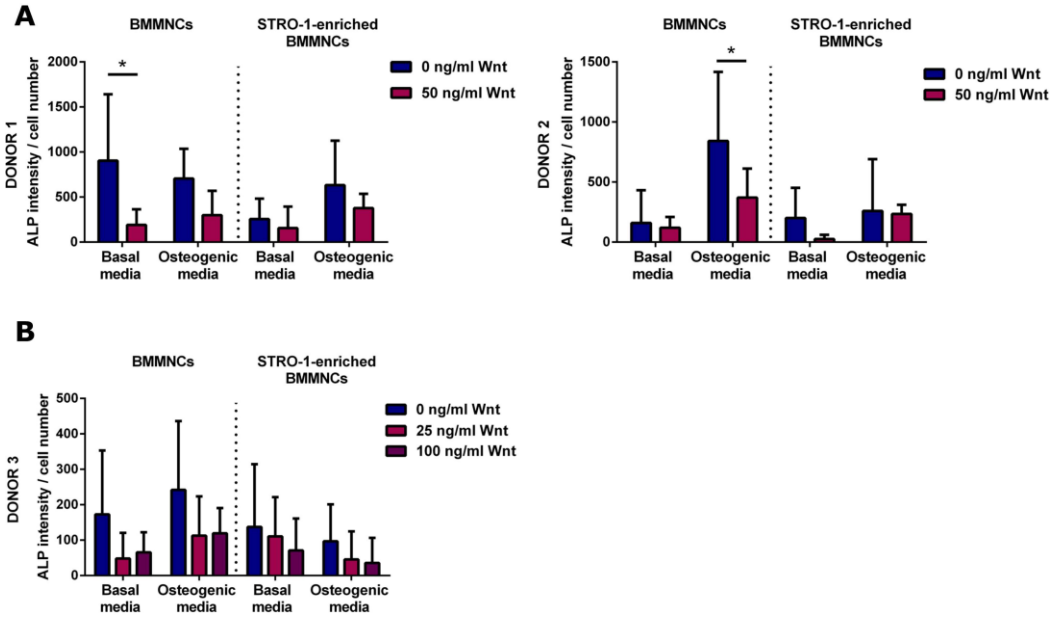

Figure A.16 ALP activity in BMMNCs and STRO-1-enriched BMMNCs after long-term Wnt induction.

Cells were cultured in monolayer for 14 days in basal or osteogenic media with 50 ng/ml (A) or 25 and 100 ng/ml (B) Wnt3A *vs.* control. ALP intensity per cell was quantified by image analysis. Data presented as mean ± SD from n = 6 wells. Statistical significance assessed by two-way ANOVA with Sidak's correction: *p<0.01, on technical replicates. Each donor sample is presented on a separate graph.

Liposome compositions

Table A.12 Lipid characteristics.

Lipid	Chemical name	Numerical code of the fatty acid chain	Tc
Cholesterol	cholest-5-en-3ß-ol		
DMPC	1,2-dimyristoyl-*sn*-glycero-3-phosphocholine	14:0 PC	24°C
DPPC	1,2-dipalmitoyl-*sn*-glycero-3-phosphocholine	16:0 PC	41°C
DSPC	1,2-distearoyl-*sn*-glycero-3-phosphocholine	18:0 PC	55°C
DOPC	1,2-dioleoyl-*sn*-glycero-3-phosphocholine	18:1 PC	-17°C
DSPE-PEG	1,2-distearoyl-*sn*-glycero-3-phosphoethanolamine-N-[amino(polyethylene glycol)-2000] (ammonium salt)	18:0 PE	74°C (for DSPE alone)

Table A.13 Liposome composition.

	Lipid composition	Molar % ratios	Hydration/extrusion temperature
1	DSPC/cholesterol/DSPE-PEG	50:45:5	56˚C
2	DSPC/cholesterol/DSPE-PEG	50:45:5	37˚C
3	DOPC/DSPE-PEG	95:5	37˚C
4	DPPC/DSPE-PEG	95:5	37˚C
5	DMPC/DSPE-PEG	95:5	37˚C
6	DMPC/DSPE-PEG Biotin	95:5	37˚C
7	DOPC/DSPE-PEG/DSPE-PEG Biotin	95:3:2	37°C

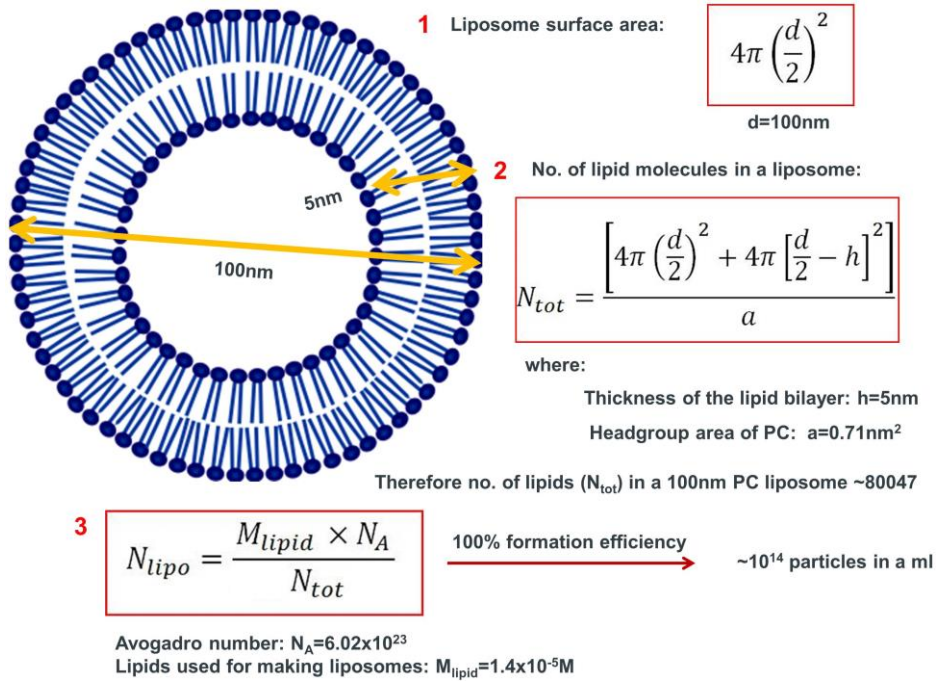

Figure A.17 Calculations of liposome concentration.

Estimation of liposome concentration was based on: the liposome surface area (1), which was calculated based on the 100 nm diameter of particles; assumption of the number of lipid molecules present per liposome (2), calculated based on the predicted size of the lipid bilayer (5 nm) as well as the area occupied by a phosphocholine headgroup (0.71 nm²); and the known concentration of lipids used in formulations (14 µM) as well as the Avogadro number (3). The calculations resulted in ~10^{14} particles per ml of preparation, which was similar to the concentration measured by Nanosight.

A

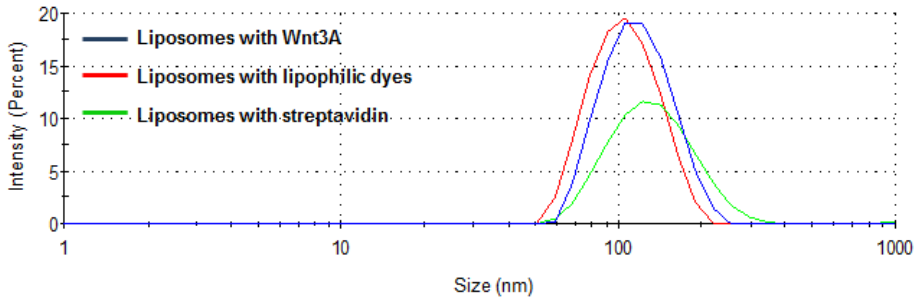

B

Liposome preparation	Liposome size (nm)
Liposomes with Wnt3A	112 ± 27 (n = 3)
Liposomes with lipophilic dyes	102 ± 29 (n = 3)
Liposomes with streptavidin	175 ± 25 (n = 3)

Figure A.18 Size distribution of Wnt3A-loaded and dye and streptavidin-labelled liposomes.

A: Representative histograms from DLS, showing narrow distribution of the Wnt3A and dye-loaded liposome preparation, and a wide distribution of streptavidin-labelled liposomes. B: Summary of size distribution, n = 3 for each sample type.

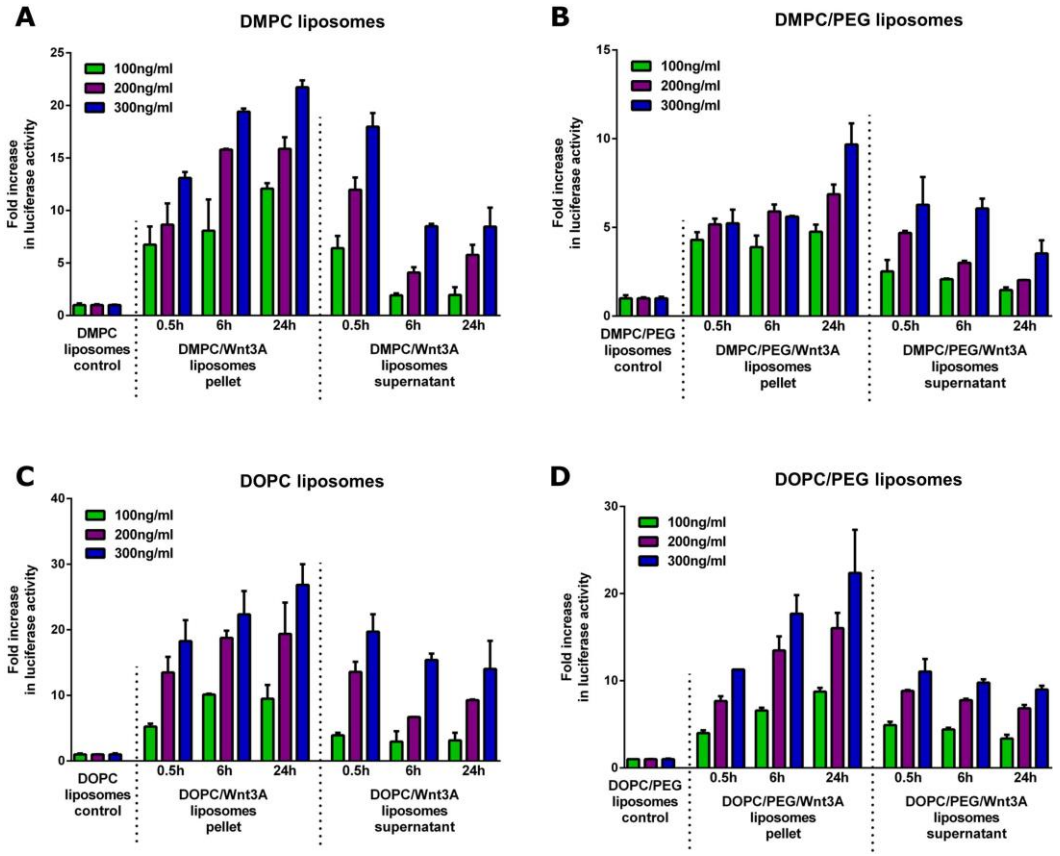

Figure A.19 Wnt3A activity in liposomes increases with incubation time.

Incorporation of Wnt3A into four liposomal preparations (A, B, C and D) during incubation following liposome formation. 0.5, 6 and 24 hour time points were assayed on the Wnt reporter cell line.

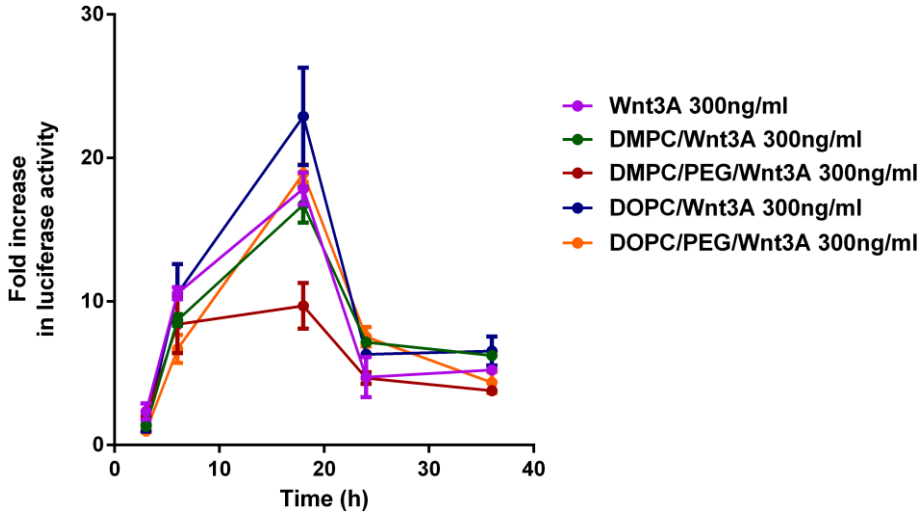

Figure A.20 Various time points for the luciferase assay readout.

The cellular response to liposome-encapsulated Wnt was tested on the murine cell line over 3, 6, 18, 24 and 36 hours of incubation. The response was optimal at 18 hours.

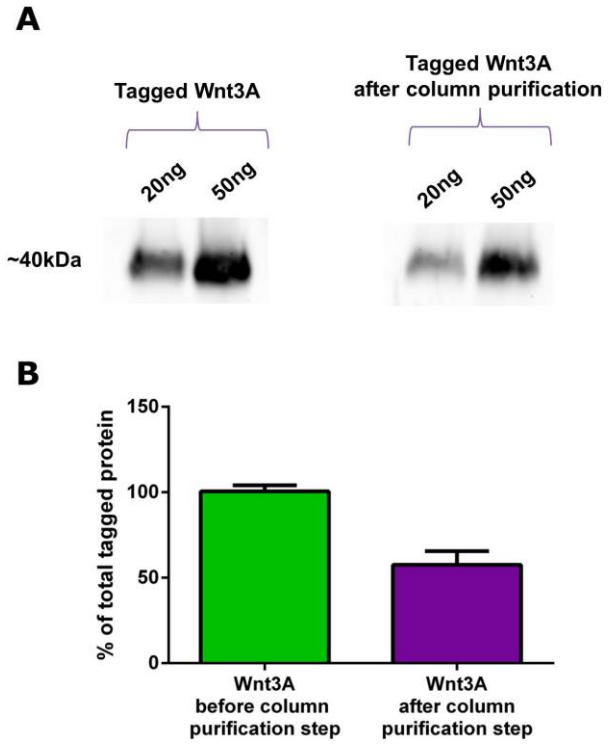

Figure A.21 Protein loss due to the column purification step.

A: Western blot analysis of tagged Wnt3A protein, before and after the column purification. B: Quantification of the Wnt3A signal. The column purification step is necessary for removal of unbound dye, but results in ~50 % protein loss.

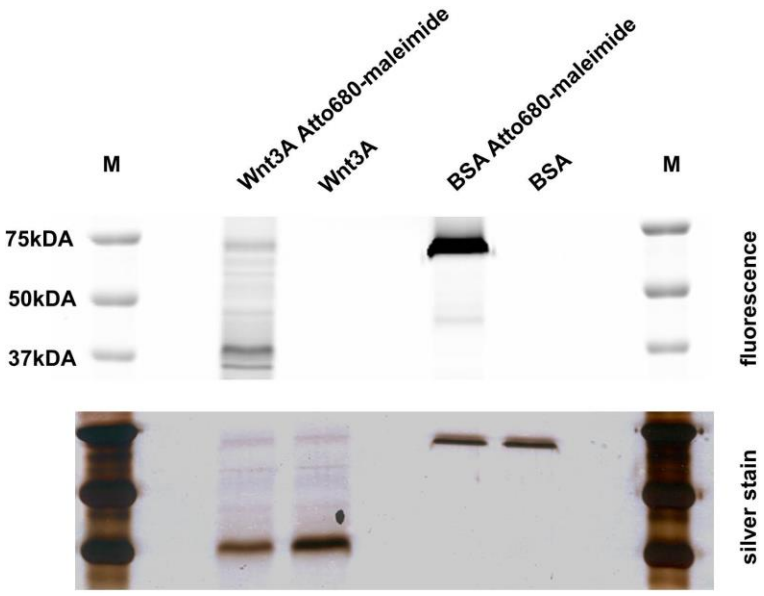

Figure A.22 SDS-PAGE of Atto680-maleimide-tagged Wnt3A.

Upper panel shows fluorescent signal from the tagged proteins, lower panel shows silver stain of all proteins presents. M, marker.

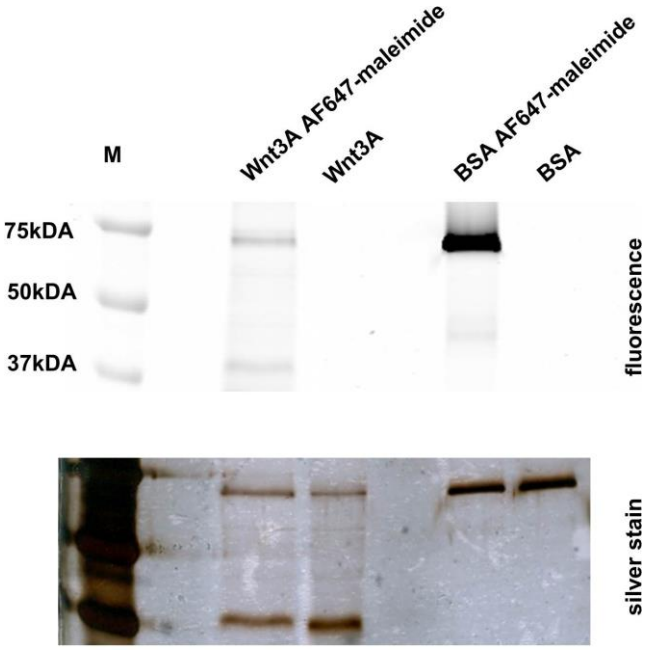

Figure A.23 SDS-PAGE of AF647-maleimide-tagged Wnt3A.

Upper panel shows fluorescent signal from the tagged proteins, lower panel shows silver stain of all proteins presents. M, marker.

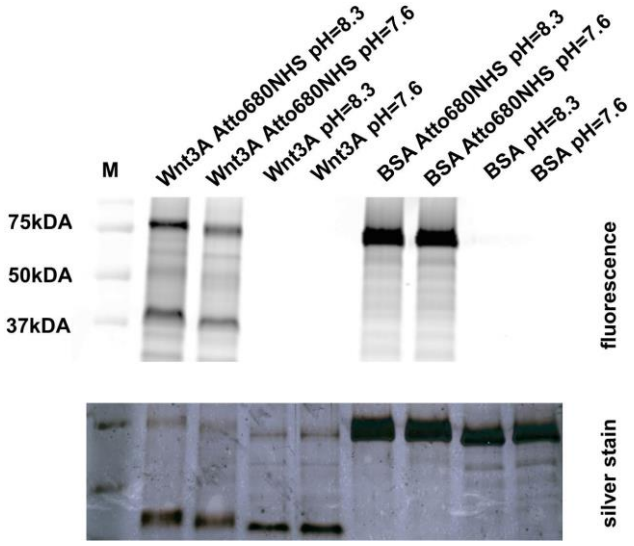

Figure A.24 SDS-PAGE of Atto680NHS-tagged Wnt3A.

Upper panel shows fluorescent signal from the tagged proteins, lower panel shows silver stain of all proteins presents. M, marker.

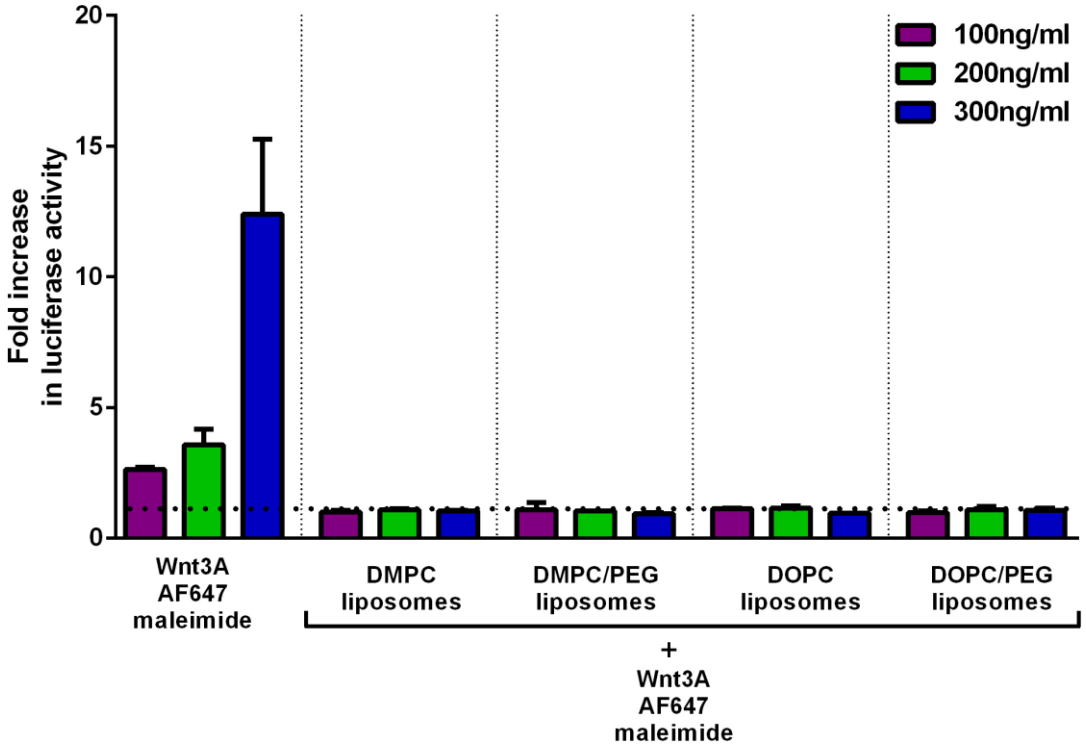

Figure A.25 Liposome activity with AF647 labelled Wnt3A protein.

Wnt3A protein conjugated with AF647-maleimide dye was inactive in DMPC and DOPC liposomal preparations. Data presented as mean ± SD, n = 3 separate experiments. 5 μM concentration of BIO resulted in 78 ± 32 fold increase in luciferase activity. All data points were normalised to controls without the addition of fluorescent proteins, as well as to cell number.

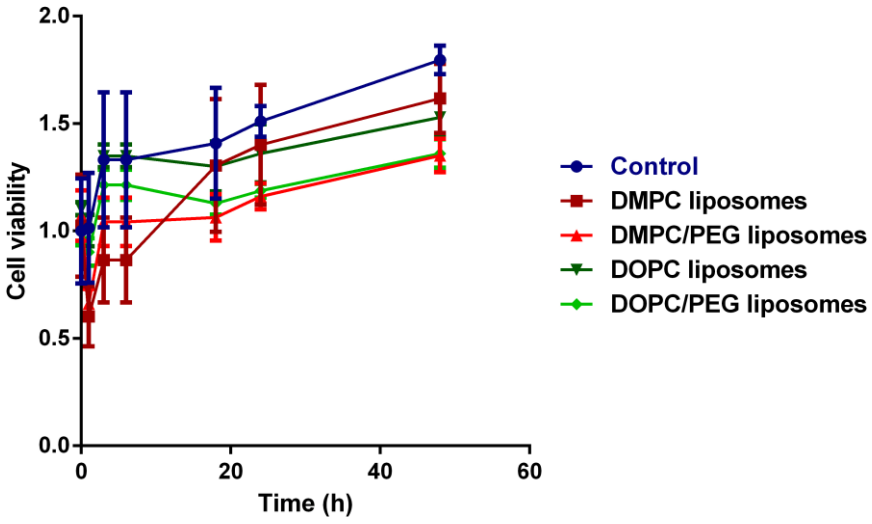

Figure A.26 Viability of cells exposed to liposomes.

No toxic effects were measured after the exposure of cells to various liposome formulations. The number of viable cells was no different to that of control at 1, 3, 6, 18, 24 and 48 hours after seeding and with continuous exposure to liposomes.

In vivo imaging

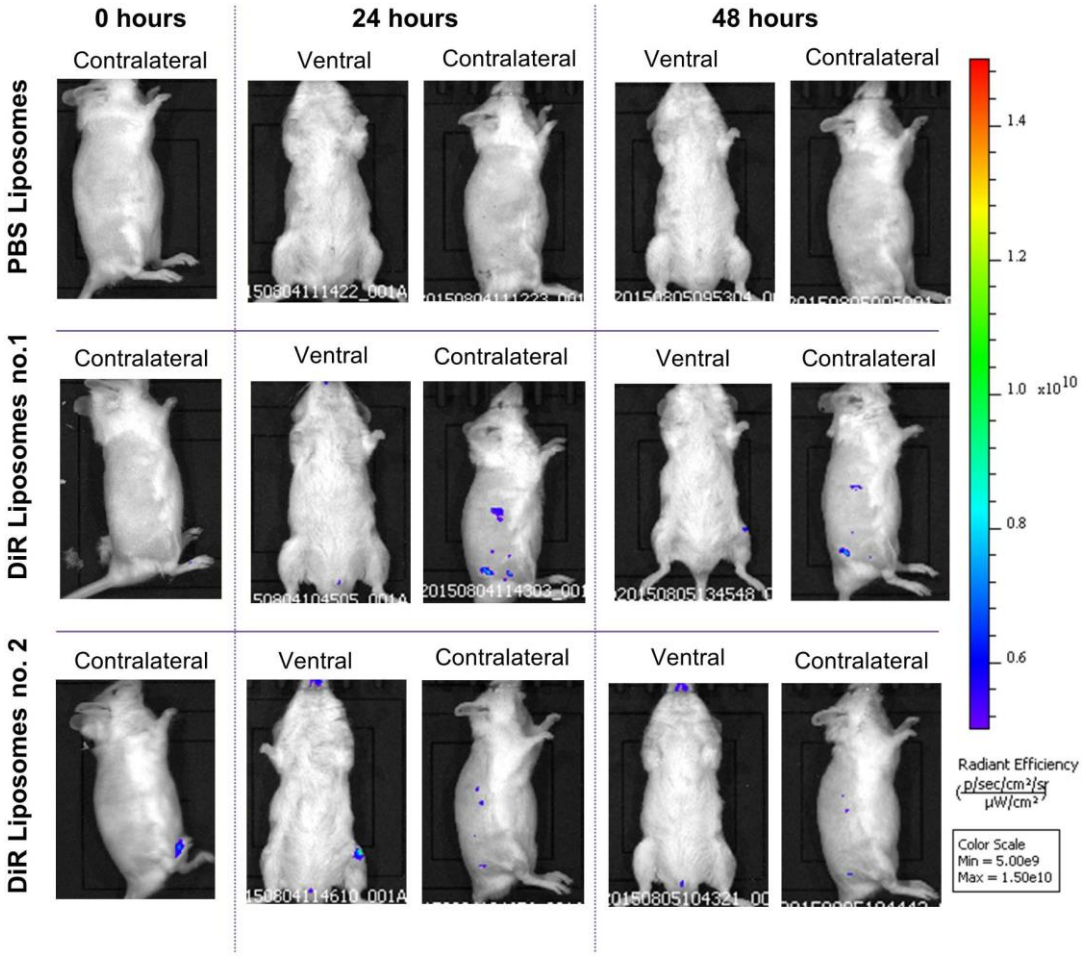

Figure A.27 IVIS whole animal imaging of liposome localisation after systemic injection in a murine bone fracture model.

DiR-labelled liposome nanoparticles were injected systemically *via* tail vein within 30 minutes of left femur drill defect formation. There was a lack of the fluorescent signal imaged at 24 and 48 hour time points in the contralateral side to the bone fracture, as well as in the ventral projections. These imaging projections served as controls.